



UNIVERSIDAD NACIONAL AUTÓNOMA DE MÉXICO

Maestría y Doctorado en Ciencias Bioquímicas

Caracterización del metabolón glucolítico en *Saccharomyces cerevisiae*

TESIS

QUE PARA OPTAR POR EL GRADO DE:

Doctor en Ciencias

PRESENTA:
Emilio Espinoza Simón

TUTOR PRINCIPAL
Dr. Salvador Uribe Carvajal
[Instituto de Fisiología Celular](#)

MIEMBROS DEL COMITÉ TUTOR
Dra. Sobeida Sánchez Nieto
[Facultad de Química](#)
Dra. Xochitl Pérez Martínez
[Instituto de Fisiología Celular](#)

Ciudad de México. Noviembre, 2020



UNAM – Dirección General de Bibliotecas

Tesis Digitales
Restricciones de uso

DERECHOS RESERVADOS ©
PROHIBIDA SU REPRODUCCIÓN TOTAL O PARCIAL

Todo el material contenido en esta tesis está protegido por la Ley Federal del Derecho de Autor (LFDA) de los Estados Unidos Mexicanos (Méjico).

El uso de imágenes, fragmentos de videos, y demás material que sea objeto de protección de los derechos de autor, será exclusivamente para fines educativos e informativos y deberá citar la fuente donde la obtuvo mencionando el autor o autores. Cualquier uso distinto como el lucro, reproducción, edición o modificación, será perseguido y sancionado por el respectivo titular de los Derechos de Autor.

RECONOCIMIENTOS

Esta tesis se realizó bajo la asesoría del Dr. Salvador Uribe Carvajal en el laboratorio 305-ote, Departamento de Genética Molecular, Instituto de Fisiología Celular, UNAM

El jurado del examen estuvo constituido por:

Presidente: Dr. Leonardo Peraza Reyes, Instituto de Fisiología Celular, UNAM

Secretario: Dr. Arturo Carlos II Becerra Camacho, Facultad de Ciencias, UNAM

Vocal: Dr. Óscar Flores Herrera, Facultad de Medicina, UNAM

Vocal: Dr. Manuel Gutiérrez Aguilar, Facultad de Química, UNAM

Vocal: Dr. José Francisco Torres Quiroz, Instituto de Fisiología Celular, UNAM

El comité tutorial que asesoró durante el desarrollo de este trabajo estuvo formado por:

Dr. Salvador Uribe Carvajal, Instituto de Fisiología Celular, UNAM

Dra. Xochitl Pérez Martínez, Instituto de Fisiología Celular, UNAM

Dra. Sobeida Sánchez Nieto, Facultad de Química, UNAM

El jurado de examen de candidatura estuvo integrado por:

Dr. Antonio Peña Diaz, Instituto de Fisiología Celular, UNAM

Dra. Emma Saavedra Lira, Instituto Nacional de Cardiología “Ignacio Chávez”

Dr. Roberto Coria Ortega, Instituto de Fisiología Celular, UNAM

Dra. Sobeida Sánchez Nieto, Facultad de Química, UNAM

Dr. Eleazar Martínez Barajas, Facultad de Química, UNAM

Dra. Xochitl Pérez Martínez, Instituto de Fisiología Celular, UNAM

Se reconoce la colaboración, asesoría y asistencia de la Dra. Natalia Chiquete Felix del laboratorio 305-Ote, Instituto de Fisiología Celular, UNAM

Se reconoce la colaboración y asesoría de la Dra. Ruth Rincón Heredia y de la Unidad de Imagenología, Instituto de Fisiología Celular, UNAM

Se reconoce el apoyo de Ramón Méndez Franco, auxiliar del laboratorio, Instituto de Fisiología Celular UNAM; María del Rocio Romualdo Martínez, Asistente ejecutivo, Instituto de Fisiología Celular, UNAM; Julio Ignacio Palacio Ordoñez, Asistente de procesos, Programa de posgrado en Ciencias Bioquímicas; Adelina González Pérez, Asistente de procesos, Programa de posgrado en Ciencias Bioquímicas; Sara Noguera Solano, Secretaria ejecutiva, Coordinación de enseñanza, Instituto de Fisiología Celular, UNAM.

El sustentante gozó de una beca para realizar los estudios de doctorado otorgada por el COMECYT y una beca de ayudante de SNI III otorgada por el CONACYT

El proyecto fue financiado por el CONACyT (239487) y por la DGAPA-PAPIIT (IN204015, IA202217 e IN209219).

ABREVIATURAS

ABP: proteína de unión a actina

ACT: actina

ALD: fructosa 1,6 bifosfato aldolasa

CCCP: carbonilcianuro-m-clorofenilhidrazona

ENO: enolasa

EtOH: etanol

FBPasa: fructosa 1,6 bifosfato fosfatasa

G6Pasa: glucosa 6 fosfatasa

G6PDH: glucosa 6 fosfato deshidrogenasa

GAPDH: gliceraldehído 3 fosfato deshidrogenasa

GLUT: transportador de glucosa

GPI: glucosa 6 fosfato isomerasa

HK: hexocinasa

LDH: lactato deshidrogenasa

PFK: fosfofructocinasa

PGK: fosfoglicerato cinasa

PGM: fosfoglicerato mutasa

PK: piruvato cinasa

ROS: especies reactivas de oxígeno

TPI: triosa fosfato isomerasa

CONTENIDO

1. Índice de figuras	1
2. Índice de tablas	2
3. Resumen	3
4. Abstract	4
5. Introducción	5
5.1 El citoplasma celular	5
5.2 Asociación enzimática	6
5.3 El citoesqueleto de actina en <i>Saccharomyces cerevisiae</i>	16
6. Hipótesis	19
7. Objetivos	19
7.1 Objetivo general	19
7.2 Objetivos particulares	19
8. Métodos	20
8.1 Materiales	20
8.2 Generación de las cepas transformadas	21
8.3 Efecto de la incubación en ausencia de actina	25
8.4 Distribución de la actina	26
8.5 Obtención de extractos citoplásmicos	26
8.6 Inmunoprecipitaciones	27
8.7 Producción de ATP	28
8.8 Cinética de fermentación	28

9. Resultados	30
9.1 Construcción de las cepas mutantes	30
9.2 La asociación de las enzimas glucolíticas con la actina F disminuyó después de la depleción de glucosa en el medio	33
9.3 La interacción entre las enzimas glucolíticas disminuyó después de la depleción de glucosa en el medio	35
9.4 El ayuno disminuyó la concentración de ATP en las levaduras, siendo este efecto mayor en las cepas fermentativas	36
9.5 A bajas concentraciones de ATP, la adición de glucosa incrementó la actividad fermentativa	38
9.6 La distribución de la proteína de unión a actina (Abp1) se modificó durante la depleción de glucosa, lo que sugiere alteraciones en la organización del citoesqueleto	42
9.7 En las cepas fermentativas obligadas incubadas en ausencia de glucosa, los parches de actina son reemplazados por cuerpos de actina inmóviles	44
9.8 En la cepa silvestre en ayunas, la adición de CCCP indujo la formación de cuerpos de actina inmóviles	45
10. Discusión	47
11. Conclusiones	55
12. Bibliografía	56
13. Anexo. Artículos publicados	63

1. ÍNDICE DE FIGURAS

Fig. 1 Construcción del fragmento Abp1-GFP

Fig. 2 PCR de comprobación

Fig. 3 Curva de crecimiento

Fig. 4 Asociación de enzimas glucolíticas con actina

Fig. 5 Asociación de enzimas glucolíticas en ausencia de glucosa

Fig. 6 Concentración de ATP en las cepas incubadas en ausencia de glucosa

Fig. 7. Producción de etanol en respuesta a la adición de glucosa

Fig. 8 Organización del citoesqueleto de actina en ausencia de glucosa

Fig. 9 Organización del citoesqueleto de actina en la cepa w303 Abp1-GFP incubada sin glucosa y con CCCP

2. ÍNDICE DE TABLAS

Tabla 1. Oligonucleótidos utilizados en este proyecto

Tabla 2. Programa de PCR utilizado para la construcción de las mutantes

Tabla 3. Programa de PCR utilizado para la verificación de las mutantes

Tabla 4. Cepas haploides construidas en este trabajo

Tabla 5. Velocidad de fermentación en las cepas incubadas en ausencia o presencia de glucosa

3. RESUMEN

Los metabolones son asociaciones dinámicas de enzimas que catalizan reacciones consecutivas en una vía determinada. Dichas asociaciones estabilizan a las enzimas y optimizan la catálisis. Los metabolones pueden usar elementos del citoesqueleto, membranas celulares y proteínas de membrana como andamios. El efecto de la eliminación de glucosa en la formación de un metabolón glucolítico anclado a los filamentos actina F (actina F) fue evaluado en tres cepas de *Saccharomyces cerevisiae*; una cepa silvestre y dos cepas fermentativas obligadas, las cuales obtienen ATP principalmente de la glucólisis. La incubación en ausencia de glucosa indujo una inhibición de la fermentación, disminución en la concentración de ATP y la disociación de las enzimas glucolíticas de la actina F. La velocidad de reactivación de la fermentación después de la reincubación en glucosa dependió de la cepa en estudio. Además, a baja concentración de ATP (< 1 nmol/mg de peso húmedo), los parches dinámicos de actina se reorganizaron en grandes cuerpos inmóviles. La adición de glucosa restauró la fermentación y la dinámica del citoesqueleto, sugiriendo que además de la concentración de ATP, el ensamblaje del metabolón glucolítico optimiza la velocidad de fermentación.

4. ABSTRACT

Metabolons are dynamic associations of enzymes catalyzing consecutive reactions within a given pathway. Association results in enzyme stabilization and increased metabolic efficiency. Metabolons may use cytoskeletal elements, membranes or membrane proteins as scaffolds. The effect of glucose withdrawal on a putative glycolytic metabolon/F-actin system was evaluated in three *Saccharomyces cerevisiae* strains: a WT and two different obligate fermentative (OxPhos-deficient) strains. Carbon source withdrawal inhibited fermentation, decrease in ATP concentration and dissociation of glycolytic enzymes from F-actin. Depending on the strain, inactivation / reactivation transitions of fermentation took place in seconds. In addition, when ATP was very low, F-actin reorganized from highly dynamic patches to large, non motile actin bodies containing proteins and enzymes. Glucose addition restored fermentation and cytoskeleton dynamics, suggesting that metabolon assembly / disassembly controls the rate of fermentation.

5. INTRODUCCIÓN.

5.1 El citoplasma

El citoplasma es una solución viscosa en la que están dispersos los componentes celulares, constituido por agua, moléculas orgánicas e inorgánicas. En las células eucariontes, el citoplasma incluye al material celular que se encuentra fuera del núcleo y está constituido por el citosol, los organelos membranosos y los ribosomas (Burr, 2007). Inicialmente se pensaba que el citoplasma era una suspensión acuosa de enzimas y otras macromoléculas distribuidas al azar (Mainland, 1931). Actualmente éste es descrito como un gel constituido por 80%-85% de agua, 10%-15% de proteínas, y 2%-4% de lípidos (Bibbo & Wilbur, 2008).

El citoplasma en los eucariontes también contiene una red de microfilamentos, microtúbulos y filamentos intermedios, proteínas de unión a citoesqueleto y varias enzimas que, en conjunto, le dan forma a la célula (Jinturkar & Misra, 2011). En el citoplasma de la bacteria *Escherichia coli*, las biomoléculas alcanzan una concentración de 200 a 400 mg/ml (Zimmerman & Trach, 1991). La organización del citoesqueleto, la presencia de organelos y la elevada concentración de proteínas en el citoplasma constituyen un sistema con una elevada acumulación de macromoléculas o “crowding” que impone límites en su difusión y en las reacciones enzimáticas secuenciales (Yu *et al.*, 2016). La disminución del volumen efectivo de disolvente tendría un efecto adverso sobre el metabolismo celular, sin embargo, la célula está adaptada a estas condiciones mediante la adsorción reversible y las interacciones transitorias entre las enzimas (Pagliaro, 2000).

5.2 Asociación enzimática

En los sesentas, David Green postuló que en el citoplasma las enzimas de una vía metabólica se asocian a estructuras como la membrana celular. Mediante el análisis de la actividad enzimática en fracciones citoplásmicas y membranales, se determinó que las enzimas glucolíticas forman un complejo unido a la cara interna de la membrana plasmática de los eritrocitos o de las levaduras (Green *et al.*, 1965).

En la enzima ALD aislada de músculo bovino se determinó que la eficiencia aumenta en presencia de actina F, particularmente cuando se incuba con el complejo actina F-tropomiosina-troponina. Además, se observó que la adición de calcio modifica la actividad de esta enzima sin afectar la formación de complejo (Walsh, 1977). También, la unión de PFK-1 a las miofibrillas de músculo disminuye su inhibición por ATP e incrementa su actividad en presencia de hexosas fosfato (Andrés *et al.*, 1996). La interacción de ALD con el citoesqueleto se ha demostrado en diferentes modelos experimentales. La incubación de ALD marcada con rodamina y actina filamentosa disminuye el coeficiente de difusión de la enzima y hasta un 36% de la enzima se une al citoesqueleto. También, se demostró que la incubación con un exceso del sustrato fructosa 1,6 bifosfato disminuye la unión de la enzima y la actina, esto sugiere que la unión de la enzima al citoesqueleto requiere que el sitio activo de la enzima esté libre (Pagliaro & Taylor, 1988). En la línea celular 3T3, la unión de la aldolasa a los filamentos de actina disminuye en presencia de la 2 desoxiglucosa o de citocalasina sugiriendo que la unión de la aldolasa depende de la estabilidad de los filamentos de actina y de la actividad de la vía glucolítica (Pagliaro & Taylor, 1992).

Paul Srere propuso que en las mitocondrias las enzimas forman complejos multienzimáticos unidos a la membrana interna (Hanson, 1972). Srere acuñó el término “metabolón” para describir al complejo de enzimas metabólicas secuenciales unidas a elementos estructurales de la célula (Srere, 1985).

La formación de metabolones optimiza las vías metabólicas mediante el incremento en la estabilidad enzimática y la canalización de sus intermediarios entre los sitios activos contiguos de las enzimas (Ovádi & Srere, 1999; Srere, 1987). En 1987 mediante la técnica de dilución de isótopos, se demostró que la ALD y la GAPDH forman un complejo que canaliza al sustrato gliceraldehído 3 fosfato (Orosz *et al.*, 1987). Este fenómeno se ha demostrado también en la síntesis de macromoléculas como el DNA, RNA y las proteínas (Srere, 1987), el ciclo de Krebs (Wu *et al.*, 2015), la síntesis de purinas (Pedley & Benkovic, 2017) y en la síntesis de flavonoides (Jørgensen *et al.*, 2005), entre otros. Además del incremento en la eficiencia enzimática por la canalización de intermediarios, los metabolones impiden la difusión de intermediarios lábiles o tóxicos (Sweetlove & Fernie, 2018).

Durante la formación del metabolón, la organización de las enzimas participantes que incrementan su actividad mediante la disminución de los tiempos de transferencia de los intermediarios entre los sitios activos, disminución de la dilución de intermediarios en el citosol (Jørgensen *et al.*, 2005) y la exclusión de los posibles inhibidores del sitio activo de las enzimas (Ellis & Minton, 2003).

El ensamble de un metabolón enzimático requiere de un elemento estructural en la célula. Algunos organismos contienen elementos membranales o proteínicos donde las enzimas son organizadas. En los tripanosomas, las enzimas glucolíticas están contenidas en pequeños organelos denominados glucosomas. En *Trypanosoma brucei*, el 90% de las proteínas contenidas en este organelo son enzimas glucolíticas y tienen un papel relevante durante el crecimiento de este organismo en condiciones de anaerobiosis (Schmitt & An, 2017). Estos organelos también pueden contener enzimas de la vía de las pentosas fosfato, oxidación de ácidos grasos y síntesis de purinas (Michels *et al.*, 2006).

En la membrana citoplasmática, las enzimas se asocian dinámicamente con transportadores celulares, formando metabolones que incrementan la eficiencia metabólica al canalizar el sustrato directamente del transportador a las enzimas que lo metabolizan. En el eritrocito, la anhidrasa carbónica forma un complejo con la banda 3 que facilita el transporte de bicarbonato a través de la membrana plasmática (Sterling *et al.*, 2001). En músculo esquelético, la unión de la hexocinasa con el GLUT4 incrementa la glucólisis y la unión del transportador con la GAPDH la disminuye (Moraes & Reithmeier, 2012).

Algunas enzimas citoplásicas del metabolismo glucolítico pueden unirse a transportadores de la membrana externa mitocondrial, canalizando los intermediarios de esta vía a la matriz mitocondrial. Esto se ha demostrado en protoplastos de *Arabidopsis thaliana*, donde mediante microscopía de fluorescencia se demostró que la enzima GAPDH unida a una proteína fluorescente se une al canal aniónico dependiente de voltaje (VDAC) (Schneider *et al.*, 2018).

Dicha interacción favorece la canalización de NADH para la generación de ATP mitocondrial, probablemente a través de la vía de las oxidases alternas. La formación de este complejo disminuyó cuando los protoplastos fueron incubados en presencia de H₂O₂ y aumentó cuando la incubación se realizó con DTT, lo que sugiere que esta interacción es un “interruptor redox” que puede organizar el metabolismo energético. Por ejemplo, bajo condiciones normales una parte de la GAPDH podría canalizar NADH a la mitocondria para la generación de ATP, en cambio un aumento en el estrés oxidativo celular disminuiría la actividad de esta enzima para permitir la reorganización del metabolismo glucolítico para la generación de NADPH con el objetivo de incrementar el número de antioxidantes en la célula (Schneider *et al.*, 2018).

En el tejido cardiaco, la enzima HKII se localiza en el citoplasma y en la membrana externa de la mitocondria interaccionando con el canal aniónico dependiente de voltaje (VDAC). Cuando este tejido sufre isquemia / reperfusión, la HKII unida a la mitocondria se despega y relocaliza en el citoplasma. Esto induce la apertura del poro de transición de la permeabilidad (mPTP), la salida de citocromo C de la mitocondria, la traslocación de las proteínas proapoptóticas y la generación de especies reactivas de oxígeno. Así, la unión de esta enzima a la mitocondria disminuye la producción de ROS y la necrosis celular (Nederlof *et al.*, 2016). En células de cáncer de ovario (células CHO) se expresan dos de las cuatro isoformas de la enzima hexocinasa (HKI y HKII). HKI se asocia principalmente a la mitocondria y se considera que promueve exclusivamente la glucólisis, mientras que la HKII se encuentra en el citoplasma y unida a la membrana mitocondrial y participa en la glucólisis y en el metabolismo del glucógeno.

La disponibilidad de glucosa y glucosa 6 fosfato en estas células modifica la localización de HKI. La remoción de glucosa del medio de incubación promueve la movilización de HKII al citoplasma y no tiene efectos importantes sobre la localización de HKI. Dicho efecto se revierte después de la adición de glucosa ó glucosa 6 fosfato. Esto sugiere que estas enzimas pueden formar complejos diferentes para la glucólisis (unidos a la membrana mitocondrial) o para la glucogenólisis (en el citoplasma). Es probable que por esto la HKII se encuentra con frecuencia en tejidos que en respuesta a la insulina promueven la síntesis de glucógeno y la HKI en tejidos primordialmente glucolíticos (Calmettes *et al.*, 2013).

El citoesqueleto es otra estructura a la cual se anclan las enzimas formando metabolones. En músculo esquelético de rata, se ha determinado que la isoforma $\alpha\alpha$ de la enzima glucolítica ENO se une a los microtúbulos en mioblastos indiferenciados, mientras que después de la diferenciación de estas células, es la isoforma $\beta\beta$ la unida a los microtúbulos en los miotubos. La unión de ENO a los microtúbulos disminuye cuando se incrementa la concentración de su producto, el 2-fosfoglicerato. Los autores postulan que la ENO y la PK se unen al microtúbulo, formando un complejo que permite producir ATP “*in situ*” para los fenómenos de contracción muscular. Además, proponen que la formación de dicho complejo se modula por las concentraciones del 2 fosfoglicerato (Keller *et al.*, 2007).

Experimentos *in vitro* mostraron que las enzimas GPI, ALD, GAPDH, TPI, ENO, PGM, PGK, PK y LDH interaccionan con tubulina y con los microtúbulos. Las constantes de disociación observadas en cada una de estas enzimas son cercanas a sus concentraciones fisiológicas, lo que sugiere que *in vivo* estas proteínas interaccionan (Walsh *et al.*, 1989).

En los eritrocitos humanos, se describió la asociación de las enzimas glucolíticas GAPDH, LDH y PK con las proteínas banda 3, β -espectrina, ankirina, actina, p55 y p4.2 (Puchulu-Campanella *et al.*, 2013). La formación de este complejo es un mecanismo de regulación sensible a las concentraciones de oxígeno circulantes. Cuando los eritrocitos están en condiciones de hipoxia, las enzimas glucolíticas se desprenden de la banda 3 incrementando la glucolisis y disminuyendo la vía de las pentosas fosfato para la producción de NADPH. En cambio, en condiciones normales de oxigenación, las enzimas glucolíticas se unen a la banda 3 y disminuyen la vía glucolítica (Lewis *et al.*, 2009).

En células musculares, también se ha demostrado el papel del citoesqueleto en la formación de un complejo multienzimático glucolítico donde se propone que la PFK se une al citoesqueleto y después se unen la ALD, la GAPDH, la LDH y finalmente la PGK, la PGM, la ENO, la TPI y la glicerol 3 fosfato deshidrogenasa (GPDH) (Menard *et al.*, 2014).

En las células vegetales, las enzimas que intervienen en la formación de metabolitos secundarios forman metabolones en la membrana del retículo endoplásmico (RE). En *Antirrhinum majus*, la flavona sintasa, la chalcona sintasa, la dihidroflavonol reductasa, la chalcona isomerasa y la flavonoide 3 hidroxilasa forman un complejo anclado a la membrana del RE para la síntesis de flavonas y antocianinas (Fujino *et al.*, 2018). En las leguminosas, la isoflavona sintasa y la cinamato 4 hidroxilasa interaccionan con las enzimas P450 en la membrana del RE, interactuando con otras enzimas que intervienen en la síntesis de isoflavonas (Dastmalchi *et al.*, 2016).

Acorde a lo descrito, las enzimas que participan en el metabolismo glucolítico forman complejos que pueden estar adosados a la membrana externa mitocondrial, a la membrana citoplásmica o al citoesqueleto.

Uno de los andamios más utilizados por las enzimas glucolíticas para formar metabolones dinámicos es el citoesqueleto. Mediante ensayos *in vitro*, se observó que la ALD y la PFK-1 forman complejos con los componentes del citoesqueleto. Cuando la PFK-1 tetramérica es diluida, se descompone en dímeros que pierden su actividad catalítica. En cambio, cuando es preincubada con la ALD, la actividad de la enzima y su conformación tetramérica se preservan. Si a este sistema se le adicionan concentraciones micromolares de microtúbulos, hay un incremento de la actividad de la PFK, probablemente debido a la formación de un complejo estable entre los microtúbulos y las enzimas glucolíticas (Rais, 2000).

Se ha propuesto que, en las células musculares, la PFK-1 interacciona directamente con la actina, y las demás enzimas se unen a la PFK mediante interacciones débiles (Menard *et al.*, 2014). En las células permeabilizadas de cáncer de ovario de hámster, la GAPDH, la G6PDH, la G6Pasa y la LDH se unen a la actina formando un complejo multienzimático. Esta interacción se interrumpe después de la adición de latrunculina A (que promueve la despolimerización de los filamentos de actina), lo que sugiere que la estabilidad de los filamentos de actina es relevante para la formación del metabolón (Hudder *et al.*, 2003).

En las células de cáncer de mama, se ha descrito la colocalización de las cuatro enzimas reguladoras del metabolismo de carbohidratos: la PFK, la FBPasa, la PK y la PEPCK.

También, se observó que el tamaño de estos complejos responde a las variaciones metabólicas de la célula. Durante la activación de la vía de las pentosas fosfato, los agregados enzimáticos son más pequeños que durante la activación de la vía glucolítica o durante la biosíntesis de serina. Este fenómeno de agregación no se observa en células sanas, lo que sugiere que durante la reorganización metabólica que ocurre en las células tumorales la formación de metabolones también se modifica (Kohnhorst *et al.*, 2017).

La interacción de las enzimas y su dinámica dependen de la disponibilidad de nutrientes en la célula. En *S. cerevisiae*, la ALD interacciona con tres regiones distintas de la ATPasa vacuolar. Dicha interacción es importante para la función de la ATPsa; las cepas mutantes en la ALD crecen a pH de 5.5, pero no a un pH de 7.5 debido a un ensamble deficiente de la ATPasa vacuolar. Esta investigación también demostró qué en cepas silvestres, la interacción entre la ALD y la ATPasa se incrementa cuando hay una elevada concentración de glucosa en la célula. Asimismo, se determinó que la enzima GAPDH también forma parte de este complejo. Los autores proponen la formación de un complejo glucolítico con las otras enzimas (aunque no lo demuestran) que facilitaría la canalización de ATP para la función de la ATPasa vacuolar (Lu *et al.*, 2004).

La organización de las enzimas que intervienen en la traducción de proteínas también depende de la disponibilidad de nutrientes. En *S. cerevisiae*, la depleción de glucosa induce una disminución en la cantidad de polirribosomas e inhibe la traducción de proteínas. Este fenómeno correlacionó con una disminución en la concentración de ATP celular. (Ashe *et al.*, 2000).

La escasez de glucosa en *S. cerevisiae* disminuye la endocitosis, el reciclaje de proteínas y la autofagia, e incrementa la hidrólisis vacuolar con el objetivo de aumentar la poza de aminoácidos para su catabolismo (Lang *et al.*, 2014). Bajo las mismas condiciones, las enzimas involucradas en la biosíntesis de los lípidos son secuestradas en regiones específicas en el citoplasma, disminuyen la reorganización mitocondrial y los contactos entre la mitocondria, el retículo endoplásmico y las vacuolas (Suresh *et al.*, 2015).

La distribución de las enzimas citoplásmicas en *S. cerevisiae* también responde al estado energético. Después de alcanzar la fase de crecimiento estacionaria o durante la depleción de glucosa, veintitrés enzimas, incluyendo a las enzimas PFK1 y PFK2 forman filamentos insolubles. La adición de glucosa revierte este fenómeno (Shen *et al.*, 2016). Esta filamentación inducida por la ausencia de glucosa también ocurre con la enzima citidina trifosfato sintetasa (Ura7p) (Noree *et al.*, 2010). Una posible explicación a este fenómeno es que, la ausencia de glucosa incrementa el *crowding* celular y estimula una disminución del pH intracelular que induce la filamentación de las enzimas. (Petrovska *et al.*, 2014).

En *S. cerevisiae*, las enzimas glucolíticas forman complejos que preservan su actividad en diferentes viscosidades. Algunas enzimas de esta vía, como la GAPDH y la PGK son muy sensibles a la inhibición por viscosidad. La ALD en cambio, es insensible a la inhibición por viscosidad y más aún, aparentemente protege la actividad de otras enzimas.

Por ejemplo, la incubación de la ALD con la GAPDH protege la actividad de esta última en condiciones crecientes de viscosidad inducida por la adición de trehalosa e inclusive la incrementa veinte veces multienzimático (Araiza-Olivera *et al.*, 2010).

Al evaluar la producción de etanol en extractos citoplásmicos, se determinó que la fermentación no se modifica en presencia de concentraciones fisiológicas de trehalosa, lo que sugiere que en el extracto citoplásmico las enzimas de esta vía están organizadas formando un complejo multienzimático (Araiza-Olivera *et al.*, 2010).

En las levaduras, la formación del metabolón glucolítico depende de la estructura de la actina. Ensayos *in vitro* mostraron que la estabilización farmacológica de los la actina F con faloidina incrementa su interacción con las enzimas HK, GPI, TPI, GAPDH, PGK y ENO. Asimismo, la monomerización de la actina F inducida por la citocalasina disminuyó la interacción antes mencionada. También se observó que la estructura de la actina modifica la interacción entre las enzimas glucolíticas; la interacción de la ALD con la GAPDH y la PGK se incrementó cuando la actina forma filamentos estables y disminuyó con su monomerización. La velocidad de fermentación también depende de la estructura del citoesqueleto; la estabilización de los filamentos de actina aumenta la producción de etanol y la monomerización de los filamentos tuvo el efecto inverso (Araiza-Olivera *et al.*, 2013).

5.3 El citoesqueleto de actina en *S. cerevisiae*

En *S. cerevisiae* el citoesqueleto de actina tiene un papel fundamental en la estructura celular, polarización de organelos, división y tráfico intracelular (Apodaca, 2001; Moseley & Goode, 2006). La actina monomérica globular (actina G) se polimeriza formando filamentos de actina (actina F), la cual tiene un papel fundamental en la regulación de la traducción y el plegamiento de proteínas. En las levaduras interviene en la formación del anillo de actomiosina durante la división celular, el transporte de organelos y de vesículas, la generación de ascosporas, la gemación, la endocitosis y la exocitosis (Sattlegger *et al.*, 2014).

Para ejecutar esta diversidad de funciones, los microfilamentos de actina F se organizan en forma de cables y parches. Los parches de actina intervienen en los procesos de endocitosis, se forman en la membrana citoplásmica y tienen una vida media que oscila entre los 20 y 40 segundos. Para su formación se requiere de la interacción de la actina F con proteínas accesorias como la proteína de unión a actina 1 (Abp1) (Smith *et al.*, 2001, Berepiki *et al.*, 2011). Los cables de actina por otro lado se requieren para el transporte de organelos, proteínas y ácidos nucleicos durante la división celular. El ensamble de estas estructuras depende de la interacción de actina F con proteínas accesorias como la Abp140 (Moseley & Goode, 2006).

La organización del citoesqueleto también depende de la disponibilidad de nutrientes en el medio. Minutos después de la incubación en ausencia de glucosa, los cables de actina se estabilizan, las miosinas liberan a su molécula cargo y permanecen inmóviles sobre los cables de actina mientras que los parches de actina pierden polaridad (Xu & Bretscher, 2014).

En la fase estacionaria, la actina se reorganiza formando unas estructuras inmóviles denominadas “cuerpos de actina”. Estas estructuras funcionan como “reservas” de actina a partir de las cuales, los cables y los parches de actina se reensamblan cuando los nutrientes están disponibles nuevamente (Sagot *et al.*, 2006).

Diversas investigaciones sugieren que el citoesqueleto interviene en la regulación del metabolismo formando complejos enzimáticos. Respecto a la vía glucolítica, se ha demostrado *in vitro* que la PFK incrementa su actividad al interaccionar con la actina F (Silva *et al.*, 2004), mientras que en las células epiteliales la ALD muestra un comportamiento inverso (Hu *et al.*, 2016). En la levadura, simulaciones por dinámica browniana sugieren que la actina no interacciona con la ALD e interacciona débilmente con la GAPDH (Waingeh *et al.*, 2006). En nuestro laboratorio, se demostró que la incubación de las enzimas GAPDH y ALD o extractos citoplásmicos con actina filamentosa estabiliza la interacción entre las enzimas e incrementa la actividad glucolítica. Este complejo enzimático o "metabolón glucolítico" protege a las enzimas de la inhibición mediada por la viscosidad del medio o por anticuerpos (Araiza-Olivera *et al.*, 2013, 2010).

Se ha reportado que la organización de las enzimas es sensible a la fase de crecimiento y a la disponibilidad de nutrientes en el medio. En levaduras, la distribución de algunas enzimas en el citoplasma está regulada por la fase de crecimiento. Durante la fase de crecimiento logarítmica, las enzimas asparagina sintetasa, glutamato sintasa y PFK marcadas con proteína verde fluorescente se distribuyen homogéneamente en el citoplasma, sin embargo, en las fases diauxica y estacionaria, se agrupan formando filamentos (Shen *et al.*, 2016).

Los autores proponen que la agrupación de estas enzimas disminuye su actividad en respuesta a la disminución en la disponibilidad de nutrientes. La adición de medio fresco estimula la redistribución de las enzimas en el citoplasma.

Así, la organización de las enzimas y el citoesqueleto depende de la disponibilidad de nutrientes y probablemente de la concentración de ATP. En las levaduras, la producción de ATP depende de la glucólisis y la producción de ATP mitocondrial. Durante la incubación en glucosa, las células transforman la glucosa en etanol. Posteriormente, el etanol es catabolizado en la mitocondria para mantener los niveles basales de ATP. Existen cepas de levaduras que solo obtienen ATP a partir de la fermentación debido a alteraciones mitocondriales. En la cepa *S. cerevisiae* p⁰ (cepa fermentativa obligada sin DNA mitocondrial) la concentración de ATP disminuye en más del 50% minutos después de la depleción de glucosa, lo que impide la fosforilación de proteínas que intervienen en vías de señalización de adaptación a la ausencia de nutrientes (Friis & Schultz, 2016). *S. cerevisiae* pet122Δ es otra cepa con metabolismo fermentativo, que carece de la proteína Pet122, relevante para el ensamble del complejo 4 de la cadena respiratoria (Kloeckener-Gruissem *et al*, 1988). En este trabajo, se determinará el efecto de la ausencia de glucosa en la organización del citoesqueleto y la formación del metabolón glucolítico en la cepa *S. cerevisiae* w303 (cepa silvestre) y en las cepas *S. cerevisiae* w303 p⁰ y *S. cerevisiae* w303 pet122Δ (cepas respiratorias).

6. HIPÓTESIS

Si la formación del metabolón glucolítico depende de la estructura del citoesqueleto de actina, entonces la alteración del citoesqueleto inducida por la carencia de glucosa modificará el ensamblaje del metabolón y la eficiencia de la vía glucolítica.

7. OBJETIVOS

7.1 Objetivo general.

Evaluar el efecto de la depleción de glucosa sobre la organización del citoesqueleto de actina, así como la formación y actividad del metabolón glucolítico en *S. cerevisiae*.

7.2 Objetivos particulares.

Observar los cambios en la organización del citoesqueleto de actina en las cepas w303, w303 ρ^0 y w303 $pet122\Delta$ durante la incubación en ausencia de glucosa.

Determinar la unión de las enzimas glucolíticas GAPDH, ALD y PGK al citoesqueleto de actina en las cepas ya mencionadas durante la depleción de glucosa.

Evaluar la velocidad de fermentación alcohólica en las cepas ya mencionadas después de la adición de glucosa.

Cuantificar la concentración de ATP en las cepas ya mencionadas después de la depleción de glucosa.

8. MÉTODOS

8.1 Materiales.

Los reactivos utilizados en el desarrollo de este trabajo fueron de calidad analítica. La glucosa, HEPES, EDTA, MES, TEA, MgCl₂, 2-mercptoetanol, SDS, glicerol, albumina sérica bovina, ADH de levadura, etanol y NAD⁺ se adquirieron de Sigma Aldrich (St. Louis MO, EUA). El KOH, acetato de magnesio, NaH₂PO, H₂SO₄, H₃PO₄, ácido tricloroacético, NaOH y K₂HPO₄ fueron obtenidos de JT Baker (Xalostoc, Mex). El extracto de levadura se obtuvo de BD Bioxon (Tepotzotlan, Mex) y la peptona de gelatina de MCD Labs (Tlalnepantla, Mex). El cocktel inhibidor de proteasas se obtuvo de SantaCruz Biotech y la proteína agarosa G fue obtenida de Roche (Basilea, Suiza). La acrilamida/bisacrilamida, TEMED, persulfato de amonio y el marcador de peso molecular se obtuvieron de Bio-Rad (Richmond CA, EUA).

Los anticuerpos monoclonales anti-ALD, anti-GAPDH, anti-PGK fueron de SantaCruz Biotechnology (SantaCruz CA, EUA). El anticuerpo monoclonal anti-actina fue donado por el Dr. JM Hernández (CINVESTAV, México). Los anticuerpos secundarios anti-conejo, anti-cabra y anti-ratón acoplados a la enzima peroxidasa fueron obtenidos de Jackson Immunoresearch Laboratories Inc. (West Grove, PA, EUA).

El kit para la cuantificación de ATP “Bioluminiscence Assay Kit CLS II” se obtuvo de la empresa Roche (California, EUA).

Para la construcción y verificación de las cepas mutantes, se utilizaron oligonucleótidos, agarosa, y sales diversas de Sigma Aldrich (St. Louis MO, EUA), PFU polimerasa y Taq polimerasa de Thermo Sci (Massachusetts , EUA).

8.2 Generación de las cepas mutantes.

Se han desarrollado diversas estrategias para observar “*in vivo*” el citoesqueleto de actina: adición de faloidina marcada, fusión de proteínas fluorescentes a la actina. Sin embargo, estas estrategias afectan el crecimiento celular o modifican la dinámica del citoesqueleto. Otra estrategia es el marcaje indirecto de actina péptidos marcados con GFP que se unen a actina (LifeAct®) (Riedl *et al.*, 2008).

En las levaduras, algunos investigadores han marcado directamente a las proteínas de unión a actina Abp1 y Abp140 con GFP para observar parches y cables de actina. Esta metodología no tiene efecto sobre el crecimiento de las levaduras ni en la organización del citoesqueleto de actina (Huckaba *et al.*, 2004). En este trabajo, se utilizó esta estrategia para marcar la proteína Abp1 con la proteína fluorescente GFP- γ .

La modificación del gen *ABP1* se realizó mediante una reacción de PCR (Longtine *et al.*, 1998). El diseño de los oligonucleótidos, la reacción de PCR y la recombinación homóloga “*in silico*” se realizaron con el software Serial Cloner (Serialbasics, Francia, 2014).

La reacción de PCR se realizó en el termociclador T100, (Bio Rad, CA, EUA) utilizando el plásmido pFA6a-link-yoEGFP-SpHis5 (donado por Wendell Lim & Kurt Thorn (Addgene plasmid 159 # 44836)) (Lee *et al.*, 2013), los oligonucleótidos Abp1 oligoF y Abp1 oligoR (Tabla 1) y la enzima polimerasa Pfu de alta fidelidad (Thermo Sci, Massachussets, EUA). El programa de PCR utilizado se indica en la Tabla 2.

Tabla 1. Oligonucleótidos utilizados en este proyecto.

Oligonucleótidos	Secuencia
ABP1 oligo F	5`- AAGACGGCTCAAAGGTCTTCCCCAGCAATTATGTGTCTTGGC AACATCGGTGACGGTGCTGGTTA-3'
ABP1 oligo R	5`- GTATTTTTTACGTAAGAATAATATAATAGCATGACGCTGACGTGTGAT TTGGATGGCGGCCTAGTATCG-3'
ABP1 oligo C	5'GACTGGGATGATGATGAAGA-3'
ADH Ter2	5'-CGTTTAAACCTAAGAGTCAC-3'

Tabla 2. Programa de PCR utilizado para la construcción de las mutantes:

Fase	Condiciones
Calentamiento 1 ciclo	95°C por 1 min
Amplificación 35 ciclos	92°C por 30 seg, 55°C por 30 seg, 72°C por 5 min
Terminación 1 ciclo	72°C por 10 min 4°C hasta 2 h

La calidad del producto de PCR obtenido y el tamaño se determinó mediante electroforesis en gel de agarosa al 3% teñido con bromuro de etidio (Sha *et al.*, 2016).

Una vez verificada la pureza e integridad del DNA, las cepas *S. cerevisiae* *w303* (*MATa ade2-1 his3-1,15 leu2-3,112 trp1-1 ura3-1*), *S. cerevisiae w303 ρ⁰* (*MATa, ade2-1 his3-1,15 leu2-3,112 trp1-1 ura3-1, rho0*) y *S. cerevisiae pet122Δ* (*MATx, ade2-1 his3-1,15 leu2-3,112 trp1-1 ura3-1, pet122::KANMX*) se transformaron con el método del acetato de litio (Gietz *et al.*, 1995).

Estas cepas se cultivaron en 5 mL de YPD toda la noche a 30°C con una velocidad de agitación de 250 rpm en la incubadora Excella E24 (New Brunswick Scientific, EUA). Posteriormente, se determinó la densidad óptica a 600 nm y se ajustó a una densidad óptica de 0.2 en un volumen de 5 mL de YPD. Las cepas se incuban a 30°C hasta alcanzar una densidad óptica de 0.5. Posteriormente, los cultivos se centrifugaron a 2900 g por 5 minutos y la pastilla de lavó dos veces con agua destilada estéril. La pastilla se transfirió a un microtubo de 2 mL y se centrifugó a 14000 rpm por un minuto y se lavó con 1 mL de buffer TE/LiOAc 3 veces. La pastilla se resuspendió en 50 uL de buffer TE/LiOAc y se mezcló con 8 µL del producto de PCR obtenido en el inciso anterior. También se adicionaron 5 µL de DNA de esperma de salmón (Sigma Aldrich, Missouri, EUA) y 300 µL de buffer PEG/LiOAc/TE, se agitó el tubo vigorosamente y se incubó a 30°C por 30 minutos. Posteriormente, se adicionaron 40 µL de DMSO estéril (Sigma Aldrich, MO, EUA) y la mezcla se incubó a 42°C por 15 minutos. Transcurrido este tiempo, se centrifugó el cultivo y se retiró el sobrenadante. La pastilla se resuspendió cuidadosamente en 1 mL de YPD y se incubó al menos 2 horas a 30°C. Una vez concluido el tiempo de incubación, las células se sembraron en placas con medio selectivo sin histidina (SD-His) por 48 h a 30°C. Las colonias aisladas que crecieron después de este tiempo se resembraron en placas con SD-His por estriado y se incubaron 24 h a 30°C. Las colonias que crecieron en estas placas se seleccionaron para evaluar las características de las mutantes obtenidas. Para determinar si las levaduras tienen el mismo patrón de marcaje de Abp1 reportado en la literatura, se sembraron las células en medio SD por 12 h y se observaron en el microscopio de epifluorescencia Nikon Eclipse E600.

Una vez seleccionadas las colonias transformadas, se verificó la adecuada inserción del gen modificado utilizando una reacción de PCR. El DNA total se extrajo con la columna de purificación Quick-DNA miniprep (Zymo Research, CA, EUA) y se verificó su pureza mediante espectrofotometría en el equipo nanodrop (Thermo Sci, MA, EUA). La reacción de PCR se realizó con los oligonucleótidos Abp1 Oligo C y ADH Ter2 (Tabla 1) y la enzima Taq polimerasa (Thermo Sci, MA, EUA) con el programa de PCR indicado en la tabla 3. El producto de PCR se corrió en un gel de agarosa al 4% y se tiñó con bromuro de etidio. El peso de las bandas se verificó utilizando un marcador de peso molecular de 1 Kb (New England Biolabs, ML, USA).

Tabla 3. Programa de PCR utilizado para la verificación de las mutantes:

Fase	Condiciones
Calentamiento 1 ciclo	95°C por 3 min
Amplificación 35 ciclos	94°C por 45 seg, 52°C por 30 seg, 72°C por 1 min
Terminación 1 ciclo	72°C por 10 min 4°C hasta 2 h

Las cepas con el producto de PCR del tamaño esperado y la distribución de la proteína Abp1-GFP reportada en la literatura (pequeños parches móviles) fueron seleccionadas para este proyecto y se enumeran en la tabla 4.

Tabla 4. Cepas haploides construidas en este trabajo.

Cepa	Proteína modificada	Marcador fluorescente	Marcador selectivo
<i>W303 ABP1-GFP Y</i>	Proteína de unión a actina 1	GFP-Y	His ⁺
<i>W303 rho⁰ ABP1-GFP Y</i>	Proteína de unión a actina 1	GFP-Y	His ⁺
<i>W303 pet122Δ ABP1-GFP Y</i>	Proteína de unión a actina 1	GFP-Y	His ⁺

8.3 Efecto de la incubación en ausencia de glucosa.

Con el objetivo de evaluar si el metabolismo energético tiene efecto sobre la distribución de las enzimas glucolíticas o el citoesqueleto, se utilizaron las cepas *S. cerevisiae* w303 (cepa WT, con metabolismo fermentativo y respiratorio), *S. cerevisiae* w303 p⁰ (cepa con metabolismo respiratorio, carente de DNA mitocondrial) (Friis & Schultz, 2016) y *S. cerevisiae* pet122Δ (cepa con metabolismo respiratorio, incapaz de formar un complejo 4 mitocondrial funcional) (Costanzo & Fox, 1988) como modelo de estudio. Para la preservación, almacén y ensayos de fermentación se cultivaron en YPD, mientras que para su observación en el microscopio se utilizó medio SD. Para evaluar que las modificaciones realizadas a la proteína Abp1 no tienen efecto sobre el crecimiento de las cepas, se realizó una curva de crecimiento en el crecimetro Bioscreen C (Labsystems, HE, Finlandia). Para evaluar la adaptación catabólica, las cepas fueron sembradas en SD-glu a 30°C por 12 h. Posteriormente las células se lavaron 3 veces con agua estéril (tiempo aproximado: 30 min) y fueron inoculadas en SD (sin glucosa) ó SD-glu por 4 h a 30°C con agitación constante. Una vez concluido este tiempo, se evaluó la distribución de actina mediante microscopía de fluorescencia; la colocalización de las enzimas glucolíticas GAPDH, PGK y ALD con la actina mediante inmunoprecipitación; la producción de ATP con un método quimioluminiscente y la velocidad de fermentación mediante un método enzimático.

8.4 Distribución de actina.

Para evaluar la colocalización de Abp1-GFP y la actina, las cepas obtenidas se tiñeron con faloidina rodaminada (Higuchi-Sanabria *et al.*, 2016). Después de que las células se incubaron en las condiciones descritas en la sección 8.3, se fijaron con formaldehído al 3.7% por 20 minutos. Después, las células se lavaron 3 veces con PBS y se tiñeron con 1.65 µM de faloidina rodaminada por 30 minutos y se lavaron 3 veces con PBS. Finalmente, las muestras fueron montadas en portaobjetos de vidrio y se observaron en el microscopio de epifluorescencia Nikon Eclipse E600 equipado con una cámara DXM 1200 de alta resolución con el filtro FITC (480/30).

Para evaluar la dinámica de los parches de actina, las levaduras fueron incubadas bajo las condiciones descritas en el apartado 7.3. Posteriormente, las células se montaron en parches de agarosa acorde a lo reportado por Pemberton (Pemberton, 2014). Después se realizaron videos de 60 segundos en un microscopio confocal Leica TCS-SP5 con un objetivo 63X. El análisis de imágenes fue realizado con el software ImageJ.

8.5 Obtención del extracto citoplásmico.

Las cepas en estudio fueron incubadas en las condiciones descritas en el apartado 8.3. Posteriormente, se lavaron con agua una vez a 676 g por 5 minutos. Se calculó el peso húmedo de las células y se resuspendieron en el amortiguador de lisis (HEPES 100 mM, acetato de potasio 600 mM, acetato de magnesio 10 mM, EDTA 1 mM, glicerol al 20%, 2-mercaptoetanol 8 mM e inhibidores de proteasas “Ultracruz” (SantaCruz Biotech, California, EUA).

Las células fueron lisadas en el Bead Beater (Biospec products, Oakland, EUA) con perlas de vidrio de 0.5 mm de diámetro (pulsos de 30 segundos de agitación por 1 minutos de reposo) en hielo. Finalmente, los extractos fueron centrifugados a 24500 g por 1h a 4°C y el sobrenadante se almacenó a -60°C. La concentración de proteínas en el extracto fue cuantificada por el método de Bradford (Bradford, 1976).

8.6 Inmunoprecipitaciones.

La asociación de la actina con las enzimas ALD, GAPDH y PGK se evaluó mediante ensayos de inmunoprecipitación (Araiza-Olivera *et al.*, 2013). Se incubaron 3 µg/mL del anticuerpo α -actina con 7 µL de proteína G agarosa durante 30 minutos a 4°C, posteriormente se mezclaron con 1 mg/mL de extracto citoplásmico y la mezcla se incubó a 4°C toda la noche en un agitador vortex. El inmunoprecipitado se colectó por centrifugación a 2000 g por 10 minutos y se lavó 3 veces con el amortiguador IP (50 mM Tris-HCl, pH 7.4, PMSF 0.1 mM, 0.1 % Tween 20 e inhibidor de proteasas “Ultracruz” (SantaCruz Biotech, California, EUA). Las muestras se resuspendieron en buffer de muestra (500 mM Tris, pH 6.8, glicerol al 10%, SDS al 10%, β -mercaptoetanol al 0.05% y azul de bromofenol al 0.01%) y hervidas durante 5 minutos. La electroforesis SDS/PAGE se realizó en un gel de poliacrilamida al 10% a 90 V en el cuarto frio (4°C). Las proteínas fueron transferidas a una membrana de PVDF en una cámara de transferencia húmeda a 4°C utilizando el amortiguador de electrotransferencia (25 mM de fosfato de potasio, 12 mM Tris, 192 mM de glicina y metanol al 20%). Las membranas se bloquearon con albumina al 0.5% en TBS-T (Tris 50 mM pH 7.6, NaCl 104 mM y 0.1 % de Tween 20) por 1h y se incubaron con el anticuerpo primario toda la noche a 4°C.

Posteriormente se lavaron con TBS-T y se incubaron 1h con el anticuerpo secundario a temperatura ambiente. Una vez lavadas, las membranas fueron reveladas con el reactivo Immobilon Western Chemiluminiscent HRP substrate (Millipore, Missouri, EUA) empleando películas radiográficas para registrar los resultados (Kodak, NY, EUA).

8.7 Producción de ATP.

La concentración intracelular de ATP se cuantificó utilizando el kit Bioluminiscence Assay Kit CLS II (Sigma, Missouri, EUA) siguiendo este protocolo: las cepas se cultivaron bajo las condiciones mencionadas en el inciso anterior. Después del tiempo indicado, 1×10^7 células se resuspendieron en 100 mM Tris-HCl pH 7.8 y 4 mM de EDTA. Después, las células fueron hervidas por 2 minutos acorde a lo indicado por el fabricante del kit. Posteriormente los residuos celulares fueron separados mediante centrifugación y el ATP se cuantificó del sobrenadante en el luminómetro POLARstar Omega (BMG Labtech, Alemania) (Mendoza-Hoffmann et al., 2018).

8.8 Cinética de fermentación.

Para evaluar el catabolismo de las fuentes de carbono utilizadas, las levaduras fueron inoculadas en 5 mL de YP o YPD y se incubaron 4h a 30°C. Las células se lavaron y la pastilla se resuspendió en YPD (control) o en YP (sin glucosa). Para evaluar la velocidad de fermentación, 1×10^7 células se incubaron en 20 mM de glucosa por 0.5, 1, 2, 4 y 6 minutos. La reacción se detuvo mediante la adición de ácido tricloroacético al 30%. Posteriormente las muestras se centrifugaron a 2900 g por 5 minutos a 4°C.

El sobrenadante se neutralizó con NaOH y el etanol se cuantificó utilizando un método enzimático acoplado a la reducción de NAD⁺ mediado por la enzima alcohol deshidrogenasa (ADH) (Araiza-Olivera *et al.*, 2010). 1 mg/mL del sobrenadante en amortiguador de cuantificación de EtOH (300 mM Na₄P₂O₇, 75 mM de hidrocloruro de semicarbazida, 22 mM de glicina, 66 mM de NaOH pH 8.8 y 1.8 mM de NAD⁺) se incubó con 100 µg/mL de ADH por 1 h a 24°C. La absorbancia final se midió a 340 nm en el espectrofotómetro Aminco-Olis DW2000 (Olis Inc., Bogart, GA, USA). Se utilizó una curva estándar de etanol y los resultados se reportaron como nanomoles de etanol (EtOH) producidos por cada mg de células por minuto.

9 RESULTADOS

9.1 Construcción de las cepas mutantes.

Para obtener cepas de levaduras con la proteína Abp1 unida a la proteína GFP- γ se construyó un fragmento de DNA que contiene el extremo final del gen *ABP1*, una región bisagra, el gen GFP y el gen *HIS3*, cuya enzima permite a las levaduras auxótrofas crecer en un medio sin histidina. La figura 1 muestra el gel obtenido después de esta reacción de PCR y la electroforesis. El producto obtenido tiene el tamaño esperado (2 Kb).

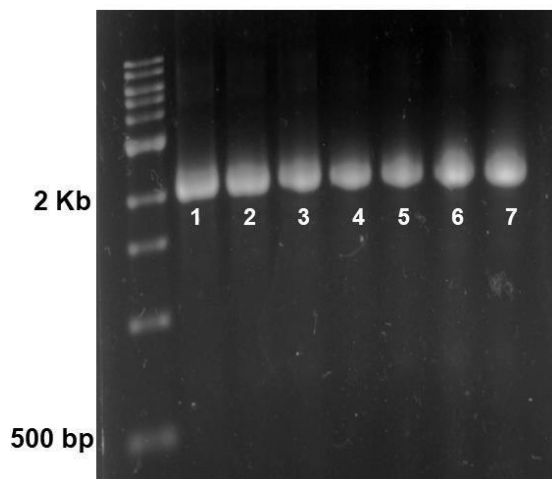


Fig 1. Construcción del fragmento Abp1-GFP. Se realizó una reacción de PCR utilizando el plásmido pFA6a-link-yoEGFP-SpHis5 y los oligonucleótidos Abp1-F y Abp1-R. El producto obtenido se corrió en un gel de agarosa al 1% y se tiñó con bromuro de etidio. Los fragmentos de DNA indicados en números blancos corresponden a experimentos de construcción independientes.

Con el producto de PCR obtenido se transformaron las cepas w303 ρ^0 y w303 pet122 Δ y se sembraron en un medio sin histidina (SD-His). Las colonias obtenidas fueron seleccionadas para evaluar el patrón de distribución de Abp1 y la señal fluorescente de la proteína GFP. Las colonias con parches de actina brillantes y dinámicos se seleccionaron y se comprobó mediante una reacción de PCR que la inserción del gen tuviera el tamaño y localización esperada. La figura 2 muestra que la construcción insertada en las levaduras tuvo el tamaño esperado (500 bp).

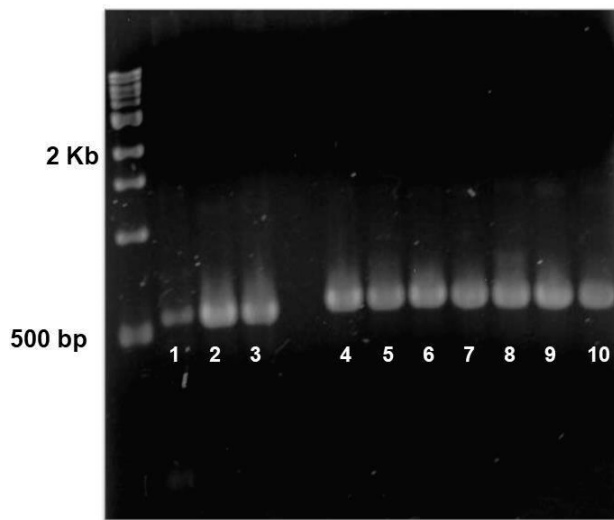


Fig 2. PCR de comprobación. Se realizó una reacción de PCR utilizando el DNA obtenido de las cepas mutantes seleccionadas y los oligonucleótidos Abp1-C y Adh Ter2. El producto obtenido se corrió en un gel agarosa al 1% y se tiñó con bromuro de etidio. 1,2 y 3 corresponden a la cepa WT, 4,5 y 6 a la cepa ρ^0 y 7,8 y 9 a la cepa pet122 Δ .

Para verificar que las modificaciones genéticas no afectaran el crecimiento de las cepas, se realizó una curva de crecimiento para todas las cepas en estudio. La figura 3 nos muestra que la modificación de la proteína Abp1 no afectó la velocidad de crecimiento en todas las cepas ($w303=5.47\pm0.54 \times 10^{-3}$ cel/min, $w303 abp1-GFP=5.25 \pm 0.62 \times 10^{-3}$ cel/min, $w303 \rho^0=11.49 \pm 0.7 \times 10^{-3}$ cel/min, $w303 abp1-GFP=11.7\pm0.8 \times 10^{-3}$ cel/min, $w303 pet122\Delta=8.79\pm1.2 \times 10^{-3}$ cel/min, $w303 pet122\Delta abp1-GFP=8.79\pm0.6 \times 10^{-3}$ cel/min). Estos resultados nos muestran también que la cepa ρ^0 creció más rápido, mientras que la cepa WT es la de crecimiento más lento.

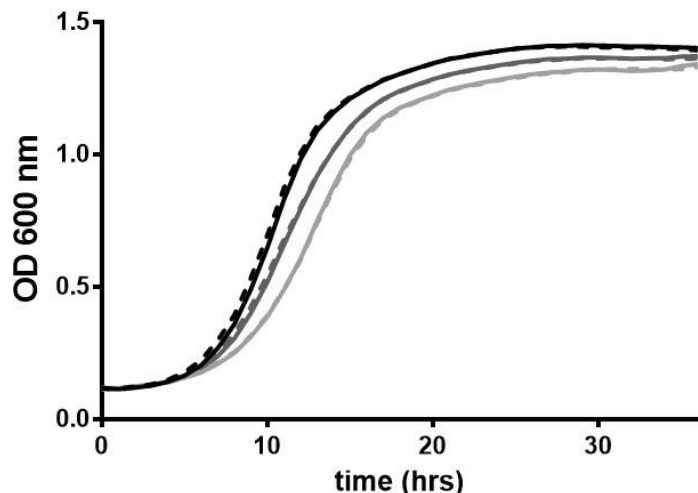


Fig 3. Curva de crecimiento. Se determinó que la modificación a la proteína Abp1 no alteró el patrón de crecimiento en SD-gluc mediante una curva de crecimiento. En línea discontinua se muestra el crecimiento de la cepa con la proteína Abp1 unida a GFP y en línea continua el crecimiento de la cepa sin modificación. En color negro se indica el crecimiento de la cepa *w303*, en gris medio la cepa *w303 pet122Δ* y en gris claro la cepa ρ^0 . Los resultados mostrados son un promedio de 3 determinaciones independientes.

9.2 La asociación de las enzimas glucolíticas con la actina F disminuyó después de la depleción de glucosa en el medio.

Para verificar las modificaciones en la asociación de las enzimas y la actina debidas a la incubación en ausencia de glucosa, se realizó un ensayo de coimmunoprecipitación de las enzimas ALD, PGK y GAPDH con actina en condiciones de ayuno (S) o en presencia de glucosa (G) en las cepas *w303*, *w303 ρ^o* y *w303 pet122Δ*. En las cepas incubadas en presencia de glucosa, se observó una interacción fuerte entre la actina y las enzimas ya mencionadas (figura 4). Estos resultados concuerdan con los reportados anteriormente en nuestro laboratorio (Araiza-Olivera *et al.*, 2013). En contraste, la interacción entre las enzimas glucolíticas y la actina disminuyó cuando las cepas son incubadas en ausencia de glucosa (figura 4). Es interesante observar que, en estas condiciones, la pérdida de interacción de GADPH con actina fue completa. Así, la interacción entre las enzimas ya mencionadas y la actina se modificó por la disponibilidad de glucosa en el medio.

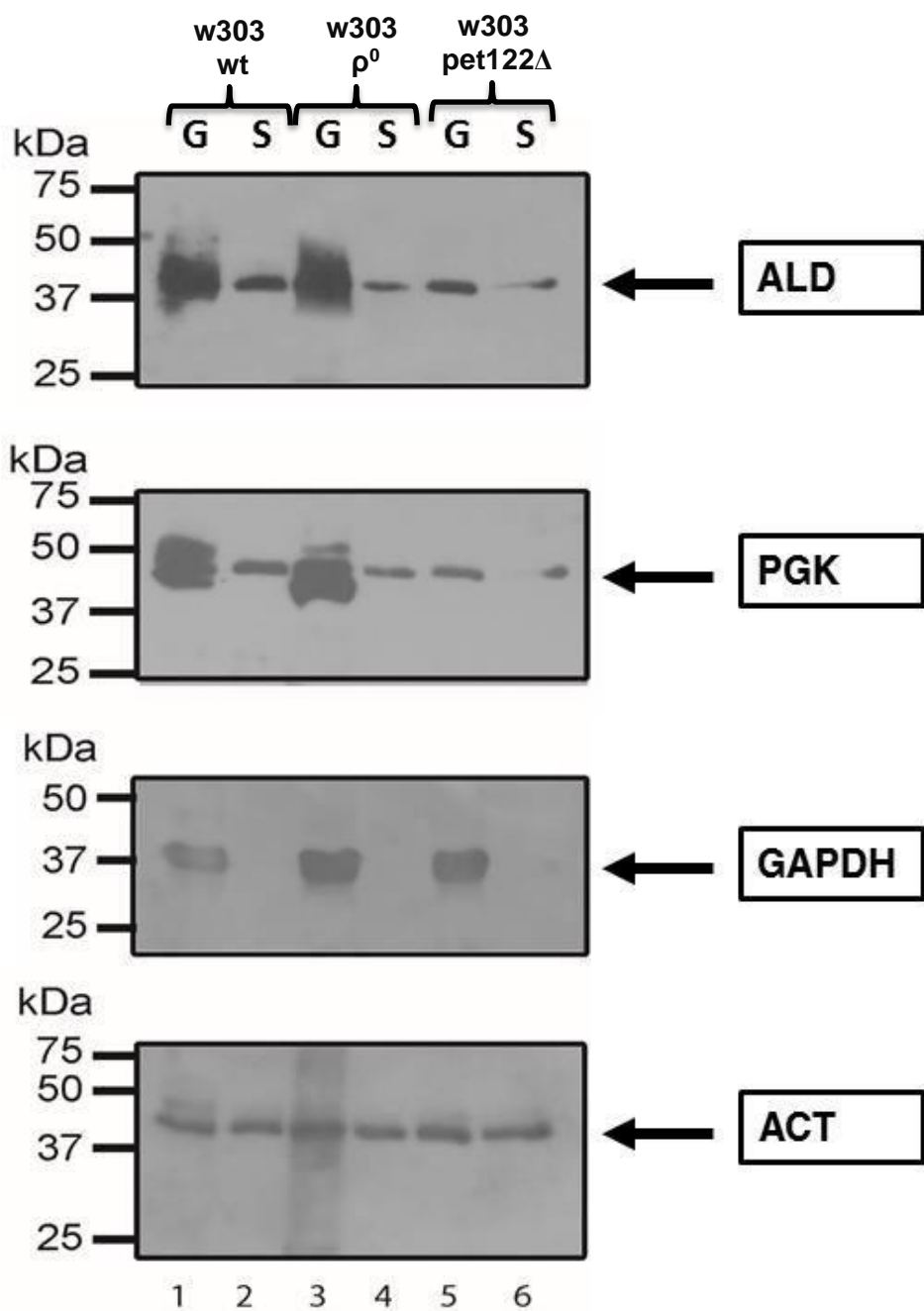


Fig 4. Asociación de enzimas glucolíticas con actina. A partir de extractos citoplásmicos se inmunoprecipitó actina y se identificó por western blot la presencia de ALD, PGK y GAPDH. Línea 1: W303 WT Abp1-GFP en SD-Gluc, Línea 2: W303 WT Abp1-GFP en SD, Línea 3: W303 ρ^0 Abp1-GFP en SD-Gluc, línea 4: W303 ρ^0 Abp1-GFP en SD, línea 5: W303 $\text{pet}122\Delta$ Abp1-GFP en SD-Gluc, línea 6: W303 $\text{pet}122\Delta$ Abp1-GFP en SD. El resultado mostrado es representativo de tres experimentos independientes.

Se ha demostrado que la desestabilización farmacológica de los filamentos de actina disminuye la interacción entre las enzimas glucolíticas (Araiza-Olivera *et al.*, 2013). Para evaluar si la ausencia de glucosa disminuye la esta interacción, se determinó la asociación de las enzimas con la actina en presencia y ausencia de glucosa.

9.3La interacción entre las enzimas glucolíticas disminuye después de la depleción de glucosa en el medio.

Para determinar si la glucosa tiene efecto en la interacción entre las enzimas glucolíticas, se realizaron ensayos de inmunoprecipitación. A partir de las muestras de las cepas w303 WT, w303 ρ^0 y w303 $pet122\Delta$, se inmunoprecipitó a la enzima aldolasa y se identificó por western blot a las enzimas PGK y ALD (figura 5). En todos los casos, la interacción de la enzima PGK disminuyó durante la ausencia de glucosa, aunque en la cepa $pet122\Delta$ la afinidad de PGK por aldolasa es menor en ambas condiciones. Respecto a la interacción de ALD con GAPDH, se observó una disminución ligera en la interacción entre ambas enzimas en ausencia de glucosa. El efecto del ayuno en la asociación GAPDH-ALD fue menor que el reportado después de la desestabilización de la actina F con latrunculina A o citocalasina (Araiza-Olivera *et al.* 2013). Así, la organización de las enzimas glucolíticas y la actina F, que probablemente conforman al metabolón glucolítico, se modificó ligeramente durante la depleción de glucosa.

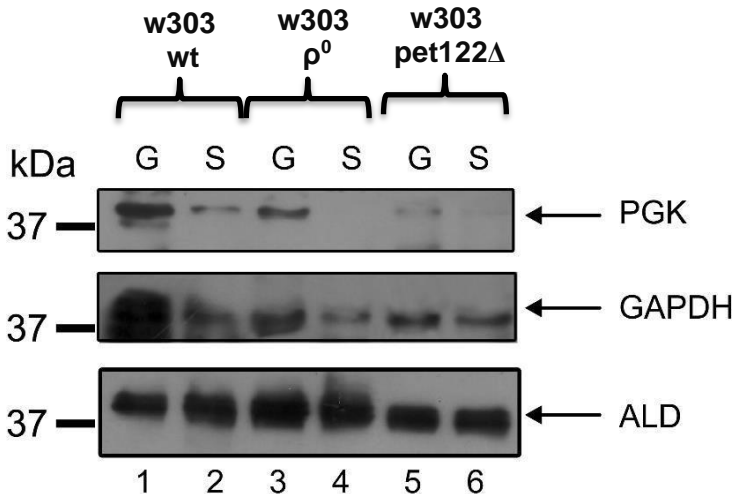


Fig. 5 Asociación de enzimas glucolíticas en ausencia de glucosa. La enzima ALD fue inmunoprecipitada a partir de los extractos citoplásmicos y las enzimas PGK y GAPDH fueron identificadas por western blot. Línea 1: w303 WT Abp1-GFP en SD-Gluc, línea 2: w303 WT Abp1-GFP en SD, línea 3: w303 ρ^0 Abp1-GFP en SD-Gluc, línea 4: w303 ρ^0 Abp1-GFP en SD, línea 5: w303 $pet122\Delta$ Abp1-GFP en SD-Gluc, línea 6: w303 $pet122\Delta$ Abp1-GFP en SD. El resultado mostrado es representativo de tres experimentos independientes.

Para evaluar si la alteración en la formación de complejos entre las enzimas y la actina modifica la actividad glucolítica en las células incubadas en ausencia de glucosa, se cuantificó la concentración de ATP.

9.4 El ayuno disminuyó la concentración de ATP en las levaduras, siendo este efecto mayor en las cepas fermentativas.

La concentración de ATP se determinó después de la depleción de glucosa en la cepa silvestre (figura 6, barra negra), en la cepa ρ^0 (fig 6, barra blanca) y en la cepa $pet122\Delta$ (figura 6, barra gris). Después de incubar las cepas por 4 h en presencia de glucosa, la concentración de ATP fue de 45.2 ± 4.4 nmol/mg de proteína en la cepa WT, y ligeramente superior en las cepas respiratorias (50.5 ± 2.5 nmol/mg de proteína para la cepa ρ^0 y 55.6 ± 2.4 nmol/mg de proteína en la cepa $pet122\Delta$) (figura 6A).

Después de un periodo de ayuno de 30 minutos (tiempo de lavado), se observó una ligera disminución en la concentración de ATP en la cepa silvestre (30.0 ± 2.0 nmol/mg de proteína), mientras que en las cepas fermentativas la disminución fue aproximadamente de un 50% (16.4 ± 1.2 nmol/mg de proteína en la cepa ρ^0 y 18.8 ± 1.6 nmol/mg de proteína para la cepa $\text{pet}122\Delta$). (figura 6B). Después de 4h en ausencia de glucosa, las diferencias anteriores fueron más evidentes. La cepa silvestre presentó niveles elevados de ATP (41.3 ± 0.8 nmol/mg de proteína), mientras que, en las cepas fermentativas, la concentración de ATP fue mucho menor (12.3 ± 0.8 nmol/mg de proteína en la cepa ρ^0 y 14.5 ± 1.0 nmol/mg de proteína para la cepa $\text{pet}122\Delta$) (figura 6C). Estos resultados sugieren que en las cepas fermentativas la concentración de ATP disminuye más en comparación a la cepa WT durante la incubación sin glucosa. A las 4h sin fuente de glucosa, la concentración de ATP disminuyó más del 60% en las cepas fermentativas, mientras que, en la cepa silvestre, esta diminución fue solo del 16%.

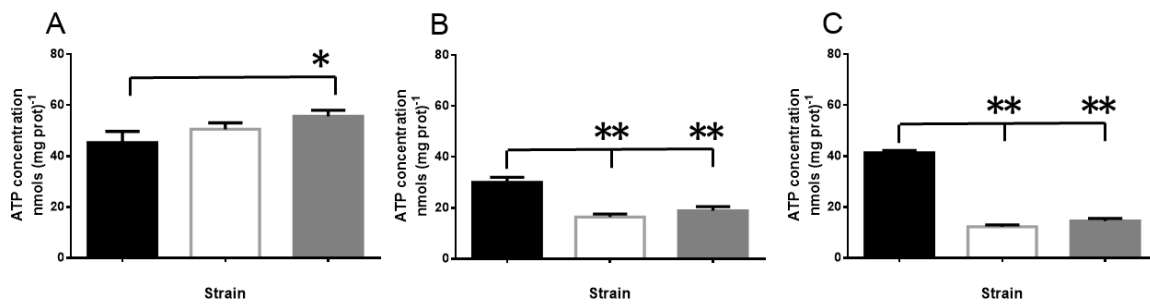


Fig. 6 Concentración de ATP en las cepas incubadas en ausencia de glucosa. La concentración de ATP en las cepas w303 Abp1-GFP (barras negras), w303 ρ^0 Abp1-GFP (barras blancas) y w303 $\text{pet}122\Delta$ Abp1-GFP (barras grises) se cuantificó utilizando un método bioluminiscente. Los valores se representan como la media \pm SD y las condiciones experimentales fueron: (A) en SD-Gluc por 4h, (B) en SD por 30 min ó (C) en SD por 4h. Los datos representan el promedio de 3 experimentos independientes. Las diferencias estadísticas fueron determinadas utilizando la prueba de ANOVA y la comparación múltiple de Tukey (* P<0.05, **P<0.01).

La disminución en la concentración de ATP podría deberse sólo a la carencia de sustrato, o podría evidenciar la desorganización del metabolón glucolítico, que a su vez podría reflejarse en una disminución en la velocidad de fermentación. Para evaluar esto se cuantificó la producción de etanol en las cepas después de la adición de glucosa

9.5 A bajas concentraciones de ATP, la adición de glucosa incrementó la actividad fermentativa.

La ausencia de glucosa disminuyó la asociación de las enzimas ALD, GAPDH y PGK con la actina F (figura 4); asimismo, se observó una disminución en la interacción entre las enzimas (figura 5) y una baja concentración del ATP intracelular en las cepas fermentativas (figura 6), sugiriendo que el metabolón glucolítico se desensambló y la glucólisis se inactivó. Para evaluar esto, se determinó la velocidad de fermentación inducida por la adición de glucosa en las cepas previamente incubadas en un medio con glucosa o en un medio sin glucosa. En las cepas incubadas en ausencia de glucosa, la velocidad de fermentación fue al menos cinco veces mayor que en las cepas preincubadas en un medio con glucosa (Tabla 5 y figura 7), sugiriendo que a bajas concentraciones de ATP se activa la glucólisis. Además, mientras que la cepa silvestre (figura 7A) y la cepa w303 ρ^0 (figura 7B) exhibieron una actividad fermentativa constante desde el inicio, la velocidad de fermentación en la cepa *pet122Δ* fue más lenta los primeros dos minutos e incrementó a tiempos posteriores (figura 7C).

Tabla 5. Velocidad de fermentación en las cepas incubadas en ausencia o presencia de glucosa.

Cepa	Velocidad de fermentación (nmol etanol/mg proteína*min)	
	Preincubación en SD-glu	Preincubación en SD
w303	9.7	1.6
w303 ρ^0	15.2	1.7
w303 pet122 Δ	10.8	1.6

La cepa WT, donde la concentración de ATP fue más alta después del ayuno fue la cepa menos activa. La cepa *pet122 Δ* tuvo una velocidad inicial de fermentación de 3 nmol de etanol/min/mg de proteína, que incrementó a 12 nmol EtOH/min/mg de proteína después de dos minutos. En contraste, las cepas incubadas con glucosa exhibieron una velocidad de fermentación muy lenta en todos los casos (figura 7, puntos negros). En los primeros cuatro minutos de fermentación se observó una ligera elevación de la fermentación que disminuyó a tiempos posteriores (Insertos en figura 7). Además, la velocidad de fermentación de las cepas con glucosa fue menor que en las cepas ayunadas. En la cepa silvestre incubada con glucosa, la velocidad de fermentación fue de 3 nmol EtOH/min/mg de proteína y disminuyó a 1.2 nmol EtOH/min/mg de proteína después de 2 minutos (Inserto en Fig 7A). La cepa w303 ρ^0 tuvo una velocidad de fermentación inicial de 3.6 nmol EtOH/min/mg de proteína, la cual disminuyó a 1.5 nmol EtOH/min/mg de proteína (inserto de fig. 7B). La cepa w303 *pet122 Δ* tuvo una velocidad de fermentación inicial de 5 nmol EtOH/min/mg de proteína que disminuyó a 2 nmol EtOH/min/mg de proteína después de 2 minutos (inserto fig 7C).

En las cepas ayunadas, la fermentación fue más activa, probablemente con el objetivo de reestablecer las concentraciones de ATP celulares. En contraste, las cepas incubadas en glucosa fueron activas desde el inicio del experimento, aunque no alcanzaron altos niveles probablemente como resultado de la presencia de concentraciones altas de ATP. Solo en la cepa *pet122Δ* se observó una fase lag de uno a dos minutos antes de que se alcanzara la actividad fermentativa completa

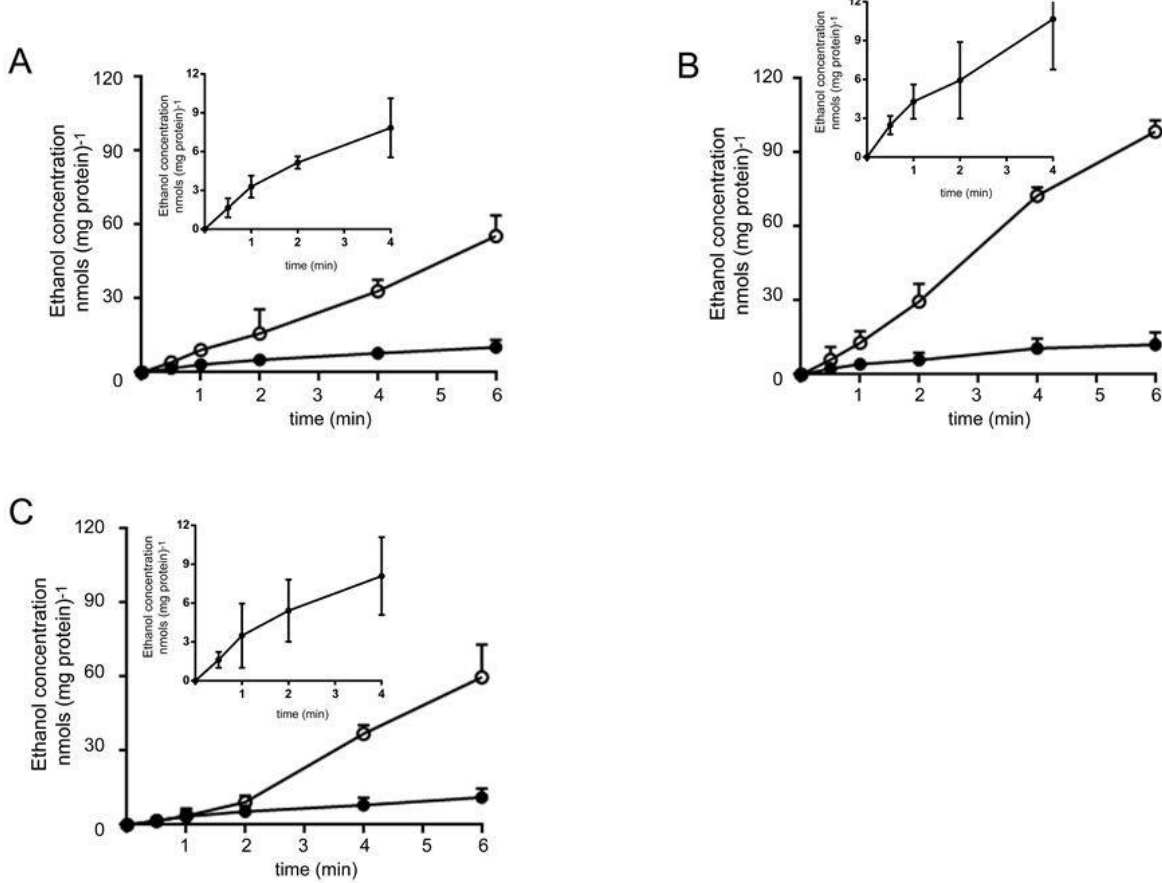


Fig. 7 Producción de etanol en respuesta a la adición de glucosa. La cinética de fermentación fue medida en la cepa w303 Abp1-GFP (A), w303 p⁰ Abp1-GFP (B) o w303 pet122Δ Abp1-GFP (C). El etanol producido fue cuantificado utilizando un ensayo enzimático acoplado. En círculos blancos se muestra la producción de etanol en las cepas incubadas en ausencia de glucosa por 4h. En círculos negros se muestra la producción de etanol en las cepas incubadas con glucosa por 4h. Los resultados son reportados como nmols EtOH/mg proteínas. Los insertos en las gráficas muestran la producción de etanol durante los primeros cuatro minutos en las cepas incubadas previamente con glucosa. Los datos representan el promedio de 3 experimentos independientes.

9.6 La distribución de la proteína de unión a actina 1 (Abp1) se modificó durante la depleción de glucosa, lo que sugiere alteraciones en la organización del citoesqueleto.

Se ha reportado que el metabolón glucolítico se forma sobre el citoesqueleto de actina (Araiza-Olivera *et al.*, 2013). Para determinar el efecto de la depleción de glucosa en la distribución de la actina, se marcó a la proteína de unión a actina 1 (Abp1) con la proteína verde fluorescente (GFP- γ).

Para determinar la distribución de Abp1 y actina en las células incubadas en ausencia de glucosa, se realizó un ensayo de co-marcaje en células fijadas con formaldehído al 3.7 % utilizando faloidina rodaminada para marcar los filamentos de actina. (Fig. 8). En las cepas incubadas con glucosa y en la cepa silvestre incubada en ausencia de glucosa, se observaron pequeños parches formados por filamentos de actina (marca roja) y por la proteína Abp1 (marca verde). En las cepas fermentativas ayunadas, se observaron cuerpos de actina grandes, tanto en la cepa w303 ρ^0 (Fig 8D) como en la cepa w303 *pet122Δ* (Fig 8F). Así, la incubación sin glucosa induce una reorganización del citoesqueleto de actina que correlaciona con una disminución en las concentraciones intracelulares de ATP. Después de la adición de glucosa, los niveles de ATP se restablecen y las modificaciones antes descritas en el citoesqueleto se revierten. Las estructuras de actina que se forman después de la incubación sin glucosa son similares a los cuerpos de actina inmóviles descritos en la literatura (Sagot *et al.*, 2006).

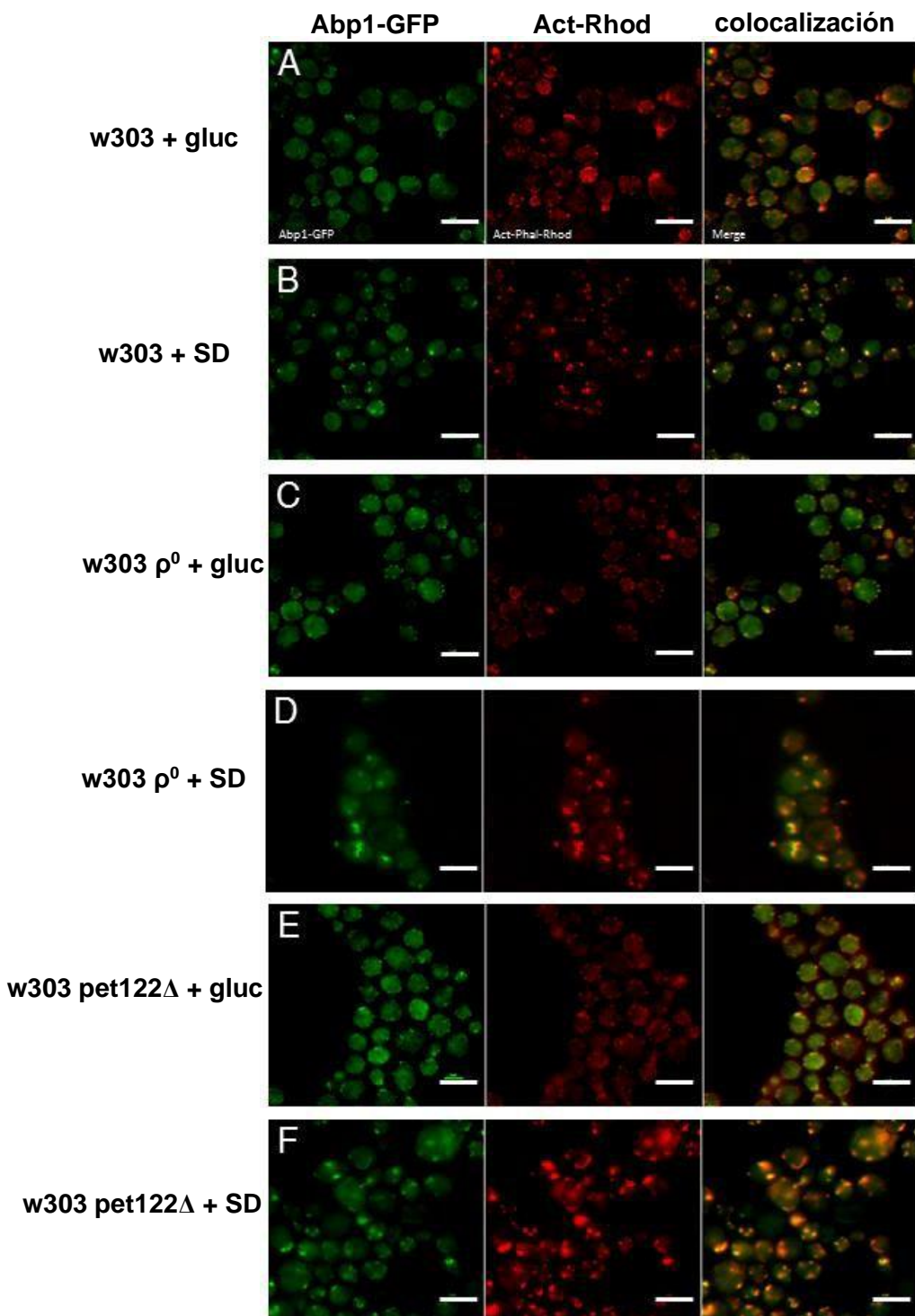


Fig. 8 Organización del citoesqueleto de actina en ausencia de glucosa. Posterior a la incubación con o sin glucosa, las células de fijaron con formaldehído y tiñeron con faloidina rodaminada por 30 minutos. Las imágenes fueron obtenidas en un microscopio de epifluorescencia. Las cepas utilizadas fueron w303 Abp1-GFP con glucosa (A) o en SD (B), w303 p⁰ Abp1-GFP con glucosa (C) o con SD (D) y w303 pet122Δ Abp1-GFP con glucosa (E) o SD (F). Barra= 10 μm.

Acorde a lo descrito en la literatura, los cuerpos de actina son estructuras estáticas de forma indefinida (Sagot *et al.*, 2006). Así, para determinar si los cuerpos de actina descritos en este trabajo presentan movilidad, se evaluó la dinámica del citoesqueleto en las condiciones experimentales previamente descritas.

9.7 En las cepas fermentativas obligadas incubadas en ausencia de glucosa, los parches de actina dinámicos son reemplazados por cuerpos de actina inmóviles.

Cuando las levaduras alcanzan la fase estacionaria de crecimiento, los cables y los parches de actina se reorganizan formando cuerpos de actina inmóviles (Sagot *et al.*, 2006). Así, se evaluaron las modificaciones en la dinámica del citoesqueleto de actina en las cepas estudiadas, utilizando microscopía de lapso de tiempo (time lapse microscopy) de la proteína de unión a actina Abp1 unida a GFP. En todas las cepas incubadas en medio con glucosa y en la cepa w303 WT incubada solo en medio SD, se observaron pequeños parches de actina móviles (Video 1, 2, 4 y 6). La cepa WT exhibió parches de actina con alta movilidad independientemente de si fue incubada en medio con glucosa (Vid 1) o en medio SD (Vid 2). En contraste, la cepa w303 p⁰ incubada en medio con glucosa mostró parches de actina con elevada movilidad (Vid 3), en cambio, al ser incubada sin glucosa los parches de actina desaparecieron y se formaron cuerpos de actina inmóviles (Vid 4). La cepa w303 *pet122Δ*, al igual que la cepa anterior, mostró parches de actina dinámicos cuando fue incubada en medio con glucosa (Vid 5) y cuerpos de actina inmóviles cuando fue incubada en medio SD (Vid 6).

En este trabajo se evaluó el papel de la glucosa en la formación de un metabolón entre las enzimas glucolíticas y el citoesqueleto de actina en levaduras. Después de 4 horas en ausencia de glucosa, el citoesqueleto de actina se reorganizó disminuyó su asociación con las enzimas glucolíticas. Aparentemente, la concentración de ATP fue el factor que reguló la organización del citoesqueleto y la capacidad fermentativa. En las cepas fermentativas obligadas, w303 ρ^0 y w303 *pet122Δ*, la ausencia de glucosa indujo la reorganización del citoesqueleto y el almacenamiento de actina en cuerpos inmóviles. Estos efectos fueron reversibles por la adición de glucosa. En la cepa w303, la producción de ATP mitocondrial durante el ayuno fue suficiente para mantener la dinámica del citoesqueleto. Para comprobar lo anterior, se observó la dinámica del citoesqueleto después del desacoplamiento farmacológico de la cadena respiratoria mitocondrial.

9.8 En la cepa silvestre en ayunas, la adición de CCCP indujo la formación de cuerpos de actina inmóviles.

La dinámica del citoesqueleto depende de la concentración intracelular de ATP. En ausencia de glucosa, hay una disminución del 80% en la concentración de ATP después de dos minutos. Bajo estas condiciones la dinámica del citoesqueleto cambia drásticamente. Probablemente, durante la depleción de glucosa, el restablecimiento de los niveles de ATP por la mitocondria es esencial para regular la dinámica de la actina. Para evaluar el papel de la función mitocondrial en la dinámica de los parches, se observó la distribución de la actina en la cepa silvestre ayunada e incubada con CCCP, un desacoplante de la cadena respiratoria mitocondrial. Después de 4h de incubación en medio SD + CCCP 20 μM se observó

que los parches de actina desaparecieron, formando cuerpos de actina inmóviles (Fig 9B). Cuando a estas células se les adicionó glucosa, la actina se redistribuyó en la célula y se observaron algunos parches con movilidad reducida (Fig 9C). Este resultado sugiere que la

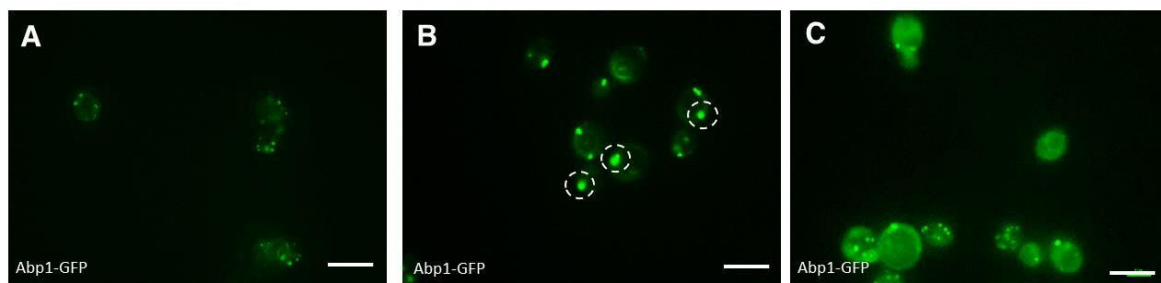


Fig. 9 Organización del citoesqueleto de actina en la cepa w303 Abp1-GFP incubada sin glucosa y con CCCP. *S. cerevisiae* w303 incubada en SD (A) SD + CCCP 20 μ M (B) y SD-gluc + CCCP 20 μ M (C) a 30°C durante 4h. Barra= 10 μ m.

10 DISCUSIÓN

El citoplasma contiene una elevada concentración de biomoléculas que forman sistemas moleculares organizados (Trevors, 2011). El movimiento de las macromoléculas en el citoplasma depende del estado metabólico celular; la depleción de energía inducida por ayuno o la incubación con 2,4 dinitrofenol (un desacoplante mitocondrial) disminuye la movilidad de proteínas y material genético por mecanismos aún no dilucidados (Parry *et al.*, 2014). En este ambiente con una concentración elevada de biomoléculas, uno de los mecanismos que permiten la organización eficiente del metabolismo es la formación de complejos multienzimáticos o “metabolones”. La formación de estas estructuras ha sido descrita en procariontes y eucariontes e intervienen en diversos mecanismos celulares; síntesis de DNA, proteínas, glucógeno, purinas, pirimidinas, aminoácidos, catabolismo de la glucosa, ciclo de Krebs y ciclo de la urea, entre otros (Srere, 1987).

La construcción de estos complejos y las interacciones establecidas entre las enzimas dependen de las características de la vía metabólica; si la vía no presenta ramificaciones las interacciones enzimáticas serán estáticas, ejemplo de estas vías son la síntesis y ruptura de ácidos nucleicos. La formación de complejos enzimáticos transitorios ocurre en vías anfibólicas con varias bifurcaciones, como en la glucólisis y el ciclo de Krebs (Ovádi, 1999).

El ensamblaje de los metabolones usualmente requiere de algún componente estructural de la célula. En eucariontes relativamente sencillos como los tripanosomas, las enzimas de la vía glucolítica se organizan en los glucosomas (Michels *et al.*, 2006).

Otros componentes estructurales de la célula como el citoesqueleto, la membrana plasmática y la membrana del retículo endoplásmico funcionan como andamios para la organización del metabolón (Trevors, 2011; Fujino *et al*, 2018). En la mitocondria, las enzimas del ciclo de Krebs se organizan en regiones cercanas a la membrana interna mitocondrial (Srere, 1985). Por otro lado, los complejos enzimáticos solubles en el citoplasma tienen variación en cuanto a su estequiometría y tiempo de estabilidad (Case *et al.*, 2019). Se ha descrito que hasta 180 enzimas que participan en el metabolismo intermediario pueden exhibir un comportamiento no difusible en el citoplasma (O'Connell *et al.*, 2012).

Así, es posible que estas enzimas puedan formar un complejo multienzimático o “interactoma” donde las enzimas de una vía determinada y los receptores de sustrato en la membrana podrían promover su canalización al citoplasma, desde su captación en la célula hasta la generación del último producto de dicha vía (Moraes & Reithmeier, 2012). Esto se ha descrito en el caso de los eritrocitos, donde la banda 3 se une al GLUT1 y a enzimas glucolíticas (Puchulu-Campanella *et al.*, 2013). La tendencia de las proteínas a formar estructuras cuaternarias para formar fibras tiende a ser alta y puede optimizar la actividad catalítica como en el caso de los purinosomas o puede generar enfermedades como en el caso de la anemia falciforme o en las enfermedades amiloideas (O'Connell *et al.*, 2012).

Otro ejemplo de asociación enzimática lo constituyen las vías de señalización (Strzyz, 2019). En la membrana plasmática, las proteínas nephrin y LAT se asocian a Nck, y WASP para iniciar la formación de los filamentos de actina (Case *et al.*, 2019).

La vía de señalización de las MAP cinasas recluta en la membrana celular proteínas como SOS, necesarias para optimizar la vía de señalización (Huang et al., 2019). Los grupos de proteínas o clusters pueden secuestrar pequeñas moléculas, como los signalosomas A_{2A} o A_{2B}, los cuales son isoformas del receptor de adenosina, la enzima adenilato ciclase y la proteína cinasa A de anclaje. Este complejo permite la acumulación de pozas de AMPc y promueve respuestas específicas para cada receptor (Guinzberg et al., 2017).

El metabolón glucolítico optimiza la catálisis y protege a las enzimas contra condiciones de estrés (Araiza-Olivera et al., 2010; Menard et al., 2014). Cuando las neuronas de *C. elegans* son sometidas a estrés, las enzimas glucolíticas se ubican cerca de las sinápsis, probablemente con el objetivo de incrementar la producción local de ATP (Jin et al., 2017). En condiciones de hipoxia, *S. cerevisiae* reorganiza sus enzimas glucolíticas en cuerpos G con el objetivo de hacer la glucólisis más eficiente (Jin et al., 2017).

En este trabajo se determinó el efecto de la disponibilidad de ATP sobre la organización del citoesqueleto y la interacción de las enzimas glucolíticas con la actina. Para evaluar esto se emplearon 3 cepas de *S. cerevisiae*; una cepa silvestre con metabolismo facultativo (w303 WT) y dos cepas fermentativas obligadas; la cepa w303 p⁰ (carente de DNA mitocondrial) y la cepa *pet122Δ* (sin el promotor PET122, requerido para la traducción de una subunidad 3 del complejo IV) (Constanzo & Fox, 1990). Las cepas ya mencionadas se incubaron durante 4 horas en medio SD-Gluc (con glucosa) o en medio SD (sin glucosa). Después de este tiempo se cuantificó la concentración de ATP con un método luminiscente.

La concentración de ATP en las cepas fermentativas obligadas disminuyó más que en la cepa silvestre (Fig 6), resultados similares a los mostrados por Friis, que demostró que en la cepa ρ^0 , la depleción rápida de glucosa induce una disminución significativa en la concentración de ATP e inhibe la fosforilación de diferentes factores de transcripción requeridos para la adaptación a este tipo de estrés (Friis & Schultz, 2016). Las condiciones empleadas en este experimento fueron reversibles cuando las levaduras ayunadas fueron reincubadas en un medio con glucosa (resultados no mostrados).

Así, las cepas empleadas y las condiciones de trabajo propuestas permiten evaluar el efecto de la baja concentración de ATP sobre la organización del citoesqueleto y la unión de este a las enzimas glucolíticas.

Una vez establecidas las condiciones de trabajo, se evaluó la interacción entre las enzimas glucolíticas y la actina. Bajo condiciones de ayuno, la interacción de las enzimas ALD, GAPDH y PGK con la actina-F disminuyó (Fig 4), y se observó también una disminución en la asociación entre las enzimas (Fig 5). Este fenómeno no había sido descrito anteriormente y complementa la información disponible sobre la adaptación de las levaduras al ayuno. En el 2015 se describió que después de incubar a *S. cerevisiae* en ausencia de glucosa hay una disminución en la movilidad de las ribonucleoproteínas y la cromatina en el núcleo celular (Joyner et al., 2016).

Otro artículo describe que cuando las levaduras son incubadas en un medio sin nutrientes, las enzimas ácido graso sintasa, CTP sintasa y glutamina sintetasa forman agregados o filamentos en el citoplasma. Estos agregados se disuelven al incubar las células en un medio rico en nutrientes (Petrovska, 2015).

Se ha propuesto que la reorganización de las enzimas bajo estas condiciones tiene como objetivo formar un “almacén” de enzimas inactivas disponibles (Noore et al, 2010). Nuestros resultados sugieren qué la distribución de las enzimas glucolíticas es sensible a las condiciones del medio; en presencia de glucosa las enzimas se unen a la actina, probablemente formando un metabolón y en ayunas esta interacción disminuye.

Este trabajo propone que el ensamble del metabolón glucolítico depende de la concentración de ATP y que la formación de este complejo de enzimas permite a las células catabolizar la glucosa de un modo eficiente. Para determinar si la presencia de estos complejos modifica la velocidad de fermentación de la glucosa, se midió la producción de etanol en las cepas preincubadas en ausencia o presencia de glucosa. Los resultados obtenidos muestran que las cepas con menor concentración de ATP tienen mayor actividad fermentativa. Nuestra hipótesis inicial sugería que la velocidad de fermentación dependería del ensamble del metabolón glucolítico, sin embargo, los resultados indican que la inactivación de la glucólisis por la disociación de enzimas no ocurre en las cepas con bajas concentraciones de ATP iniciales, solo la cepa w303 *pet122Δ* exhibió un grado de inactivación por ayuno, el cuál rápidamente fue revertido después de dos minutos (Fig 7C). En contraste, la velocidad de fermentación en las cepas preincubadas en glucosa no fue tan alta como en las células ayunadas y ésta disminuyó después de dos minutos.

Nosotros sugerimos que la concentración interna de ATP controla la velocidad de fermentación. El retardo de dos minutos en la actividad fermentativa en la cepa w303 *pet122Δ* probablemente refleja la necesidad de reensamble de un

metabolón glucolítico, aunque esto no fue observado en la cepa w303 ρ^0 , quizás por la incapacidad de esta cepa de responder a la depleción rápida de glucosa (Friis & Schultz, 2016).

La respuesta a la ausencia de glucosa fue más pronunciada en las cepas fermentativas obligadas que dependen principalmente de la glucólisis para la producción de energía. Las cepas fermentativas obligadas disminuyeron su concentración total de ATP hasta un 80%, mientras que en la cepa WT se observó una disminución del 10%. Además, se observó una reorganización importante del citoesqueleto, los parches pequeños y dinámicos de actina formaron cuerpos de actina inmóviles, los cuales probablemente se forman para disminuir el gasto energético asociado a la dinámica del citoesqueleto, además de funcionar como reservas de actina (Sagot *et al.*, 2006). Así, es posible que durante la formación de estas estructuras de almacenamiento de actina se detengan funciones como el transporte de moléculas cargo y la endocitosis, donde se requiere un gasto de energía considerable (Goode *et al.*, 2014).

El papel del citoesqueleto como andamio para la organización de las enzimas glucolíticas (Menard *et al.*, 2014), podría perderse también durante la formación de los grandes cuerpos de actina. El papel crítico del metabolón durante la producción de energía se ha documentado en otros sistemas, como el descrito en las moscas mutantes nulas del gen *gpdh-3*, que no exhiben organización de las enzimas glucolíticas alrededor del citoesqueleto en células musculares, lo cual resulta en la incapacidad de volar de estas moscas (Wojtas *et al.*, 1997).

La redistribución del citoesqueleto de actina en cuerpos inmóviles correlaciona con la disponibilidad de ATP. En las mutantes fermentativas obligadas, la disminución en la concentración de ATP durante el ayuno condujo a la reorganización del citoesqueleto. Sin embargo, en la cepa WT fue necesario desacoplar la cadena respiratoria durante el ayuno para inducir la formación de cuerpos de actina. En este trabajo, la redistribución del citoesqueleto se observó marcando a la proteína de unión a actina 1 con GFP. Dicha proteína permaneció unida a actina bajo las condiciones estudiadas, lo que sugiere una reorganización de la actina y sus proteínas accesorias durante estos procesos.

En nuestras cepas de *S. cerevisiae*, la concentración de ATP previa a la adición de glucosa reguló la velocidad inicial de fermentación. Es probable que el mecanismo de control involucra el ensamblaje y desensamblaje del metabolón glucolítico que utiliza a la actina F como andamio. Además, la concentración de ATP fue el principal factor que controló la velocidad máxima de fermentación. La organización del citoesqueleto y el metabolismo de las cepas fermentativas obligadas fueron más sensibles al ayuno (Fig 10).

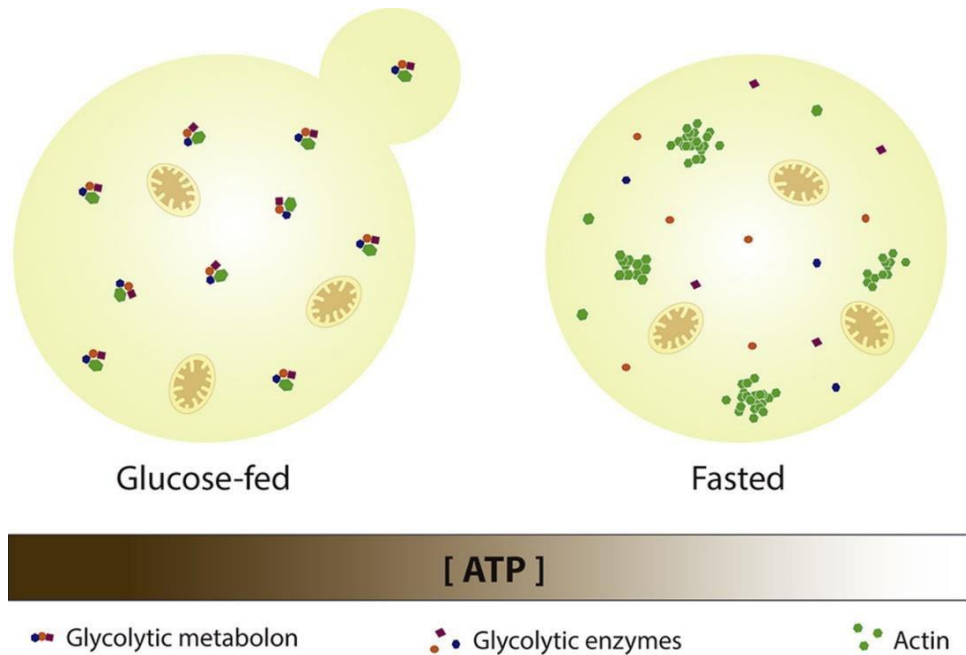


Fig. 10 La organización del citoesqueleto y la formación del metabolón glucolítico depende de la concentración de ATP. En respuesta a la disminución de ATP (disminución en la intensidad de color de la barra café), el citoesqueleto de actina se reorganiza formando parches y las enzimas glucolíticas pierden su interacción con la actina.

11 CONCLUSIONES

- La interacción de las enzimas ALD, GAPDH y PGK con la actina disminuye cuando *S. cerevisiae* es incubada en ausencia de glucosa.
- La concentración intracelular de ATP disminuye en todas las cepas después de la incubación en ausencia de glucosa. Las cepas w303 ρ^0 y w303 *pet122Δ* son incapaces de restaurar los niveles basales de ATP a los 30 minutos y 4h de ayuno.
- La velocidad de fermentación depende de los niveles de ATP celulares.
- Concentraciones bajas de ATP aumentan la velocidad de fermentación.
- La incubación en ausencia de glucosa induce la formación de cuerpos de actina inmóviles en las cepas w303 ρ^0 y w303 *pet122Δ*.

12 REFERENCIAS

- Andrés, V., Carreras, J., & Cussó, R. (1996). Myofibril-bound muscle phosphofructokinase is less sensitive to inhibition by ATP than the free enzyme, but retains its sensitivity to stimulation by bisphosphorylated hexoses. *International Journal of Biochemistry and Cell Biology*, 28(10), 1179–1184.
- Apodaca, G. (2001). Endocytic traffic in polarized epithelial cells: role of the actin and microtubule cytoskeleton. *Traffic (Copenhagen, Denmark)*, 2(3), 149–159.
- Araiza-Olivera, D., Chiquete-Felix, N., Rosas-Lemus, M., Sampedro, J. G., Peña, A., Mujica, A., & Uribe-Carvajal, S. (2013). A glycolytic metabolon in *Saccharomyces cerevisiae* is stabilized by F-actin. *FEBS Journal*, 280(16), 3887–3905.
- Araiza-Olivera, D., Sampedro, J. G., Mújica, A., Peña, A., & Uribe-Carvajal, S. (2010). The association of glycolytic enzymes from yeast confers resistance against inhibition by trehalose. *FEMS Yeast Research*, 10(3), 282–289.
- Ashe, M. P., Long, S. K. De, & Sachs, A. B. (2000). Glucose Depletion Rapidly Inhibits Translation Initiation in Yeast. *Molecular Biology of the Cell*, 11(March), 833–848.
- Berepiki, A., Lichius, A., Read, N.D., 2011. Actin organization and dynamics in filamentous fungi. *Nat. Rev. Microbiol.* 9, 876–887.
- Bibbo, M., & Wilbur, D. C. (2008). The Cell: Basic Structure and Function. *Comprehensive Cytopathology*.
- Bradford, M. (1976). A rapid and Sensitive Method for the Quantitation of Microgram Quantities of Protein Utilizing the Principle of Protein-Dye Binding. *Analytical Biochemistry*, 72(1), 248–254.
- Burr, J. G. (2007). Tools of the Cell Biologist. *Medical Cell Biology: Third Edition*, 1–26.
- Calmettes, G., John, S. A., Weiss, J. N., & Ribalet, B. (2013). Hexokinase-mitochondrial interactions regulate glucose metabolism differentially in adult and neonatal cardiac myocytes. *Journal of General Physiology*, 142(4), 425–436.
- Case, L. B., Zhang, X., Ditlev, J. A., & Rosen, M. K. (2019). Stoichiometry controls activity of phase-separated clusters of actin signaling proteins. *Science*, 363(6431), 1093–1097.
- Constanzo, M., & Fox, T. D. (1990). Control of mitochondrial gene expression in *Saccharomyces cerevisiae*. *Annual Review of Genetics*, 24(1), 91–113.
- Costanzo, M. C., & Fox, T. D. (1988). Specific translational activation by nuclear gene products occurs in the 5' untranslated leader of a yeast mitochondrial mRNA. *Proc. Natl. Acad. Sci. USA*, 85(8), 2677–2681.

- Dastmalchi, M., Bernards, M. A., & Dhaubhadel, S. (2016). Twin anchors of the soybean isoflavanoid metabolon: Evidence for tethering of the complex to the endoplasmic reticulum by IFS and C4H. *Plant Journal*, 85(6), 689–706.
- Ellis, R., & Minton, A. (2003). Cell Biology: join the crowd. *Nature*, 425(1), 27–28.
- Friis, R. M. N., & Schultz, M. C. (2016). Attenuation of transcriptional and signaling responses limits viability of ρ 0 *Saccharomyces cerevisiae* during periods of glucose deprivation. *Biochimica et Biophysica Acta (BBA) - General Subjects*, 1860(11), 2563–2575.
- Fujino, N., Tenma, N., Waki, T., Ito, K., Komatsuzaki, Y., Sugiyama, K., ... Nakayama, T. (2018). Physical interactions among flavonoid enzymes in snapdragon and torenia reveal the diversity in the flavonoid metabolon organization of different plant species. *Plant Journal*, 94(2), 372–392.
- Gietz, R. D., Schiestl, R. H., Willems, A. R., & Woods, R. A. (1995). Studies on the transformation of intact yeast cells by the LiAc/SS???DNA/PEG procedure. *Yeast*, 11(4), 355–360.
- Goode, B. L., Eskin, J. A., & Wendland, B. (2015). Actin and endocytosis in budding yeast. *Genetics*, 199(2), 315–358.
- Green, D. E., Murer, E., Richardson, S. H., Salmon, B., Brierley, G. P., & Baum, H. (1965). Association of integrated Metabolic Pathways with Membranes. *Archives of Biochemistry and Biophysics*, 112(1), 635–647.
- Guinzberg, R., Díaz-Cruz, A., Acosta-Trujillo, C., Vilchis-Landeros, M. M., Vázquez-Meza, H., Lozano-Flores, C., ... Piña, E. (2017). Newly synthesized cAMP is integrated at a membrane protein complex signalosome to ensure receptor response specificity. *FEBS Journal*, 284(2), 258–276.
- Hanson, R. H. I. (1972). Energy Metabolism and the Regulation of Metabolic Processes in Mitochondria. *Energy Metabolism and the Regulation of Metabolic Processes in Mitochondria*.
- Higuchi-Sanabria, R., Swayne, T. C., Boldogh, I. R., & Pon, L. A. (2016). Imaging of the Actin Cytoskeleton and Mitochondria in Fixed Budding Yeast Cells. In R. H. Gavin (Ed.), *Cytoskeleton Methods and Protocols: Methods and Protocols* (pp. 63–81).
- Hu, H., Juvekar, A., Lyssiotis, C. A., Lien, E. C., Albeck, J. G., Oh, D., ... Wulf, G. M. (2016). Phosphoinositide 3-Kinase Regulates Glycolysis through Mobilization of Aldolase from the Actin Cytoskeleton. *Cell*, 164(3), 433–446.
- Huang, W. Y. C., Alvarez, S., Kondo, Y., Lee, Y. K., Chung, J. K., Yue, H., ... Groves, J. T. (2019). A molecular assembly phase transition and kinetic proofreading modulate Ras activation by SOS. *Science*, 1103(March), 1098–1103.
- Huckaba, T. M., Gay, A. C., Pantalena, L. F., Yang, H. C., & Pon, L. A. (2004). Live cell imaging of the assembly, disassembly, and actin cable-dependent movement of endosomes and actin patches in the budding yeast, *Saccharomyces cerevisiae*. *Journal of Cell Biology*, 167(3), 519–530.

- Hudder, A., Nathanson, L., & Deutscher, M. P. (2003). Organization of Mammalian Cytoplasm. *Molecular and Cellular Biology*, 23(24), 9318–9326.
- Jin, M., Han, T., Yao, Y., Alessi, A. F., Freeberg, M. A., Inoki, K., ... Han, T. (2017). Glycolytic Enzymes Coalesce in G Bodies under Hypoxic Stress. *Cell Reports*, 20(4), 895–908.
- Jinturkar, K. A., & Misra, A. (2011). Challenges and Opportunities in Gene Delivery. In *Challenges in Delivery of Therapeutic Genomics and Proteomics* (First Edit).
- Jørgensen, K., Rasmussen, A. V., Morant, M., Nielsen, A. H., Bjarnholt, N., Zagrobelny, M., ... Møller, B. L. (2005). Metabolon formation and metabolic channeling in the biosynthesis of plant natural products. *Current Opinion in Plant Biology*, 8(3 SPEC. ISS.), 280–291.
- Keller, A., Peltzer, J., Carpentier, G., Horváth, I., Oláh, J., Duchesnay, A., ... Ovádi, J. (2007). Interactions of enolase isoforms with tubulin and microtubules during myogenesis. *Biochimica et Biophysica Acta - General Subjects*, 1770(6), 919–926.
- Kloeckener-Gruissem, B., McEwen, J. E., & Poyton, R. O. (1988). Identification of a third nuclear protein-coding gene required specifically for posttranscriptional expression of the mitochondrial COX3 gene in *Saccharomyces cerevisiae*. *Journal of Bacteriology*, 170(3), 1399–1402.
- Kohnhorst, C. L., Kyoung, M., Jeon, M., Schmitt, D. L., Kennedy, E. L., Ramirez, J., ... An, S. (2017). Identification of a multienzyme complex for glucose metabolism in living cells. *Journal of Biological Chemistry*, 292(22), 9191–9203.
- Lang, M. J., Martinez-Marquez, J. Y., Prosser, D. C., Ganser, L. R., Buelto, D., Wendland, B., & Duncan, M. C. (2014). Glucose starvation inhibits autophagy via vacuolar hydrolysis and induces plasma membrane internalization by down-regulating recycling. *Journal of Biological Chemistry*, 289(24), 16736–16747.
- Lee, S., Lim, W. A., & Thorn, K. S. (2013). Improved Blue, Green, and Red Fluorescent Protein Tagging Vectors for *S. cerevisiae*. *PLoS ONE*, 8(7), 4–11.
- Lewis, I. A., Campanella, M. E., Markley, J. L., & Low, P. S. (2009). Role of band 3 in regulating metabolic flux of red blood cells. *Proceedings of the National Academy of Sciences of the United States of America*, 106(44), 18515–18520.
- Longtine, M. S., McKenzie, A., Demarini, D. J., Shah, N. G., Wach, A., Brachet, A., ... Pringle, J. R. (1998). Additional modules for versatile and economical PCR-based gene deletion and modification in *Saccharomyces cerevisiae*. *Yeast*, 14(10), 953–961.
- Lu, M., Sautin, Y. Y., Holliday, L. S., & Gluck, S. L. (2004). The Glycolytic Enzyme Aldolase Mediates Assembly, Expression, and Activity of Vacuolar H⁺-ATPase. *Journal of Biological Chemistry*, 279(10), 8732–8739.
- Mainland, D. (1931). The Early Development of the Ferret: The Cytoplasm. *Journal of Anatomy*, 65(Pt 4), 411-426.3.

- Menard, L., Maughan, D., & Vigoreaux, J. (2014). The Structural and Functional Coordination of Glycolytic Enzymes in Muscle: Evidence of a Metabolon? *Biology*, 3(3), 623–644.
- Mendoza-Hoffmann, F., Pérez-Oseguera, Á., Cevallos, M. Á., Zarco-Zavala, M., Ortega, R., Peña-Segura, C., ... García-Trejo, J. J. (2018). The Biological Role of the ζ Subunit as Unidirectional Inhibitor of the F₁F_O-ATPase of *Paracoccus denitrificans*. *Cell Reports*, 22(4), 1067–1078.
- Michels, P. A. M., Bringaud, F., Herman, M., & Hannaert, V. (2006). Metabolic functions of glycosomes in trypanosomatids. *Biochimica et Biophysica Acta - Molecular Cell Research*, 1763(12), 1463–1477.
- Minascheck, G., Groschel-Stewart, U., Blum, S., & Bereiter-Hahn, J. (1992). Microcompartmentation of glycolytic enzymes in cultured cells. *European Journal of Cell Biology*, 58, 418–428.
- Moraes, T. F., & Reithmeier, R. A. F. (2012). Membrane transport metabolons. *Biochimica et Biophysica Acta - Biomembranes*, 1818(11), 2687–2706.
- Moseley, J. B., & Goode, B. L. (2006). The yeast actin cytoskeleton: from cellular function to biochemical mechanism. *Microbiology and Molecular Biology Reviews : MMBR*, 70(3), 605–645.
- Nederlof, R., Gürel-Gurevin, E., Eerbeek, O., Xie, C., Deijs, G. S., Konkel, M., ... Zuurbier, C. J. (2016). Reducing mitochondrial bound hexokinase II mediates transition from non-injurious into injurious ischemia/reperfusion of the intact heart. *Journal of Physiology and Biochemistry*, 73(3), 323–333.
- Noree, C., Sato, B. K., Broyer, R. M., & Wilhelm, J. E. (2010). Identification of novel filament-forming proteins in *Saccharomyces cerevisiae* and *Drosophila melanogaster*. *The Journal of Cell Biology*, 190(4), 541–551.
- O'Connell, J. D., Zhao, A., Ellington, A. D., & Marcotte, E. M. (2012). Dynamic Reorganization of Metabolic Enzymes into Intracellular Bodies. *Annual Review of Cell and Developmental Biology*, 28(1), 89–111.
- Orosz, F., Ovfidi, J., & Ovhdi, J. (1987). A simple approach to identify the mechanism of intermediate transfer enzyme system related to triose phosphate metabolism. *Biochimica et Biophysica Acta - General Subjects*, 915, 53–59.
- Ovádi, J., & Srere, P. A. (1999). Macromolecular Compartmentation and Channeling. *International Review of Cytology*, 192, 255–280.
- PA, S. (1987). Complexes of Sequential metabolic enzymes. *Annual Review of Biochemistry*, 56(1), 89–124.
- Pagliaro, L., & Taylor, D. L. (1988). Aldolase exists in both the fluid and solid phases of cytoplasm. *The Journal of Cell Biology*, 107(3), 981–991.

- Pagliaro, Len. (2000). Mechanisms for Cytoplasmic Organization : An Overview. In *Microcompartmentation and Phase Separation in Cytoplasm: Volume 192*(Vol. 192).
- Pagliaro, Len, & Taylor, D. L. (1992). 2-Deoxyglucose and cytochalasin D modulate aldolase mobility in living 3T3 cells. *Journal of Cell Biology*, 118(4), 859–863.
- Parry, B. R., Surovtsev, I. V., Cabeen, M. T., O'Hern, C. S., Dufresne, E. R., & Jacobs-Wagner, C. (2014). The bacterial cytoplasm has glass-like properties and is fluidized by metabolic activity. *Cell*, 156(1–2), 183–194.
- Pedley, A. M., & Benkovic, S. J. (2017). A New View into the Regulation of Purine Metabolism: The Purinosome. *Trends in Biochemical Sciences*, 42(2), 141–154.
- Pemberton, L. F. (2014). Preparation of Yeast Cells for Live-Cell Imaging and Indirect Immunofluorescence. In J. S. Smith & D. J. Burke (Eds.), *Yeast Genetics: Methods and Protocols* (pp. 79–90).
- Petrovska, I., Nüske, E., Munder, M. C., Kulasegaran, G., Malinovska, L., Kroschwald, S., ... Alberti, S. (2014). Filament formation by metabolic enzymes is a specific adaptation to an advanced state of cellular starvation. *ELife*, 2014(3), 1–19.
- Puchulu-Campanella, E., Chu, H., Anstee, D. J., Galan, J. A., Tao, W. A., & Low, P. S. (2013). Identification of the components of a glycolytic enzyme metabolon on the human red blood cell membrane. *Journal of Biological Chemistry*, 288(2), 848–858.
- Ra, B. (2000). Quantitative characterization of homo- and heteroassociations of muscle phosphofructokinase with aldolase. 1479, 303–314.
- Riedl, J., Crevenna, A. H., Kessenbrock, K., Yu, J. H., Bista, M., Bradke, F., ... Francisco, S. (2008). Lifeact: a versatile marker to visualize F-actin. *Nature Methods*, 5(7), 605–607.
- Sagot, I., Pinson, B., Salin, B., & Daignan-Fornier, B. (2006). Actin Bodies in Yeast Quiescent Cells: An Immediately Available Actin Reserve? *Molecular Biology of the Cell*, 17(11), 4645–4655.
- Sattlegger, E., Chernova, T. A., Gogoi, N. M., Pillai, I. V., Chernoff, Y. O., & Munn, A. L. (2014). Yeast studies reveal moonlighting functions of the ancient actin cytoskeleton. *IUBMB Life*, 66(8), 538–545.
- Schmitt, D. L., & An, S. (2017). *Current Topic / Perspective Spatial Organization of Metabolic Enzyme Complexes in Cells Spatial Organization of Metabolic Enzyme Complexes in Cells University of Maryland Baltimore County*.
- Schneider, M., Knuesting, J., Birkholz, O., Heinisch, J. J., & Scheibe, R. (2018). Cytosolic GAPDH as a redox-dependent regulator of energy metabolism. *BMC Plant Biology*, 18(1), 1–14.

- Berepiki, A., Lichius, A., Read, N.D., 2011. Actin organization and dynamics in filamentous fungi. *Nat. Rev. Microbiol.* 9, 876–887. <https://doi.org/10.1038/nrmicro2666>
- Joyner, R.P., Tang, J.H., Helenius, J., Dultz, E., Brune, C., Holt, L.J., Huet, S., Müller, D.J., Weis, K., 2016. A glucose-starvation response regulates the diffusion of macromolecules. *eLife* 5, 1–26. <https://doi.org/10.7554/eLife.09376>
- Sha, S.P., Anupama, A., Pradhan, P., Prasad, G.S., Tamang, J.P., 2016. Identification of yeasts by polymerase-chain-reaction-mediated denaturing gradient gel electrophoresis in marcha, an ethnic amylolytic starter of India. *J. Ethn. Foods* 3, 292–296. <https://doi.org/10.1016/j.jef.2016.11.009>
- Shen, Q. J., Kassim, H., Huang, Y., Li, H., Zhang, J., Li, G., ... Liu, J. L. (2016). Filamentation of Metabolic Enzymes in *Saccharomyces cerevisiae*. *Journal of Genetics and Genomics*, 43(6), 393–404.
- Silva, A. P. P., Alves, G. G., Araújo, A. H. B., & Sola-Penna, M. (2004). Effects of insulin and actin on phosphofructokinase activity and cellular distribution in skeletal muscle. *Anais Da Academia Brasileira de Ciencias*, 76(3), 541–548.
- Smith, M. G., Swamy, S. R., & Pon, L. a. (2001). The life cycle of actin patches in mating yeast. *Journal of Cell Science*, 114(Pt 8), 1505–1513.
- Srere, P. A. (1985). The metabolon. *Trends in Biochemical Sciences*, 10(3), 109– 110.
- Sterling, D., Reithmeier, R. A. F., & Casey, J. R. (2001). A transport metabolon: Functional interaction of carbonic anhydrase II and chloride/bicarbonate exchangers. *Journal of Biological Chemistry*, 276(51), 47886–47894.
- Strzyz, P. (2019). Phase separation tunes signal transduction. *Nature Reviews Molecular Cell Biology*, 20(5), 263.
- Suresh, H. G., da Silveira dos Santos, A. X., Kukulski, W., Tyedmers, J., Riezman, H., Bukau, B., & Mogk, A. (2015). Prolonged starvation drives reversible sequestration of lipid biosynthetic enzymes and organelle reorganization in *Saccharomyces cerevisiae*. *Molecular Biology of the Cell*, 26(9), 1601–1615.
- Sweetlove, L. J., & Fernie, A. R. (2018). The role of dynamic enzyme assemblies and substrate channelling in metabolic regulation. *Nature Communications*, Vol. 9.
- Trevors, J. T. (2011). The Composition and Organization of Cytoplasm in Prebiotic Cells. *International Journal of Molecular Sciences*, 12(1), 1650–1659.
- Waingeh, V. F., Gustafson, C. D., Kozliak, E. I., Lowe, S. L., Knull, H. R., & Thomasson, K. A. (2006). Glycolytic enzyme interactions with yeast and skeletal muscle F-actin. *Biophysical Journal*, 90(4), 1371–1384.
- Walsh, J. L., Keith, T. J., & Knull, H. R. (1989). Glycolytic enzyme interactions with tubulin and microtubules. *Biochimica et Biophysica Acta (BBA)/Protein Structure and Molecular*, 999(1), 64–70.
- Walsh TP, C. F. and M. C. (1977). Modification of the Kinetic Parameters of Aldolase on

- Binding to the Actin-Containing Filaments of Skeletal Muscle. *Biochemical Journal*, 165(1), 165–167.
- Wojtas, K., Laurence, S., & Sullivan, D. (1997). Flight Muscle Function in Drosophila Requires Colocalization of Glycolytic Enzymes. *Molecular Biology of the Cell*, 8(September), 1665–1675.
- Wu, F., Pelster, L. N., & Minteer, S. D. (2015). *Krebs cycle metabolon formation : metabolite compartmentation of sequential enzymes*. 1244–1247.
- Xu, L., & Bretscher, A. (2014). Rapid glucose depletion immobilizes active myosin v on stabilized actin cables. *Current Biology*, 24(20), 2471–2479.
- Yu, I., Mori, T., Ando, T., Harada, R., Jung, J., Sugita, Y., & Feig, M. (2016). Biomolecular interactions modulate macromolecular structure and dynamics in atomistic model of a bacterial cytoplasm. *ELife*, 5(NOVEMBER2016), 1–22.
- Zimmerman, S. B., & Trach, S. O. (1991). Estimation of macromolecule concentrations and excluded volume effects for the cytoplasm of Escherichia coli. *Journal of Molecular Biology*, 222(3), 599–620.

12 ANEXO. Artículos publicados

1. Gutiérrez-Aguilar M, López-Carbajal HM, Uribe-Alvarez C, Espinoza Simón E, Rosas Lemus M, Chiquete Feliz N, Uribe-Carvajal S. Effects of ubiquinone derivatives on the mitochondrial unselective channel of *Saccharomyces cerevisiae*. *J Bioenerg Biomembr.* 2014. 46(6): 519-27.
2. Espinoza-Simón E, Rosas-Lemus M, Cabrera-Orefice A, Uribe-Alvarez C, Chiquete-Felix N, Uribe-Carvajal S. Oxygen, for better and for worse. (in spanish). *Revista de la Facultad de Medicina*. 2014. Vol 57, 6.
3. Mónica Rosas-Lemus, Cristina Uribe-Alvarez, Martha Contreras-Zentella, Luis Alberto Luévano-Martínez, Natalia Chiquete-Félix, Norma Lilia Morales-García, Emilio Espinoza Simón, Adriana Muhlia-Almazán, Edgardo Escamilla-Marván and Salvador Uribe-Carvajal. Oxygen: From Toxic Waste to Optimal (Toxic) Fuel of Life. *Free Radicals and Diseases*, InTech. 2016.
4. Rodríguez-González M, Kawasaki L, Velázquez-Zavala N, Domínguez- Martín E, Trejo-Medecigo A, Martagón N, Espinoza-Simón E, Vázquez-Ibarra A, Ongay-Larios L, Georgellis D, de Nadal E, Posas F, Coria R. Role of the Sln1- phosphorelay pathway in the response to hyperosmotic stress in the yeast *Kluyveromyces lactis*. *Mol Microbiol*. 2017 Jun;104(5):822-836.
5. Francisco Mendoza-Hoffmann, Ángeles Pérez Oseguera, Miguel Ángel Cevallos, Mariel Zarco-Zavala, Raquel Ortega, Claudia Peña-Segura, Emilio Espinoza-Simón, Salvador Uribe-Carvajal and José J. García-Trejo. The Biological Role of the ζ Subunit as Unidirectional Inhibitor of the F1F0-ATPase of *Paracoccus denitrificans*. *Cell Reports*. 2018. 22(4):1067-1078.
6. Lilia Morales-García, Salvador Uribe-Carvajal, Natalia Chiquete-Félix, Emilio Espinoza-Simón. The Reversible Opening of Muc Demonstrates a High Potential as a Cellular Protection System. *Biophysical Journal*. 2019. 116(3): 419 a.
7. Espinoza-Simón Emilio, N. Chiquete-Félix, L. Morales-García, U. Pedroza Dávila, X. Perez-Martínez, D. Araiza-Olivera, F. Torres-Quiroz and S. Uribe- Carvajal. In *Saccharomyces cerevisiae*, withdrawal of the carbon results in detachment of glycolytic enzymes from the cytoskeleton and in actin reorganization. *Fungal Biol*. Nov, 2019.
8. Pedroza-Dávila, Ulrik; Uribe-Alvarez, Cristina; Morales-García, Lilia; Espinoza-Simón, Emilio; Méndez-Romero Ofelia, Muhlia-Almazán, Adriana; Chiquete-Felix, Natalia and Uribe-Carvajal, Salvador. Metabolism, ATP production and biofilm generation by *Staphylococcus epidermidis* in either respiratory or fermentative conditions. *AMB Express*, 10;31, 2020.

Effects of ubiquinone derivatives on the mitochondrial unselective channel of *Saccharomyces cerevisiae*

Manuel Gutiérrez-Aguilar · Helga M. López-Carbajal ·
Cristina Uribe-Alvarez · Emilio Espinoza-Simón · Mónica Rosas-Lemus ·
Natalia Chiquete-Félix · Salvador Uribe-Carvajal

Received: 15 June 2014 / Accepted: 25 November 2014 / Published online: 3 December 2014
© Springer Science+Business Media New York 2014

Abstract Ubiquinone derivatives modulate the mammalian mitochondrial Permeability Transition Pore (PTP). Yeast mitochondria harbor a similar structure: the respiration- and ATP-induced *Saccharomyces cerevisiae* Mitochondrial Unselective Channel (*ScMUC*). Here we show that decylubiquinone, a well-characterized inhibitor of the PTP, suppresses *ScMUC* opening in diverse strains and independently of respiratory chain modulation or redox-state. We also found that naturally occurring derivatives such as hexaprenyl and decaprenyl ubiquinones lacked effects on the *ScMUC*. The PTP-inactive ubiquinone 5 (Ub₅) promoted the *ScMUC*-independent activation of the respiratory chain in most strains tested. In an industrial strain however, Ub₅ blocked the protection elicited by dUb. The results indicate the presence of a ubiquinone-binding site in the *ScMUC*.

Keywords Ubiquinone analogues · Mitochondria · Permeability transition pore · Yeast

Abbreviations

dUb	Decylubiquinone
dVO ₄	Decavanadate
Δψ	Mitochondrial transmembrane potential
FCCP	Carbonyl cyanide <i>p</i> -trifluoro-methoxyphenyl-hydrazone

M. Gutiérrez-Aguilar (✉)
Dalton Cardiovascular Research Center, University of Missouri-Columbia, 134 Research Park Dr, Columbia, MO 65211, U.S.A.
e-mail: gutierrezaguilar@missouri.edu

H. M. López-Carbajal · C. Uribe-Alvarez · E. Espinoza-Simón ·
M. Rosas-Lemus · N. Chiquete-Félix · S. Uribe-Carvajal
Department of Molecular Genetics, Instituto de Fisiología Celular, Universidad Nacional Autónoma de México, UNAM, Mexico City, Mexico

Cyclosporine A	CsA
PTP	Mitochondrial permeability transition pore
<i>ScMUC</i>	<i>Saccharomyces cerevisiae</i> mitochondrial unselective channel
Ub ₅	Ubiquinone 5
Ub ₃₀	Hexaprenylquinone
Ub ₅₀	Decaprenylquinone

Introduction

The mitochondrial permeability transition can be defined as the rise in unselective conductance to ions and metabolites triggered by the opening of an unidentified non-selective pore (Brenner and Moulin 2012). In mammalian mitochondria, the permeability transition pore (PTP) depletes the protonmotive force and exhibits a molecular mass cutoff of up to 1.5 kDa (Bernardi 2013). The *Saccharomyces cerevisiae* Mitochondrial Unselective Channel (*ScMUC*) is probably an equivalent of the PTP (Uribe-Carvajal et al. 2011).

The biochemistry and physiopathology of the PTP has been studied *ad extenso*. Most hypotheses suggest that this pore opens irreversibly during several disease states, inducing a collapse in mitochondrial homeostasis (for a review, see Di Lisa and Bernardi 2006). In contrast, PTP transient opening or flickering has also been proposed to regulate Ca²⁺ homeostasis in mitochondria (Ichas and Mazat 1998). Less is known in terms of the molecular composition of the PTP; earlier models proposing that the Adenine Nucleotide Translocator and the Voltage Dependent Anion Channel could form the PTP have not successfully passed genetic tests (reviewed in Bonora et al. 2014). When the mitochondrial phosphate carrier is deleted, this results in changes in the properties of both, the PTP (Kwong et al. 2014) and the *ScMUC* (Gutiérrez-Aguilar et al. 2010) likely by controlling inorganic phosphate

(Pi) availability in mitochondria. However, a moderate change in the expression levels of the Pi carrier does not impact the Ca^{2+} -induced PTP (Gutiérrez-Aguilar et al. 2014). Up to now, Cyclophilin D (CypD) and mitochondrial Complex I are the only widely accepted modulators of the PTP (Giorgio et al. 2010; Di Lisa et al. 2011; Li et al. 2012). Topical studies suggest that CypD regulates F_1F_0 -ATP synthase. In addition, the purified dimeric enzyme from both mouse and *S. cerevisiae* mitochondria forms a multiple conductance channel with PTP-like behavior (Giorgio et al. 2013; Carraro et al. 2014). This has led to propose that the unselective pores observed in yeast and higher eukaryotes are equivalent structures that form at the interface of two F_0 sectors of ATP synthase and that the F_0 sector may play an important role in PTP formation (Bernardi 2013; Bonora et al. 2013).

The s_c MUC probably participates in energy surplus dissipation processes (Prieto et al. 1995). Although the s_c MUC and the mammalian PTP present similar molecular exclusion properties, it was earlier proposed that the s_c MUC could be hardly considered a yeast counterpart of the PTP (Manon et al. 1998). Since *S. cerevisiae* lacks a mitochondrial Ca^{2+} -uniporter (Uribe et al. 1992), Ca^{2+} does not activate the s_c MUC unless *S. cerevisiae* mitochondria are incubated in the presence of the Ca^{2+} ionophore ETH129 (Yamada et al. 2009; Carraro et al. 2014). In regard to similarities in their properties, s_c MUC and PTP are both regulated by ADP, octylguanidine, Mg^{2+} , Pi, mercurials and mastoparan (Uribe-Carvajal et al. 2011). Indeed it has been suggested that MUCs are conserved throughout the eukaryotic domain (for reviews see Azzolin et al. 2010; Bernardi and Von Stockum 2012).

Different ubiquinone analogues seem to interact with mammalian mitochondria on a specific site. Then, depending on the analogue substituent, PTP may be activated, unaffected or inhibited (Walter et al. 2000). In addition, since ubiquinones are natural ligands of respiratory complexes I, II and III, certain analogues can also interfere with respiration thus making difficult to detect off-site effects (Walter et al. 2000). Here we aimed to determine whether ubiquinone analogues modulate the s_c MUC. This is interesting as *S. cerevisiae* mitochondria lack respiratory complex I. Our results show that known PTP inhibitors modulate s_c MUC activity and support the notion of a conserved ubiquinone-binding site on the channel.

Materials and methods

Materials

All chemicals were reagent grade. dUB, Ub₅, Ub₃₀, Ub₅₀, Mannitol, MES, ethanol, safranine-O, CaCl₂, MgCl₂, ADP, FCCP and bovine serum albumin type V were from Sigma

Chem Co. (St. Louis, MO). All other reagents were of the highest purity commercially available.

Industrial and laboratory yeast strains

A commercial strain of the baker's yeast *S. cerevisiae* (La Azteca) was purchased from a local bakery. The industrial strain Yeast Foam (YF) was obtained from a previous collaboration (Díaz-Ruiz et al. 2008). The laboratory strains were BY4741 (BY) (*MATA*; *his3* Δ1; *leu2* Δ0; *met15* Δ0; *ura3* Δ) and W303 (*MATα*; *ura3*-1; *trp1*Δ 2; *leu2*-3,112; *his3*-11,15; *ade2*-1; *can1*-100).

Isolation of Yeast Mitochondria

For experiments in Figs. 1, 2A, B, C, 3, 4B and 5, an industrial strain of *S. cerevisiae* (La Azteca) was used. Cells (40 g) were suspended and incubated in a rich liquid medium under aeration (3 L/min) for 16 h, washed, suspended in distilled water and starved overnight under aeration (de Kloet et al. 1961). Cells were washed by centrifugation three times and suspended in 0.6 M mannitol, 5 mM MES, 0.1 % bovine serum albumin, pH 6.8 adjusted with triethanolamine (TEA). Cells were disrupted using a Braun cell-homogenizer and 0.45 mm diameter glass beads. Mitochondria were isolated by differential centrifugation in a SS34 rotor (Sorvall) (Cortés et al. 2000). Protein concentration was determined by a biuret method. For experiments in Figs. 2D and 4, the strains YF, W303 and BY were also used. The *S. cerevisiae* industrial strain Yeast Foam (YF) was subcultured 8 hours in YPD and cultured in YPLac until reaching an optical density of 3.0–3.5. The *S. cerevisiae* laboratory strains W303 and BY were subcultured in YPD for 24 hours and cultured in YPLac for 24 hours. All cultures were grown under constant agitation (250 rpm) at 30 °C. Mitochondria were isolated from the YF, W303 and BY strains after spheroplast homogenization and differential centrifugation (for detailed protocols see Gutiérrez-Aguilar et al. 2010).

Oxygen consumption

The rate of oxygen consumption was measured in the resting state (State 4) and in the phosphorylating state (State 3) using an YSI model 5,300 oxygraph equipped with a Clark-Type electrode at room temperature in a 1.5 mL chamber containing mitochondria at a final concentration of 0.5 mg protein/mL. Samples were suspended in respiration buffer (0.6 M mannitol, 5 mM MES pH 6.8 (TEA) plus 5 μL/mL 96 % ethanol as respiratory substrate, unless indicated otherwise). The concentrations of Pi and K⁺ used are indicated under each figure. Stock solutions were 1.0 M MgCl₂, 2.0 M KCl, and either 1.0

or 0.1 M PO₄³⁻ buffer, pH 6.8 (TEA) and 20 mM dUb, Ub₅, Ub₃₀, Ub₅₀.

Transmembrane potential ($\Delta\psi$)

The $\Delta\psi$ was determined using 10 μ M safranine-O, following the absorbance changes at 511–533 nm in a DW2000 Aminco spectrophotometer in dual mode (Akerman and Wikström 1976). At the end of each trace, $\Delta\psi$ was collapsed by adding 6 μ M FCCP.

Mitochondrial swelling

The K⁺-mediated swelling of mitochondria was measured as described before (Castrejón et al. 2002). Typically, coupled isolated mitochondria are impermeable to K⁺. However, when the *S_cMUC* opens, it allows unselective transport of externally added K⁺ along with anions present in the medium, resulting in the transport of osmotically active species. This will result in the transport of water towards the mitochondrial matrix following swelling of the organelles, which is optically measured as a decrease in light scattering of isolated mitochondria in suspension. Swelling buffer, containing 0.3 M mannitol, 5 mM MES, pH 6.8 (TEA), plus 5 μ L/mL ethanol or NADH was used to promote swelling under energized conditions. Swelling was promoted by adding 20 mM KCl where indicated by an arrow. The absorbance changes were measured at 540 nm in a DW2 Aminco spectrophotometer in split mode equipped with a magnetic stirrer. Sample volume was kept constant at 4 mL of respiration buffer. Mitochondrial concentration was 0.5 mg protein/mL.

NADH:NAD⁺ ratio determination

In order to determine whether the increase in alcohol dehydrogenase activity led to an increase in the percentage of reduced NADH, we made a NADH concentration curve, which we used to determine the amount of NADH present in samples incubated in the presence of increasing ethanol. Then, the 100 % percent NADH concentration was evaluated after adding 3 μ M sodium dithionite, which was prepared within one hour (Quinlan et al. 2013). NADH absorbance was read at 340 nm in a Varian 50 Bio-UV/Vis spectrophotometer.

Results

In isolated mitochondria, dUb inhibits opening of the *S_cMUC*

The ubiquinone derivative dUb closes the PTP in mitochondria from different cell lines and mammalian sources (Walter

et al. 2000; Devun et al. 2010). With this in mind, we decided to assess whether other ubiquinone derivatives also regulate *S_cMUC* opening (Fig. 1A). We first monitored oxygen consumption of isolated *S. cerevisiae* mitochondria from the industrial strain La Azteca under control conditions where the *S_cMUC* is typically closed by high phosphate (Fig. 1B, “c”). Under these conditions, the respiration rate of isolated mitochondria remained low. Respiration was significantly increased when phosphate was decreased, indicating opening of *S_cMUC* (Fig. 1B, “0”). This high respiration rate phenotype was gradually attenuated with dUb in a concentration-dependent manner (Fig. 1B “10” to “30”). We next wanted to assess if the protective effects of dUb on respiration were derived from a direct interaction with the respiratory chain (Fig. 1C). To address this possibility we tested the effects of increasing amounts of dUb in mitochondria incubated with the uncoupler FCCP. Under these conditions, dUb failed to decrease the respiration rate of isolated mitochondria suggesting that the protection was not at the level of the respiratory chain. The *S_cMUC* can be regulated by fluctuations in the NADH:NAD⁺ ratio (Bradshaw and Pfeiffer 2013). This is of particular relevance as *S. cerevisiae* lacks respiratory complex I, which has been proposed to regulate PTP opening (Li et al. 2012). To further address if dUb regulates the *S_cMUC* through modifications of the NADH dehydrogenase activity, we performed state 4 oxygen consumption experiments in the presence of increasing concentrations of ethanol (which generates NADH), in the absence and presence of dUb (Fig. 1D). As expected, increasing concentrations of ethanol enhanced the rate of respiration, being maximal at 20 mM ethanol. The presence of dUb under these conditions resulted in a decreased state four respiration, reaching significance at 20 mM ethanol. Further Lineweaver-Burk processing of these results suggests that dUb behaves as a non-competitive inhibitor of NADH-linked respiration and further implying that the dUb effects on *S_cMUC* activity are not related to NADH:NAD⁺ ratio fluctuations (Fig. 1E). Furthermore, the NADH:NAD⁺ ratio did not change in any of the ethanol concentrations tested (result not shown); this probably indicates that alcohol dehydrogenase is much slower than NADH dehydrogenase activities and thus it cannot affect the NADH reduction percentage.

Opening of the *S_cMUC* prevents energized mitochondria from building up a stable $\Delta\psi$ (Gutiérrez-Aguilar et al. 2010). With this in mind, we tested the effects of dUb on the $\Delta\psi$ of isolated mitochondria from La Azteca strain under the same conditions as those used for oxygen consumption. The results show that in the presence of high phosphate, mitochondria are able to sustain a high, constant and FCCP-sensitive $\Delta\psi$ (Fig. 2A trace a). Decreasing phosphate in the incubation media resulted in a fast drop in $\Delta\psi$, indicative of *S_cMUC* opening. This $\Delta\psi$ reading was not sensitive to further

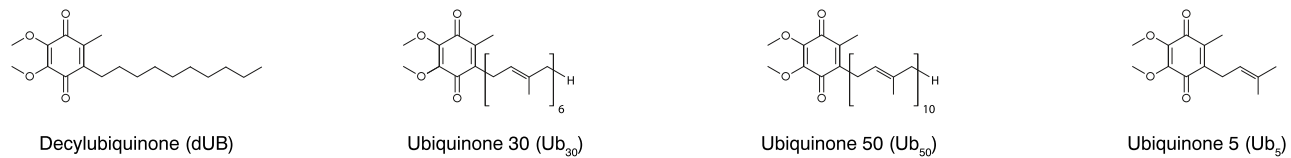
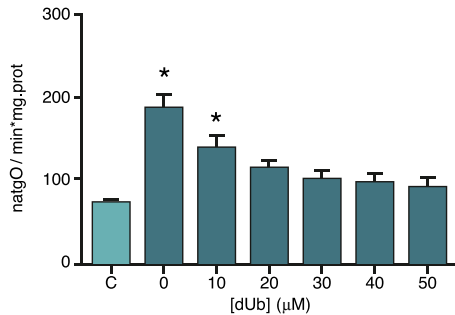
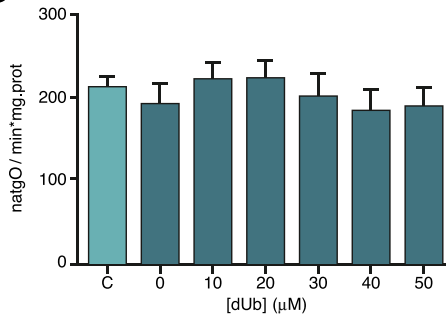
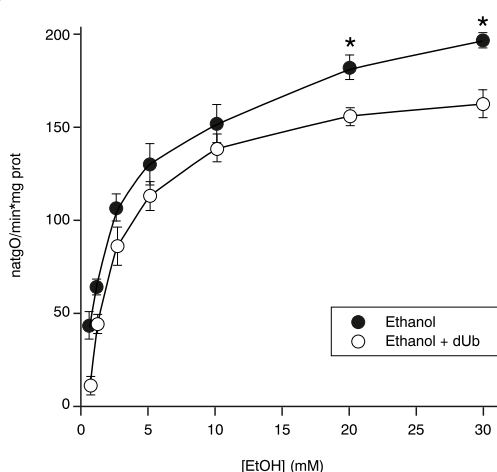
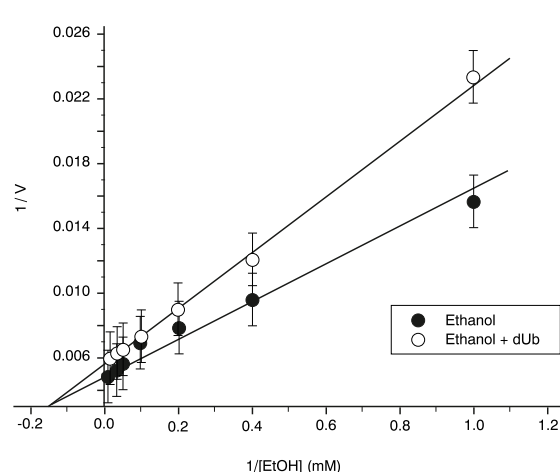
A**B****C****D****E**

Fig. 1 Ubiquinone derivatives used in this study and effects of dUb on the rates of oxygen consumption in closed/open *S_cMUC* conditions in mitochondria isolated from *S. cerevisiae* La Azteca strain. Chemical structures in (A) represent the ubiquinone derivatives used in this study. For panels B-E, experimental conditions were: 0.6 M Mannitol, 5 mM MES, pH 6.8, 20 mM KCl, pH 6.8 (TEA), 5 μ L ethanol /mL. To obtain the uncoupled state respiration, 6 μ M FCCP was added in the experiments on panel C. Measurements were conducted in a water-jacketed chamber (30 °C) connected to an oxymeter interfaced to a computer. Rates of oxygen consumption are expressed in natoms gram O ($\text{min} \cdot \text{mg prot}$) $^{-1}$. Isolated mitochondria were used at a final concentration of

0.5 mg prot/mL. Bars in both B and C were: “C”=4 mM Pi, no dUb, 0=0.4 mM Pi no dUb, 10=0.4 mM Pi plus 10 μ M dUb, 20=0.4 mM Pi plus 20 μ M dUb, 30=0.4 mM Pi plus 30 μ M dUb, 40=0.4 mM Pi plus 40 μ M dUb, 50=0.4 mM Pi plus 50 μ M dUb. In (D), oxygen uptake in open MUC (0.4 mM Pi) condition was evaluated in the presence (●) or absence (○) of 30 μ M dUb. Rates of respiration were calculated at different ethanol concentrations (0.5 mM, 1 mM, 2.5 mM, 5 mM, 10 mM, 20 mM, 30 mM) with and without dUb added. (E) Lineweaver-Burk plot from data presented in (D), which indicates a non-competitive inhibition of dUb. Each point represents the mean of three experiments \pm Standard Deviation. *P<0.05 vs. “C”

addition of FCCP (Fig. 2A trace b). Under this condition, increasing dUb resulted in the gradual buildup of a $\Delta\psi$ (Fig. 2A traces c to h), reaching maximal values at 50 and 100 μ M dUb (Fig. 2A traces g, h).

A typical parameter used to measure *S_cMUC* (and PTP) activity is the swelling resulting from opening of the pore (Castrejón et al. 2002). Mitochondria suspended in buffer with ethanol as respiratory substrate and high levels of phosphate were not sensitive to K⁺-induced swelling (Fig. 2B trace a).

Isolated mitochondria in the presence of ethanol plus low phosphate levels rapidly swelled following K⁺ addition (Fig. 2B trace b). Then increasing levels of dUb, attenuated mitochondrial swelling confirming a direct inhibition of the *S_cMUC* (Fig. 2B traces c-h). The experiments above show that dUb closed the *S_cMUC* in the presence of 0.4 mM phosphate. However, all experiments were performed in the presence of ethanol as respiratory substrate. Ethanol reduces NAD⁺ to NADH+H⁺, which in turn is reoxidized by the internal

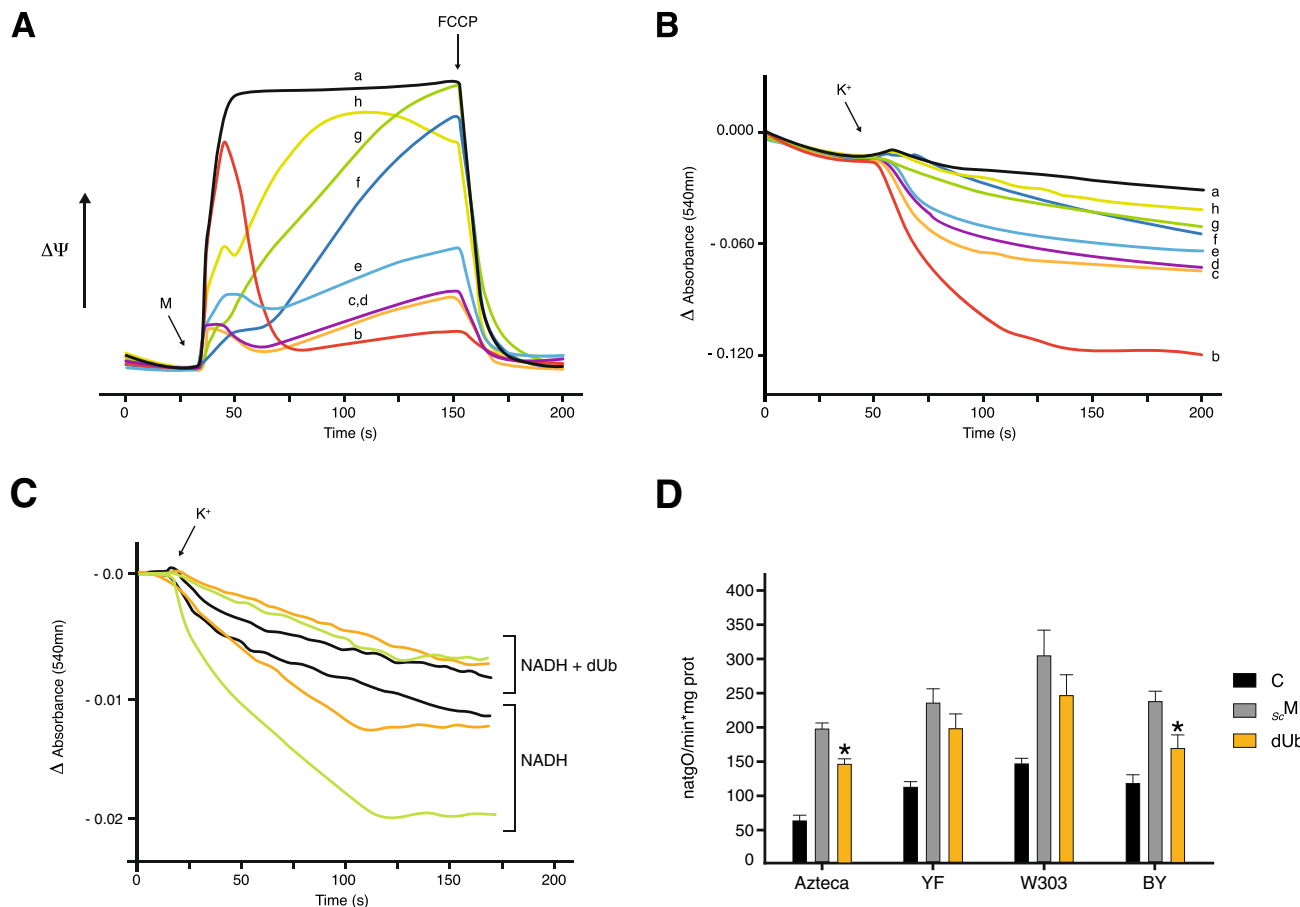


Fig. 2 Effect of dUb on the (A) $\Delta\Psi$ and (B) swelling of mitochondria isolated from different industrial and laboratory strains of *S. cerevisiae*. Experimental conditions: As in Fig. 1 except in (A), 10 μ M safranine-O. Traces in both (A) and (B) were: a=4 mM Pi, no dUb, b=0.4 mM Pi no dUb, c=0.4 mM Pi plus 10 μ M dUb, d=0.4 mM Pi plus 20 μ M dUb, e=0.4 mM Pi plus 30 μ M dUb, f=0.4 mM Pi plus 40 μ M dUb, g=0.4 mM Pi plus 50 μ M dUb, h=0.4 mM Pi plus 100 μ M dUb. Mitochondria (M) were added at the arrow. Representative experiment from $n=3$. For the experiments detailed in (C), externally added NADH was used instead of ethanol to energize mitochondria in the presence of 0.4 mM Pi being

0 mM NADH (black traces), 1 mM NADH (yellow traces) and 2 mM NADH (green traces) in the absence or presence of 30 μ M dUb as indicated. Representative experiment from $n=3$. In (D), data are presented as oxygen uptake rate in $natgO\text{ (min}^{-1}\text{mg prot)}^{-1}$. Bars labeled “C” represent the oxygen uptake rate in the presence of 4 mM phosphate. Bars labeled “dUb” represent the oxygen uptake rate in the presence of 30 μ M dUb. Please refer to section “Industrial and laboratory yeast strains” for information of the strains used in these experiments. Each bar represents the mean of three independent experiments \pm Standard Error. * $P < 0.05$ vs. values of “ $ScMUC$ ” labeled bars

NADH dehydrogenase. In our hands the redox state of the pyridine nucleotides did not vary under these conditions. Nonetheless, it has been reported that increased NADH:NAD⁺ ratios and/or high respiratory rates can result in $ScMUC$ or PTP opening (Leverve and Fontaine 2001; Manon 1999; Manon et al. 1998). To determine whether dUb inhibited $ScMUC$ opening in the presence of increasing NADH, we directly added NADH to isolated mitochondria (Fig. 2C). As expected, at 1 and 2 mM, NADH promoted $ScMUC$ opening as indicated by an increase in mitochondrial swelling (Fig. 2C, “NADH” traces). In contrast, in the presence of 30 μ M dUb swelling was prevented regardless of the NADH addition (Fig. 2C, “NADH+dUb” traces). Thus it may be concluded that the effect of dUb is independent of the purine nucleotide pool redox state.

Early studies assessing the regulation and transport properties of the $ScMUC$ concluded that industrial and laboratory strains of *S. cerevisiae* presented a mitochondrial pore with different effector sensitivities (Manon et al. 1998). These differences were later proposed to be context-specific and were abolished under appropriate experimental conditions (Bradshaw and Pfeiffer 2013). In mammalian mitochondria, cell type-dependent differential response to ubiquinone derivatives has been reported (Devun et al. 2010). With this in mind, we assessed the sensitivity of different industrial and laboratory strains of *S. cerevisiae* to dUb (Fig. 2D). We performed state 4 oxygen uptake rate experiments on the industrial strains La Azteca and Yeast Foam (YF) and the laboratory W303 and BY strains. As expected, conditions leading to closure of the $ScMUC$ induced a typical-baseline oxygen uptake rate phenotype in isolated mitochondria from

all strains (Fig. 2D, black bars). In the presence of low phosphate loads (S_c MUC), oxygen consumption was enhanced (Fig. 2D, gray bars). In agreement with Fig. 1A, addition of 30 μ M dUb reduced the oxygen uptake rate in the industrial and laboratory strains (Fig. 2D, yellow bars). The effect was S_c MUC-specific and concentration-dependent as confirmed with $\Delta\psi$ and swelling experiments performed in the laboratory W303 and BY strains (results not shown).

Effects of naturally occurring ubiquinones on the S_c MUC of industrial and laboratory strains

Based on our results showing that dUb-induced S_c MUC closure does not depend on a potential interaction of the ubiquinone derivative with the respiratory chain, we next wanted to assess whether naturally occurring ubiquinones such as hexaprenyl (Ub₃₀) and decaprenyl quinone (Ub₅₀) could potentially influence S_c MUC activity in addition to its physiological role in the respiratory chain (Fig. 3). We performed $\Delta\psi$ experiments on isolated mitochondria from the industrial strain La Azteca under control conditions where we detected a high and stable $\Delta\psi$ (Fig. 3A, trace a). As shown before, opening of the S_c MUC led to a decrease in $\Delta\psi$ (Fig. 3A, trace b). Increasing concentrations of Ub₃₀ (10–100 μ M) did not confer any potential protection on the S_c MUC-dependent $\Delta\psi$ decrease (Fig. 3A, traces c-f). Oxygen consumption experiments in the presence of Ub₃₀ under the same experimental conditions resulted in no protection against S_c MUC-mediated increase in the oxygen consumption rate (not shown). We measured $\Delta\psi$ of isolated mitochondria from La Azteca strain in the presence of Ub₅₀ (Fig. 3B). Although we occasionally measured weak, concentration-independent increases in $\Delta\psi$ (see Fig. 3B, trace d), oxygen consumption experiments

evidenced lack of Ub₅₀ protection against S_c MUC-dependent increase in respiration (not shown).

Ub₅ does not modulate the S_c MUC

We decided to test whether Ub₅, which has been reported to behave as a PTP-inactive derivative, could modulate the S_c MUC in isolated mitochondria from the industrial and laboratory strains of *S. cerevisiae* used in this study. Consequently, we measured state 4 oxygen uptake rates of isolated mitochondria from La Azteca YF, W303 and BY strains under control conditions (C), where oxygen uptake rates were low (Fig. 4A, black bars) and in the presence of low phosphate loads, which trigger S_c MUC opening (Fig. 4A, gray bars). Addition of 200 μ M Ub₅ under S_c MUC conditions had no effects on the uptake rates of mitochondria from La Azteca strain. Conversely, Ub₅ increased oxygen uptake rates ~2–3 fold under S_c MUC conditions in the YF, W303 and BY strains (Fig. 4A, white bars). Further oxygen uptake experiments in the presence of high phosphate loads (closed S_c MUC) resulted in a concentration-dependent increase in mitochondrial respiration mediated by Ub₅ in all strains (Fig. 4B). The increase in oxygen uptake was significantly lower in La Azteca strain (Fig. 4B, ●). Such effects in the oxygen uptake of all strains were S_c MUC-independent, given Ub₅ failed to modulate $\Delta\psi$ on isolated mitochondria from all strains in the presence of either low or high phosphate loads (not shown).

Ub₅ suppresses dUb protective effects in La Azteca strain

While dUb promoted closure of S_c MUC, Ub₅ did not exhibit measurable S_c MUC-related effects in La Azteca strain. Therefore, to determine if Ub₅ could still bind (but not

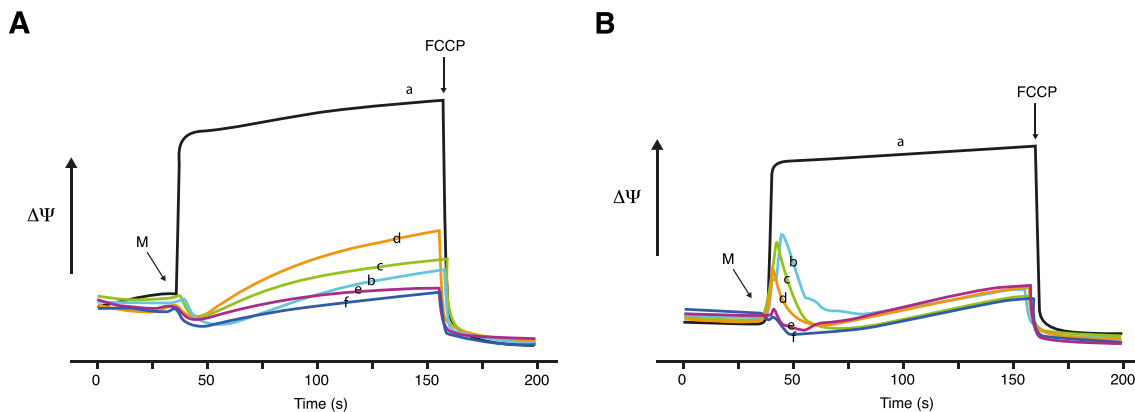


Fig. 3 Effects of Ub₃₀ and Ub₅₀ on the $\Delta\psi$ of isolated mitochondria of *S. cerevisiae* La Azteca strain. Experimental conditions were as in Fig. 2. Traces in (A) were: a=4 mM Pi, no Ub₅₀, b=0.4 mM Pi, no Ub₅₀, c=0.4 mM Pi plus 10 μ M Ub₅₀, d=0.4 mM Pi plus 30 μ M Ub₅₀, e=0.4 mM Pi plus 50 μ M Ub₅₀, f=0.4 mM Pi plus 100 μ M Ub₅₀. Traces in (B) were:

a=4 mM Pi, no Ub₅₀, b=0.4 mM Pi, no Ub₅₀, c=0.4 mM Pi plus 10 μ M Ub₅₀, d=0.4 mM Pi plus 30 μ M Ub₅₀, e=0.4 mM Pi plus 50 μ M Ub₅₀, f=0.4 mM Pi plus 100 μ M Ub₅₀. Mitochondria (M) were added at the arrow. Representative experiment from $n=3$

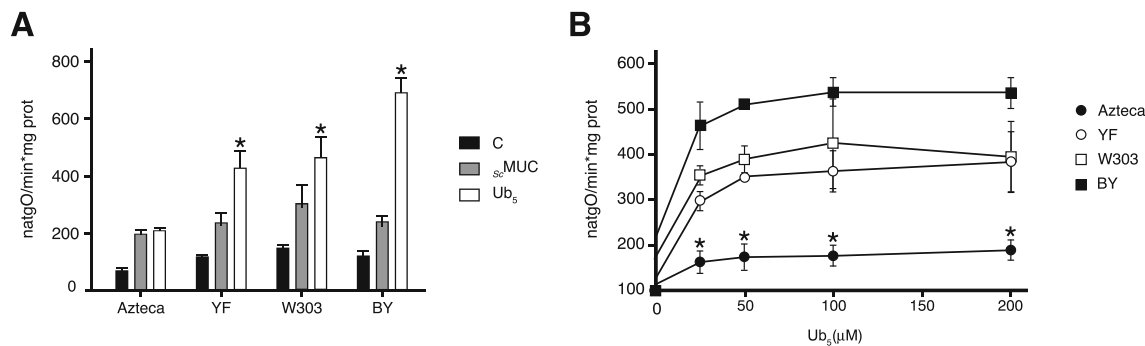


Fig. 4 Effects of Ub₅ on the oxygen uptake rates of mitochondria isolated from different industrial and laboratory strains of *S. cerevisiae*. Experimental conditions: As in Fig. 2. A, B=oxygen uptake rates. Bars labeled “ s_c MUC” represent oxygen uptake rates in the presence of 0.4 mM phosphate. Bars labeled “C” represent percent oxygen uptake rates in the presence of 4 mM phosphate. Bars labeled “Ub₅” represent percent oxygen uptake rates in the presence of 200 μM Ub₅. Please refer to section “Industrial and laboratory yeast strains” for information of the strains used in these experiments. Each bar represents the mean of three independent experiments±Standard Deviation. *P<0.05 vs. values of “ s_c MUC” labeled bars.

Deviations. *P<0.05 vs. values of “ s_c MUC” labeled bars. In (B), oxygen uptake rates were evaluated with increasing concentrations of Ub₅ using isolated mitochondria from La Azteca (●), YF (○), W303 (□), and by (■) strains. Data are presented as oxygen uptake rate in natgO (min*mg prot)⁻¹. Rates of respiration were calculated at different Ub₅ concentrations (0 μM, 25 μM, 50 μM, 100 μM, 200 μM). Each value represents the mean of three independent experiments±Standard Deviation. *P<0.05 vs. values of YF, W303 and BY strains

modulate) the s_c MUC in this strain, we designed a competition protocol measuring the rate of oxygen consumption in the presence of dUb and increasing concentrations of Ub₅ (Fig. 5). At 0.4 mM Pi, addition of 50 μM dUb promoted the return to a basal rate. Further additions of Ub₅ from 25 to 200 μM increased oxygen consumption similarly to uncoupled rates (Fig. 5A). These results were confirmed with Δψ experiments under the same conditions. At 4 mM Pi, Δψ values were high and stable but low at 0.4 mM Pi. Δψ values returned to high values at 0.4 mM Pi plus 50 μM dUb. Then, in the presence of increasing Ub₅ concentrations Δψ values decreased again

(Fig. 5B). These results indicate that dUb-mediated closure of s_c MUC was reverted by Ub₅, suggesting that these ubiquinone derivatives compete for the same binding site.

Discussion

The PTP-modulating effects of ubiquinone analogues have been proposed to be downstream from the regulatory role of CypD (Basso *et al.* 2005). Fontaine *et al.* (1998) previously proposed that the ubiquinone effect-site was respiratory

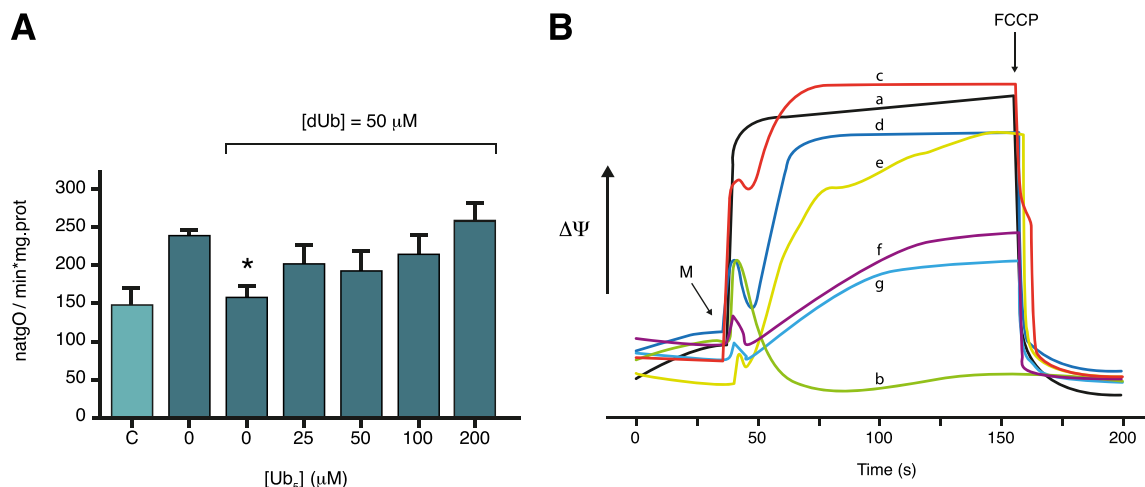


Fig. 5 Combined effects of dUb and Ub₅ on the rates of oxygen consumption and Δψ of mitochondria isolated from *S. cerevisiae* La Azteca strain. Experimental conditions: As in Fig. 2. A=oxygen consumption, B=Δψ. Bars in A were: “C”=4 mM Pi, no Ub₅ or dUb, 0=0.4 mM Pi no Ub₅ or dUb, 25=0.4 mM Pi plus 25 μM Ub₅, 50=0.4 mM Pi plus 50 μM Ub₅, 100=0.4 mM Pi plus 100 μM Ub₅, 200=0.4 mM Pi plus 200 μM Ub₅. Where indicated, 50 μM dUb was present

in the reaction mixture. Each point represents the mean of three experiments±Standard Deviation. *P<0.05 vs. C. Traces in B were: a= 4 mM Pi, no Ub₅, b=0.4 mM Pi and no Ub₅, c=0.4 mM Pi and no Ub₅, d=0.4 mM Pi plus 25 μM Ub₅ e=0.4 mM Pi plus 50 μM Ub₅, f=0.4 mM Pi plus 100 μM Ub₅, g=0.4 mM Pi plus 200 μM Ub₅. For traces c-g, 50 μM dUb was present in the reaction mixture. Mitochondria (M) were added where indicated by an arrow. Representative experiment from n=3

complex I. It is important to note that these analogues present divergent modulating properties depending on the ubiquinone side chain (Walter et al. 2002). In addition such divergent properties are cell line-specific (Devun et al. 2010). This implies that PTPs (and probably the *S. cerevisiae* MUC) may present context-specific accessory components. Indeed, (Li et al. 2012) proposed that rotenone-mediated inhibition of complex I may be even more protective against PTP opening than CsA as long as CypD levels do not exceed those of discrete complex I subunits. Manon (1999) also concluded that *S. cerevisiae* MUC activity is strictly dependent on respiratory chain activity. These data suggest that MUCs are likely modulated by the pyridine nucleotide redox state. In fact, Hunter and Haworth (1979) were the first to report NADH-induced PTP inhibition indicating that the PTP remained closed upon inhibition of complex I with rotenone or through the regulation of the NADH:NAD⁺ ratio using β-hydroxybutyrate and acetoacetate. Ubiquinone derivatives regulate the PTP downstream of mitochondrial CypD, strongly indicating that these molecules bind directly to the pore or to another regulatory factor (Basso et al. 2005). Since the *S. cerevisiae* MUC is probably not regulated by the yeast mitochondrial Cyclophilin (Cpr3), but is still sensitive to ubiquinone derivatives, the *S. cerevisiae* MUC and the PTP still present conserved characteristics. To this, the utilization of *S. cerevisiae* as a model to understand the PTP constitutes a powerful genetic tool to unveil the molecular componentry of the *S. cerevisiae* MUC as recently proposed by Carraro et al. (2014). Here, we provide evidence supporting the notion that the *S. cerevisiae* MUC presents a conserved ubiquinone-sensitive site and that the effects of ubiquinone derivatives are independent of the presence of mitochondrial complex I, which is naturally absent in our yeast model. We also show that dUb blocks the *S. cerevisiae* MUC, like the PTP, in a similar concentration range. Then we confirm that the effects of dUb are not related to the regulation of the mitochondrial respiration nor changes in the matrix NADH:NAD⁺ ratio, which are also known pore effectors (Leverve and Fontaine 2001). This suggests that respiration-induced *S. cerevisiae* MUC opening and dUb-mediated *S. cerevisiae* MUC closure likely occur through unrelated mechanisms.

We finally show that although the PTP-inactive Ub₅ counteracts the effects of dUb on the *S. cerevisiae* MUC of La Azteca strain, this derivative also strongly activates *S. cerevisiae* MUC-independent respiration in several yeast strains tested. To this, the Ub₅-mediated increase in respiration has also been reported for the laboratory CEN.PK2–1C strain of *S. cerevisiae* (James et al. 2005). Although the cause for such divergent phenotype between La Azteca and the rest of the strains tested is unknown and is subject of further research in our laboratory, adaptive evolution could account for the differences monitored herein, where close to 22 % of the total transcripts detected in industrial strains do not match annotated sequences for laboratory strains (Varela et al. 2005).

We have discussed this possibility for the strain-specific differences in *S. cerevisiae* MUC activity reported before (Uribe-Carvajal et al. 2011).

Altogether, our results suggest that ubiquinone analogues can regulate the *S. cerevisiae* MUC as seen with the mammalian PTP. Consequently, ubiquinone analogues may bind to a conserved/discrete site and its lateral chain may be involved in the gating of the *S. cerevisiae* MUC as well as the PTP. This likely explains why ubiquinone derivatives with disparate side chains have similar properties on the PTP and the *S. cerevisiae* MUC. The results presented here also imply that ubiquinone analogues display its permeability-modulating effects in a complex I-independent context.

Acknowledgments M.G.-A. is currently supported by an American Heart Association Midwest Affiliate Postdoctoral Fellowship (13POST14060013). HLC is a CONACyT fellow enrolled in the Ms. Sc. Biochemistry program at UNAM. CUA, EGS and MRL are CONACyT fellows enrolled in the Ph. D. Biochemistry program at UNAM. Partially funded by DGAPA/PAPIIT Project IN202612. We acknowledge the technical assistance of Ramón Méndez. Mariana Valenzuela kindly helped to build the figures.

References

- Akerman KE, Wikström MK (1976) Safranine as a probe of the mitochondrial membrane potential. FEBS Lett 68:191–197
- Azzolin L, Von Stockum S, Basso E et al (2010) The mitochondrial permeability transition from yeast to mammals. FEBS Lett 584: 2504–2509
- Basso E, Fante L, Fowlkes J et al (2005) Properties of the permeability transition pore in mitochondria devoid of Cyclophilin D. J Biol Chem 280:18558–18561
- Bernardi P (2013) The mitochondrial permeability transition pore: a mystery solved? Front Physiol 4:95
- Bernardi P, Von Stockum S (2012) The permeability transition pore as a Ca²⁺ release channel: new answers to an old question. Cell Calcium 52:22–27
- Bonora M, Bononi A, De Marchi E et al (2013) Role of the c subunit of the F₀ ATP synthase in mitochondrial permeability transition. Cell Cycle 12:674–683
- Bonora M, Wieckowski MR, Chinopoulos C, et al. (2014) Molecular mechanisms of cell death: central implication of ATP synthase in mitochondrial permeability transition. Oncogene. doi:doi:10.1038/onc.2014.96
- Bradshaw PC, Pfeiffer DR (2013) Characterization of the respiration-induced yeast mitochondrial permeability transition pore. Yeast 30: 471–483
- Brenner C, Moulin M (2012) Physiological roles of the permeability transition pore. Circ Res 111:1237–1247
- Carraro M, Giorgio V, Sileikyté J, et al. (2014) Channel Formation by Yeast F-ATP Synthase and the Role of Dimerization in the Mitochondrial Permeability Transition. J Biol Chem 289:15980–15985
- Castrejón V, Peña A, Uribe S (2002) Closure of the yeast mitochondria unselective channel (YMUC) unmasks a Mg²⁺ and quinine sensitive K⁺ uptake pathway in *Saccharomyces cerevisiae*. J Bioenerg Biomembr 34:299–306

- Cortés P, Castrejón V, Sampedro JG, Uribe S (2000) Interactions of arsenate, sulfate and phosphate with yeast mitochondria. *Biochim Biophys Acta* 1456:67–76
- de Kloet S, van Wermeskerken R, Koningsberger VV (1961) Studies on protein synthesis by protoplasts of *Saccharomyces carlsbergensis*. I. The effect of ribonuclease on protein synthesis. *Biochim Biophys Acta* 47:138–143
- Devun F, Walter L, Belliere J et al (2010) Ubiquinone analogs: a mitochondrial permeability transition pore-dependent pathway to selective cell death. *PLoS ONE* 5:e11792
- Díaz-Ruiz R, Averet N, Araiza D, Pinson B, Uribe-Carvajal S, Devin A et al (2008) Mitochondrial oxidative phosphorylation is regulated by fructose 1,6-bisphosphate. A possible role in Crabtree effect induction? *J Biol Chem* 283:26948–26955
- Di Lisa F, Bernardi P (2006) Mitochondria and ischemia-reperfusion injury of the heart: fixing a hole. *Cardiovasc Res* 70:191–199
- Di Lisa F, Carpi A, Giorgio V, Bernardi P (2011) The mitochondrial permeability transition pore and cyclophilin D in cardioprotection. *Biochim Biophys Acta* 1813:1316–1322
- Fontaine E, Eriksson O, Ichas F, Bernardi P (1998) Regulation of the permeability transition pore in skeletal muscle mitochondria. Modulation By electron flow through the respiratory chain complex I. *J Biol Chem* 273:12662–12668
- Giorgio V, Soriano ME, Basso E et al (2010) Cyclophilin D in mitochondrial pathophysiology. *Biochim Biophys Acta* 1797:1113–1118
- Giorgio V, Von Stockum S, Antoniel M et al (2013) Dimers of mitochondrial ATP synthase form the permeability transition pore. *Proc Natl Acad Sci U S A* 110:5887–5892
- Gutiérrez-Aguilar M, Douglas DL, Gibson AK et al (2014) Genetic manipulation of the cardiac mitochondrial phosphate carrier does not affect permeability transition. *J Mol Cell Cardiol* 72:316–325
- Gutiérrez-Aguilar M, Pérez-Martínez X, Chávez E, Uribe-Carvajal S (2010) In *Saccharomyces cerevisiae*, the phosphate carrier is a component of the mitochondrial unselective channel. *Arch Biochem Biophys* 494:184–191
- Hunter DR, Haworth RA (1979) The Ca^{2+} -induced membrane transition in mitochondria. I. The protective mechanisms. *Arch Biochem Biophys* 195:453–459
- Ichas F, Mazat JP (1998) From calcium signaling to cell death: two conformations for the mitochondrial permeability transition pore. Switching from low- to high-conductance state. *Biochim Biophys Acta* 1366:33–50
- James AM, Cochemé HM, Smith RAJ, Murphy MP (2005) Interactions of mitochondria-targeted and untargeted ubiquinones with the mitochondrial respiratory chain and reactive oxygen species. Implications for the use of exogenous ubiquinones as therapies and experimental tools. *J Biol Chem* 280:21295–21312
- Kwong JQ, Davis J, Baines CP et al (2014) Genetic deletion of the mitochondrial phosphate carrier desensitizes the mitochondrial permeability transition pore and causes cardiomyopathy. *Cell Death Differ* 21(8):1209–1217
- Leverve XM, Fontaine E (2001) Role of substrates in the regulation of mitochondrial function in situ. *IUBMB Life* 52(3–5):221–229
- Li B, Chauvin C, De Paulis D et al (2012) Inhibition of complex I regulates the mitochondrial permeability transition through a phosphate-sensitive inhibitory site masked by cyclophilin D. *Biochim Biophys Acta* 1817:1628–1634
- Manon S (1999) Dependence of yeast mitochondrial unselective channel activity on the respiratory chain. *Biochim Biophys Acta* 1410:85–90
- Manon S, Roucou X, Guérin M et al (1998) Characterization of the yeast mitochondria unselective channel: a counterpart to the mammalian permeability transition pore? *J Bioenerg Biomembr* 30:419–429
- Prieto S, Bouillaud F, Rial E (1995) The mechanism for the ATP-induced uncoupling of respiration in mitochondria of the yeast *Saccharomyces cerevisiae*. *Biochem J* 307(Pt 3):657–661
- Quinlan CL, Peresvoshchikova IV, Hey-Mogensen M, Orr AL, Brand MD (2013) Sites of reactive oxygen species generation by mitochondria oxidizing different substrates. *Redox Biol* 1:304–312
- Uribe S, Rangel P, Pardo JP (1992) Interactions of calcium with yeast mitochondria. *Cell Calcium* 13:211–217
- Uribe-Carvajal S, Luévanos-Martínez LA, Guerrero-Castillo S et al (2011) Mitochondrial unselective channels throughout the eukaryotic domain. *Mitochondrion* 11:382–390
- Varela C, Cárdenas J, Melo F, Agosin E (2005) Quantitative analysis of wine yeast gene expression profiles under winemaking conditions. *Yeast* 22:369–383
- Walter L, Miyoshi H, Leverve X et al (2002) Regulation of the mitochondrial permeability transition pore by ubiquinone analogs. a progress report. *Free Radic Res* 36:405–412
- Walter L, Nogueira V, Leverve X et al (2000) Three classes of ubiquinone analogs regulate the mitochondrial permeability transition pore through a common site. *J Biol Chem* 275:29521–29527
- Yamada A, Yamamoto T, Yoshimura Y et al (2009) Ca^{2+} -induced permeability transition can be observed even in yeast mitochondria under optimized experimental conditions. *Biochim Biophys Acta* 1787: 1486–1491

Oxígeno, para bien y para mal

*Emilio Espinoza Simón^a, Mónica Rosas Lemus^a, Alfredo Cabrera Orefice^a,
Cristina Uribe Álvarez^a, Natalia Chiquete Félix^a, Salvador Uribe Carvajal^a*

El oxígeno ayuda a aprovechar la energía de los nutrientes, sin embargo, también produce especies reactivas de oxígeno (ERO), que en exceso, reaccionan con las moléculas del organismo y las destruyen. Esto provoca envejecimiento y, eventualmente, la muerte. Las diferentes especies biológicas han evolucionado para regular la formación de las ERO. La alimentación y el estilo de vida ejercen una fuerte influencia sobre la capacidad del organismo para lidiar con las ERO.

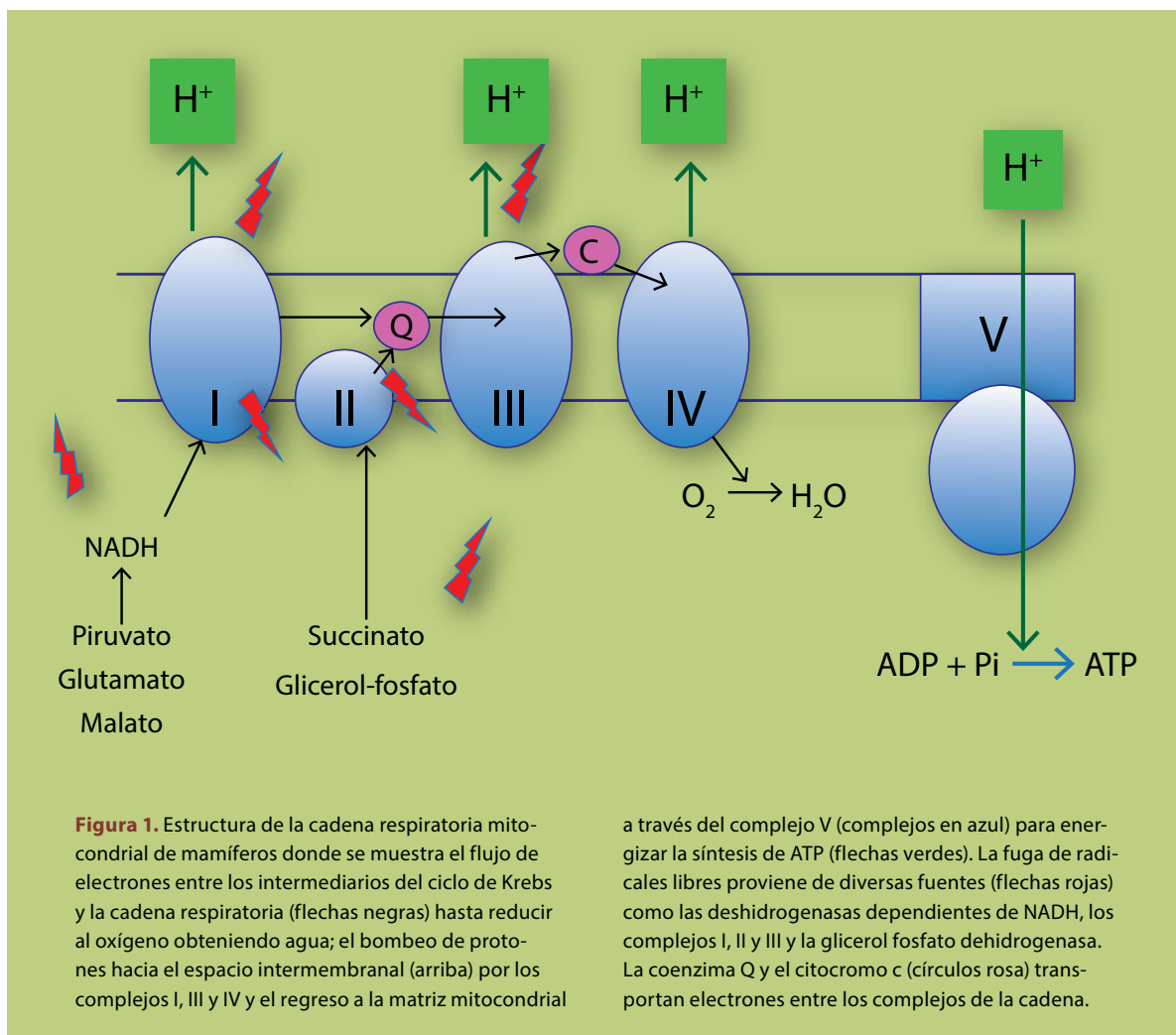
Desde su aparición hace 3,500 millones de años, los seres vivos proliferaron y se diversificaron hasta que hace 2,000 millones de años la concentración de oxígeno atmosférico aumentó 100,000 veces, lo que indujo la extinción de alrededor del 80% de las especies biológicas. Este aumento se debió a la actividad de las cianobacterias fotosintéticas cuya actividad metabólica libera oxígeno como subproducto y a la toxicidad de los derivados parcialmente reducidos del oxígeno que se conocen como ERO.

A partir de las especies que sobrevivieron a la oxigenación masiva de la atmósfera se desarrolla-

ron los organismos aerobios. Es decir, células que utilizan al oxígeno como aceptor de electrones, lo que libera grandes cantidades de energía en un proceso conocido como respiración aerobia. La cadena respiratoria aerobia se localiza en la membrana plasmática de las bacterias o en la membrana interna mitocondrial de los eucariotas.

La fosforilación oxidativa mitocondrial resulta del acoplamiento entre 2 procesos (**figura 1**). Primero, la cadena respiratoria bombea protones al espacio extramembranal usando la energía del flujo de electrones desde diversos donadores hasta el oxígeno, este proceso genera un “gradiente” de protones, es decir una diferencia de sus concentraciones a cada lado de la membrana. Luego el complejo V o adenosintrifosfato (ATP) sintetasa libera la energía almacenada en el gradiente de protones para la fosforilación, es decir la síntesis de ATP, a partir de una molécula de adenosindifosfato (ADP) y un fosfato. La cadena respiratoria acepta equivalentes reductores de diversos sustratos como el nicotinamida adenindinucleótido reducido (NADH) y el flavín adenin dinucleótido reducido (FADH₂). El nicotinamida adenindinucleótido (NAD⁺) es reducido a NADH por diversas enzimas entre las que se encuentran algunas del ciclo de Krebs, como

^aLaboratorio 305 Oriente. Departamento de Genética Molecular. Instituto de Fisiología Celular. UNAM. México, DF.



la piruvato deshidrogenasa, la alfa-ceto glutarato deshidrogenasa y la malato deshidrogenasa; luego el NADH es oxidado en el complejo I (NADH: coenzima Q óxido-reductasa). El FADH₂ proviene de la succinato dehidrogenasa o de la glicerol fosfato deshidrogenasa y alimenta al complejo II (FADH₂: coenzima Q óxido-reductasa). Los electrones captados en los complejos I y II son cedidos a través de la coenzima Q al complejo III (coenzima Q: citocromo c óxido-reductasa) y luego, a través del citocromo C al complejo IV (citocromo-oxidasa). El complejo IV reduce al oxígeno para producir agua.

El flujo de electrones es ilustrado con flechas negras (**figura 1**). Los electrones arrastran protones y 3 de los complejos respiratorios (I, III y IV)

aprovechan la liberación de energía de las óxido-reducciones catalizadas para bombear los protones al espacio intermembranal y así almacenar la energía en forma de un gradiente de protones (**figura 1**, flechas y cuadros verdes). Los protones fluyen de regreso al interior mitocondrial a través de la ATP sintetasa o complejo V liberando energía que se usa para sintetizar ATP (**figura 1**).

La eficiencia del metabolismo aerobio es unas 15 veces mayor que la del metabolismo anaerobio y por ello, los organismos que generaron un metabolismo aerobio pudieron crecer y llegaron a dominar la Tierra. Sin embargo, esa eficiencia tiene un elevado precio. Durante la respiración se generan radicales libres (especies químicas con electrones desapareados)

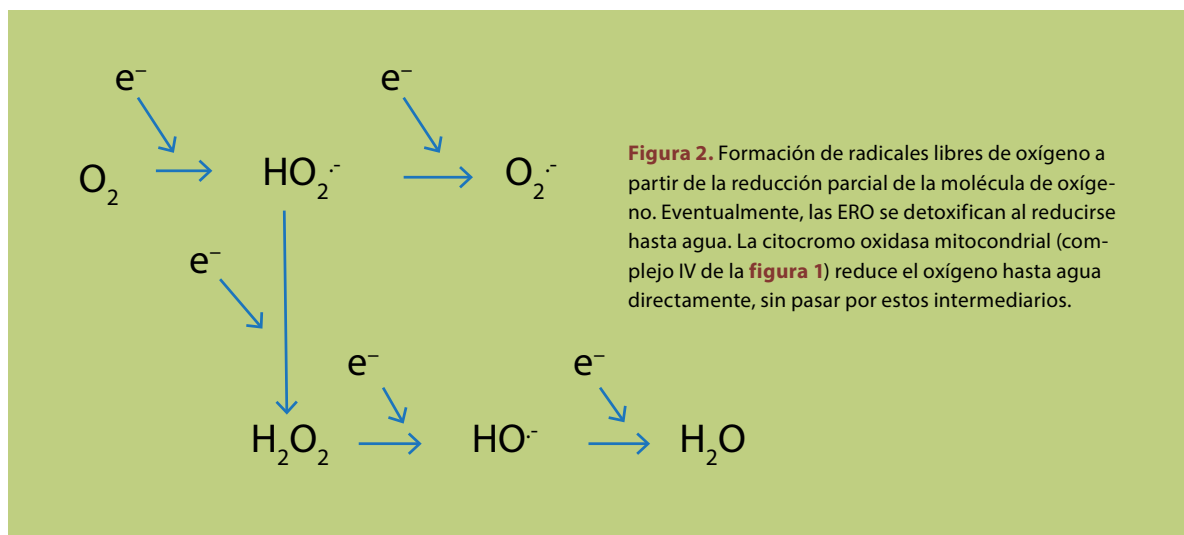


Figura 2. Formación de radicales libres de oxígeno a partir de la reducción parcial de la molécula de oxígeno. Eventualmente, las ERO se detoxifican al reducirse hasta agua. La citocromo oxidasa mitocondrial (complejo IV de la **figura 1**) reduce el oxígeno hasta agua directamente, sin pasar por estos intermediarios.

dos) que pueden reaccionar inespecíficamente con el oxígeno del medio y generar ERO (**figura 1**, flechas rojas).

Las ERO, que también son radicales libres, reaccionan rápidamente con los lípidos formando malondialdehido y 4-hidroxinonenal, oxidan las bases del DNA formando 8- hidroxiguanosina, además de carbonilar, nitrar y glutationilar a las proteínas. Estas modificaciones eventualmente conducen a la muerte celular.

Las principales ERO son el ion superóxido (O_2^-), el ion hidroperóxido (HOO^-) y el ion hidroxilo (HO^-), además del peróxido de hidrógeno (H_2O_2) que no es un radical libre pero es muy reactivo. Su génesis por introducción de electrones individuales provenientes de radicales libres se muestra en la **figura 2**.

Los organismos, lo mismo una bacteria que un humano, necesitan defenderse de las ERO. Las defensas son de 2 tipos: el primero es la desactivación de las ERO catalizada por enzimas como la superóxido-dismutasa (SOD), la catalasa y el sistema de la glutatión-peroxidasa/reductasa. La SOD convierte al radical superóxido en peróxido de hidrógeno, mientras que la catalasa transforma al peróxido de hidrógeno en agua. Estas 2 reacciones deben estar estrechamente coordinadas. Por ejemplo, en humanos la SOD se codifica en el cromosoma 21; si hay 3 cromosomas 21, en lugar de 2, se expresa

La glucólisis anaerobia genera 2 moléculas de ATP por glucosa consumida, mientras que la combinación de glucólisis con fosforilación oxidativa genera entre 36 y 38 moléculas de ATP por glucosa.

un exceso de SOD que produce tanto peróxido de hidrógeno que la catalasa no logra eliminarlo y daña a las células. El sistema de la glutatión peroxidasa/reductasa usa al glutatión, un tripeptido antioxidante que contiene cisteína.

El segundo mecanismo de protección consiste en abatir la formación intracelular de las ERO. La aceleración de la velocidad del paso de electrones por la cadena respiratoria abate la producción de las ERO mediante 2 mecanismos: disminuye la concentración de oxígeno en la célula y elimina rápidamente a los radicales libres, antes de que puedan participar en reacciones inespecíficas.

Las mitocondrias, paradójicamente parecen ser la clave del manejo de las ERO. Si bien la cadena respiratoria mitocondrial produce una gran cantidad de radicales libres, es también gracias a la actividad de la cadena respiratoria mitocondrial que se evita que esos radicales libres se combinen con oxígeno y se produzcan ERO.

En humanos, las ERO tienen un papel relevante en procesos tan variados como el síndrome de Down (trisomía 21), la gangrena, el daño postis-



El ejercicio regular, físico y muy probablemente intelectual y la ingesta de antioxidantes polifenólicos incrementan la biogénesis y la respiración mitocondrial en tejido nervioso, adiposo y muscular. En modelos animales se observó que la biogénesis y la función mitocondrial neuronal de la descendencia son beneficiadas por la práctica constante de ejercicio.

químico, cerebral o miocárdico, el envejecimiento fisiológico de los organismos y las enfermedades neurodegenerativas.

En pacientes con la enfermedad de Parkinson se observó una actividad deficiente del complejo I mitocondrial en la sustancia nigra, mientras que en la enfermedad de Huntington existe una baja actividad del complejo II en el cerebro de pacientes en etapas avanzadas y en la corteza temporal de pacientes con síndrome de Alzheimer se observa deficiencia del complejo III.

Diversos estudios demostraron que el ejercicio regular, físico y muy probablemente intelectual y la ingesta de antioxidantes polifenólicos incrementan la biogénesis y la respiración mitocondrial en tejido nervioso, adiposo y muscular en sujetos obesos, diabéticos y sanos. En modelos animales se observó que la biogénesis y la función mitocondrial neuronal de la descendencia son beneficiadas por la práctica

constante de ejercicio. Asimismo, la restricción calórica preserva la función mitocondrial promoviendo la biogénesis mitocondrial y mejorando la eficiencia bioenergética.

Elelixir de la juventud es el propio sudor. Conforme acumulamos años, es necesario luchar (en el gimnasio y en la pista de atletismo) por formar biomasa muscular y mantener el metabolismo aerobio funcionando. Así se producirán más mitocondrias y se evitará el daño inducido por las ERO. En este sentido, se ha demostrado que aún cuando un sujeto físicamente activo no necesariamente viva más tiempo, su calidad de vida será muy superior al que es sedentario. Evitar el exceso en la ingesta en alimentos también ayuda a aumentar la población mitocondrial. ●

BIBLIOGRAFÍA

- Gregory MA, Gill DP, Petrella RJ. Brain health and exercise in older adults. *Curr Sport Med Rep*. 2013;12(4):256-71.
- Lane N. Oxygen: the molecule that made the world. Oxford: Oxford University Press; 2003.
- Sena LA, Chandel NS. Physiological roles of mitochondrial reactive oxygen species. *Mol Cell*. 2012;48(2):158-67.
- Toledo FG, Goodpaster BH. The role of weight loss and exercise in correcting skeletal muscle mitochondrial abnormalities in obesity, diabetes and aging. *Mol Cell Endocrinol*. 2013;379(1-2):30-4.

We are IntechOpen, the world's leading publisher of Open Access books Built by scientists, for scientists

4,100

Open access books available

116,000

International authors and editors

120M

Downloads

154

Countries delivered to

TOP 1%

most cited scientists

12.2%

Contributors from top 500 universities



WEB OF SCIENCE™

Selection of our books indexed in the Book Citation Index
in Web of Science™ Core Collection (BKCI)

Interested in publishing with us?
Contact book.department@intechopen.com

Numbers displayed above are based on latest data collected.

For more information visit www.intechopen.com



Oxygen: From Toxic Waste to Optimal (Toxic) Fuel of Life

Mónica Rosas-Lemus, Cristina Uribe-Alvarez,
Martha Contreras-Zentella,
Luis Alberto Luévano-Martínez,
Natalia Chiquete-Félix, Norma Lilia Morales-García,
Emilio Espinosa Simón, Adriana Muhlia-Almazán,
Edgardo Escamilla-Marván and
Salvador Uribe-Carvajal

Additional information is available at the end of the chapter

<http://dx.doi.org/10.5772/63667>

Abstract

Some 2.5 billion years ago, the great oxygenation event (GOE) led to a 10^5 -fold rise in atmospheric oxygen [O_2], killing most species on Earth. In spite of the tendency to produce toxic reactive oxygen species (ROS), the highly exergonic reduction of O_2 made it the ideal biological electron acceptor. During aerobic metabolism, O_2 is reduced to water liberating energy, which is coupled to adenosine triphosphate (ATP) synthesis. Today, all organisms either aerobic or not need to deal with O_2 toxicity. O_2 -permeant organisms need to seek adequate [O_2], for example, aquatic crustaceans bury themselves in the sea bottom where O_2 is scarce. Also, the intestinal lumen and cytoplasm of eukaryotes is a microaerobic environment where many facultative bacteria or intracellular symbionts hide from oxygen. Organisms such as plants, fish, reptiles and mammals developed O_2 -impermeable epithelia, plus specialized external respiratory systems in combination with O_2 -binding proteins such as hemoglobin or leg-hemoglobin control [O_2] in tissues. Inside the cell, ROS production is prevented by rapid O_2 consumption during the oxidative phosphorylation (OxPhos) of ATP. When ATP is in excess, OxPhos becomes uncoupled in an effort to continue eliminating O_2 . Branched respiratory chains, unspecific pores and uncoupling proteins (UCPs) uncouple OxPhos. One last line of resistance against ROS is deactivation by enzymes such as super oxide dismutase and catalase. Aerobic organisms profit from the high energy released by the reduction of O_2 , while at the same time they need to avoid the toxicity of ROS.

Keywords: oxygen, ROS, oxidative stress, oxyconformers, oxyregulators, adaptative metabolism

1. At the beginning, all life was anaerobic

The early Earth atmosphere contained high $[H_2]$, $[NH_3]$ and $[CH_4]$, while $[O_2]$ was less than 10^{-5} the present atmospheric level (PAL) [1, 2]. All life forms were anaerobic [3, 4]. Early redox reactions involved electron donors such as H_2 , CO_2 or HS [5, 6], while electron acceptors were sulfur and NO_3 [7]. Eukaryotes were present before O_2 rose [8, 9] and contained anaerobic mitochondrion-like organelles [10, 11].

2. The massive increase in $[O_2]$ and the need to counteract its toxicity

Approximately 2.5 billion years ago, the great oxygenation event (GOE) was precipitated by both geological processes [12] and by the photosynthetic activity of cyanobacteria [13, 14]. Today, O_2 is the preferred electron acceptor used by facultative microorganisms and the only one used by aerobes. The highly exergonic reduction of O_2 provided the energy needed for the development of multicellular organisms. In addition, the high energy of activation required for O_2 reduction ensures that this reaction occurs mostly through catalyzed reactions. For instance, oxidases bind their substrate tightly, preventing the liberation of reactive oxygen species (ROS) [15]. At low concentrations, ROS are useful as signaling molecules, while at higher concentrations ROS damage and kill cells. Cells need much less $[O_2]$ than what is found in the atmosphere and thus, to prevent ROS production internal O_2 is kept at a low level [16]. Cells have developed two mechanisms to deal with surplus O_2 : (1) avoiding it and (2) rapidly reducing it. Furthermore, cellular O_2 is found mostly bound to proteins such as hemoglobin, leg-hemoglobin and myoglobin. Early oxy-conformer organisms are permanent to O_2 , and thus, at different stages in their life cycle, they have to migrate to microaerobic or anaerobic spaces (**Table 1**) to cope with variations in O_2 . More evolved oxyregulator organisms from fish to mammals enveloped themselves in an O_2 -impermeable epithelium, while at the same time developing highly specialized systems that control tissue $[O_2]$ (**Figure 1**). Oxyconformers and oxyregulators display different strategies to manage O_2 -by-product toxicity (**Figure 1**).

In oxyconformers, all cells are exposed to environmental $[O_2]$. O_2 -permeable organisms do have O_2 transport proteins and intracellular O_2 -binding proteins, but in addition, they need to implement diverse strategies to deal with changing O_2 . These include searching for microaerophilic or anaerobic environments. Arthropoda, the most abundant and widely distributed phylum on Earth, are oxyconformers [17]; it comprises subphyla Chelicerata (spiders), Myriapoda (centi- and millipedes), Hexapoda (Insects) and Crustacea, all of them protected by an exoskeleton. Nonaquatic insects possess a hard waterproof cuticle and branched invaginated tubules forming a specialized respiratory structure that works well at constant

$[O_2]$. Aquatic organisms, including most of the crustacea, are exposed to highly variant $[O_2]$, which may be 26 times lower than in the atmosphere [18, 19]. In water, $[O_2]$ varies with temperature, depth, mechanical aeration and tidal movements. Only few invertebrates (Plathelmythes, Nematoda, Molluska, Anellida and Sypuncula) have been thoroughly studied in regard to their mechanisms to deal with fluctuating $[O_2]$ [20, 21]. Remarkably, very few studies on Crustacea are available.

Environment	O_2 concentration (μM)	References
Atmosphere	1000m ASL 256.0 Sea level 1028.0	[88]
Alveoles	143.0	[89]
Arteries	123.0 <i>Hb bound</i> 120.5 <i>Not bound</i> 2.5	[89] [90]
Capillaries	130.0	[89]
Interstitial fluid	55.0	[89]
Tissue cells	31.0	[89]
Veins	59.0	[89]
Mitochondria	Minimal for coupling 0.1 Minimal reported 20.0	[91]
Distilled water	223.0	[92]
Sea water	Surface 198-397.0 250.0 MOZ < 20.0	[93] [34] [94]
Estuaries	Surface 375.0 Bottom 62.5	[95] [96]

Oxygen concentrations reported were modified from partial pressures to micromolar concentration (μM) using Henry's law at 310.15K ASL (above sea level).

Table 1. Oxygen concentrations in different environments.

In order to control the release of ROS oxyconformers reduce aerobic activity during hypoxia/anoxia cycles, marine crustaceans display different responses to hypoxia/anoxia. To avoid hyperoxygenated or anoxic waters, crustaceans migrate between open sea and coastal lagoons (Figure 2), or migrate vertically through the water column to flee the O_2 -minimum zone (OMZ) and into $[O_2]$ compatible with their metabolic needs [22, 23]. Some shrimp species, such as the burrowing thalassinids *Upogebia major* and *Callianassa japonica*, which commonly inhabit the extremely hypoxic or even anoxic intertidal flats, can reduce their respiratory rate in dugout burrows, surviving up to 5 h of anoxia for *U. major* and 19 h for *C. japonica* [24]. *Artemia franciscana* is well known for its high tolerance to anoxia; the embryos of this species survive without O_2 for years through the complete depression of their metabolic rates [25, 26]. Metabolic rate depression is also observed in ectotherms, which lower their mitochondrial activity in function of temperature adjusting their O_2 consumption machinery accordingly [27]. However, it is not clear how mitochondria from oxyconformers respond to hypoxia, how respiratory activity adapts to reduced metabolic rates and how the cellular redox balance and energetic homeostasis are preserved [28, 29].

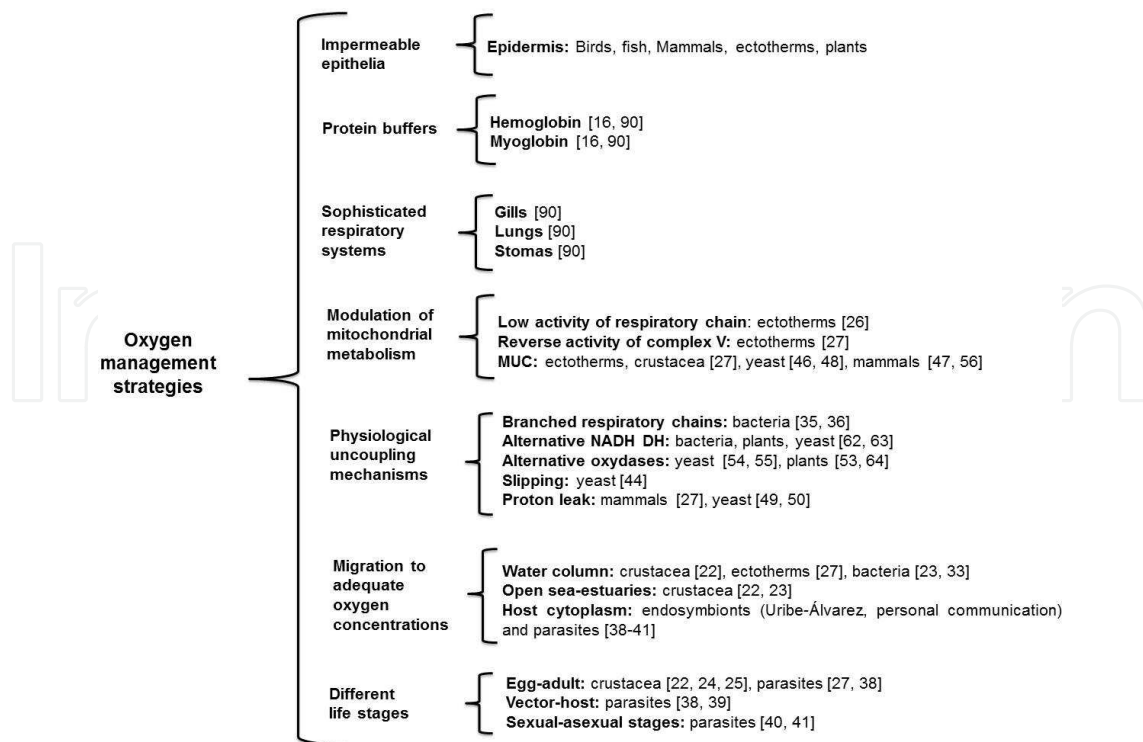


Figure 1. Oxygen management strategies in different organisms. Organisms need to adapt to the O_2 concentration in the environment. Therefore, either they move to environments with adequate O_2 or they engineer different mechanisms to process O_2 at varying rates (electron transport chain (ETC) activity, mitochondrial unspecific channels (MUC), uncoupling proteins (UCPs). Additionally, oxyregulators have developed O_2 -excluding mechanisms such as impermeable epithelia, external respiratory systems (lungs, gills, stomas) and O_2 -transporting proteins (hemoglobin, myoglobin).

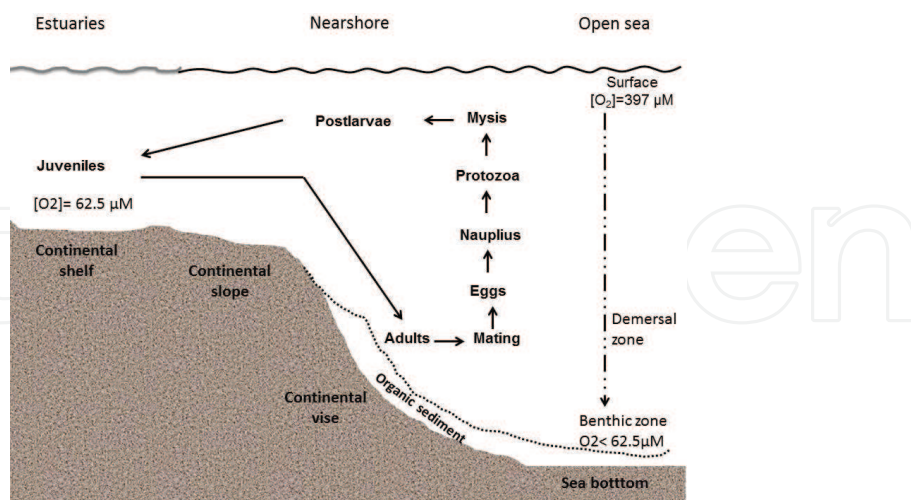


Figure 2. Migration of shrimp during their life cycle. Shrimp spend most of their life in the open sea, where they mate and lay eggs which hatch and undergo different larval stages (Nauplius, Protozoa, Mysis). Once in the postlarval stage, they travel to estuaries where they mature reaching the juvenile stage, and burying themselves in the sand for long periods. Once maturity is reached, they begin the cycle again returning to the open sea. This migration pattern takes shrimp to waters with widely different O_2 concentrations.

Among unicellular organisms, diverse yeast species can survive at almost any $[O_2]$. *Saccharomyces cerevisiae* can thrive at very low $[O_2]$ through fermentation, although it does possess a facultative aerobic metabolism. The anaerobic metabolism of *S. cerevisiae*, *D. hansenii* and other yeast species is the basis for the fermentation industry of bread, wine and cheese. For example, during wine fermentation, *S. cerevisiae* produces large amounts of ethanol, while *D. hansenii* produces volatile products conferring the characteristic aroma of wine [30]. Also, *S. cerevisiae* participates in cheese fermentation, whereas *D. hansenii* protects against other filamentous fungi during ripening [31, 32]. Yeast and other organisms have developed diverse systems to detoxify oxygen through physiological uncoupling and these are discussed later.

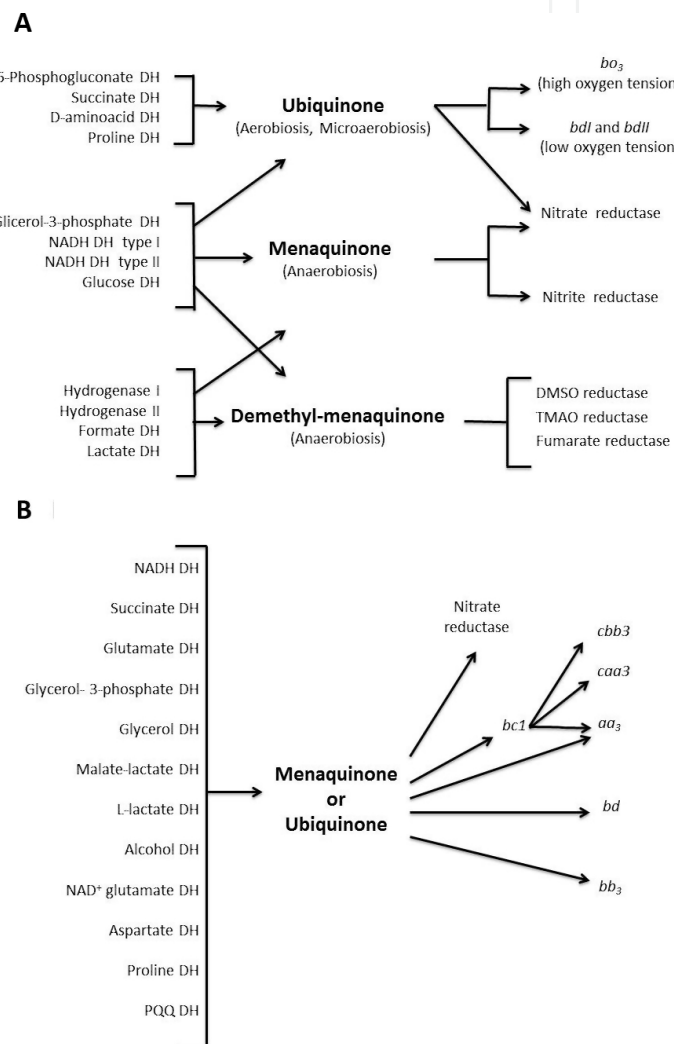


Figure 3. Diversity of bacterial respiratory chains at different $[O_2]$. **A.** The respiratory chain from *Escherichia coli* during aerobiosis, micro-aerobiosis and anaerobiosis. Modified from [35, 36]. Ubiquinone is expressed at high $[O_2]$ and NADH DH type II is overexpressed as compared to the NADH DH type I, which in turn is expressed at low $[O_2]$. The major final oxidase is cytochrome *bo*. During anaerobiosis, the respiratory chain in *Escherichia coli* succinate dehydrogenase is not expressed, whereas fumarate reductase or nitrate reductase may be the final electron acceptors. **B.** Hypothetical respiratory chain of *Wolbachia pipiensis* constructed from BLAST and genome sequences reported in [76, 77]. At high $[O_2]$ cytochrome, *bc1* and different cytochrome oxidases are expressed. Under microaerobic conditions, cytochrome *bd* is expressed. Then, under anaerobiosis, nitrate reductase is expressed.

Many bacteria are facultative. Among these, *Escherichia coli* is a very illustrative representative that may thrive both in microaerobic environments such as the intestinal lumen and in the external environment in a wide range of $[O_2]$. Bacteria respond to environmental $[O_2]$ variations or other conditions such as the need to fixate N_2 [33, 34] by varying the composition of their branched respiratory chains (**Figure 3A**), which vectorially transport from 0 to 10 protons, as many as those in orthodox respiratory chains [35, 36]. Still, when motile, bacteria will swim toward environments containing the ideal $[O_2]$.

Obligate endosymbionts, such as *R. prowazekii*, *Wolbachia* sp. or *Sodalis*, live in cytoplasmic vacuoles of multicellular organisms. The cytoplasm is a microaerophilic environment equipped with O_2 -consuming organelles and ROS-detoxifying enzymes. Remarkably, most endosymbionts contain a respiratory chain that at least in the case of *Wolbachia* seems to aid host mitochondria to deplete intracellular O_2 (**Figure 3B**).

Many parasites exhibit various life-cycle stages, which have different sensitivities to ROS engineered to endure attacks from macrophages. *Leishmania* sp. undergoes a relatively simple life cycle with two stages: the flagellated mobile promastigote living in the gut of the sand fly vector and the intracellular amastigote within phagolysosomal vesicles of the vertebrate host macrophage [37]. Promastigotes contain respiratory complexes I, II, III and IV, while it is not clear whether amastigotes possess an oxidative phosphorylation (OxPhos) machinery. Strikingly, amastigotes exhibit a succinate-dependent, uncoupler-sensitive transmembrane potential. Differences in sensitivity to oxidants are also observed between them, *in vitro*, promastigotes are more resistant to H_2O_2 than amastigotes [38].

In the bloodstream, *Trypanosoma cruzi* trypomastigotes contain high complex II and III activities. Interestingly, cytochrome c oxidase (COX) activity decreases creating an “electron bottleneck” that favors an increase in electron leakage, thus overproducing ROS. The oxidative preconditioning provided by this mechanism confers protection to bloodstream trypomastigotes against ROS liberated by the host immune system. These changes in mitochondrial activity, during the *T. cruzi* life cycle, are probably a key metabolic adaptation for survival in different hosts [39].

Malarial parasites are vulnerable to oxidative stress during their intraerythrocyte life stages. They contain the canonical respiratory chain (complex I, II, III and IV) plus an alternative electron transport pathway. Moreover, malarial mitochondria coordinate the biosynthesis of pyrimidine, heme and coenzyme Q [40]. *Plasmodium falciparum* possesses genes for two different superoxide dismutases (SOD), a cytosolic, Fe^{2+} -dependent, (SOD-1) expressed throughout the intraerythrocytic life of the parasite. The second, SOD-2, is mitochondrial and possesses a reminiscent apicoplast-targeting sequence. The host immune response to malaria involves phagocytosis and the production of nitric oxide and ROS that end up contributing to the pathology of the disease [41].

Regardless the organism studied, cytoplasmic $[O_2]$ can vary widely, so damage control is needed at two levels. Either O_2 is reduced independently of adenosine triphosphate (ATP) production in a process known as physiological uncoupling, or the ROS-handling enzymes are activated. We shall briefly describe only physiological uncoupling as many reviews on

ROS-handling enzymes, such as superoxide dismutase and catalase are found elsewhere [42, 43].

3. Physiological uncoupling as an O₂-depleting mechanism and prevents ROS production

Both in oxyconformers and in oxyregulators, once O₂ enters the cell it has to be reduced at a high rate. When ATP is needed the respiratory chain rapidly catalyzes this reduction. When there is energy surplus, O₂ consumption has to be uncoupled from ATP synthesis with the aim of preventing ROS overproduction [44]. A review on the physiological uncoupling mechanisms observed in mitochondria from different species of yeasts has been published recently [45]. Yeast mitochondrial uncoupling mechanisms may be (a) proton sinks, such as the mitochondrial unspecific channels [46–48] and the uncoupling protein (UCP) [49, 50], or (b) nonpumping redox alternative enzymes found in branched respiratory chains [51–55].

(a). Proton sinks: The opening of the mitochondrial permeability transition pore (MPTP) leads to mitochondrial uncoupling and to the activation of signaling events leading to apoptosis [56], which was first detected in mammalian mitochondria as a response to the disruption of intracellular calcium homeostasis. In crustaceans subjected to hypoxia, mitochondrial functions are downregulated [57, 58, 20] and there is an anoxia-triggered intracellular increase in both calcium and phosphate, while ATP production is inhibited, probably as a result of the opening of a MPTP. In *Artemia franciscana* [26] and in the ghost shrimp *Lepidophthalmus louisianensis* [59], the proteins needed to form the MPTP are present. However, whether these crustaceans possess MPTPs is to be defined. Both in crustacean mitochondria and in other known hypoxia-tolerant invertebrates (mussels, oysters, and cnidarians among others), the role of a putative MPTP is an interesting question.

(b). Branched respiratory chains: Bacteria do not exhibit a permeability transition. This seems to be a mitochondrial trait. Instead, bacteria (and many mitochondria) exhibit branched respiratory chains. Indeed, different species of mitochondria may exhibit from none to three alternative enzymes. In contrast, bacteria may contain as much as twenty electron entry ports and as many exits. Thus, in most prokaryotes, branched respiratory chains seem to be the mechanism of choice to maintain a high rate of O₂ consumption, while adjusting ATP production to the energy requirements of the cell. In this regard, the bioenergetic efficiency for each entry point is defined as the stoichiometry of H⁺ pumped per e⁻ traveling through the respiratory chain [60]. In addition, terminal oxidases are remarkably varied and their active site orientation, to the cytoplasm or to the periplasm determines their pumping efficiency [36].

Alternative oxidoreductases is the term designating all components of the respiratory chain different to the usual complexes I through IV. Most alternative oxidoreductases lack proton-pumping activity and may coexist with, or substitute for the respiratory proton-pumping complexes. Alternative enzymes catalyze the rapid, uncoupled flow of electrons towards O₂. Alternative NADH dehydrogenases may either substitute for (*S. cerevisiae*) or coexist with (bacteria, plants and diverse fungi) complex I [61, 62].

Alternative oxidases (AOXs) catalyze the oxidation of ubiquinol to quinone and the reduction of O₂ to H₂O in the absence of proton translocation [53]. Although highly represented among plants, fungi and protist species, animal AOXs have been predicted to exist only in Molluska, Nematoda and Chordata [63]. Recently, the number of phyla that probably possess AOX has increased including Placozoa, Porifera, Cnidaria, Annelida, Echinodermata, Hemichordata and Chordata. In some marine vertebrates, such as sipunculids, annelids (*Nereis pelagica*, and *Arenicola marina*) and in bivalves (*Arctica islandica*), AOX has been detected [64–66]. However, there are no confirmed reports for AOX in mitochondria from crustaceans [51]. In different plant and animal species, cells lacking AOX show an increased susceptibility to death due to H₂O₂, hypoxia and pathogens [67]. The ultimate decoupling of electron flow occurs when NADH dehydrogenases act in concert with alternative oxidases. The yeast *Yarrowia lipolytica* is a strict aerobic organism for which several biotechnological applications have been developed, such as in the cheese fermentation, obtention of extracellular enzymes [68], production of organic acids [69] and interconversion of fatty acids and alkenes [70]. In *Y. lipolytica*, metabolism occurs in a complex network between compartments, such as peroxisomes, endoplasmic reticulum, lipid bodies and mitochondria [69]. Mitochondria play an important role in ATP production, as well as in the maintenance of the NADH/NAD⁺ redox ratio [71]. The respiratory chain is composed of the classic complexes: I, II, III and IV, one alternative NADH dehydrogenase external (NADH2) [72] and two isoforms of AOX [73]. During the logarithmic growth phase, NADH2 interacts with supercomplexes III–IV channeling the electrons to oxygen, while pumping protons at both complex III and IV [74]. In contrast, during the stationary growth phase, electrons are directly transferred from alternative NDH2 to AOX, thus uncoupling oxidative phosphorylation and decreasing the production of ROS [54, 55]. This is a very illustrative example, which suggests that physiological uncoupling systems are present in all living organisms. Furthermore, in *Y. lipolytica*, both proton sinks and branched chains are observed [50, 54].

Bacterial cytochrome-containing oxidases are many. These enzymes are differentially expressed in response to different oxygen concentrations and on whether an organism is an obligate aerobic or a facultative species. In addition, oxidases may coexist depending on the species under study and they may play different roles in the cell [75]. In *E. coli*, different oxidases are expressed depending on [O₂]. At high O₂, bo3 is expressed, while at low O₂, bd cytochromes are observed. Furthermore, *E. coli* is capable of growth under anaerobiosis, using respiratory chains reminiscent of the early Earth that use ubiquinone, menaquinone or demethylmenaquinone to donate electrons to enzymes that use terminal acceptors different to O₂ (**Figure 3A**) [35, 36]. Branched respiratory chains provide the possibility of consuming O₂ without producing ATP. In the yeast *Y. lipolytica*, in the bacterium *E. coli* and probably in the Rickettsial *Wolbachia* sp., the arrangement of the respiratory chain varies such that when [O₂] is high, or ATP is needed, high proton pumping efficiency is observed. In contrast, factors such as arrival to the stationary phase or microaerophilic conditions probably trigger overexpression of the alternative NADH dehydrogenase and/or the AOX leading to the futile reduction of O₂ [61]. A possible arrangement of the respiratory chain of *Wolbachia* sp is illustrated (**Figure 3B**) where a large number of possible electron-donating enzymes reduce

menaquinone or ubiquinone that in turn reduce final electron-accepting enzymes that are expressed according to the presence of O₂ in the cytoplasm of the host [76, 77].

4. N-fixating bacteria are a special case

Nitrogen-fixating bacteria may be facultative as *Klebsiella pneumonia* or strict aerobics as *Azotobacter vinelandii* or *Gluconobacter diazotrophicus*. As they contain fragile, oxygen-sensitive nitrogen-fixating enzymes that need to be protected, these bacteria have developed many strategies to detoxify [O₂]. Thus, in N-fixating bacteria, both N-reductases and different oxidases are expressed: *A. vinelandii* contains a highly active respiratory chain and is able to adjust the expression of its three oxidases to a wide range of [O₂]. Among these, cytochrome *bd* has high O₂ affinity (KmO₂=5 μM) and becomes active during N fixation [15, 78–80]. Indeed, during N fixation the H⁺/O index is low, at 1 [81]. In *Ga. diazotrophicus* different periplasmic membrane enzymes such as glucose-, acetaldehyde- or ethanol-dehydrogenase reduce a quinone, which in turn donates its electrons to two different oxidases, *ba* which is coupled to ATP synthesis and *bb*₃ which is not coupled, but its role is to deplete O₂ in the vicinity of nitrogen reductases [82].

5. ROS detoxification

In spite of the production-prevention mechanisms outlined earlier, ROS may reach high concentrations, for example, during ischemia-reperfusion. The last line of defense is detoxification. Enzymes such as superoxide dismutases (SODs) and catalases deactivate ROS. SODs have been grouped on the basis of the metal cofactor, which can be Fe, Mn, Ni or Cu/Zn [83]. The Fe-SODs are mostly found in microaerophiles and anaerobes. Microorganisms in aerobic environments prefer Mn-SOD [84]. Catalase dismutates hydrogen peroxide to water plus O₂ [85]. Several genes capable of H₂O₂ dismutation evolved from ancestral genomes. The most abundant was heme-containing enzymes spread among bacteria, Archaea and Eukarya [86].

In *Clostridium acetobutylicum*, a strict anaerobic that survives little time when exposed to O₂, no catalases are found [87], and a function has yet to be found for the annotated SODs.

6. Conclusion

During the early paleoproterozoic period, a massive death toll resulted from a 10⁵ times rise in atmospheric O₂. In order to survive, organisms had to learn to cope with O₂ toxicity while profiting from the large energy release coupled to its reduction. Several O₂-management strategies are revised here. Among these is hiding away from O₂, moving to adequate O₂

concentrations or excluding O₂ with impermeable epithelia. Once O₂ enters the cell, other mechanisms are designed to handle it. Its reactivity is controlled by O₂-quenching proteins or by rapidly reducing it with specific oxidases. In order to avoid side reactions, the rate of reduction had to be kept at optimal pace, independently of ATP production and thus several mechanisms of physiological uncoupling of oxidative phosphorylation evolved. Physiological uncoupling was achieved either by opening proton sinks or by using O₂ independently of the proton gradient. Today, these mechanisms are expressed in many cells. Proton sinks include unspecific channels and uncoupling proteins, while proton gradient-independent consumption of O₂ involved alternative oxido-reductases found in the branched respiratory chains of fungi, plants and arthropods. In spite of the function of all these O₂-management machines, O₂ can still react unspecifically to form ROS, which destroy the cell through processes such as aging, apoptosis or necrosis. Once formed, ROS may still be eliminated by enzymes such as SOD and catalase, which are reviewed elsewhere [43] O₂ is a great source of energy for the cell, but its high toxicity has to be dealt with, through mechanisms that we are only beginning to understand.

Acknowledgements

Authors thank Ramón Méndez-Franco for technical assistance. Partially funded by the PAPIIT program and DGAPA/UNAM (grant IN202612). MRL, NLMG and CUA are CONACYT fellows enrolled in the Biochemistry Graduate Program at UNAM.

Declaration of Interest. The authors do not have any interests to disclose.

Author details

Mónica Rosas-Lemus¹, Cristina Uribe-Alvarez¹, Martha Contreras-Zentella², Luis Alberto Luévano-Martínez³, Natalia Chiquete-Félix¹, Norma Lilia Morales-García¹, Emilio Espinosa Simón¹, Adriana Muñoz-Almazán⁴, Edgardo Escamilla-Marván⁵ and Salvador Uribe-Carvajal^{1*}

1 Department of Molecular Genetics, Institute of Cellular Physiology, UNAM, CDMX, México

2 Department of Cellular Biology and Development, Institute of Cellular Physiology, UNAM, CDMX, México

3 Department of Biochemistry, Institute of Chemistry, U de São Paulo, São Paulo, SP, Brazil

4 Laboratory of Bioenergetics and Molecular Genetics CIAD, Hermosillo, Sonora, México

5 Posthumous paper

References

- [1] Lane N. Oxygen the molecule that made the world. Oxford: Oxford University Press; 2002. p. 384.
- [2] Sessions AL, Doughty DM, Welander PV, Summons RE, Newman DK. The continuing puzzle of the great oxidation event. *Current Biology*. 2009;19(14):R567–74.
- [3] Pavlov AA, Kasting JF. Mass-independent fractionation of sulfur isotopes in Archean sediments: strong evidence for an anoxic Archean atmosphere. *Astrobiology*. 2002;2(1):27–41.
- [4] Martin W, Rotte C, Hoffmeister M, Theissen U, Gelius-Dietrich G, Ahr S, et al. Early cell evolution, eukaryotes, anoxia, sulfide, oxygen, fungi first (?), and a tree of genomes revisited. *IUBMB Life*. 2003;55(4–5):193–204.
- [5] Nisbet EG, Sleep NH. The habitat and nature of early life. *Nature*. 2001;409(6823):1083–91.
- [6] Martin W, Muller M. The hydrogen hypothesis for the first eukaryote. *Nature*. 1998;392(6671):37–41.
- [7] Castresana J, Saraste M. Evolution of energetic metabolism: the respiration-early hypothesis. *Trends in Biochemical Sciences*. 1995;20(11):443–8.
- [8] Gray MW. Evolution of organellar genomes. *Current Opinion in Genetics & Development*. 1999;9(6):678–87.
- [9] Kurland CG, Andersson SG. Origin and evolution of the mitochondrial proteome. *Microbiology and Molecular Biology Reviews*. 2000;64(4):786–820.
- [10] Hellemond JJv, Klei Avd, Weelden SHv, Tielens AGM. Biochemical and evolutionary aspects of anaerobically functioning mitochondria. *Philosophical Transactions of the Royal Society of London Series B: Biological Sciences*. 2003;358(1429):205–15.
- [11] Mentel M, Martin W. Energy metabolism among eukaryotic anaerobes in light of Proterozoic ocean chemistry. *Philosophical Transactions of the Royal Society of London Series B, Biological Sciences*. 2008;363(1504):2717–29.
- [12] Hayes JM, Waldbauer JR. The carbon cycle and associated redox processes through time. *Philosophical Transactions of the Royal Society B: Biological Sciences*. 2006;361(1470):931–50.
- [13] Holland HD. The oxygenation of the atmosphere and oceans. *Philosophical Transactions of the Royal Society of London Series B, Biological Sciences*. 2006;361(1470):903–15.
- [14] Golblatt C, Lenton TM, Watson AJ. Bistability of atmospheric oxygen and the Great Oxidation. *Nature*. 2006;443(7112):683–6.

- [15] Poole RK, D'Mello R, Hill S, Ioannidis N, Leung D, Wu G. The oxygen reactivity of bacterial respiratory haemoproteins: oxidases and globins. *Biochimica et Biophysica Acta*. 1994;1187(2):226–31.
- [16] Hinton HE. Respiratory systems of insect egg shells. *Annual review of entomology*. 1969;14:343–68.
- [17] Hochachka PW, Somero GN. Biochemical adaptation: mechanism and process in physiological evolution. United States Of America: Oxford University Press; 2002. 467 p.
- [18] Hill RW, Wyse GA, Anderson M. Animal physiology. MA, USA: Sinauer Associates Inc. Publishers; 3rd Ed., 2012, P.799.
- [19] Abele D. Toxic oxygen: the radical life-giver. *Nature*. 2002;420(6911):27.
- [20] Martinez-Cruz O, Calderon de la Barca AM, Uribe-Carvajal S, Muhlia-Almazan A. The function of mitochondrial F(O)F(1) ATP-synthase from the whiteleg shrimp Litopenaeus vannamei muscle during hypoxia. *Comparative Biochemistry and Physiology Part B, Biochemistry & Molecular Biology*. 162(4):107–12.
- [21] Müller M, Mentel M, van Hellemond JJ, Henze K, Woehle C, Gould SB, et al. Biochemistry and evolution of anaerobic energy metabolism in eukaryotes. *Microbiology and Molecular Biology Reviews*. 2012;76(2):444–95.
- [22] Dall W, Hill BJ, Rothlisberg PC, Sharples DJ. The biology of the Penaeidae. *Advances in Marine Biology*; 1990. pp 489, 27. CSIRO Marine Laboratories, P.O. Box 120, Cleveland, Qld. 4163, Australia 1990.
- [23] Ekau W, Auel H, Pörtner HO, Gilbert D. Impacts of hypoxia on the structure and processes in pelagic communities (zooplankton, macro-invertebrates and fish). *Biogeosciences*. 2010;7(5):1669–99.
- [24] Mukai H, Koike I. Behavior and respiration of the Burrowing Shrimps Upogebia major (de Haan) and Callianassa japonica (de Haan). *Journal of Crustacean Biology*. 1984;4(2):191–200.
- [25] Clegg J. Embryos of Artemia franciscana survive four years of continuous anoxia: the case for complete metabolic rate depression. *Journal of Experimental Biology*. 1997;200(3):467–75.
- [26] Menze MA, Hutchinson K, Laborde SM, Hand SC. Mitochondrial permeability transition in the crustacean Artemia franciscana: absence of a calcium-regulated pore in the face of profound calcium storage. *American Journal of Physiology – Regulatory, Integrative and Comparative Physiology*. 2005;289(1):R68–76.
- [27] Galli GJ, Richards J. Mitochondria from anoxia-tolerant animals reveal common strategies to survive without oxygen. *Journal of Comparative Physiology B*. 2014;184(3):285–302.

- [28] Strahl J, Dringen R, Schmidt MM, Hardenberg S, Abele D. Metabolic and physiological responses in tissues of the long-lived bivalve *Arctica islandica* to oxygen deficiency. *Comparative Biochemistry and Physiology Part A, Molecular & Integrative Physiology*. 2011;158(4):513–9.
- [29] Buttemer WA, Abele D, Costantini D. From bivalves to birds: oxidative stress and longevity. *Functional Ecology*. 2010;24(5):971–83.
- [30] Rosi I, Vinella M, Domizio P. Characterization of beta-glucosidase activity in yeasts of oenological origin. *The Journal of Applied Bacteriology*. 1994;77(5):519–27.
- [31] Roostita R, Fleet GH. Growth of yeasts in milk and associated changes to milk composition. *International Journal of Food Microbiology*. 1996;31(1–3):205–19.
- [32] Eliskases-Lechner F, Ginzinger W, Rohm H, Tschager E. Raw milk flora affects composition and quality of Bergkäse. 1. Microbiology and fermentation compounds. *Lait*. 1999;79(4):385–96.
- [33] Baracchini O, Sherris JC. The chemotactic effect of oxygen on bacteria. *The Journal of Pathology and Bacteriology*. 1959;77(2):565–74.
- [34] Ulloa O, Canfield DE, DeLong EF, Letelier RM, Stewart FJ. Microbial oceanography of anoxic oxygen minimum zones. *Proceedings of the National Academy of Sciences of the United States of America*. 2012;109(40):15996–6003.
- [35] Ingledew WJ, Poole RK. The respiratory chains of *Escherichia coli*. *Microbiological Reviews*. 1984;48(3):222–71.
- [36] Unden G, Bongaerts J. Alternative respiratory pathways of *Escherichia coli*: energetics and transcriptional regulation in response to electron acceptors. *Biochimica et Biophysica Acta*. 1997;1320(3):217–34.
- [37] Chakraborty B, Biswas S, Mondal S, Bera T. Stage specific developmental changes in the mitochondrial and surface membrane associated redox systems of *Leishmania donovani* promastigote and amastigote. *Biochemistry Biokhimiia*. 2010;75(4):494–518.
- [38] Van Assche T, Deschacht M, da Luz RA, Maes L, Cos P. Leishmania-macrophage interactions: insights into the redox biology. *Free Radical Biology & Medicine*. 2011;51(2):337–51.
- [39] Gonçalves RL, Barreto RF, Polycarpo CR, Gadelha FR, Castro SL, Oliveira MF. A comparative assessment of mitochondrial function in epimastigotes and bloodstream trypomastigotes of *Trypanosoma cruzi*. *Journal of Bioenergetics and Biomembranes*. 2011;43(6):651–61.
- [40] Krungkrai J. The multiple roles of the mitochondrion of the malarial parasite. *Parasitology*. 2004;129(Pt 5):511–24.
- [41] Muller S. Redox and antioxidant systems of the malaria parasite *Plasmodium falciparum*. *Molecular Microbiology*. 2004;53(5):1291–305.

- [42] McCord JM, Keele BB, Jr., Fridovich I. An enzyme-based theory of obligate anaerobiosis: the physiological function of superoxide dismutase. *Proceedings of the National Academy of Sciences of the United States of America*. 1971;68(5):1024–7.
- [43] D'Autreux B, Toledano MB. ROS as signalling molecules: mechanisms that generate specificity in ROS homeostasis. *Nature Reviews Molecular Cell Biology*. 2007;8(10):813–24.
- [44] Kadenbach B. Intrinsic and extrinsic uncoupling of oxidative phosphorylation. *Biochimica et Biophysica Acta*. 2003;1604(2):77–94.
- [45] Guerrero-Castillo S, Araiza-Olivera D, Cabrera-Orefice A, Espinasa-Jaramillo J, Gutierrez-Aguilar M, Luevano-Martinez LA, et al. Physiological uncoupling of mitochondrial oxidative phosphorylation. Studies in different yeast species. *Journal of Bioenergetics and Biomembranes*. 2011;43(3):323–31.
- [46] Manon S, Roucou X, Guerin M, Rigoulet M, Guerin B. Characterization of the yeast mitochondria unselective channel: a counterpart to the mammalian permeability transition pore? *Journal of Bioenergetics Biomembranes*. 1998;30(5):419–29.
- [47] Bernardi P. The mitochondrial permeability transition pore: a mystery solved? *Frontiers in Physiology*. 2013;4:95.
- [48] Uribe-Carvajal S, Luevano-Martinez LA, Guerrero-Castillo S, Cabrera-Orefice A, Corona-de-la-Pena NA, Gutierrez-Aguilar M. Mitochondrial unselective channels throughout the eukaryotic domain. *Mitochondrion*. 2011;11(3):382–90.
- [49] Nicholls DG, Rial E. A history of the first uncoupling protein, UCP1. *Journal of Bioenergetics and Biomembranes*. 1999;31(5):399–406.
- [50] Luevano-Martinez LA, Moyano E, de Lacoba MG, Rial E, Uribe-Carvajal S. Identification of the mitochondrial carrier that provides *Yarrowia lipolytica* with a fatty acid-induced and nucleotide-sensitive uncoupling protein-like activity. *Biochimica et Biophysica Acta*. 2010;1797(1):81–8.
- [51] McDonald AE, Vanlerberghe GC, Staples JF. Alternative oxidase in animals: unique characteristics and taxonomic distribution. *Journal of Experimental Biology*. 2009;212(Pt 16):2627–34.
- [52] McDonald AE, Vanlerberghe GC. Alternative oxidase and plastoquinol terminal oxidase in marine prokaryotes of the Sargasso Sea. *Gene*. 2005;349:15–24.
- [53] Vanlerberghe GC, McIntosh L. Alternative oxydase: from gene to function. *Annual Review of Plant Physiology and Plant Molecular Biology*. 1997;48:703–34.
- [54] Guerrero-Castillo S, Cabrera-Orefice A, Vazquez-Acevedo M, Gonzalez-Halphen D, Uribe-Carvajal S. During the stationary growth phase, *Yarrowia lipolytica* prevents the overproduction of reactive oxygen species by activating an uncoupled mitochondrial respiratory pathway. *Biochimica et Biophysica Acta*. 2012;1817(2):353–62.

- [55] Cabrera-Orefice A, Chiquete-Felix N, Espinasa-Jaramillo J, Rosas-Lemus M, Guerrero-Castillo S, Pena A, et al. The branched mitochondrial respiratory chain from Debaryomyces hansenii: components and supramolecular organization. *Biochimica et Biophysica Acta*. 2013;1837(1):73–84.
- [56] Bernardi P. Mitochondrial transport of cations: channels, exchangers, and permeability transition. *Physiological Reviews*. 1999;79(4):1127–55.
- [57] Kwast KE, Hand SC. Acute depression of mitochondrial protein synthesis during anoxia: contributions of oxygen sensing, matrix acidification, and redox state. *The Journal of Biological Chemistry*. 1996;271(13):7313–9.
- [58] Eads BD, Hand SC. Mitochondrial mRNA stability and polyadenylation during anoxia-induced quiescence in the brine shrimp *Artemia franciscana*. *The Journal of Experimental Biology*. 2003;206(Pt 20):3681–92.
- [59] Holman JD, Hand SC. Metabolic depression is delayed and mitochondrial impairment averted during prolonged anoxia in the ghost shrimp, *Lepidophthalmus louisianensis* (Schmitt, 1935). *Journal of Experimental Marine Biology and Ecology*. 2009;376(2):85–93.
- [60] Borisov VB, Murali R, Verkhovskaya ML, Bloch DA, Han H, Gennis RB, et al. Aerobic respiratory chain of *Escherichia coli* is not allowed to work in fully uncoupled mode. *Proceedings of the National Academy of Sciences*. 2011;108(42):17320–4.
- [61] Kerscher SJ. Diversity and origin of alternative NADH:ubiquinone oxidoreductases. *Biochimica et Biophysica Acta (BBA) - Bioenergetics*. 2000;1459(2–3):274–83.
- [62] Büschges R, Bahrenberg G, Zimmermann M, Wolf K. Nadh: Ubiquinone oxidoreductase in obligate aerobic yeasts. *Yeast*. 1994;10(4):475–9.
- [63] McDonald A, Vanlerberghe G. Branched mitochondrial electron transport in the Animalia: presence of alternative oxidase in several animal phyla. *IUBMB Life*. 2004;56(6):333–41.
- [64] Tschischka K, Abele D, Portner HO. Mitochondrial oxyconformity and cold adaptation in the polychaete *Nereis pelagica* and the bivalve *Arctica islandica* from the Baltic and White Seas. *The Journal of Experimental Biology*. 2000;203(Pt 21):3355–68.
- [65] Buchner T, Abele D, Portner HO. Oxyconformity in the intertidal worm *Sipunculus nudus*: the mitochondrial background and energetic consequences. *Comparative Biochemistry and Physiology Part B, Biochemistry & Molecular Biology*. 2001;129(1):109–20.
- [66] Hildebrandt TM, Grieshaber MK. Three enzymatic activities catalyze the oxidation of sulfide to thiosulfate in mammalian and invertebrate mitochondria. *FEBS Journal*. 2008;275(13):3352–61.

- [67] Vanlerberghe GC, Robson CA, Yip JY. Induction of mitochondrial alternative oxidase in response to a cell signal pathway down-regulating the cytochrome pathway prevents programmed cell death. *Plant Physiology*. 2002;129(4):1829–42.
- [68] Beckerich JM, Boisrame-Baudevin A, Gaillardin C. *Yarrowia lipolytica*: a model organism for protein secretion studies. *International Microbiology: The Official Journal of the Spanish Society for Microbiology*. 1998;1(2):123–30.
- [69] Otto C, Holz M, Barth G. Production of Organic Acids by *Yarrowia lipolytica*. In: Barth G, editor. *Yarrowia lipolytica: Biotechnological Applications*. Berlin, Heidelberg: Springer Berlin Heidelberg; 2013. p. 137–49.
- [70] Darvishi Harzevili F. *Yarrowia lipolytica*: An Overview. Chapter 1, *Biotechnological Applications of the Yeast *Yarrowia lipolytica**. SpringerBriefs in Microbiology, Springer International Publishing; 2014. p. 1–16.
- [71] Kerscher S, Dröse S, Zwicker K, Zickermann V, Brandt U. *Yarrowia lipolytica*, a yeast genetic system to study mitochondrial complex I. *Biochimica et Biophysica Acta (BBA) – Bioenergetics*. 2002;1555(1–3):83–91.
- [72] Kerscher SJ, Okun JG, Brandt U. A single external enzyme confers alternative NADH:ubiquinone oxidoreductase activity in *Yarrowia lipolytica*. *Journal of Cell Science*. 1999;112(Pt 14):2347–54.
- [73] Medentsev AG, Arinbasarova AY, Golovchenko NP, Akimenko VK. Involvement of the alternative oxidase in respiration of *Yarrowia lipolytica* mitochondria is controlled by the activity of the cytochrome pathway. *FEMS Yeast Research*. 2002;2(4):519–24.
- [74] Guerrero-Castillo S, Vazquez-Acevedo M, Gonzalez-Halphen D, Uribe-Carvajal S. In *Yarrowia lipolytica* mitochondria, the alternative NADH dehydrogenase interacts specifically with the cytochrome complexes of the classic respiratory pathway. *Biochimica et Biophysica Acta*. 2009;1787(2):75–85.
- [75] Cook GM, Poole RK. Oxidase and periplasmic cytochrome assembly in *Escherichia coli* K-12: CydDC and CcmAB are not required for haem-membrane association. *Microbiology*. 2000;146(Pt 2):527–36.
- [76] Wu M, Sun LV, Vamathevan J, Riegler M, Deboy R, Brownlie JC, et al. Phylogenomics of the reproductive parasite *Wolbachia pipiensis* wMel: a streamlined genome overrun by mobile genetic elements. *PLoS Biology*. 2004;2(3):E69.
- [77] Klasson L, Walker T, Sebaihia M, Sanders MJ, Quail MA, Lord A, et al. Genome evolution of *Wolbachia* strain wPip from the *Culex pipiens* group. *Molecular Biology and Evolution*. 2008;25(9):1877–87.
- [78] Haddock BA, Jones CW. Bacterial respiration. *Bacteriological Reviews*. 1977;41(1):47–99.

- [79] Jones K. Acetilene reduction by mats of blue-green algae in sub-tropical grassland: possible contribution by other micro-organisms. *New Phytologist*. 1977;78(2):437–40.
- [80] Ng TCN, Laheri AN, Maier RJ. Cloning, sequencing, and mutagenesis of the cytochrome c4 gene from *Azotobacter vinelandii*: characterization of the mutant strain and a proposed new branch in the respiratory chain. *Biochimica et Biophysica Acta (BBA) – Bioenergetics*. 1995;1230(3):119–29.
- [81] Bertsova YV, Bogachev AV, Skulachev VP. Two NADH:ubiquinone oxidoreductases of *Azotobacter vinelandii* and their role in the respiratory protection. *Biochimica et Biophysica Acta*. 1998;1363(2):125–33.
- [82] González PJ, Correia C, Moura I, Brondino CD, Moura JJJG. Bacterial nitrate reductases: molecular and biological aspects of nitrate reduction. *Journal of Inorganic Biochemistry*. 2006;100(5–6):1015–23.
- [83] Whittaker MM, Whittaker JW. A glutamate bridge is essential for dimer stability and metal selectivity in manganese superoxide dismutase. *The Journal of Biological Chemistry*. 1998;273(35):22188–93.
- [84] Cannio R, Fiorentino G, Morana A, Rossi M, Bartolucci S. Oxygen: friend or foe? Archaeal superoxide dismutases in the protection of intra- and extracellular oxidative stress. *Frontiers in Bioscience: A Journal and Virtual Library*. 2000;5:D768–79.
- [85] Klotz MG, Loewen PC. The molecular evolution of catalatic hydroperoxidases: evidence for multiple lateral transfer of genes between prokaryota and from bacteria into eukaryota. *Molecular Biology and Evolution*. 2003;20(7):1098–112.
- [86] Zamocky M, Furtmuller PG, Obinger C. Evolution of catalases from bacteria to humans. *Antioxidants & Redox Signaling*. 2008;10(9):1527–48.
- [87] Nölling J, Breton G, Omelchenko MV, Makarova KS, Zeng Q, Gibson R, et al. Genome sequence and comparative analysis of the solvent-producing bacterium *Clostridium acetobutylicum*. *Journal of Bacteriology*. 2001;183(16):4823–38.
- [88] Peacock AJ. ABC of oxygen: oxygen at high altitude. *British Medical Journal*. 1998;317(7165):1063–6.
- [89] Hall JE, Guyton AC. Unit VII Respiration. In: Hall J, editor. *Textbook of Medical Physiology*. 12. Philadelphia, PA, USA: Elsevier; 2012.
- [90] Popel AS. Theory of oxygen transport to tissue. *Critical Reviews in Biomedical Engineering*. 1989;17(3):257–321.
- [91] Wilson DF, Rumsey WL, Green TJ, Vanderkooi JM. The oxygen dependence of mitochondrial oxidative phosphorylation measured by a new optical method for measuring oxygen concentration. *The Journal of Biological Chemistry*. 1988;263(6):2712–8.

- [92] Geng M, Duan Z. Prediction of oxygen solubility in pure water and brines up to high temperatures and pressures. *Geochimica et Cosmochimica Acta*. 2010;74(19):5631–40.
- [93] Chapelle G, Peck LS. Amphipod crustacean size spectra: new insights in the relationship between size and oxygen. *Oikos*. 2004;106(1):167–75.
- [94] Beman JM, Carolan MT. Deoxygenation alters bacterial diversity and community composition in the ocean's largest oxygen minimum zone. *Nature Communications*. 2013;4:2705.
- [95] Borsuk ME, Stow CA, Luettich Jr RA, Paerl HW, Pinckney JL. Modelling oxygen dynamics in an intermittently stratified estuary: estimation of process rates using field data. *Estuarine, Coastal and Shelf Science*. 2001;52(1):33–49.
- [96] Engle V, Summers JK. Refinement, validation, and application of a benthic condition index for Northern Gulf of Mexico estuaries. *Estuaries*. 1999;22(3):624–35.

Role of the Sln1-phosphorelay pathway in the response to hyperosmotic stress in the yeast *Kluyveromyces lactis*

Miriam Rodríguez-González,^{1#} Laura Kawasaki,^{1#}
 Nancy Velázquez-Zavala,¹ Eunice Domínguez-Martín,¹
 Abraham Trejo-Medecigo,¹ Natalia Martagón,¹
 Emilio Espinoza-Simón,² Araceli Vázquez-Ibarra,¹
 Laura Ongay-Larios,³ Dimitris Georgellis,¹
 Eulàlia de Nadal,⁴ Francesc Posas⁴ and
 Roberto Coria  ^{1*}

¹Departamento de Genética Molecular, Instituto de Fisiología Celular, Universidad Nacional Autónoma de México, México, D.F., México.

²Departamento de Bioquímica, Instituto de Fisiología Celular, Universidad Nacional Autónoma de México, México, D.F., México.

³Unidad de Biología Molecular, Instituto de Fisiología Celular, Universidad Nacional Autónoma de México, México, D.F., México.

⁴Cell Signaling Research Group, Departament de Ciències Experimentals i de la Salut, Universitat Pompeu Fabra, Barcelona, E-08003, Spain.

Summary

The *Kluyveromyces lactis* SLN1 phosphorelay system includes the osmosensor histidine kinase Sln1, the phosphotransfer protein Ypd1 and the response regulator Ssk1. Here we show that *K. lactis* has a functional phosphorelay system. *In vitro* assays, using a heterologous histidine kinase, show that the phosphate group is accepted by KIYpd1 and transferred to KISsk1. Upon hyperosmotic stress the phosphorelay is inactivated, KIYpd1 is dephosphorylated in a KISln1 dependent manner, and only the version of KISsk1 that lacks the phosphate group interacts with the MAPKKK KISsk2. Interestingly, inactivation of the KIPtp2 phosphatase in a Δ Klsln1 mutant did not lead to KIHog1 constitutive phosphorylation. KIHog1 can replace ScHog1p and activate the hyperosmotic response in *Saccharomyces cerevisiae*, and when ScSln1 is inactivated, KIHog1 becomes phosphorylated and induces cell lethality. All these observations indicate that the phosphorelay

Accepted 7 March, 2017. *For correspondence. E-mail: rcoria@ifc.unam.mx; Tel. (+52) 55 56 22 56 52; Fax (+52) 55 56 22 56 52.
 #These authors contributed equally to this work.

negatively regulates KIHog1. Nevertheless, in the absence of KISln1 or KIYpd1, no constitutive phosphorylation is detected and cells are viable, suggesting that a strong negative feedback that is independent of KIPtp2 operates in *K. lactis*. Compared with *S. cerevisiae*, *K. lactis* has only a moderate accumulation of glycerol and fails to produce trehalose under hyperosmotic stress, indicating that regulation of osmolyte production is different in *K. lactis*.

Introduction

The HOG pathway from *Saccharomyces cerevisiae* consists of two branches (SHO1 and SLN1) that sense osmotic changes in the environment. The Sho1 branch contains one scaffold protein localized to the plasma membrane (Sho1). Sho1 recruits Pbs2 (Maeda *et al.*, 1995; Reiser *et al.*, 2000), which is also a scaffold protein with MAPKK activity (Posas and Saito, 1997). Several other proteins, including Ste11 (MAPKKK), Ste50, Ste20, Cla4 and Cdc42 are needed to activate Pbs2 in the SHO1 branch (Saito and Posas, 2012). The SLN1 branch consists of a phosphorelay system that is analogous to bacterial two-component systems. It is composed of a hybrid histidine sensor kinase, Sln1, an intermediate phosphotransfer protein, Ypd1, and two response regulators, Ssk1 and Skn7. Sln1 is distributed uniformly throughout the plasma membrane. At its N- terminus, Sln1 has two transmembrane segments connected by an extracellular loop (Ostrander and Gorman, 1999). In isosmotic conditions, the kinase domain of Sln1 is catalytically active. It appears that the active form of Sln1 is dimeric (Ostrander and Gorman, 1999), which suggests that activation is promoted by trans-autophosphorylation. The His-P residue of the kinase domain donates the phosphoryl group to an aspartate residue located in the C-terminus receiver domain (Saito and Posas, 2012). The phosphoryl group of Sln-Asp-P is then transferred to the intermediate phosphotransfer protein, Ypd1, which is a cytoplasmic protein that contains a histidine phosphotransfer domain (Hpt). The histidine residue located in the Hpt domain is the acceptor of the phosphoryl group, which in turn is delivered to an aspartate residue of the response regulator. In the cytosol

and under isosmotic conditions, Ypd1 transfers the phosphoryl group to the response regulator Ssk1. Ssk1 phosphorylation by Ypd1 under isosmotic conditions renders Ssk1 inactive, which indicates that the phosphorelay plays a negative role in the hyperosmotic response (Posas *et al.*, 1996). Under hyperosmotic stress, turgor pressure decreases, inhibiting Sln1 kinase with subsequent dephosphorylation of Ssk1 (Reiser *et al.*, 2003). Unphosphorylated Ssk1 may bind and promote autophosphorylation of the redundant MAPKKKs Ssk2 or Ssk22 (Posas and Saito, 1998; Horie *et al.*, 2008). These proteins in turn phosphorylate and activate the scaffold MAPKK Pbs2, which finally phosphorylates and activates MAPK Hog1. Phosphorylated Hog1 is imported into the nucleus, where it regulates transcription and cell cycle progression (Gustin, *et al.*, 1998; Clotet and Posas, 2007; de Nadal and Posas, 2015). Iso-osmotic conditions keep the Sln1 phosphorelay system active and therefore Hog1 remains unphosphorylated. Permanent inactivation of Sln1 and/or Ypd1 induces constitutive Hog1 phosphorylation and ultimately cell lethality through uncontrolled Hog1 activity (Maeda *et al.*, 1994; Vendrell *et al.*, 2011).

The mechanisms to signal stress conditions in other yeast species have diverged significantly. For instance, the fission yeast *Schizosaccharomyces pombe* has a phosphorelay system composed of three cytosolic sensor kinases, including Mak1, Mak2 and Mak3, one phosphotransfer protein, Mpr1, and two response regulators, Mcs4 and Prr1 (Santos and Shiozaki, 2001). These proteins are connected to Sty1, which plays a role analogous to Hog1. Although a variety of stress conditions may activate the STY1 pathway (George *et al.*, 2007), the pathway seems to be dedicated mainly to the adaptation to oxidative stress (Degols *et al.*, 1996). In contrast to *S. cerevisiae*, null mutations that eliminate sensor kinases are viable but result in early entry into the mitotic phase of the cell cycle (Aoyama *et al.*, 2001; Nakamichi *et al.*, 2002). In addition, mutants of the Mpr1 phosphotransfer protein are viable but the cell shows a stubby phenotype (Aoyama *et al.*, 2000).

Although *Candida albicans* is more closely related to *S. cerevisiae* than *S. pombe*, the phosphorelay system is mainly implicated in the detection of oxidative stress (Santos and Shiozaki, 2001; Chauhan *et al.*, 2003). *C. albicans* contains three different histidine kinases, Sln1, which is homologous to *S. cerevisiae* Sln1 (Nagahashi *et al.*, 1998), Chk1 which is homologous to Mak2 and Mak3 from *S. pombe* (Calera and Calderone, 1999a), and Nik1, which seems to be more closely related to the histidine kinase Nik1 from *Neurospora crassa*, which was implicated in osmosensing (Alex *et al.*, 1998; Nagahashi *et al.*, 1998). *C. albicans* contains one phosphotransfer protein, Ypd1 (Calera *et al.*, 2000a), and three response regulators, Ssk1 (Calera and Calderone, 1999b), Skn7

(Singh *et al.*, 2004), and Srr1 (Desai *et al.*, 2011). Inactivation of phosphorelay components in *C. albicans* does not affect cell viability but significantly reduces virulence (Yamada-Okabe *et al.*, 1999; Calera *et al.*, 2000b).

Kluyveromyces lactis contains a similar repertoire of proteins dedicated to respond to hyperosmotic stress (Krantz *et al.*, 2006); however, it diverged before the genome duplication that gave rise to *Saccharomyces* species (Wolfe and Shields, 1997), therefore *K. lactis* displays lower gene redundancy. MAPKKK Ssk22, which is not present in the *K. lactis* genome, is a good example of that lower redundancy (Krantz *et al.*, 2006). When *K. lactis* cells are exposed to hyperosmotic stress the KIHog1 is phosphorylated and accumulated in the nucleus (Kawasaki *et al.*, 2008; Velázquez-Zavala *et al.*, 2015). KIHog1 activation minimally depends on the activity of a SHO1 branch consisting of the transmembrane protein KISho1, the PAK Ste20, the MAPKKK KISte11 and its adaptor protein KISte50, which are connected to the MAPKK KIPbs2. KIPbs2 is essential for activation by phosphorylation of MAPK KIHog1 (Velázquez-Zavala *et al.*, 2015). In addition, genomic analysis has determined that *K. lactis* contains a phosphorelay system that is composed of the histidine kinase sensor KISln1, the phosphotransfer protein KIYpd1, and the response regulator KISSk1. This system is presumably connected to the MAPKK KIPbs2 via the MAPKKK KISsk2 (Krantz *et al.*, 2006). In this study, we describe the participation of the phosphorelay system in the response of *K. lactis* cells to hyperosmotic stress and discuss differences and similarities with the model yeast *S. cerevisiae*.

Results

Disruption of KISln1, KIYPD1 or KISSk1 genes produces viable cells with no sensitivity to high osmotic stress

In *S. cerevisiae*, inactivation of either the histidine-kinase Sln1 or the phosphotransfer protein Ypd1 induces cell lethality (Maeda *et al.*, 1994; Posas *et al.*, 1996). This lethality is due to constitutive activation of Hog1, which generates cell growth arrest and uncontrolled glycerol production and promotes cell death that resembles apoptosis. The high conservation of the phosphorelay proteins in *K. lactis* prompted us to study the effects of the mutation of the proteins involved in this system. We constructed *Klsln1* and *Klypd1* disruption mutants in diploid cells by introducing an *URA3* cassette to generate the disrupted alleles. Surprisingly, meiotic segregation of diploid cells transfected with both *sln1::URA3* and *YPD1::URA3* constructs produced four viable spores, two of which were *URA3⁺* (Supporting Information Fig. 1). Southern blot analysis showed that meiotic segregants **b** and **c** carried

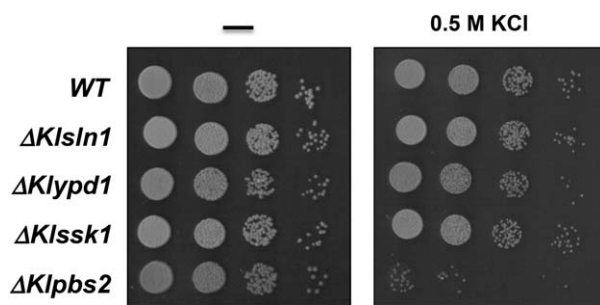


Fig. 1. Hyperosmotic stress does not affect growth of cells lacking proteins of the *K. lactis* phosphorelay system. Cells of the indicated strains were grown overnight at 30°C in liquid YPD, collected, washed and diluted in fresh medium. Cells were grown until OD₆₀₀ was 0.4 and spotted as 10-fold serial dilutions onto YPD with or without 0.5 M KCl. The plates were incubated at 30°C for 48 h and photographed.

the disrupted allele for *KISLN1* and meiotic clones **a** and **c** carried disrupted *KIYPD1*. This outcome shows that in contrast to *S. cerevisiae*, inactivation of either *KISln1* or *KIYPD1* does not induce cell lethality in *K. lactis*. In addition, we tested the Δ *KISln1* and Δ *Klypd1* haploid mutants by their ability to grow under high osmotic conditions. While inactivation of the scaffold kinase *KIPbs2* resulted in severe growth deficiency in high salt medium, we found that Δ *KISln1* and Δ *Klypd1* mutants showed a similar resistance to 0.5 M KCl as wild type cells when the mutants were tested in a spot dilution assay (Fig. 1). Finally, we disrupted the *KISSK1* gene, which encodes the response regulator in *K. lactis*, and found that, similar to the above results, the disruption did not affect growth in high salt media (Fig. 1). These results indicate that elimination of both *KISln1* and *KIYPD1* does not affect the viability of *K. lactis* haploid cells.

KIHog1 is not constitutively phosphorylated in the Δ *KISln1*, Δ *Klypd1* and Δ *KISln1* Δ *Klptp2* mutants

It has been shown that Hog1p becomes phosphorylated and constitutively active when the phosphorelay system is inactivated in *S. cerevisiae* (Maeda *et al.*, 1994; Posas *et al.*, 1996), and the lack of Sln1 or Ypd1 is lethal for the cells. Therefore, we decided to analyze the phosphorylation status of *KIHog1* in the Δ *KISln1* and Δ *Klypd1* mutants. First, we established the conditions in which *KIHog1* could be phosphorylated by a hyperosmotic treatment. When *K. lactis* wild type cells were exposed to increasing KCl concentrations for 5 min, *KIHog1* became barely phosphorylated at 0.1 M KCl. Robust phosphorylation was reached at approximately 0.2 M KCl, and did not seem to vary much with higher concentrations (Fig. 2 panel A). When cells were exposed to 0.4 M KCl in a time course, *KIHog1* phosphorylation reached its maximum within 5 min and then gradually decreased (Fig. 2 panel B).

Then, we tested whether *KIHog1* was phosphorylated in the *K. lactis* mutants that lacked the phosphorelay components *KISln1*, *KIYPD1* and *KISSK1*. We did not observe constitutive phosphorylation of *KIHog1* in the Δ *KISln1*, Δ *Klypd1* and Δ *KISSK1* mutants under iso-osmotic conditions (Fig. 3 panel A). Interestingly, *KIHog1* phosphorylation was induced in the mutants that lacked the phosphorelay system after a treatment with high osmolarity (Fig. 3 panel A). For comparison, we tested *S. cerevisiae* Hog1 phosphorylation in a strain carrying a thermo-sensitive allele of *SLN1* (*sln1-ts*) (Maeda *et al.*, 1994). When the cells were incubated in an iso-osmotic medium at 37°C for 30 min (which inactivated the *sln1-ts*), *ScHog1* became phosphorylated and this phosphorylation did not vary when a hyperosmotic treatment was used (Fig. 3 panel B). Taken together, these observations indicate that in contrast to *S. cerevisiae*, *KIHog1* is not constitutively phosphorylated in *K. lactis* cells when *KISln1* or *KIYPD1* have been inactivated.

In *S. cerevisiae* cells, negative feedback of the HOG signalling system is obtained by Hog1 dephosphorylation (Martín *et al.*, 2005). The tyrosine phosphatases, Ptp2 and Ptp3, inactivate Hog1 by dephosphorylation of Tyr-176. Ptp2 is found in the nucleus and exerts a major feedback on Hog1 activity (Mattison and Ota, 2000). To analyse the participation of KIPtp2 in the regulation of the HOG signalling pathway in *K. lactis*, we constructed the single Δ *Klptp2* and the double Δ *KISln1* Δ *Klptp2*

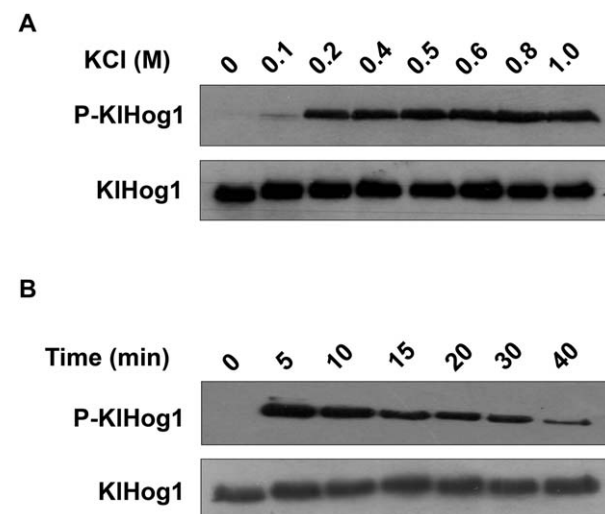


Fig. 2. *K. lactis* Hog1p phosphorylation kinetics upon hyperosmotic stress. Wild type cells were grown in YPD medium until the OD₆₀₀ reached 0.4. Cells were washed, suspended in fresh YPD medium and treated or not treated with KCl. Cells were lysed, and 20 µg of protein extracts were loaded in each line and subjected to SDS-PAGE, transferred to nylon membranes, and probed with anti-p38 antibody (P-KIHog1). Membranes were stripped and re-probed with anti-Hog1 antibody. **(A)** KIHog1 phosphorylation after treatment for 5 min with the indicated KCl concentrations. **(B)** KIHog1 phosphorylation after treatment with 0.4 M KCl for the indicated times.

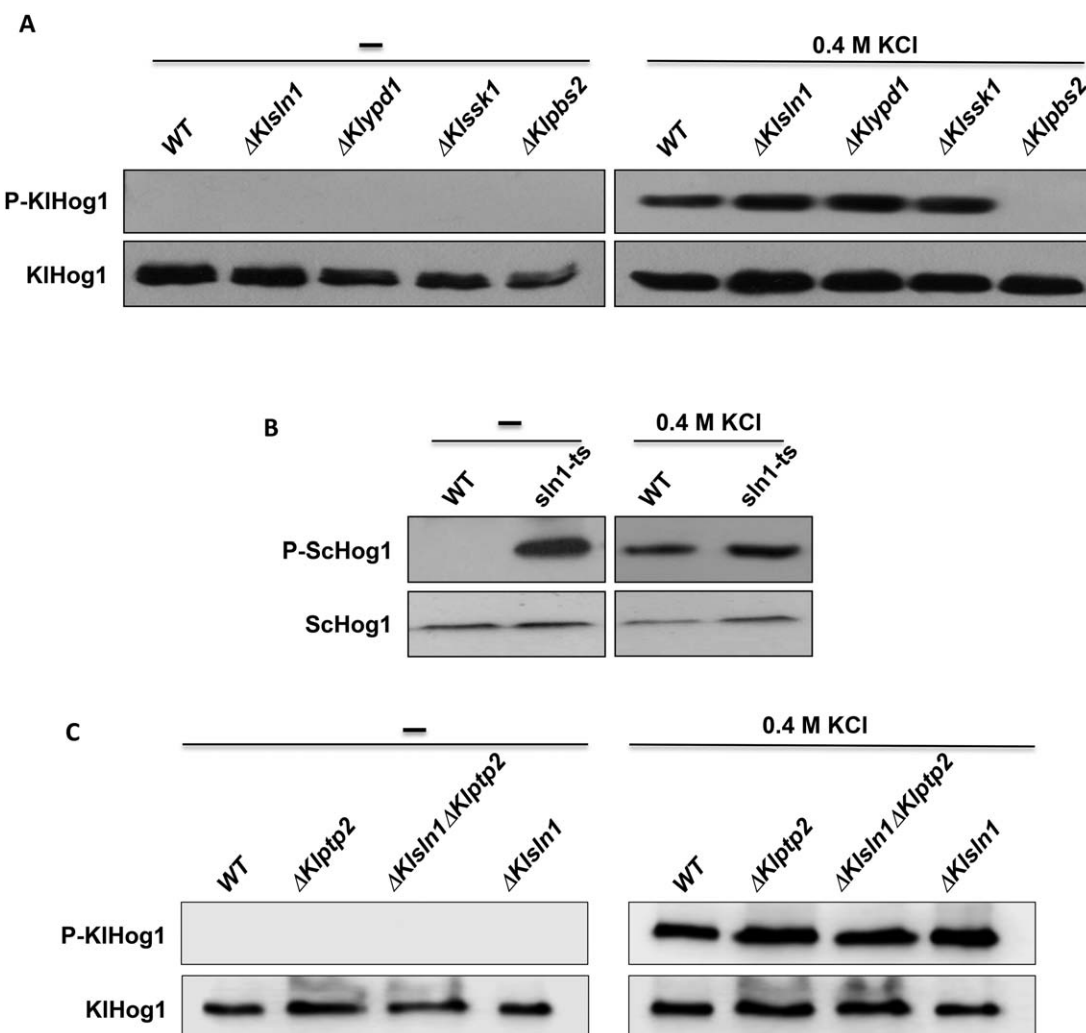


Fig. 3. *K. lactis* Hog1 phosphorylation in mutants lacking components of the Sln1 phosphorelay system. Protein extracts were obtained from wild type and mutant cells and subjected to western blot as described in the legend of Figure 2. (A) *KlHog1* phosphorylation in wild type and in the indicated mutant strains treated or not treated with 0.4 M KCl for 5 min. ΔKlpbs2 strain was included as a control of lack of *KlHog1* phosphorylation. (B) Hog1 phosphorylation in *S. cerevisiae* wild type and *sln1-ts* strains. Cells were incubated 5 min at 37°C in YPD or YPD containing 0.4 M KCl and subjected to Western blot analysis. (C) *K. lactis* Hog1 phosphorylation in mutants lacking the KIPtp2 phosphatase. Cells of the indicated strains were treated or not treated with 0.4 M KCl for 5 min and subjected to Western blot analysis.

mutants as described in the methods section. Both, the single and double mutants grew normally in iso-osmotic medium (data not shown). Phosphorylated *KlHog1* was detected when the cells were treated with hyperosmotic stress (Fig. 3 panel C). Interestingly, the level of phosphorylation of these mutants was similar to that observed in the wild type and ΔKlsln1 mutant. Under iso-osmotic conditions no phosphorylation was detected in any of the mutants. These results showed that *KlHog1* could not be constitutively phosphorylated in cells lacking the phosphorelay system, even in the absence of KIPtp2, which indicates that a strong feedback is still present in cells where the KIPtp2 phosphatase has been inactivated.

*Strong sensitivity to hyperosmotic stress is obtained by inactivation of both branches of the *K. lactis* HOG pathway*

In *S. cerevisiae*, inactivation of either *SLN1* or *SHO1* branches has no effect on growth under hyperosmotic conditions, but inactivation of both branches results in strong sensitivity (Posas and Saito, 1997). Our results showed that in *K. lactis* inactivation of the phosphorelay system alone had no effect on either viability or the hyperosmotic response. We then evaluated whether inactivation of both branches in *K. lactis* had the same effects as those seen in *S. cerevisiae*. For this purpose, we constructed a double mutant, $\Delta\text{Klsln1} \Delta\text{Klsho1}$, and evaluated its growth in high osmotic medium compared with

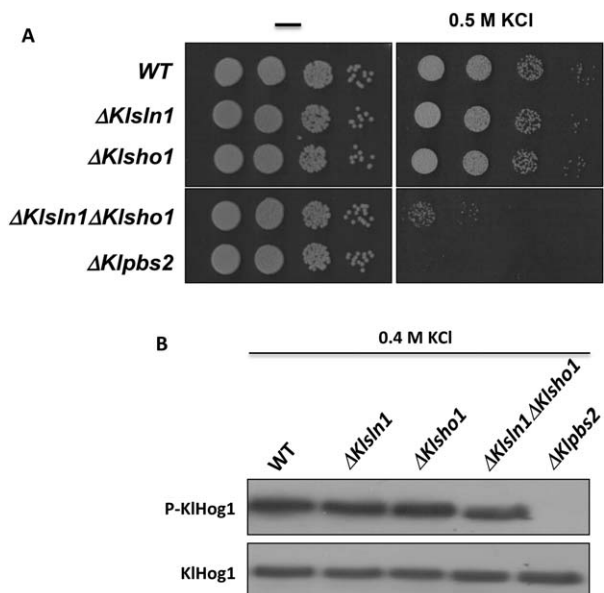


Fig. 4. Hyperosmotic stress induces growth defects in a mutant strain lacking both *KISLN1* and *KISHO1* genes. **(A)** Cells of the indicated strains were grown overnight at 30°C in liquid YPD, collected, washed and diluted in fresh medium. Cells were grown until OD₆₀₀ was 0.4 and spotted as 10-fold serial dilutions onto YPD with or without 0.5 M KCl. The plates were incubated at 30°C for 48 h and photographed. **(B)** *K. lactis* Hog1p phosphorylation in mutant strains upon hyperosmotic stress. Protein extracts were obtained from wild type and mutant cells and subjected to western blot as described in the legend of Figure 2. Cells of the indicated strains were treated with 0.4 M KCl for 5 min and subjected to Western blot analysis.

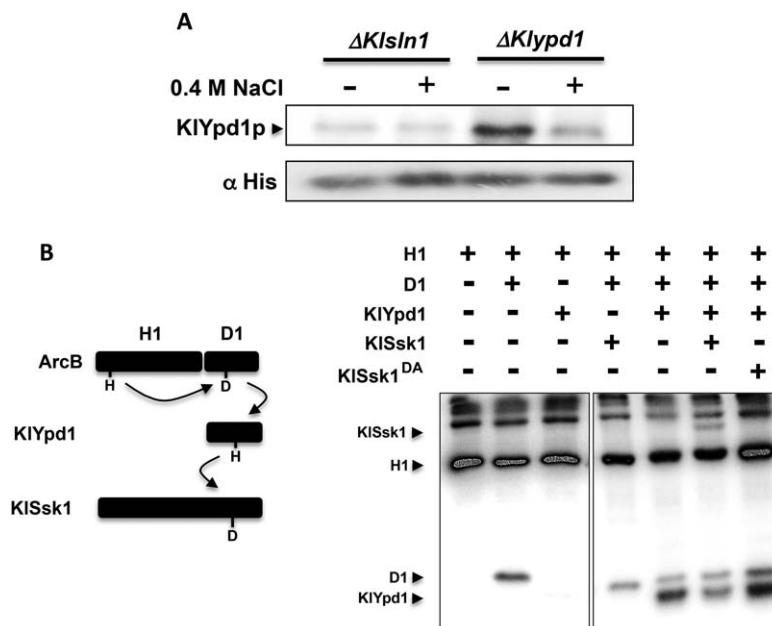
the single mutants (Fig. 4A). We observed that the double $\Delta Klsln1\Delta Klsho1$ mutant showed strong sensitivity to hyperosmotic conditions while the single mutants had similar growth to the wild type strain. This observation indicates that *K. lactis* responds to hyperosmotic stress by activating both the SLN1 and SHO1 branches and that KISln1 is required to generate an appropriate response to the hyperosmotic stress. In addition, we determined the effects of high salt concentration on the KlHog1 phosphorylation in these mutants. We found that KlHog1 became phosphorylated after 5 min of treatment with 0.4 M KCl not only in the single mutants but also in the double $\Delta Klsln1\Delta Klsho1$ mutant (Fig. 4B), even though this mutant was highly sensitive to hyperosmotic stress. This observation agreed with the amount of KlHog1 phosphorylation that was detected in the double $\Delta Klsln1\Delta Klssk2$ mutant (Velázquez-Zavala et al., 2015).

Phosphorylation of KIYpd1 occurs under iso-osmotic conditions and is dependent on KISln1

It has been shown that the phosphorelay system works as a negative regulator of the HOG pathway in *S. cerevisiae*. Therefore, the phosphorelay is activated

by iso-osmotic conditions and it is turned off when cells are exposed to high osmolarity (Maeda et al., 1994). The phenotypes observed in the *K. lactis* $\Delta Klsln1$ and $\Delta Klypd1$ mutants might suggest that the phosphorelay system is working differently in this yeast species compared with the one in *S. cerevisiae*. To address this question, we measured the phosphorylation of KIYpd1 under iso-osmotic and hyperosmotic conditions and in absence and presence of KISln1. We established an *in vivo* metabolic labelling system in the absence and presence of 0.4 M KCl in $\Delta Klypd1$ or $\Delta Klsln1$ mutants that expressed a His(6)-tagged KIYpd1 protein. His(6)-tagged KIYpd1 protein was purified in nickel columns as described in the methods section. A gel containing cell extracts from the different strains that was used as input of the nickel column is shown in Supporting Information Fig. 2. We observed that KIYpd1 was phosphorylated in cells growing under normal conditions and that it became unphosphorylated when the cells were treated with high osmotic medium (Fig. 5A). As expected, phosphorylation of KIYpd1 was dependent on the presence of KISln1. These observations indicate that KISln1 is catalytically active under iso-osmotic conditions and under these conditions, a phosphate group may be transferred to KIYpd1. In contrast, when KISln1 was inactivated by the hyperosmotic shock, KIYpd1 became unphosphorylated. Taken together, the above observations indicate that the molecular transfer of the phosphate in the phosphorelay system in *K. lactis* seems to be working similar to *S. cerevisiae*.

To understand the activity of the SLN1 phosphorelay system in *K. lactis*, we determined if KIYpd1 was able to accept phosphate groups from a donor protein and transfer them to KISsk1. For this experiment, we expressed and purified these proteins according to the strategy described in the Experimental procedures section. A purification profile of KISsk1 and Klypd1 is shown in Supporting Information Fig. 3A and B. First, we tried to use a recombinant cytoplasmic portion of KISln1 as a donor protein, but it showed high instability when it was purified from bacterial extracts (data not shown). Therefore, we tested whether KIYpd1 could be phosphorylated by a heterologous donor. For this approach, we used the purified hybrid histidine-kinase ArcB from *Escherichia coli* (Georgellis et al., 1997). In our assays, we used the ArcB histidine-kinase H1 transmitter domain (ArcB⁷⁸⁻⁵²¹) and the D1 receiver domain (ArcB⁵²¹⁻⁶⁶¹) which were purified separately. The H1 domain was able to transfer a phosphate group to the receiver D1 domain when they were incubated with a radiolabeled ATP nucleotide (Alvarez and Georgellis, 2010). We tested if the D1 domain could donate the phosphate group to KIYpd1 and if this protein, in turn, might phosphorylate KISsk1 as depicted in the scheme shown in Fig. 5B. KIYpd1 was phosphorylated



only when incubated with both, the H1 and the D1 domains. When the response regulator KISsk1 was added to the reaction mix, it became phosphorylated only when KIYpd1 was present, which indicated that the phosphate group cannot go directly from the D1 domain of ArcB to KISsk1p (Fig. 5B). These observations indicate that KIYpd1 is capable of accepting a phosphate group from a receiver domain and transferring it to KISsk1. In addition, we constructed a KISsk1 mutant in which the Asp(444) residue was replaced by Ala to create KISsk1^{DA}. It has been shown that in *S. cerevisiae* the substitution of the equivalent Asp(554) residue prevents Ssk1 from being phosphorylated by Ypd1 (Posas *et al.*, 1996; Horie *et al.*, 2008). We observed that the *K. lactis* mutant protein was not phosphorylated in our *in vitro* assay (Fig. 5B), which indicates that the Asp(444) residue is the acceptor of the phosphate group in *K. lactis* Ssk1.

The unphosphorylated form of KISsk1 interacts with the MAPKKK KISsk2

Next, we investigated if the *K. lactis* phosphorelay system is connected to the MAPK module as it is in *S. cerevisiae* (Posas and Saito, 1998). For this experiment, we measured KISsk1 and KISsk2 interaction using the two-hybrid system in which we fused KISsk1 to the LexA binding domain and KISsk2 to the B42 activator domain. It is worth noting that *K. lactis* lacks an Ssk22, which is redundant for Ssk2 in *S. cerevisiae*. We observed that the wild type versions of KISsk1 and KISsk2 proteins failed to interact (Fig. 6), as shown by the lack of blue color from the β-galactosidase reporter.

Fig. 5. *In vivo* and *In vitro* phosphorylation assays. (A) *K. lactis* strains were transfected with YEpkDGal-His-KIYPD1. Transformants were grown in phosphate-depleted media and pulsed with [³²P]orthophosphate. Cell aliquots were treated or not treated with 0.4 M NaCl for 1 min at RT. KIYPD1-His was purified using a Nickel column and applied to SDS-PAGE. Proteins were transferred to nylon membranes and analysed with a phospho-imager scanner. The nylon membrane was subjected to western blot analysis using an anti-His antibody. (B) *In vitro* phosphotransfer assay. ArcB (fragments H1 and D1), KIYPD1, and KISsk1 or KISsk1^{DA} were purified as described in the methods section. ArcB (H1) was incubated at RT for 10 min with [γ -³²P]ATP and then ArcB (D1), His-KIYPD1 and Mal-KISsk1 or Mal-KISsk1^{DA} were added in the depicted combination. After 10 min incubation at RT, proteins were applied to SDS-PAGE and the dried gel was analyzed with a phosphoimager scanner.

However, when we tested the KISsk1^{DA} mutant, which cannot be phosphorylated by KIYPD1, there was a very strong interaction between KISsk1 and the MAPKKK KISsk2. Taken together, the above results indicate that, similar to *S. cerevisiae*, the *K. lactis* phosphorelay system acts on the HOG pathway when it is inhibited by hyperosmotic stress.

	Binding domain	Activation domain	β-galactosidase activity (units/mg $\times 10^{-3}$)
KISsk1	KISsk2		2.4 ± 0.9
KISsk1 ^{DA}	KISsk2		35.2 ± 5.7
KISsk1	—		0.9 ± 0.7
KISsk1 ^{DA}	—		0.8 ± 0.5

Fig. 6. Physical interaction determined by the two-hybrid system. The binding domain corresponds to LexA-fused proteins cloned into pEG202 and the activation domain corresponds to B42-fused proteins cloned into pJG4-5. Two-hybrid plasmids were introduced into strain EGY48, and two independent clones were plated on SGal plates containing 1 mg/ml X-Gal. Photographs were taken 24 h after incubation at 30°C. Quantitation of β-galactosidase activity was determined as described (Ongay-Larios *et al.*, 2000). The β-galactosidase activity corresponds to the average value of three independent clones.

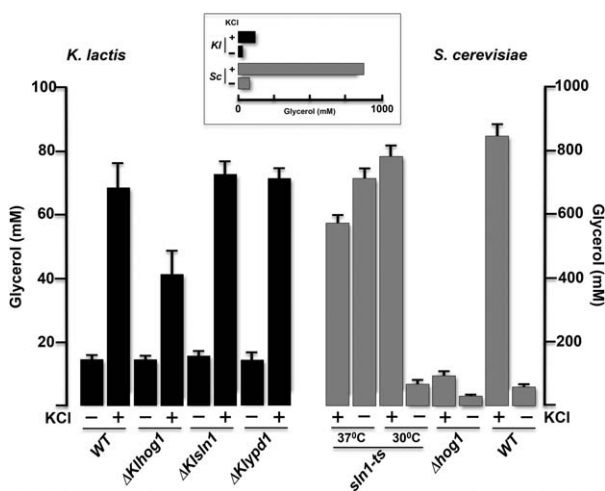


Fig. 7. Comparison of glycerol accumulation in *K. lactis* and *S. cerevisiae* strains. Cultures of the indicated strains were grown in YPD at 30°C until OD₆₀₀ 0.4. Cells were transferred to the same medium with or without 0.4 M KCl and incubated for 6 h at 30°C, except for one aliquot of strain *sln1-ts* which was incubated at 37°C. Glycerol content was determined as described in the methods section. Insert; comparison of intracellular glycerol content in wild type cells of *K. lactis* and *S. cerevisiae*.

Kluyveromyces lactis osmolyte production to cope with osmotic stress differs from that of *S. cerevisiae*

Activation of Hog1 in *S. cerevisiae* cells induces growth arrest and accumulation of several osmolytes, especially glycerol, to avoid plasmolysis (Saito and Posas, 2012). Moreover, inactivation of Sln1 causes constitutive activation of Hog1 and therefore, uncontrolled glycerol production (Hohmann, 2002). To determine whether glycerol accumulation occurs in *K. lactis* cells following hyperosmotic stress, we measured glycerol content in wild type and mutant strains and compared it to glycerol production in *S. cerevisiae*. We found that the glycerol content in *K. lactis* wild type cells increased approximately 5- to 7-fold under hyperosmotic stress, which is in agreement with previous reports (Cialfi *et al.*, 2011). The glycerol content under osmotic stress in *K. lactis* slightly decreased in the Δ Klhog1 mutant and remained unaltered in the Δ Klsln1 and Δ Klypd1 mutants (Fig. 7). Furthermore, mutants with an inactivated phosphorelay in *K. lactis* did not have sustained production of glycerol under iso-osmotic conditions, which was consistent with the lack of Hog1 phosphorylation in these mutants. Δ Klsln1 and Δ Klypd1 mutants accumulated as much glycerol as the wild type strain only when they were treated with a hyperosmotic stimulus (Fig. 7). In contrast, *S. cerevisiae* wild type strain accumulated glycerol approximately 18- to 20-fold when cells were treated with a hyperosmotic shock. The *S. cerevisiae* hog1 mutant was unable to produce glycerol under hyperosmotic stress, while the cells carrying the *sln1-ts*

allele accumulated glycerol, under the restrictive temperature, at a similar level compared with the wild type strain. In this assay, we found that *K. lactis* wild type cells accumulated ten times less glycerol than *S. cerevisiae* wild type cells (Fig. 7, insert). This result suggests that this amount of glycerol is sufficient to protect *K. lactis* cells against the hyperosmotic stress or that this strain uses alternative osmolytes, in addition to glycerol, to cope with high osmolarity. It has been proposed that trehalose might act as osmolyte in *S. cerevisiae*. Previous studies have shown that *S. cerevisiae* accumulated approximately 10 times more trehalose when cells were exposed to hyperosmotic stress (Hounsa *et al.*, 1998). With this in mind, we determined whether trehalose could be used as osmoprotectant in *K. lactis* cells. For this assay wild type cells were grown until early stationary phase and treated with 0.4 M NaCl for 6 h. In these conditions, we found that *K. lactis* cells did not accumulate trehalose, instead, a 50% reduction of trehalose concentration was detected after the NaCl shock, as compared with untreated cells (Table 1). The Δ Klhog1 mutant behaved as the wild type strain, suggesting that Klhog1 does not play a significant role in trehalose production in these conditions. In contrast, in wild type *S. cerevisiae* cells the trehalose content increased 15-fold upon hyperosmotic stress. This increment was dependent on Hog1, since the Δ hog1 mutant failed to increase the trehalose content under hyperosmotic stress.

Klhog1 rescues a Δ Schog1 mutant from its sensitivity to hyperosmotic stress

In *S. cerevisiae*, Hog1 participates in a feedback regulatory mechanism to regulate the basal signaling in the pathway and the fine tuning of the signaling (Macia *et al.*, 2009; Sharifian *et al.*, 2015). To understand the basis for the differential outcomes of the inactivation of the phosphorelay in *K. lactis*, we assessed whether this result could be attributed to Hog1. Thus, we asked if Klhog1 could substitute for Schog1 in the *S. cerevisiae*

Table 1. Comparison of trehalose production between *K. lactis* and *S. cerevisiae* cells. Trehalose concentration is given in [mg/g dry wt]. Cells were grown as described in the Experimental procedures section and treated or not treated with 0.4 M NaCl for 6 h.

		NaCl	
<i>K. lactis</i>	WT	0.54 ± 0.06	0.22 ± 0.05
	hog1	0.63 ± 0.07	0.28 ± 0.05
<i>S. cerevisiae</i>	WT	0.20 ± 0.03	3.02 ± 0.09
	hog1	0.32 ± 0.05	0.27 ± 0.08

Numbers are the average value of three-independent experiments (± SD).

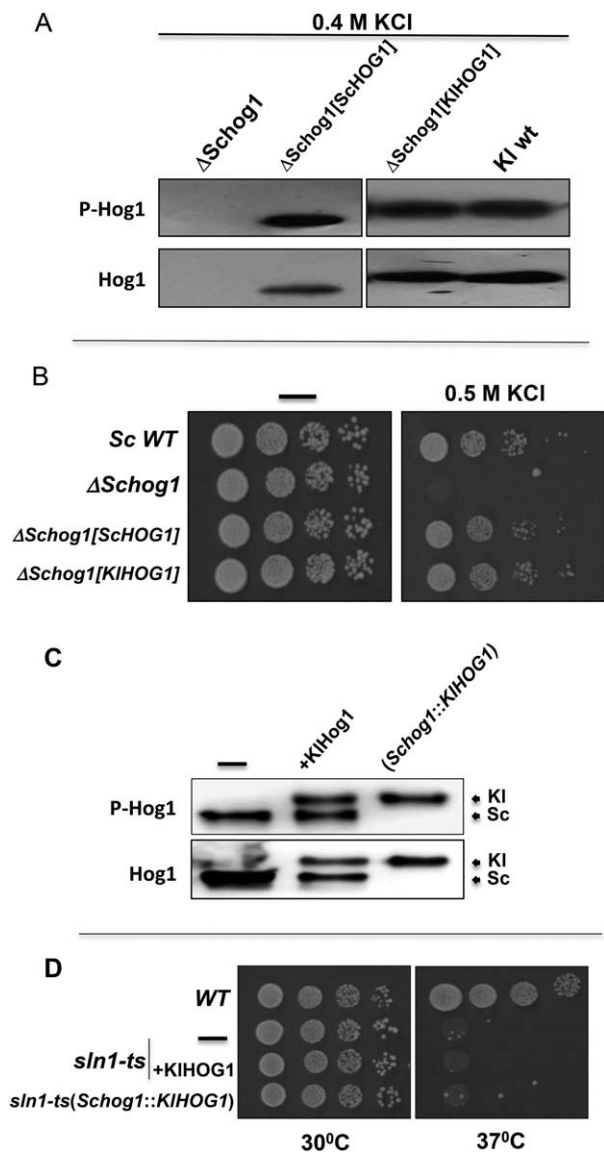


Fig. 8. Effect of KIHog1 expression on the *S. cerevisiae* *hog1* and *sln-ts* strains. The strains were transfected with empty pYES2 (-) or pYES2 containing either *KIHOG1* or *ScHOG1*. Transformants were grown overnight in SD medium at 30°C. Cells were collected, washed and suspended in fresh SD medium and allowed to reach OD₆₀₀ 0.4. Cells were then used for western blot or plating. (A) Cells were washed and transferred to SGal medium for 4 h to allow expression of *KIHOG1* and *ScHOG1*. Cultures were treated or not treated with 0.4 M KCl for 5 min. Protein extracts were obtained from wild type and mutant cells and subjected to western blot as described in the legend of Figure 2. An extract protein aliquot from the *K. lactis* wild type strain was used as a control. (B) Mid-log cells were collected, washed and spotted as 10-fold serial dilutions onto YPD with or without 0.75M KCl. The plates were incubated at 30°C for 48 h and photographed. Sc WT strain is BY4742. (C) Cells of the indicated strains were washed and transferred to SGal medium for 3 h to allow expression of *KIHOG1*, followed by incubation at 37°C for 3 h. Cells were lysed and protein extracts were obtained and subjected to Western blot analysis as described. (D) Mid-log cells of strain TM141 or its isogenic *sln1-ts* with empty plasmid (dash), pYES-KIHOG1 or with integrated *KIHOG1* were spotted as 10-fold serial dilutions onto YPD plates. Plates were incubated at 30°C or 37°C for 48 h and photographed.

HOG pathway. First, we investigated whether KIHog1 could be phosphorylated in *S. cerevisiae* when expressed in the Δ *Schog1* mutant. For this test, we cloned the *K. lactis* gene into the pYES2 vector and expressed it under the *GAL1* promoter. We found that after 5 min of a hyperosmotic treatment, KIHog1 was phosphorylated in *S. cerevisiae* at a similar level as ScHog1 (Fig. 8 panel A). We observed that expression of *KIHOG1* was able to reverse the sensitivity to hyperosmotic stress displayed by the *S. cerevisiae* Δ *hog1* mutant to the same level as *ScHOG1* (Fig. 8 panel B). We also tested if KIHog1 was phosphorylated in the absence of stress in *S. cerevisiae* cells when the phosphorelay system was inactivated. For this experiment, we expressed KIHog1 in the cells carrying the thermo-sensitive *sln1-ts* allele and monitored phosphorylation at 37°C. We took advantage of the differences in MW between KIHog1 and ScHog1 to distinguish them in the same gel. KIHog1 and endogenous ScHog1 were both phosphorylated at the same level when the cells were shifted to 37°C (Fig. 8 panel C). When the growth of these strains was analyzed, we observed that the *sln1-ts* strain and the strain carrying the plasmid copy of *KIHOG1* were unable to grow at 37°C in YPD medium due to constitutive activation of endogenous ScHog1 (Fig. 8 panel D). To evaluate the effects of KIHog1 alone on the growth of the *sln1-ts* strain, we integrated the *KIHOG1* gene into the *ScHOG1* locus (*sln1-ts(Schog1::KIHOG1)*), and placed it under the control of the *ScHOG1* promoter. Under these conditions, we observed that when the temperature shifted to 37°C, KIHog1 phosphorylation was induced (Fig. 8 panel C), and the temperature shift also induced cell lethality in the *sln1-ts* strain (Fig. 8 panel D). Taken together, these results indicate that Hog1 from *K. lactis* can replace ScHog1 in terms of its capability to respond to hyperosmotic stress, and its ability to induce cell lethality when the phosphorelay is inactivated.

*ScHog1p does not induce lethality in *K. lactis* upon inactivation of the phosphorelay*

We finally asked if ScHog1 would be able to induce cell lethality in *K. lactis* upon phosphorelay inactivation as it does in *S. cerevisiae*. For this experiment, we used the double mutant Δ *Klypd1* Δ *Klhog1*. When overexpressed, both KIHog1 and ScHog1 proteins were able to reverse the sensitivity to hyperosmotic stress that was displayed in the cells transformed with the vector alone (Fig. 9). In the absence of the hyperosmotic stimulus, KIHog1 slightly impaired the growth of the double mutant strain (which probably occurred due to a KIHog1 overdose). However, ScHog1p did not affect the growth of the

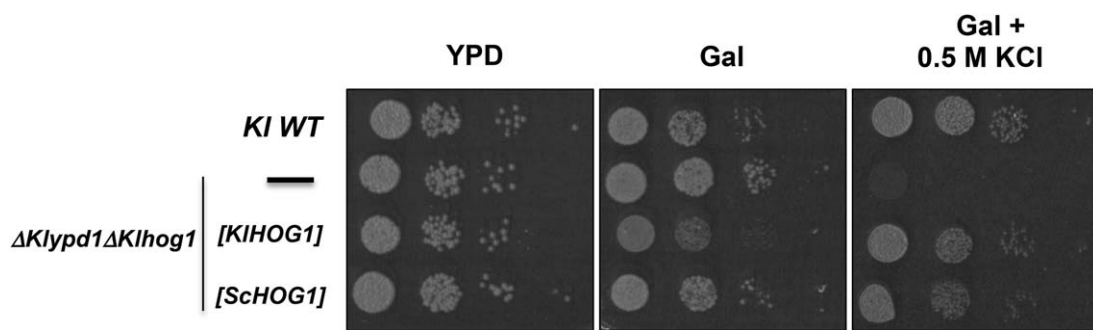


Fig. 9. Effect of *ScHog1* expression on *K. lactis* *Ypd1* and *Hog1* deficient mutant. The $\Delta Klypd1\Delta Klhog1$ strain was transfected with empty YEpkD-Gal or YEpkD-Gal containing either *KIHOG1* or *ScHOG1*. Transformants were grown overnight in SD medium at 30°C. Cells were collected washed and suspended in fresh SD medium and allowed to reach OD₆₀₀ 0.4. Cells were collected, washed and spotted as 10-fold serial dilutions onto YPD or YPGal with or without 0.75M KCl. The plates were incubated at 30°C for 48 h and photographed.

$\Delta Klypd1\Delta Klhog1$ strain. These results indicate that *ScHog1* is able to replace *Klhog1* when *K. lactis* cells are under hyperosmotic stress and the substitution does not induce lethality when the *K. lactis* phosphorelay is inactivated.

Discussion

Saccharomyces cerevisiae has been considered a useful yeast model organism for studying the osmostress response pathway. Previous studies have shown that the *SLN1* phosphorelay system plays a negative regulatory role for *Hog1*, and null mutants of *SLN1* and *YPD1* showed constitutive phosphorylation of *Hog1* and cell death due to overactivation of the HOG pathway (Posas *et al.*, 1996; Hohmann, 2000). *K. lactis*, which is a close relative of *S. cerevisiae*, contains most of the proteins required for the hyperosmotic stress response, except the ortholog of redundant MAPKKK *Ssk22* (Krantz *et al.*, 2006). All *K. lactis* proteins have high structural similarity to the proteins in *S. cerevisiae*. This similarity suggests that *K. lactis* has a similar architecture and mechanisms to cope with hyperosmotic stress. We constructed deletion mutants of both, *KISln1* and *KIYpd1* in diploid cells to determine their contribution to the stress response. To our surprise, we found that haploid null mutants of either gene were viable and insensitive to hyperosmotic stress. The observed phenotypes agreed with the phenotypes of *S. pombe* (Nakamichi *et al.*, 2002) and *C. albicans* (Yamada-Okabe *et al.*, 1999), for which, inactivation of the sensor kinase and the phosphotransfer proteins did not affect cell viability. In addition, we found that a mutant of the response regulator *KISsk1* was also insensitive to hyperosmotic stress. When we tested the effects of the elimination of *KISln1* and *KIYpd1* on *Klhog1* phosphorylation, *Klhog1* remained unphosphorylated when grown under iso-osmotic conditions. This would mean that in *K. lactis*,

the phosphorelay system either does not participate in the response to hyperosmotic stress or that the *K. lactis* phosphorelay pathway acts in a different manner in this yeast species. The first hypothesis was discarded since a double *ΔKlsln1 ΔKlsho1* mutant was osmosensitive, which contrasted the observed phenotype of the single *ΔKlsho1* mutant, which was osmoreistant (Velázquez-Zavala *et al.*, 2015). This indicated that both *K. lactis* branches were active and worked in parallel for hyperosmotic adaptation.

Surprisingly, we observed that in cells where both *KISln1* and *Klsho1* were eliminated, *Hog1* was in fact phosphorylated when the cells were grown in high osmotic medium. However, this phosphorylation failed to protect the cells against hyperosmotic stress, which was contrary to the outcome we expected. These results correlate with the phenotype displayed by a *ΔKlssk2ΔKlste11* mutant (Velázquez-Zavala *et al.*, 2015) in which *Klhog1* was phosphorylated under hyperosmotic stress. This could mean that phosphorylation of *Klhog1*, under these conditions, was performed in a different manner that made the reaction inefficient for an osmostress response or that *Klhog1* activity has not reached a threshold to trigger an osmoreponse. Nevertheless, our results showed that *KIYpd1* and *KISsk1* had phosphotransfer activity *in vitro*, which indicated that those proteins were functional and conserved the structural characteristics to accept and transfer phosphate groups. Moreover, substitution of the Asp444 residue from the response regulator *KISsk1*, failed to hyper-activate the *K. lactis* HOG1 pathway as observed in *S. cerevisiae* (Horie *et al.*, 2008), although it did eliminate its capacity to accept phosphate groups from *KIYpd1p*. In addition, we found that *KIYpd1* could be phosphorylated *in vivo* and that this phosphorylation was dependent on the presence of *KISln1* and could occur under iso-osmotic conditions, which indicated that the *SLN1* system in *K. lactis* conserved activation properties similar to *S. cerevisiae* (Maeda *et al.*, 1994). In this study,

we also demonstrated that KISsk1 made contact with KISsk2 when the Asp444 residue was substituted, while the wild type KISsk1 was unable to interact with KISsk2. This result suggested that the un-phosphorylated form of KISsk1p was the one that was associated with KISsk2. These data showed that activation properties of the SLN1 system in *K. lactis* were similar to *S. cerevisiae*, and, that the connection between the phosphorelay system and the MAPK module in *K. lactis* could be carried out in a similar manner as in *S. cerevisiae*.

Interestingly, in contrast to the high glycerol accumulation observed in *S. cerevisiae* cells upon hyperosmotic stress, *K. lactis* cells treated with high salt accumulated 10 times less glycerol. Moreover, while elimination of thermosensitive Sln1 activity by a temperature shift induces constitutive glycerol accumulation in *S. cerevisiae*, even under iso-osmotic conditions, *K. lactis* cells devoid of phosphorelay proteins failed to increase the glycerol concentration. Finally, glycerol production decreased approximately ten times in the *S. cerevisiae* Δ hog1 mutant under hyperosmotic treatment, while it decreased just to half in the *K. lactis* Δ hog1 mutant. Although hyperosmotic stress increased glycerol production in *K. lactis* cells, its level was significantly lower compared with *S. cerevisiae*, which suggests that this amount of glycerol is sufficient to exert osmotic protection, or that other compatible solutes are used by this yeast species. In *S. cerevisiae* the activity of the glycerol-3-phosphate dehydrogenase (Gpd1) is required to provide osmostress resistance (Albertyn *et al.*, 1994), therefore inactivation of the ortholog protein in *K. lactis* will be a useful approach to determine if this amount of glycerol is serving as osmoprotectant in this yeast species. It has been demonstrated that trehalose plays a role in protecting yeast cells from different stress insults (Argüelles, 2000; Sampedro and Uribe, 2004). For this reason, we determined production of trehalose in *K. lactis* cells grown under hyperosmotic stress. We found that trehalose did not accumulate in *K. lactis*, which is in contrast with the accumulation observed in *S. cerevisiae* (Parrou *et al.*, 1997). This observation could mean that this osmolyte is not used as osmoprotectant in *K. lactis* or that the conditions used in this study did not allow trehalose accumulation. An important observation is that hyperosmotic stress induces recycling of trehalose due to increased synthesis by the trehalose 6-phosphate synthase (Tps1) and increased degradation by the neutral trehalase (Nth1) (Parrou *et al.*, 1997). Therefore, it will be interesting to construct mutants that inactivate these enzymes in *K. lactis* to determine their contribution to the hyperosmotic response.

It is important to mention that KIHog1 conserves structural similarities with ScHog1. In fact, as we have shown here, it can fully complement the lack of Hog1 in *S.*

cerevisiae and allow for growth of Δ hog1 cells in high osmotic medium. In addition, KIHog1 was phosphorylated constitutively and induced lethality when expressed in *S. cerevisiae* cells devoid of phosphotransfer activity. In the same manner, ScHog1 can substitute for KIHog1 and does not induce lethality in *K. lactis* lacking the phosphorelay system. All these observations suggest that Hog1 of either species could induce negative feedback efficiently in *K. lactis*, which would allow the cells to survive, even if they lack an active phosphorelay (Sharifian *et al.*, 2015). However, in *S. cerevisiae* KIHog1, as well as ScHog1, is not capable of establishing this negative feedback and would be constitutively active in *sln1* cells. Several mechanisms participate in the negative feedback that attenuates Hog1 activity (Saito and Posas, 2012). Among these, activity of Hog1 phosphatases contribute to downregulate the hyperosmotic transduction system. The nuclear phosphatase Ptp2 is responsible for Hog1 dephosphorylation in the nucleus (Mattison and Ota, 2000). Accordingly, we deleted the gene that encodes the Ptp2 phosphatase in *K. lactis* and we found that KIHog1 was not phosphorylated in cells grown in iso-osmotic conditions, surprisingly, this was true even in cells where the phosphotransfer systems had also been inactivated (Δ Klsln1 Δ Klptp2 mutant). The KIPtp2 inactivation in the Δ Klsln1 mutant did not affect growth on iso-osmotic conditions. These observations suggest that KIPtp2 does not participate in the negative feedback or that it has a marginal contribution in this mechanism. It would be important to investigate which negative feedback mechanisms are present in *K. lactis* and what will be their contribution to the regulation of the hyperosmotic response pathway.

In this study, we showed that the phosphorelay system composed of KISln1-KIYpd1-KISsk1 had phosphotransfer activity both *in vitro* and *in vivo*, that was active under normal osmotic conditions and that was turned off under hyperosmotic stress. These observations indicate that this system negatively regulates KIHog1p. However, the absence of the transfer of phosphate in the Δ Klsln1 and Δ Klypd1 mutants did not induce constitutive activation of KIHog1p. Furthermore, phosphorylation of KIHog1 was not observed in the Δ Klsln1 mutant even when the KIPtp2 phosphatase was inactivated. In *S. cerevisiae*, inactivation of Sln1 leads to constitutive Hog1 phosphorylation and to cell lethality due to hyperactivation of the HOG pathway. In this condition, the activity of Ptp2 phosphatase, which dephosphorylates Hog1, seems to be insufficient to attenuate Hog1 activity. In contrast, in *K. lactis*, our results indicate that a strong feedback mechanism, independent of Ptp2 is operating and will inactivate Hog1 in a mutant lacking KISln1. Our data suggest that the attenuation of the KIHog1 activity could take place in the cytoplasm and might be carried out by either KIPtp3 or by the type 2C Ser/Thr phosphatases. In resting conditions, inactivation

of the phosphorelay system would not be sufficient to overtake the negative feedback imposed by these phosphatases, and under hyperosmotic shock the activation of K1Yhog1 would trigger a canonical osmo-response. Our data indicate that despite the high conservation in components and architecture, the high osmolarity pathway in *K. lactis* operates under different mechanisms. ■

Experimental procedures

Strains and media

The *K. lactis* strains used in this study were MD2/1 (*MAT α* , *argA* *lysA* *ura3*), 12/8 (*MAT α* , *lysA*, *argA*, *ura3*) and 155 (*Mat α* , *ade2*, *his3*, *uraA*), which have all been described in a previous study (Saviñón-Tejeda *et al.*, 2001). *K. lactis* diploids were obtained by crossing strains MD2/1 and 155. The *S. cerevisiae* strains were BY4742 (*MAT α* , *his3*, *leu2*, *lys2*, *ura3*), and its isogenic Δ *hog1* mutant (*MAT α* *his3*, *leu2*, *lys2*, *ura3*, *hog1::G418*). The TM141 (*Mata*, *ura3*, *leu2 trp1 his3*) and *sln1^{ts}* (*Mata*, *ura3*, *leu2 trp1 his3*, *sln1^{ts}*) strains were described in (Maeda *et al.*, 1994; Posas *et al.*, 1996). The EGY48 (*MAT α* *his3* *trp1* *ura3* *leu2::pLeu-Lex-Aop6*) strain (Golemis *et al.*, 1997) was used for the two hybrid assays. *E. coli* strain DH5 α was used to propagate plasmids. BL21 (New England Biolabs) was used to express and purify K1Ssk1p and M15 Z2291 (Qiagen) was used for K1Ypd1p expression and purification. YPD medium consisted of 1% yeast extract, 2% Bacto-peptone and 2% Glucose. YPGal medium was the same as YPD except that it contained galactose instead of glucose. YPGal-Pi is a phosphate depleted medium and was prepared as previously described (Warner, 1991). SD minimal medium consisted of a 0.67% yeast nitrogen base without amino acids (Difco) and 2% glucose. SGal was the same as SD except for the substitution of glucose with galactose. For plasmid selection SD and SGal were supplemented with the required amino acids and nitrogen bases (50 μ g/ml). 1 mg/ml 5-fluoroorotic acid (FOA) was added to YPD for negative selection of the URA3 marker. Sporulation medium consisted of 5% Malt extract (Difco) and 3% agar. Media were supplemented with KCl at different concentrations for osmo-sensitivity assays. LB medium supplemented with ampicillin (100 μ g/ml) was used to propagate recombinant bacteria.

Gene constructs and mutagenesis

A fragment of *KISLN1* was amplified by PCR from genomic DNA employing the forward primer Sln1F +2321 AGTC-GAACCCGAAACG +2306 and the backward primer Sln1R +3570 GGAAACCATCCATTCC +3585, which generated a 1083-base pair product. The product was subcloned into pGEM-T Easy (Promega) to yield pGEM-SLN1. A 1037-bp *Eco*RI-*Eco*RI fragment was obtained from pGEM-SLN1 and subcloned into Ylp352 (Saviñón-Tejeda *et al.*, 2001), which was opened at the *Eco*RI site. This construct was digested with *Bgl*II, which cuts twice into *SLN1*. The resulting molecule was integrated into the *KISLN1* locus in diploid cells and yielded a 600 bp deletion.

KIYPD1 was amplified from genomic DNA using primers Ypd1F -231 TTGTATATACACCGGGTTCTTTGT -257 and Ypd1R +529 CAGCACAGATCCGGGTCAATATA +552, which contained *Sma*I restriction sites (underlined). The 809-bpr product was cloned into pGEM-T Easy. The resulting pGEM-YPD1 plasmid was digested with *Sma*I and ligated into Ylp352, which was opened at the *Sma*I site. Ylp352-YPD1 was digested with *Eco*RI and employed for transformation of diploid cells. This step produced a 243 bp deletion in *KIYPD1*.

KISSK1 was amplified by PCR using the primers SSK1F -47 TGTTGAATTCTTGAGAA -65 and SSK1R +2079 AAGATGTTGAATTCGTGATG +2060. Both primers contained an *Eco*RI restriction site (underlined). The PCR product was subcloned into the pGEM-T Easy vector and sequenced in full. A 2131-bp fragment obtained by *Eco*RI-*Eco*RI digestion was subcloned into Ylp352 digested with the same enzymes. The resulting construct was opened at the *Cla*I site and used for transformation.

To construct the unphosphorylated form of KISSK1 (*KISSK1^{DA}*) we designed the mutagenic primer SSK1MF +1318 CTTATCCTTATGGCTTGCAATTGCC +1344, and its reverse complement SSK1MR, which had A instead of C at position +1331 (underlined) and produced alanine instead of the aspartate at position 444 of Ssk1p. We used the mutagenic primers along with SSK1R and SSK1F, respectively, in separated PCR reactions. Amplified products were mixed together for a second PCR reaction using SSK1F and SSK1R primers. The final PCR product was ligated into the pGEM-T Easy vector and sequenced in full.

Both wild type and mutated KISSK1 were obtained from a pGEM-T Easy plasmid and subcloned into YEpkDGal for *K. lactis* expression. For the two hybrid assays, we separately subcloned the genes encoding KISSK1 and KISSK1^{DA} into pJG4-5. This cloning was achieved by PCR mediated amplification using primers Ssk1DHF -12 TAACCGGAATTCATGCAAGAA +9 and Ssk1DHR +1920 CCATGGCTCGAGTACGG +1900, which introduced *Eco*RI and *Xba*I sites to the construct respectively (underlined). The PCR products were ligated back into the pGEM-T Easy plasmid. Both KISSK1 genes were obtained as *Eco*RI and *Xba*I fragments and subcloned into pJG4-5, which was opened at the same sites. This fused both forms of K1Ssk1 with the B42 activation domain. KISSK2 was amplified from genomic DNA using primers Ssk2DHF -12 TCGTTCCCGGGCATGTCGCAA +9 and Ssk2DHR +4662 TTATGTCCGCGCCTAGTTATG +4639, which introduced *Sma*I and *Not*I sites respectively (underlined). The PCR product was ligated into pGEM-T Easy. KISSK2 was obtained with *Sma*I and *Not*I restriction enzymes and ligated into pEG202, which was opened with the same enzymes. This fused K1Ssk2 with the LexA binding domain. The construct pJG4-5-CTS1 (Ongay-Larios *et al.*, 2000) was used as a negative interaction control.

K1YPD1 was subcloned into *E. coli* expression vector pQE30 (Qiagen) by amplifying it from the pGEM-T Easy clone. For this step, we used primers YPD1A -16 AAAAG-CACAAGAGCTCATGTCCCAAACA +12 and YPD1B +445 AGAGAAAAGCTGCCTG +429 which contained *Sac*I and *Hind*III restriction sites respectively (underlined). The PCR product was cloned back into the pGEM-T Easy vector and sequenced in full. This construct was digested with *Sac*I

and *Hind*III and subcloned into pQE30, which was opened with the same enzymes. The product was a KIYpd-His(6) tagged protein. The KIYpd-His(6) encoding gene was obtained from the pQE30 plasmid as a *Xho*1-*Hind*III fragment and was subcloned into YEpkDGal opened at the *Eco*RI site (filled in) for expression in *K. lactis*.

The plasmids pMAL-KISSK1 and pMAL-KISSK1^{DA} were constructed by PCR using the pGEM-T Easy clones as templates. Primers SSK1rrA -1138 GGATCCGATAAG-CAAGGCAA -1158 and SSK1rrB +1943 AAATATTCTT GCGGCCGCAAGCTCTGATGACCAT +1908 introduced the *Bam*HI and *Hind*III sites, respectively (underlined), which were used in a standard PCR reaction. The PCR products were cloned into a pGEM-T Easy vector and sequenced. *Bam*HI-*Hind*III fragments were obtained from these plasmids and subcloned into pMAL (which was opened with the same enzymes) (New England BioLabs).

KIHOG1 was obtained from a pGEM-T Easy clone (Kawasaki *et al.*, 2008) as an *Eco*RI and *Xho*1 fragment, and it was ligated into pYES2 opened with the same enzymes. ScHOG1 was obtained from a pGEM-ScHOG1 clone as a *Hind*III-*Xba*I fragment and subcloned into pYES2 opened at the same restriction sites. This step placed both HOG1 genes under the control of the *GAL1* promoter for *S. cerevisiae* expression. KIHOG1 and ScHOG1 were obtained from the pYES2 clones as *Hind*III-*Xba*I and *Hind*III-*Xba*I fragments respectively. These fragments were filled with Klenow and were ligated into YEpkDGal opened at *Eco*RI site (filled in) for expression in *K. lactis*.

The *ptp2*-clonNAT construct was obtained by PCR employing the following hybrid primers: PTP2-Nat-F: tggtcg ctatactgtcgTTCAATCACCAAATAAAAGAAC that contains 20 nucleotides complementary to the clonNAT promoter (lowercase) and 22 nucleotides complementary to the KIPTP2 gene, coordinates +2189 to +2210 (uppercase); PTP2-Nat-R: aagcttaaacagactggcgCACCTTCGATTAAAGCT-GATC that contains 19 nucleotides complementary to the clonNAT terminator (lowercase) and 20 nucleotides complementary to the KIPTP2 gene, coordinates +622 to +603 (uppercase). These primers were used to amplify the full clonNAT cassette including its promoter using the pAG25 plasmid (obtained from Dr. Francisco Torres) as template. Extension of PTP2 recombinant ends was performed by PCR using the clonNAT PCR product and primers: PTP2-F, +1 ATGAGAATGCAAATGAGTATG +21, and PTP2-R +2712 TTATATGTGCTCCTTCAAATA +2691, using genomic DNA as template. The PTP2-clonNAT final product contained the clonNAT cassette flanked by 622 bp and 523 bp recombinant PTP2 ends.

Gene disruptions and gene integrations

KISLN1, *KIYPD1* and *KISSK1* gene disruptions were achieved by homologous recombination using the Yip352 clones. Disruption of *KISLN1* and *KIYPD1* genes were performed in *K. lactis* diploid cells by introducing the *sln1*::*URA3* and *YPD1*::*URA3* cassettes, respectively, and selecting for *URA3*⁺ transformants. Disruption of *KIPTP2* was performed in wild type and diploid *sln1*::*URA3*/*SLN1* strains introducing the *ptp2*::*clonNAT* cassette and selecting

for clonNAT resistant transformants. Diploids were sporulated by incubation in sporulation medium for 24 to 48 h. Tetrad dissection was achieved by micromanipulation using standard protocols (Sherman *et al.*, 1986). Spores were germinated in YPD and tested for the *URA3* marker (Δ *KISLN1*, Δ *KIYPD1*, Δ *KIPTP2*) and *URA3*+ clonNAT resistance (Δ *KISLN1* Δ *KIPTP2*).

The *KISSK1* disruption was obtained by introducing the Yip352-KISSK1 plasmid (opened at the *Cla* site) into the haploid MD2/1 strain and selecting for *URA3*⁺ transformants.

Both Δ *Klsho1* Δ *KISLN1* and Δ *KIYPD1* Δ *Klhog1* double mutants were obtained by introducing the *sln1*::*URA3* or *hog1*::*URA3* cassettes, by homologous recombination, into the 5-FOA resistant mutants Δ *Klsho1* and Δ *Klhog1* respectively. All gene disruptions were confirmed by standard Southern blot hybridization. Disruption of the genes *KIHOG1*, *KIPBS2* and *KISHO1* has been previously described (Kawasaki *et al.*, 2008; Velázquez-Zavala *et al.*, 2015).

The Δ *Schog1* mutant was obtained from the Yeast Knockout Collection. The integration of the *KIHOG1* gene was accomplished through homologous recombination by selecting for the hygromycin resistance cassette.

KIYpd1p and KISsk1p purification

The *E. coli* M15 strain was transformed with the pQE30-KIYPD1 construct. A purified clone was then grown overnight in 100 ml LB plus ampicillin medium at 37°C. When OD₆₀₀ reached 0.6, isopropyl-β-D-thiogalactoside (IPTG) was added to a final concentration of 1 mM, and the culture was shaken for 4 h at 37°C. The cells were harvested and resuspended in 8 ml of buffer A containing 1% NP40, 500 mM NaCl, 40 mM Tris-HCl, 5 mM imidazole. Bacteria were lysed by sonication, and the suspensions were centrifuged at 5000 rpm for 15 min at 4°C. Then, 1 ml of the supernatant was applied to a nickel resin (Novagen) that was previously washed, loaded and balanced with buffer A. KIYPD1-His purification was performed following the instructions of the Novagen His Bind purification kit. KIYpd1p-His was eluted with buffer A, which contained 100 mM imidazole.

The *E. coli* BL21 strain was transformed separately with pMAL-KISSK1 and pMAL-KISSK1^{DA} constructs. The cells were grown in 250 ml of LB plus ampicillin at 37°C. When the OD₆₀₀ reached 0.5, IPTG was added to a final concentration of 0.3 mM, and the cultures were incubated for additional 12 h at 15°C with shaking. The cells were concentrated by centrifugation at 5000 rpm for 15 min at 4°C, and the supernatant was removed. Bacteria were resuspended in 20 ml of buffer B (20 mM Tris-HCl, 200 mM NaCl, 1 mM EDTA pH 7.5). The cells were lysed by sonication and the lysates were centrifuged at 5000 rpm for 15 min at 4°C. The supernatant (3 ml) was applied to the amylose resin. Mal-KISsk1 and Mal-KISsk1^{DA} were purified according the New England Amylose Resin protocol.

Osmotic stress assays

The strains to be tested were grown overnight at 30°C on SD supplemented with the required amino acids. The cells

were washed and suspended in YPD or YPGal (for strains carrying plasmids) at OD₆₀₀ 0.1 and were grown until OD₆₀₀ 0.5. Serial dilutions were spotted on YPD or YPGal plates containing 0.5 or 0.75 M KCl and incubated at 30°C for 48 h.

Protein interactions

Assays of physical interactions were performed with a LexA-B42 two-hybrid system, as described previously (Ongay-Larios *et al.*, 2000). Strain EGY48 was transfected with two-hybrid plasmids and grown on an SD plate for 48 h at 30°C. Selected clones were streaked on SGal medium containing 1 mg/ml XGal (5-bromo-4-chloro-3-indolyl-β-D-galactopyranoside; pH 7.0) and incubated for 24 h at 30°C. The protein interactions were determined by the ability of hybrid proteins to induce blue colonies through expression of a LACZ reporter. Quantification of β-galactosidase activity was done as described previously (Ongay-Larios *et al.*, 2000).

Phosphorylation assays and immunoblotting

The amounts of total and phosphorylated KIHog1p were detected in exponentially growing cells that were treated or not treated with different concentrations of KCl for different periods of time. The cells were then treated with 85% trichloroacetic acid (TCA). The cells were concentrated by centrifugation, and the supernatant was removed. The yeasts were lysed with SB-DTT buffer, as described previously (Velázquez-Zavala *et al.*, 2015). When needed, protein concentration was determined by the Bradford assay. The proteins were separated by SDS-PAGE and transferred to an Immobilon-Polyvinylidene difluoride membrane (Millipore). The total and dually phosphorylated KIHog1p were detected with an anti-Hog1p antibody (yC-20 Santa Cruz Biotechnology) and with a monoclonal anti-phospho-p38 antibody (Cell Signaling Technology) respectively as previously described (Velázquez-Zavala *et al.*, 2015). KIYpd1-His protein was detected with a conjugated anti-His6-Peroxidase antibody (Roche). All Westerns were repeated three times and representative blots are shown in figures. Total Hog1 was used as loading control.

In vitro phosphotransfer assay

Escherichia coli ArcB⁷⁸⁻⁵²¹ (H1) and ArcB⁵²¹⁻⁶⁶¹ (D1) domains were purified as described previously (Alvarez and Georgellis, 2010). KIYpd1-His, Mal-KISsk1 and Mal-KISsk1^{DA} were expressed and purified as described above. ArcB⁷⁸⁻⁵²¹ (H1) protein was incubated with 0.05 mM [γ -³²P]ATP (specific activity 2 Ci/mmol) in phosphorylation buffer (165 mM HEPES, 250 mM KCl, 25 mM MgCl₂, 5 mM DTT, 50% glycerol, pH 7.5) at room temperature, and after 10 min ArcB⁵²¹⁻⁶⁶¹ (D1), His-KIYpd1 and Mal-KISsk1 or Mal-KISsk1^{DA} were added to the reaction. Phosphotransfer reactions were carried out at RT for 10 min. The reactions were stopped by the addition of loading buffer (10% SDS, 0.2 M Tris pH 7.5, 10% glycerol, 0.14 M β-Mercaptoethanol, 0.04 mM of bromophenol blue). The

samples were subjected to SDS-PAGE, and the dried gels were analyzed with a phospho-imager scanner.

In vivo phosphotransfer assay

The *K. lactis* ΔKlsln1 and ΔKlypd1 strains were transfected with YEpkDGal-HIS-KIYPD1 or empty YEpkDGalHis plasmids. Transfected cells were grown in liquid YPGal-Pi (phosphate-depleted selective) medium until OD₆₀₀ 0.6. The cells were centrifuged and resuspended in 1 ml of YPGal-Pi. In vivo KIYpd1 labelling with [³²P]orthophosphate and osmotic shock were conducted as previously described (Posas *et al.*, 1996). The cells were treated with 85% TCA, centrifuged briefly and the supernatant was removed by aspiration. The cells were suspended in lysis buffer (250 mM Tris pH 6.8, 0.5 M DTT, 10% SDS, 20% glycerol, 0.5% bromophenol blue) and lysed with 0.5-mm glass beads with 3 min of vigorous vortexing. The extracts were centrifuged for 1 min and the supernatant was transferred to a clean tube and incubated at 95°C for 5 min. Purified His-KIYpd1 protein using a Nickel column was applied to 15% SDS-polyacrylamide gel electrophoresis and transferred to nylon membranes. The membranes were rinsed with water, dried and analyzed with a phospho-imager scanner. In addition, His-Ypd1 was detected by Western blot using an anti-His antibody (Santa Cruz Biotechnology) according to the manufacturer's directions.

Glycerol and trehalose quantification

Intracellular glycerol was determined enzymatically as described previously (Bergmeyer, 1984). The cells were grown to OD₆₀₀ of 0.5 in YPD at 30°C, washed and suspended in fresh YPD. All cell cultures were treated or not treated for with 0.4 M KCl for 6 h at 30°C, except for one aliquot of strain sln-ts which was incubated at 37°C. The cells were concentrated by centrifugation and washed with water. The cells were resuspended in 1 ml of water, boiled for 15 min and centrifuged at 14000 rpm for 2 min. Aliquots of supernatant were mixed with 137 mM Glycine, 686 mM Hydrazine, 1.37 mM MgCl₂, 1.23 mM ATP, 0.49 mM NAD⁺, and 2–15 μM of glycerol and 17 kU/l Glycerol-3-phosphate dehydrogenase and the OD₃₄₀ was determined (A₁). After addition of 0.85 kU/l glycerol kinase, a second reading was obtained (A₂). The subtraction between A₂ and A₁ was used to calculate the glycerol concentration according to the formula C = [Vεdv]ΔA mmol/l, where V is the final reaction volume; ε is the NADH Molar Extinction Coefficient at 340 nm; d, is the distance across the beam (cm) and v, is the sample volume.

Trehalose accumulation was determined according to the protocol described previously (Hounsa *et al.*, 1998), except that cells were grown and treated with NaCl as described for the glycerol determination. Trehalase, glucose oxidase and radish peroxidase were obtained from SIGMA.

Acknowledgments

This research was supported by grant IN206513 from PAPIIT-DGAPA, UNAM and grant CB-166734 from CONACyT (México). MR received a student fellowship from CONACyT

and was a PhD student of the Biochemical Science Program while working in this project. The laboratory of FP is supported by grants from the Spanish Government BFU2015-64437 P and FEDER, the Catalan Government (2014 SGR 599) and supported by Fundación Botín, by Banco Santander through its Santander Universities Global Division. FP and EdN are recipients of an ICREA Acadèmia (Generalitat de Catalunya). We received invaluable technical assistance from Laia Subirana (UPF); Guadalupe Codiz and Minerva Mora at the Molecular Biology Unit (IFC); and from Gerardo Coello, Ana María Escalante and Juan Manuel Barbosa at the Computer Unit, (IFC).

Conflict of Interest

The authors have no conflict of interest to declare.

References

- Albertyn, J., Hohmann, S., Thevelein, J.M., and Prior, B.A. (1994) GPD1, which encodes glycerol-3-phosphate dehydrogenase, is essential for growth under osmotic stress in *Saccharomyces cerevisiae*, and its expression is regulated by the high-osmolarity glycerol response pathway. *Mol Cell Biol* **14**: 4135–4144.
- Alex, L.A., Korch, C., Selitrennikoff, C.P., and Simon, M.I. (1998) COS1, a two-component histidine kinase that is involved in hyphal development in the opportunistic pathogen *Candida albicans*. *Proc Natl Acad Sci USA* **95**: 7069–7073.
- Alvarez, A., and Georgellis, D. (2010) *In vitro* and *in vivo* analysis of the ArcB/A redox signalling pathway. *Methods Enzymol* **471**: 205–228.
- Aoyama, K., Aiba, H., and Mizuno, T. (2001) Genetic analysis of the His-to-Asp phosphorelay implicated in mitotic cell cycle control: involvement of histidine-kinase genes of *Schizosaccharomyces pombe*. *Biosci Biotechnol Biochem* **65**: 2347–2352.
- Aoyama, K., Mitsubayashi, Y., Aiba, H., and Mizuno, T. (2000) Spy1, a histidine-containing phosphotransfer signaling protein, regulates the fission yeast cell cycle through the Mcs4 response regulator. *J Bacteriol* **182**: 4868–4874.
- Argüelles, J.C. (2000) Physiological roles of trehalose in bacteria and yeast: comparative analysis. *Arch Microbiol* **174**: 217–224.
- Bergmeyer, H.U. (1984) *Methods of Enzymatic Analysis: Metabolites 1: Carbohydrates*. Wiley-Blackwell USA, p. 701.
- Calera, J.A., and Calderone, R.A. (1999a) Flocculation of hyphae is associated with a deletion in the putative CaHK1 two component histidine kinase gene from *Candida albicans*. *Microbiology* **145**: 1431–1442.
- Calera, J.A., and Calderone, R.A. (1999b) Identification of a putative response regulator two-component phosphorelay gene (CaSSK1) from *Candida albicans*. *Yeast* **15**: 1243–1254.
- Calera, J.A., Herman, D., and Calderone, R.A. (2000a) Identification of YPD1, a gene of *Candida albicans* which encodes a two component phosphohistidine intermediate protein. *Yeast* **16**: 1053–1059.
- Calera, J.A., Zhao, X.J., and Calderone, R.A. (2000b) Defective hyphal development and avirulence caused by a deletion of the SSK1 response regulator gene in *Candida albicans*. *Infect Immun* **68**: 518–525.
- Chauhan, N., Inglis, D., Roman, E., Pla, J., Li, D., Calera, J.A., and Calderone, R.A. (2003) *Candida albicans* response regulator gene SSK1 regulates a subset of genes whose functions are associated with cell wall biosynthesis and adaptation to oxidative stress. *Eukaryot Cell* **2**: 1018–1024.
- Cialfi, S., Uccelletti, D., Carducci, A., Wésolowski-Louvel, M., Mancini, P., Heipieper, H.J., and Saliola, M. (2011) KIH1 is a component of glycerol response pathways in the milk yeast *Kluyveromyces lactis*. *Microbiology* **157**: 1509–1518.
- Clotet, J., and Posas, F. (2007) Control of cell cycle in response to osmostress: lessons from yeast. *Methods Enzymol* **428**: 63–76.
- Degols, G., Shiozaki, K., and Russell, P. (1996) Activation and regulation of the Spc1 stress-activated protein kinase in *Schizosaccharomyces pombe*. *Mol Cell Biol* **16**: 2870–2877.
- de Nadal, E., and Posas, F. (2015) Osmostress-induced gene expression – a model to understand how stress-activated protein kinases (SAPKs) regulate transcription. *FEBS J* **282**: 3275–3285.
- Desai, C., Mavrianos, J., and Chauhan, N. (2011) *Candida albicans* SRR1, a putative two-component response regulator gene, is required for stress adaptation, morphogenesis and virulence. *Eukaryot Cell* **10**: 1370–1374.
- George, V.T., Brooks, G., and Humphrey, T.C. (2007) Regulation of cell cycle and stress responses to hydrostatic pressure in fission yeast. *Mol Biol Cell* **18**: 4168–4179.
- Georgellis, D., Lynch, S.A., and Lin, E.C.C. (1997) *In vitro* phosphorylation study of two-component signal transduction system of *Escherichia coli*. *J Bacteriol* **179**: 5429–5435.
- Golemis, E.A., Serebriiskii, Gyuris, I.J., and Brent, R. (1997) Interaction trap/two-hybrid system to identify interacting proteins. *Curr. Protoc. Neurosci* Chapter 4: 4.4.1–4.4.36.
- Gustin, M.C., Albertyn, J., Alexander, M., and Davenport, K. (1998) MAP kinase pathways in the yeast *Saccharomyces cerevisiae*. *Microbiol Mol Biol Rev* **62**: 1264–1300.
- Hohmann, S. (2002) Osmotic stress signaling and osmoadaptation in yeast. *Microbiol Mol Biol Rev* **66**: 300–372.
- Horie, T., Tatebayashi, K., Yamada, R., and Saito, H. (2008) Phosphorylated Ssk1 prevents unphosphorylated Ssk1 from activating the Ssk2 mitogen-activated protein kinase kinase in the yeast high-osmolarity glycerol osmoregulatory pathway. *Mol Cell Biol* **28**: 5172–5183.
- Hounsa, C.-G., Brandt, E.V., Thevelein, J., Hohmann, S., and Prior, B.A. (1998) Role of trehalose in survival of *Saccharomyces cerevisiae* under osmotic stress. *Microbiology* **144**: 671–680.
- Kawasaki, L., Castañeda-Bueno, M., Sánchez-Paredes, E., Velázquez-Zavala, N., Torres-Quiroz, F., Ongay-Larios, L., and Coria, R. (2008) Protein kinases involved in mating and osmotic stress in the yeast *Kluyveromyces lactis*. *Eukaryot Cell* **7**: 78–85.
- Krantz, M., Becht, E., and Hohmann, S. (2006) Comparative genomics of the HOG-signalling system in fungi. *Curr Genet* **49**: 137–151.

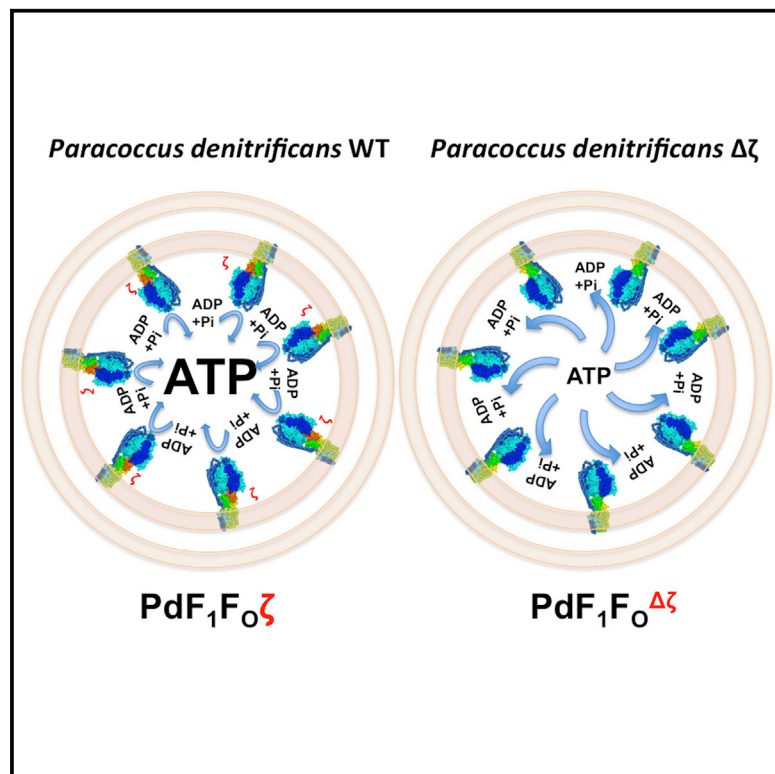
- Macia, J., Regot, S., Peeters, T., Conde, N., Solé, R., and Posas, F. (2009) Dynamic signaling in the Hog1 MAPK pathway relies on high basal signal transduction. *Sci Signal* **2**: ra13.
- Maeda, T., Takekawa, M., and Saito, H. (1995) Activation of yeast PBS2 MAPKK by MAPKKKs or by binding of an SH3-containing osmosensor. *Science* **269**: 554–558.
- Maeda, T., Wurgler-Murphy, S., and Saito, H. (1994) A two-component system that regulates an osmosensing MAP kinase cascade in yeast. *Nature* **369**: 242–245.
- Martín, H., Flández, M., Nombela, C., and Molina, M. (2005) Protein phosphatases in MAPK signalling: we keep learning from yeast. *Mol Microbiol* **58**: 6–16.
- Mattison, C.P., and Ota, I.M. (2000) Two protein tyrosine phosphatases, Ptp2 and Ptp3, modulate the subcellular localization of the Hog1 MAP kinase in yeast. *Genes Dev* **14**: 1229–1235.
- Nagahashi, S., Mio, T., Ono, N., Yamada-Okabe, T., Arisawa, M., Bussey, H., and Yamada-Okabe, H. (1998) Isolation of CaSLN1 and CaNIK1, the genes for osmo-sensing histidine kinase homologues, from the pathogenic fungus *Candida albicans*. *Microbiology* **144**: 425–432.
- Nakamichi, N., Yamada, H., Aoyama, K., Ohmiya, R., Alba, H., and Mizuna, T. (2002) His-to-asp phosphorelay circuitry for regulation of sexual development in *Schizosaccharomyces pombe*. *Biosci Biotechnol Biochem* **66**: 2662–2672.
- Ongay-Larios, L., Saviñón-Tejeda, A., Williamson, M., Durán-Avelar, M.J., and Coria, R. (2000) The Leu132 of the Ste4(Gβ) subunit is essential for proper coupling of the G protein with the Ste2 α-factor receptor during the mating pheromone response in yeast. *FEBS Lett* **467**: 22–26.
- Ostrander, D.B., and Gorman, J.A. (1999) The extracellular domain of the *Saccharomyces cerevisiae* Sln1p membrane osmolarity sensor is necessary for kinase activity. *J Bacteriol* **181**: 527–534.
- Parrou, J.L., Teste, M.-A., and Francois, J. (1997) Effects of various types of stress on the metabolism of reserve carbohydrates in *Saccharomyces cerevisiae*: genetic evidence for a stress-induced recycling of glycogen and trehalose. *Microbiology* **143**: 1891–1900.
- Posas, F., and Saito, H. (1997) Osmotic activation of the HOG MAPK pathway via Ste11p MAPKKK: scaffold role of Pbs2p MAPKK. *Science* **276**: 1702–1705.
- Posas, F., and Saito, H. (1998) Activation of the yeast SSK2 MAP kinase kinase kinase by the SSK1 two-component response regulator. *EMBO J* **17**: 1385–1394.
- Posas, F., Wurgler-Murphy, S.M., Maeda, T., Witten, E.A., Thai, T.C., and Saito, H. (1996) Yeast HOG1 MAP kinase cascade is regulated by a multistep phosphorelay mechanism in the SLN1-YPD1-SSK1 “two-component” osmo-sensor. *Cell* **86**: 865–875.
- Reiser, V., Raitt, D.C., and Saito, H. (2003) Yeast osmosensor Sln1 and plant cytokinin receptor Cre1 respond to changes in turgor pressure. *J Cell Biol* **161**: 1035–1040.
- Reiser, V., Salah, S.M., and Ammerer, G. (2000) Polarized localization of yeast Pbs2 depends on osmostress, the membrane protein Sho1 and Cdc42. *Nat Cell Biol* **2**: 620–627.
- Saito, H., and Posas, F. (2012) Response to hyperosmotic stress. *Genetics* **192**: 289–318.
- Sampedro, J.G., and Uribe, S. (2004) Trehalose-enzyme interactions result in structure stabilization and activity inhibition. The role of viscosity. *Mol Cell Biochem* **256**: 257: 319–327.
- Santos, J.L., and Shiozaki, K. (2001) Fungal histidine kinases. *Science STKE* **2001**: re1.
- Saviñón-Tejeda, A., Ongay-Larios, L., Valdés-Rodríguez, J., and Coria, R. (2001) The *KIGpa1* gene encodes a G-protein α subunit that is a positive control element in the mating pathway of the budding yeast *Kluyveromyces lactis*. *J Bacteriol* **183**: 229–234.
- Sharifian, H., Lampert, F., Stojanovski, K., Regot, S., Vaga, S., Buser, R., et al. (2015) Parallel feedback loops control the basal activity of the HOG MAPK signaling cascade. *Integr Biol (Camb)* **7**: 412–422.
- Sherman, F., Fink, G.R., and Hicks, J. (1986) *Laboratory Course Manual for Methods in Yeast Genetics*. Plainview, NY: Cold Spring Harbor Laboratory Press.
- Singh, P., Chauhan, N., Ghosh, A., Dixon, F., and Calderone, R.A. (2004) SKN7 of *Candida albicans*: mutant construction and phenotype analysis. *Infect Immun* **72**: 2390–2394.
- Velázquez-Zavala, N., Rodríguez-González, M., Navarro-Olmos, R., Ongay-Larios, L., Kawasaki, L., Torres-Quiroz, F., and Coria, R. (2015) Ineffective phosphorylation of mitogen-activated protein kinase Hog1p in response to high osmotic stress in the yeast *Kluyveromyces lactis*. *Eukaryot Cell* **14**: 922–930.
- Vendrell, A., Martínez-Pastor, M., González-Novo, A., Pascual-Ahuir, A., Sinclair, D.A., Proft, M., and Posas, F. (2011) Sir2 histone deacetylase prevents programmed cell death caused by sustained activation of the hog1 stress-activated protein kinase. *EMBO Rep* **12**: 1062–1068.
- Warner, J. (1991) Labeling of RNA and phosphoproteins in *Saccharomyces cerevisiae*. *Methods Enzymol* **246**: 423–428.
- Wolfe, K.H., and Shields, D.C. (1997) Molecular evidence for an ancient duplication of the entire yeast genome. *Nature* **387**: 708–713.
- Yamada-Okabe, T., Mio, T., Ono, N., Kashima, Y., Matsui, M., Arisawa, M., and Yamada-Okabe, H. (1999) Roles of three histidine kinase genes in hyphal development and virulence of the pathogenic fungus *Candida albicans*. *J Bacteriol* **181**: 7243–7247.

Supporting information

Additional supporting information may be found in the online version of this article at the publisher's web-site.

The Biological Role of the ζ Subunit as Unidirectional Inhibitor of the F_1F_O -ATPase of *Paracoccus denitrificans*

Graphical Abstract



Authors

Francisco Mendoza-Hoffmann,
Ángeles Pérez-Oseguera,
Miguel Ángel Cevallos, ...,
Emilio Espinoza-Simón,
Salvador Uribe-Carvajal,
José J. García-Trejo

Correspondence

jjgartre@unam.mx

In Brief

The ATP synthase nanomotor provides most of the chemical energy for life in the form of ATP. Mendoza-Hoffmann et al. resolve the role and mechanism of a natural bacterial ζ inhibitor protein working as a unidirectional pawl-ratchet to block wasteful ATP cleavage by this nanomotor, thus favoring energy preservation for life.

Highlights

- We obtained a knockout of an F₁F_O-ATPase inhibitor Δζ with a clear phenotype
- The *Paracoccus denitrificans* Δζ mutant grows more slowly than the WT in respiratory media
- ζ is a unidirectional F₁F_O-ATPase inhibitor, not affecting the ATP synthase turnover
- ζ works as a pawl-ratchet favoring clockwise ATP synthase rotation and cell division



The Biological Role of the ζ Subunit as Unidirectional Inhibitor of the F_1F_O -ATPase of *Paracoccus denitrificans*

Francisco Mendoza-Hoffmann,¹ Ángeles Pérez-Oseguera,² Miguel Ángel Cevallos,² Mariel Zarco-Zavala,³ Raquel Ortega,¹ Claudia Peña-Segura,⁴ Emilio Espinoza-Simón,⁴ Salvador Uribe-Carvajal,⁴ and José J. García-Trejo^{1,5,*}

¹Departamento de Biología, Facultad de Química, Ciudad Universitaria, Universidad Nacional Autónoma de México (U.N.A.M.), Delegación Coyoacán, Ciudad de México (CDMX) 04510, México

²Programa de Genómica Evolutiva, Centro de Ciencias Genómicas, U.N.A.M., Cuernavaca, Morelos, México

³University of Tokyo, Hongo, Bunkyo-ku, Tokyo, Japan

⁴Instituto de Fisiología Celular, U.N.A.M., Ciudad de México (CDMX), México

⁵Lead Contact

*Correspondence: jjgartre@unam.mx

<https://doi.org/10.1016/j.celrep.2017.12.106>

SUMMARY

The biological roles of the three natural F_1F_O -ATPase inhibitors, ϵ , ζ , and IF_1 , on cell physiology remain controversial. The ζ subunit is a useful model for deletion studies since it mimics mitochondrial IF_1 , but in the F_1F_O -ATPase of *Paracoccus denitrificans* (PdF_1F_O), it is a monogenic and supernumerary subunit. Here, we constructed a *P. denitrificans* 1222 derivative ($Pd\Delta\zeta$) with a deleted ζ gene to determine its role in cell growth and bioenergetics. The results show that the lack of ζ *in vivo* strongly restricts respiratory *P. denitrificans* growth, and this is restored by complementation in *trans* with an exogenous ζ gene. Removal of ζ increased the coupled PdF_1F_O -ATPase activity without affecting the PdF_1F_O -ATP synthase turnover, and the latter was not affected at all by ζ reconstitution *in vitro*. Therefore, ζ works as a unidirectional pawl-ratchet inhibitor of the PdF_1F_O -ATPase nanomotor favoring the ATP synthase turnover to improve respiratory cell growth and bioenergetics.

INTRODUCTION

ATP synthases are the cornerstone of cellular bioenergetics in bacteria, mitochondria, and chloroplasts; these F_1F_O -ATP synthases synthesize more than 90% of the ATP required by most organisms to live. The F_1F_O complex harnesses the energy stored in electrochemical gradients ($\Delta\mu_{H^+}$) generated by electron transport chains (Mitchell, 1961) by coupling the proton flow through the F_O channel to drive ATP synthesis from ADP and Pi at the F_1 water-soluble portion. The F_1 part has five essential subunits—namely, α , β , γ , δ , and ϵ —and can be isolated as a water-soluble F_1 -ATPase (Boyer, 1997). In α -proteobacteria such as *Paracoccus denitrificans*, the F_1 portion also contains a sixth supernumerary subunit named ζ (de la Rosa-Morales, 2005; Morales-Ríos et al., 2010). The F_O proton channel is composed

of three essential subunits, a , b , and c . In eukaryotes, the mitochondrial enzyme includes the mitochondrial inhibitor (IF_1), which is a regulatory (Pullman and Monroy, 1963) and stabilizing factor of dimeric and oligomeric forms of the mitochondrial ATP synthase (García et al., 2006).

The F_1F_O -ATP synthase is a rotary reversible nanomotor (Duncan et al., 1995; Noji et al., 1997; Sabbert et al., 1996); i.e., the central rotor gyrates in a clockwise (CW) direction (viewed from F_O to F_1) to synthesize ATP (Rondelez et al., 2005) and in a counterclockwise (CCW) sense to hydrolyze it (Noji et al., 1997). In the absence of oxygen or of a final electron acceptor, or during uncoupling (i.e., without a proton gradient), the F_1F_O nanomotor becomes thermodynamically prone to rotate in the reverse CCW ATP hydrolysis turnover, consuming the cellular ATP. Therefore, the CCW F_1F_O -ATPase turnover has to be somehow controlled to favor the F_1F_O -ATP synthase activity and prevent the wasteful F_1F_O -ATPase from functioning. In mitochondria, the protein in charge of blocking the F_1F_O -ATPase activity is the inhibitor protein of the F_1 -ATPase, or IF_1 (Pullman and Monroy, 1963), whereas in bacteria such as *Escherichia coli*, it is the rotor subunit ϵ with the inhibitory function (Sternweis and Smith, 1980). Both inhibitor proteins (IF_1 and ϵ) insert an α -helix at the $\alpha_{DP}/\beta_{DP}/\gamma$ interface of their respective F_1 -ATPases to block γ rotation (Cingolani and Duncan, 2011; Shirakihara et al., 2015).

In α -proteobacteria, which are closely related to the mitochondrial protoendosymbiont (John and Whatley, 1975; Ku et al., 2015; Margulis and Chapman, 1998), the ϵ subunit does not have an inhibitory function; instead, this has been transferred to a natural inhibitor that we discovered in *Paracoccus denitrificans* and related α -proteobacteria and named as the ζ subunit (de la Rosa-Morales, 2005; Morales-Ríos et al., 2010). We found the open reading frame (ORF) of ζ (DUF1476) conserved along the α -proteobacteria class and identified the inhibitory domain at the N terminus of ζ . The latter preserves some similarity with the inhibitory domain of IF_1 (Zarco-Zavala et al., 2014), notwithstanding that the full ζ structure (PDB: 2LL0) is different from those of mitochondrial IF_1 and bacterial ϵ (Serrano et al., 2014; Zarco-Zavala et al., 2012, 2014). Cross-linking studies showed that the ζ N terminus blocks rotation of the γ subunit of



the F₁-ATPase of *P. denitrificans*, similarly to IF₁ (Minauro-Sanmiguel et al., 2002). Crystals of the native PdF₁- ζ complex lacked the γ , δ , ε , and ζ subunits (Morales-Ríos et al., 2015a); thus, further structural alignment of the ζ N terminus with the inhibitory domain of IF₁, together with functional studies, showed that ζ also binds into the $\alpha_{DP}/\beta_{DP}/\gamma$ interface-blocking γ rotation, very similarly to mitochondrial IF₁ (García-Trejo et al., 2016). In other words, the ζ subunit blocks the intrinsic rotation of the *P. denitrificans* nanomotor by mimicking IF₁. This binding site of ζ at the $\alpha_{DP}/\beta_{DP}/\gamma$ interface was found before the release of the crystallographic PdF₁F_O structure of *P. denitrificans* (PDB: 5DN6), which confirmed that ζ binds to the $\alpha_{DP}/\beta_{DP}/\gamma$ interface (Morales-Ríos et al., 2015b). Taken together, the ζ nuclear magnetic resonance (NMR) structure (Serrano et al., 2014; Zarco-Zavala et al., 2012, 2014), the functional and modeling studies (García-Trejo et al., 2016), and the crystallographic data (Morales-Ríos et al., 2015b) show that the ζ N terminus shifts from an intrinsically disordered region (IDR) to an inhibitory α -helix that can be superimposed with the inhibitory IF₁ N terminus bound to the mitochondrial F₁ (Cabezón et al., 2003). In summary, ζ is an α -proteobacterial inhibitor protein that blocks the activity of the F₁F_O-ATPase complex of *P. denitrificans* with an IF₁-like N-terminal structure and mechanism; therefore, it can be used as a model to study the structure, function, and mechanism of these F₁-ATPase inhibitors. These data also support the endosymbiotic origin of mitochondria as derived from α -proteobacteria (John and Whatley, 1975; Ku et al., 2015; Margulis and Chapman, 1998), as shown by the close similarity of the primary and tertiary structures of the F₁ subunits from *P. denitrificans* and bovine heart mitochondria (García-Trejo et al., 2016).

The physiological role of the ATP synthase's natural inhibitor proteins has been a subject of a number of studies. For instance, IF₁ knockouts in yeast (*Saccharomyces cerevisiae*) and mice have shown that IF₁ is non-essential, and its absence did not exert a major effect in yeast growth or in mouse development and bioenergetics, respectively (Lu et al., 2001; Nakamura et al., 2013). Furthermore, mitochondrial IF₁ is encoded by 2–3 different genes, depending on the species; besides, there are two IF₁ homologous stabilizing factors of 9 kDa (Stf1) and 15 kDa (Stf2) in mitochondria (Hashimoto et al., 1983, 1984, 1987, 1990a), with Stf1 also working as an F₁-ATPase inhibitor (Hashimoto et al., 1987, 1990b). Furthermore, the three simultaneous yeast knockouts of the IF₁ (INH1), 9-kDa (STF1), and 15-kDa (STF2) genes showed no significant effects on cell growth, mitochondrial bioenergetics, and/or ATP synthase dimerization (Dienhart et al., 2002), unless the cells are exposed to severe starvation (Lu et al., 2001). Similar results have been observed with the homologous protein of IF₁ (MAI-2) in *Caenorhabditis elegans* (Fernández-Cárdenas et al., 2017). On the other hand, bacterial ε is an important structural subunit, forming a key connection between the rotary γ and c-ring subunits of the enzyme (see, for instance, Figure 7); thus, bacterial ε cannot be deleted without disassembling F₁ from F_O (Klionsky et al., 1984). Then again, the ζ subunit is encoded by a single supernumerary gene in α -proteobacteria (Morales-Ríos et al., 2010; Zarco-Zavala et al., 2014). Taken together, these precedents indicate that, since ζ mimics IF₁, it is a suitable model to assess the biological role of the natural ATP synthase inhibitors, espe-

cially because *P. denitrificans* can grow in a respiratory medium where it relies exclusively on its mitochondrial-like electron transport chain (Berry and Trumper, 1985; Iwata et al., 1995; Kleinschroth et al., 2011; Ludwig and Schatz, 1980; Penoyer et al., 1988; Yagi, 1986).

Once it was predicted that the ζ subunit would be a suitable model to study the role of the natural F₁-ATPase inhibitors, we analyzed the effect of the deletion of the ζ subunit of the F₁F_O-ATPase from *Paracoccus denitrificans* 1222 (Pd1222) on bacterial growth and cell bioenergetics, and the results are here presented. This was carried out by construction of a stable *P. denitrificans* $\Delta\zeta$ mutant strain (Pd $\Delta\zeta$), as well as a complemented strain (Pd $\Delta\zeta+\zeta$). The comparison of their growth curves in rich lysogeny broth (LB) medium and succinate respiratory minimal medium show clearly that removal of a natural inhibitor of the ATP synthase has strong and deleterious effects on the bacterial respiratory growth and bioenergetics. The ATP synthesis and hydrolysis of inside-out membrane vesicles of Pd1222 (PdWT) and Pd $\Delta\zeta$ mutant strains, and the PdF₁-ATPase activity of the enzyme purified from both strains, were also analyzed; these activities correlate well with the phenotype observed in the mutant Pd $\Delta\zeta$. Finally the kinetic effects of the ζ deletion and reconstitution on the F₁F_O-ATPase and F₁F_O-ATP synthase turnovers strongly support that the ζ subunit works unidirectionally as the previously proposed pawl-ratchet (García-Trejo et al., 2016) to block selectively the CCW rotation of the PdF₁F_O central rotor and, thus, favoring ATP synthesis over its hydrolysis to improve bacterial respiratory growth.

RESULTS AND DISCUSSION

Construction of a Mutant Lacking the ζ Gene and Complementation of the Knockout Strain

A suicidal plasmid, pFMMCJG- $\Delta\zeta$ (see Table S1), replaced the entire ζ gene with the kanamycin resistance cassette by homologous recombination. To confirm that the observed effects of the mutant strain are derived exclusively from the deletion of the ζ subunit ($\Delta\zeta$), the best control is to complement the Pd $\Delta\zeta$ strain with an expression plasmid containing the recombinant ζ gene. Therefore, a pBBR derivative ζ construction (pFMMCJG- $\Delta\zeta+\zeta$) was obtained using a multi-host plasmid, pBBR1 MCS-5 (Kovach et al., 1995) (Table S1). The Pd $\Delta\zeta+\zeta$ strain was subsequently obtained by conjugation of S17/pFMMCJG+ ζ into the Pd $\Delta\zeta$ strain, as explained in Experimental Procedures.

Our Pd $\Delta\zeta$ knockout mutant was confirmed by PCR and western blotting. In the PCR, the ζ gene was amplified correctly from the chromosomal DNA of the Pd1222 (PdWT), but, as expected, it could not be amplified at all from the Pd $\Delta\zeta$ strain (Figure 1A). Furthermore, the wild-type (WT) ζ gene can be also amplified from the complemented Pd $\Delta\zeta+\zeta$ strain. We also confirmed that the kanamycin resistance (Km^R) was amplified only from the Pd $\Delta\zeta$ and Pd $\Delta\zeta+\zeta$ strains, but not from the Pd1222 (PdWT) (data not shown). On the other hand, anti- ζ western blot analyses of cell extracts from the three strains confirmed that the ζ protein is totally absent in the Pd $\Delta\zeta$ strain and that ζ reappeared in the Pd $\Delta\zeta+\zeta$ strain, as shown in Figure 1B.

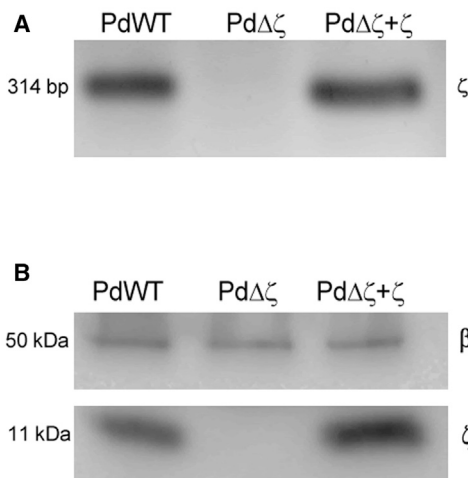


Figure 1. Confirmation of the Inhibitory ζ Subunit Depletion in $Pd\Delta\zeta$
 (A) The ζ gene (314 bp) was PCR-amplified from the genomic DNA of three different *P. denitrificans* strains: the wild-type PdWT, the mutant lacking the ζ gene Pd $\Delta\zeta$, and the mutant Pd $\Delta\zeta$ complemented with the ζ gene Pd $\Delta\zeta+\zeta$. DNA amplifications were resolved by 2% agarose gel electrophoresis.
 (B) PdWT, Pd $\Delta\zeta$, and Pd $\Delta\zeta+\zeta$ were grown for 24 hr on LB medium. Cell lysates were resolved by SDS-PAGE and western blotted for β and ζ proteins. Data are representative of three separate experiments.

Cell Growth

Cells from Pd1222 (PdWT), Pd $\Delta\zeta$, and Pd $\Delta\zeta+\zeta$ strains were grown separately in either rich LB medium or respiratory succinate minimal medium at 30°C for 48 hr. It was observed that, in LB-rich medium, there are no significant differences in the growth rate of all three strains other than a slight delay in the lag phase of the Pd $\Delta\zeta$ mutant (Figure 2A). In marked contrast, when the bacterial growth was followed in the minimal succinate medium, we clearly observed a phenotype in the Pd $\Delta\zeta$ strain in that it grows much more slowly than the Pd1222 (PdWT). In the first 24 hr, the mutant (Pd $\Delta\zeta$) barely starts to grow in this respiratory medium, whereas the WT (Pd1222) has already reached saturation (Figure 2B). In addition, the complemented mutant (Pd $\Delta\zeta+\zeta$) reverted to the WT phenotype, thus discarding the possibility that the slow growth observed for the Pd $\Delta\zeta$ strain could result from other non-specific changes in the mutant strain. The complemented Pd $\Delta\zeta+\zeta$ phenotype reached a similar growth rate compared to that of the Pd1222 (PdWT) strain (Figure 2B). In summary, these results show that the ζ gene is not essential for bacterial growth and not very important physiologically in rich LB medium. However, when *P. denitrificans* is forced to respire with oxygen and to obtain ATP exclusively from oxidative phosphorylation (Ox-Phos), the mutant has serious difficulties growing in the absence of ζ , which then becomes a key ATP synthase regulatory subunit (Figure 2).

The Effect of ζ Deletion on ATP Synthesis and ATP Hydrolysis of SBPs

We prepared sub-bacterial particles (SBPs) from the PdWT and mutant Pd $\Delta\zeta$ strains grown in both the LB-rich medium and the

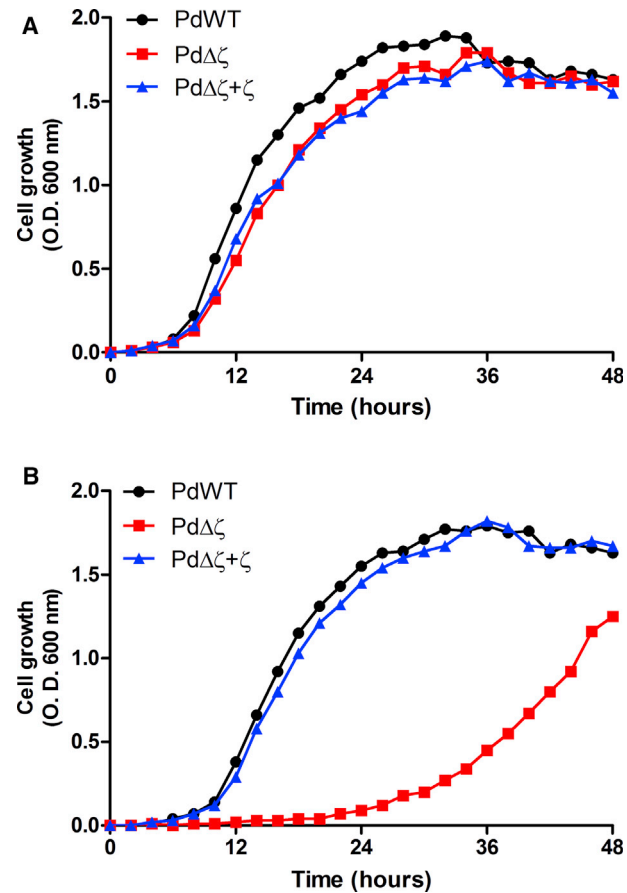


Figure 2. Effect of ζ Deletion on the Growth of *P. denitrificans*

Approximately 4.8×10^8 cells per milliliter of each strain of *P. denitrificans*: the wild-type PdWT (black circles), the mutant lacking the ζ gene Pd $\Delta\zeta$ (red squares), or the mutant Pd $\Delta\zeta$ complemented with the ζ gene Pd $\Delta\zeta+\zeta$ (blue triangles) were inoculated separately into 60 mL of LB or succinate liquid medium and incubated at 30°C for 48 hr at 200 rpm. Aliquots were taken every 2 hr, and the optical density (O.D.) was read spectrophotometrically at 600 nm.
 (A) The growth curve in LB medium.
 (B) The growth curve in succinate medium.

Data are representative from at least three experiments. SD is not shown for clarity but is $\leq 15\%$.

minimal respiratory succinate medium. The SBPs were used to measure their ATP synthesis rates as described in [Experimental Procedures](#). We found no significant differences in the F₁F_O-ATP synthase rates of the WT (Pd1222) and the mutant (Pd $\Delta\zeta$) (Figure 3A). However, both preparations are more active in their synthetic activities when grown in succinate compared to LB medium. The higher ATP synthesis rates obtained in succinate are in concordance with an increased expression of the respiratory chain in oxidative media in *P. denitrificans* (Cox et al., 1978; Hederstedt, 2002; Scholes and Smith, 1968) and with a higher succinate-driven proton-pumping activity obtained in succinate than in LB media (Figure 4). In concordance, the succinate dehydrogenase (SDH) activity of complex II increases slightly when *P. denitrificans* is grown in the presence of succinate versus its absence, together with a several-fold

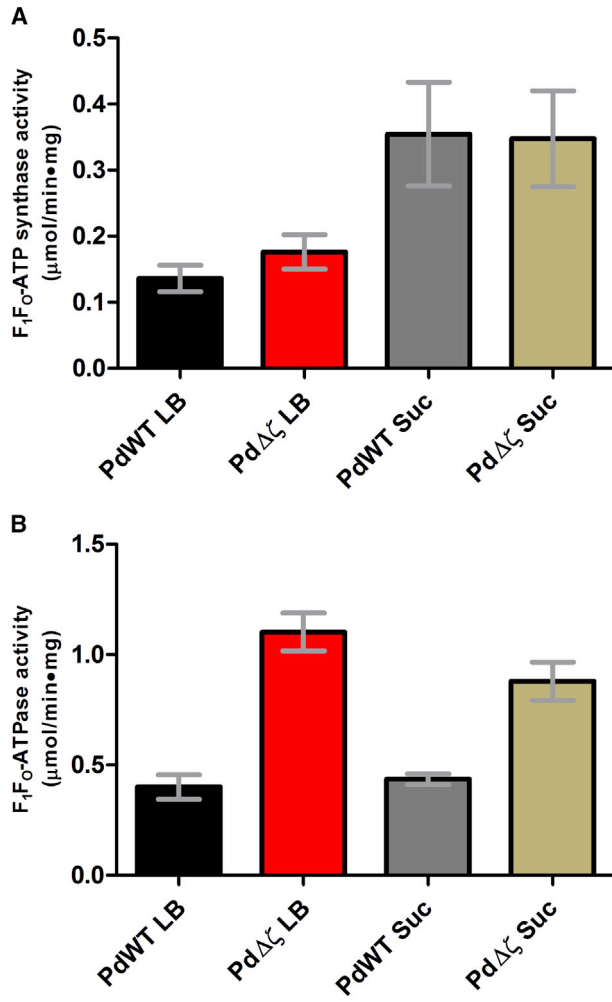


Figure 3. The ζ Subunit Inhibits the F_1F_0 -ATPase Activity, but Not the F_1F_0 -ATP Synthase Activity, in SBPs

The wild-type PdWT and the mutant Pd $\Delta\zeta$ strains were grown in LB or succinate (Suc) medium, cells were harvested, and coupled sub-bacterial particles (SBPs) were prepared.

(A) The F_1F_0 -ATP-synthase-specific activity (micromolar/minute • milligrams) of the wild-type PdWT grown in LB (black), the Pd $\Delta\zeta$ strain grown in LB (red), the PdWT grown in succinate medium (gray), and the mutant Pd $\Delta\zeta$ strain grown in succinate medium (green).

(B) The F_1F_0 -ATPase-specific activity (micromolar/minute • milligrams). Activities were measured in the presence of LDAO (0.15%) as an activator. From left to right: the wild-type PdWT grown in LB (black); the mutant strain Pd $\Delta\zeta$ grown in LB medium (red); the wild-type PdWT grown in succinate (gray); and the mutant strain Pd $\Delta\zeta$ grown in succinate (green).

The average of three experiments is shown with SD.

increase in the mRNA of the *sdh* operon (Hederstedt, 2002). To confirm this, we carried out anti-SD70 western-blot analyses of SBPs isolated from PdWT and Pd $\Delta\zeta$ strains grown in LB or succinate media and confirmed that there is actually a modest but significant increase in the amount of succinate dehydrogenase in both PdWT and Pd $\Delta\zeta$ strains (Figure S2). Thus, the higher ATP synthase and proton-pumping activities in succinate media for SBPs isolated from PdWT and Pd $\Delta\zeta$ cells could

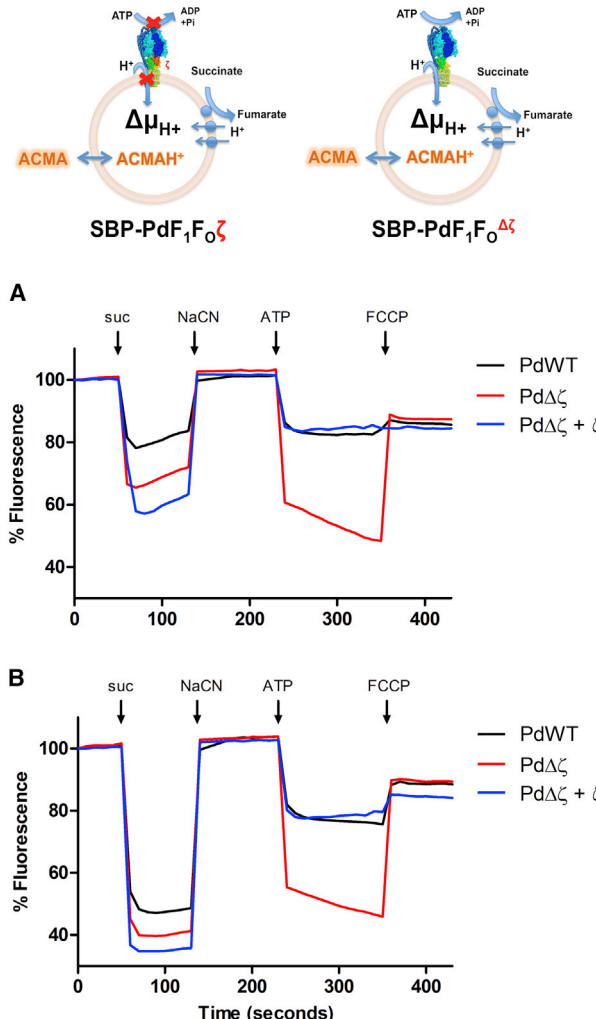


Figure 4. Effect of the ζ Deletion on Membrane Energization of SBPs from *Paracoccus denitrificans*

Upper diagram: the ACMA quenching fluorescence assay. Proton pumping is coupled either to succinate oxidation by the respiratory chain or to ATP hydrolysis carried out by the PdF1F0 complex (see *Supplemental Experimental Procedures* for details).

(A and B) SBPs were prepared from wild-type PdWT and the Pd $\Delta\zeta$ strains grown in (A) LB medium or (B) succinate medium (suc). Two subsequent events of membrane energization and collapse were induced, with succinate/NaCN and Mg-ATP/FCCP as described in *Experimental Procedures*. 300 μg of each SBP were diluted in 3 mL ACMA medium directly in the fluorescence cell. Black and red indicate membrane energization of PdWT and Pd $\Delta\zeta$, respectively. As a control, shown in blue, 120 μg of exogenous recombinant ζ was added to 300 μg of SBPs from Pd $\Delta\zeta$ (Pd $\Delta\zeta$ + ζ) in conditions where ζ inhibits essentially all of the PdF1F0-ATPase activity (see Figure 5D). ACMA fluorescence data shown are the average of three different experiments.

be, at some extent, the result of a higher expression of the succinate-oxidizing respiratory chain. Nevertheless, and more importantly, aside from the differences in Ox-Phos and $\Delta\mu_{\text{H}^+}$ observed in LB and succinate media used to grow *P. denitrificans*, it was clearly observed that the ATP synthesis

rates of both the control Pd1222 (PdWT) and the Pd $\Delta\zeta$ strains are essentially the same (Figure 3A). We also corroborated that the ATP synthase was expressed in similar amounts in PdWT and Pd $\Delta\zeta$ strains and in both LB and succinate media (Figures S2 and S4), indicating that the $\Delta\zeta$ deletion or the shift from LB to succinate does not alter the amounts of ATP synthase, thus confirming that the observed changes in activities or proton pumping described later are not due to changes in the number of ATP synthase enzymes. In brief, the complete removal of the ζ subunit does not have any significant effect on the full oxidative phosphorylation of *P. denitrificans*, as supported by succinate oxidation. At this point, it seems worth mentioning that, in contrast to the *E. coli* ATP synthase, which has a low (0.1) control coefficient of the full Ox-Phos *in vivo* (Jensen et al., 1993), the PdF₁F_O-ATP synthase has a control coefficient of 1.0 of the full Ox-Phos in the SBPs of *P. denitrificans* (Pérez and Ferguson, 1990); this means that the major rate-limiting step of the full Ox-Phos of the SBPs is the ATP synthase of this bacterium; therefore, the effect of an inhibitor of the PdF₁F_O-ATP synthase on the full Ox-Phos reaction can be correlated directly with its rotary kinetic mechanism. In summary, this indicates that ζ does not have any effect at all on the rate of the synthetic CW intrinsic rotation of the PdF₁F_O ATP synthase coupled to ATP synthesis.

We had previously shown the inhibitory function of the ζ subunit on the PdF₁-ATPase and PdF₁F_O-ATPase activities by homologous reconstitution of the recombinant ζ subunit (Morales-Ríos et al., 2010; Zarco-Zavala et al., 2014) and by the observation that partial removal of the ζ subunit increased the PdF₁-ATPase activity. Now, thanks to this ζ deletion study, we are in optimal conditions to confirm whether there is a higher increase in PdF₁-ATPase and PdF₁F_O-ATPase activities associated with full ζ removal, as expected from the inhibitory function of ζ . The effect of ζ deletion on ATP hydrolysis was measured in SBPs prepared from the Pd1222 (PdWT) and Pd $\Delta\zeta$ strains grown in LB or succinate media (Figure 3B). It was clearly observed that the removal of ζ produced a higher hydrolytic activity of the Pd $\Delta\zeta$ samples grown in LB or in succinate media, compared to the WT (Pd1222) samples. The Pd $\Delta\zeta$ preparations reached about 200% of the activities of the Pd1222 (PdWT) SBPs, regardless of the media used (275.5% for LB and 202.1% for succinate). Since ζ works as a total PdF₁-ATPase inhibitor (Zarco-Zavala et al., 2014), if all PdF₁F_O-ATPases were inhibited by ζ , there should not be residual PdF₁F_O-ATPase activity in the PdWT strain; therefore, the \approx 50% residual PdF₁F_O-ATPase (Figure 3B) and PdF₁-ATPase (Figure 5C, LDAO [lauryl dimethylamine oxide]) activities observed for the PdWT in the presence of LDAO, as compared to the $\Delta\zeta$ mutant, are likely due to a fraction of enzymes lacking ζ that are susceptible to inhibition by exogenous recombinant ζ *in vitro*, as we showed previously (Morales-Ríos et al., 2010; Zarco-Zavala et al., 2014). In summary, the PdF₁-ATPase and PdF₁F_O-ATPase activations induced by the total ζ removal, together with the null effect of the ζ deletion on ATP synthesis, strongly suggest that ζ does not affect ATP synthesis, but it strongly inhibits the F-ATPase activity. Therefore, it works as unidirectional inhibitor of the PdF₁F_O-ATPase.

Effect of ζ Deletion on the Proton-Pumping Activity of the PdF₁F_O-ATPase

As in other bacterial systems, the reverse PdF₁F_O-ATPase activity should work physiologically as a primary proton pump, energizing the membrane at the expense of ATP hydrolysis. However, since this reversal PdF₁F_O-ATPase activity is strongly inhibited and latent in *P. denitrificans* (Pacheco-Moisés et al., 2000; Pérez and Ferguson, 1990), the proton-pumping activity should be relatively low in the Pd1222 (PdWT) strain, as compared with that of the Pd $\Delta\zeta$ strain, if the increased PdF₁F_O $^{\Delta\zeta}$ -ATPase activity (Figure 3B) is catalyzed by a coupled PdF₁F_O $^{\Delta\zeta}$ complex pumping protons properly. The low proton-pumping PdF₁F_O-ATPase activity of the WT strain has been evidenced previously by a very low ATP \leftrightarrow [³²P]P_i exchange reaction observed in *P. denitrificans* SBPs, which relies on the formation of the ATP-driven membrane potential (Pacheco-Moisés et al., 2000; Pérez and Ferguson, 1990). To test the effect of ζ removal on the proton pumping of the PdF₁F_O-ATPase, we prepared SBPs from Pd1222 (PdWT) and Pd $\Delta\zeta$ strains grown in both LB and succinate media. Coupled SBPs have the entire respiratory chain; therefore, we assayed qualitatively the formation of succinate-driven and ATP-driven proton gradients by fluorescence quenching of the membrane potential probe ACMA. The first control around the first 100 s of proton pumping with succinate indicates that the SBPs are properly coupled (Figure 4). When SBPs were prepared from cells grown in succinate, formation of the proton gradient was higher than when grown in LB media (compare first 100 s in Figures 4A and 4B). After the addition of cyanide, respiratory formation of the proton gradient is collapsed (as shown by fluorescence recovery); thus, the subsequent proton gradient was formed by the coupled PdF₁F_O-ATPase. Regardless of the media used to grow *P. denitrificans* (LB or succinate medium), it was clear that the ATP-driven proton gradient was much higher when the ζ subunit was deleted (Figures 4A and 4B, red traces) than in control SBPs isolated from the Pd1222 (PdWT) strain (Figures 4A and 4B, black traces). To confirm that the increase in proton pumping is derived from the removal of ζ in the Pd $\Delta\zeta$ mutant, control experiments were carried out by pre-incubating the SBPs of the Pd $\Delta\zeta$ mutant with a molar excess of recombinant ζ in conditions that block completely the PdF₁ and PdF₁F_O-ATPase activity (Zarco-Zavala et al., 2014). As expected from an inactive reconstituted PdF₁F_O- ζ complex unable to pump protons, the ATP-driven ACMA fluorescence quenching returned to very low levels, similar to those observed with the Pd1222 (PdWT) strain expressing the endogenous ζ (Figures 4A and 4B, blue traces); thus, the increase in proton pumping of the mutant was completely abolished by the PdF₁F_O-ATPase inhibition by exogenous ζ . In summary, these results show, on one hand, that the deletion of the ζ subunit does not affect the functional coupling between the F₁ and F_O sectors of the PdF₁F_O complex, as expected from a non-essential regulatory subunit, and that, on the other hand, removal of the ζ subunit from *P. denitrificans* increases the coupled proton-pumping PdF₁F_O $^{\Delta\zeta}$ -ATPase activity, leading to a higher membrane energization than with the control PdF₁F_O- ζ complex in the Pd1222 (PdWT) strain. It is worthwhile to mention that a similar enhancement in ATP-driven H⁺ pumping has been described previously when the mitochondrial IF₁ and

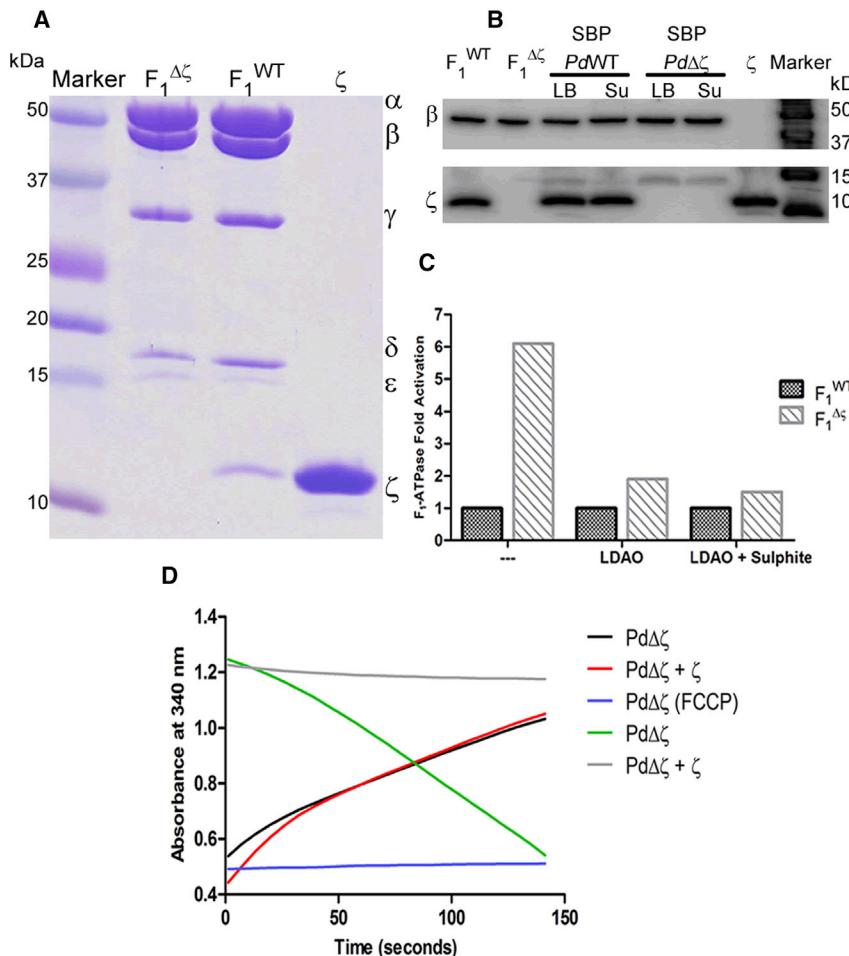


Figure 5. Activation of the Isolated PdF₁-ATPase by the ζ Deletion

(A) SDS-PAGE (from left to right) of the purified mutant PdF₁ $^{\Delta\zeta}$, the wild-type PdF₁, and pure recombinant Pd ζ ; size markers are shown in the first lane.

(B) Western blot (from left to right) of the PdF₁ WT , the PdF₁ $^{\Delta\zeta}$ mutant, SBPs of the wild-type grown in LB or succinate medium (Su), SBPs of the mutant grown in LB or succinate (Su), and the purified Pd ζ ; size markers are in the last lane. The polyvinylidene fluoride (PVDF) membrane was cut in three pieces; the upper part was exposed to the anti- β antibody, the lower part was exposed to the anti-Pd ζ antibody, and the molecular weight markers (MWM) lane was exposed to the Strept-Tactin-HRP conjugate.

(C) The normalized ATPase activities of the wild-type (PdF₁ WT -ATPase; dark gray) and the mutant (PdF₁ $^{\Delta\zeta}$; light gray) are shown as activation-fold relative to the PdF₁ WT activity. Specific activities are shown in the [Supplemental Experimental Procedures](#). Data are the average of three experiments.

(D) Effect of the reconstitution of the ζ subunit on the PdF₁F_O-ATPase and PdF₁F_O-ATP synthase activities of SBPs from Pd $^{\Delta\zeta}$. The PdF₁F_O-ATPase (absorbance decay in green and gray) and the PdF₁F_O $^{\Delta\zeta}$ -ATP synthase (absorbance increase in black, red, and blue) activities were followed spectrophotometrically by coupled assays in real time. In red and gray traces, 100 μ g SBPs from Pd $^{\Delta\zeta}$ were pre-incubated during 20 min at room temperature with 110 μ g exogenous recombinant ζ . The ATP synthesis blank shown in blue was made in the presence of uncoupler FCCP (4 μ M) and venturicidin (4 μ g), which completely block ATP synthesis. Turnover rates were obtained from the linear slopes and were obtained from at least three experiments.

its two stabilizing factors (Stf1 and Stf2) were deleted simultaneously in yeast mitochondria (Lu et al., 2001), indicating further similarities between α -proteobacterial ζ and mitochondrial IF₁ functioning *in vivo*. In a further effort to confirm the effect of ζ deletion on the membrane potential *in vivo*, we took advantage of the fluorescent probe DiOC₂(3), which is instrumental to evidence bacterial membrane energization by its increase in red/green fluorescence ratio in flow cytometry experiments (Novo et al., 1999). Thus, the WT (PdWT), mutant (Pd $^{\Delta\zeta}$), and complemented (Pd $^{\Delta\zeta}+\zeta$) *P. denitrificans* cells were incubated with this probe for 30 min before the determination of the red/green fluorescence ratio by flow cytometry. It was observed that the membrane potential (as evidenced by the CCCP-sensitive change in red/green fluorescence ratio) increased in response to the $\Delta\zeta$ mutation, particularly when the cells were grown in succinate media, and that this increase was reverted by the complementation of the mutant with the exogenous recombinant ζ gene (Figure S3), i.e., similar to the membrane energization of SBPs followed with ACMA (Figure 4). These data confirm that, not only *in vitro* in SBPs but also *in vivo* in whole bacterial cells, and particularly in succinate media, the removal of the ζ subunit activates the H⁺-PdF₁F_O-ATPase working as a primary pump,

thus increasing the proton motive force across the bacterial cell membrane in comparison with the PdWT strain, which is inhibited in the proton-pumping H⁺-PdF₁F_O-ATPase activity by its endogenous ζ subunit.

Purification of the PdF₁-ATPase from Pd1222 and Pd $^{\Delta\zeta}$

The F₁-ATPases from the PdWT and Pd $^{\Delta\zeta}$ strains were purified as described previously (Zarco-Zavala et al., 2014) and are detailed in [Experimental Procedures](#). The absence of the ζ subunit in the pure PdF₁ of the Pd $^{\Delta\zeta}$ mutant was confirmed by anti- ζ and anti- β western blot analyses carried out with both PdF₁ samples and also with SBPs prepared from both strains grown either on LB or succinate medium (Figure 5B). The specific F₁-ATPase activity (SF₁A; units = μ mol/min \times mg of protein) was measured as described in the [Experimental Procedures](#). The WT PdF₁-ATPase exhibited an SF₁A of 0.140 ± 0.003 U without activators, while the PdF₁ $^{\Delta\zeta}$ reached 0.87 ± 0.12 U of SF₁A; i.e., removal of ζ exerted a 6.2-fold increase in PdF₁-ATPase turnover. The same PdF₁ WT -ATPase sample in the presence of LDAO showed an SF₁A of 2.38 ± 0.23 U, and the mutant reached 4.49 ± 1.20 U, 1.9-fold of the WT. The SF₁A in the presence of 0.15% of LDAO and residual 1.5 mM sulfite for the WT was

19.75 ± 1.45 U, and for the mutant, it reached 30.07 ± 1.2 , a 1.5-fold increase relative to the WT (Figure 5C). This activity of the $\text{PdF}_1^{\Delta\zeta}$ mutant is the highest reported so far through the studies of the PdF_1 -ATPase (Zarco-Zavala et al., 2014), likely due to the full removal of the ζ subunit. In all cases, the mutant achieved an increase ≥ 1.5 -fold of the hydrolytic activity of the WT. In order to assess the productive binding of the recombinant ζ to the isolated $\text{PdF}_1^{\Delta\zeta}$ -ATPase, the latter was subjected to an homologous reconstitution by preincubation with increasing concentrations of the recombinant $\text{Pd}\zeta$ in the presence of 60 mM sulfite, 1 mM ATP and MgCl_2 , as described in [Experimental Procedures](#). This preincubation improves the binding of ζ , which requires some partial MgATP hydrolysis turnovers to effectively inhibit the PdF_1^{WT} -ATPase (Zarco-Zavala et al., 2014). Under these conditions, we observed a total $\text{PdF}_1^{\Delta\zeta}$ -ATPase inhibition with a concentration of inhibitor that decreases the enzyme activity to 50% (IC_{50}) of 0.015 μM , which is in the nanomolar range, similar to that previously observed with PdF_1^{WT} -ATPase (Zarco-Zavala et al., 2014). Taken together, the activation of the $\text{PdF}_1^{\Delta\zeta}$ -ATPase (Figure 5C) and that of the $\text{PdF}_1\text{F}_0^{\Delta\zeta}$ -ATPase of SBPs (Figure 3B) confirm that removal of the ζ subunit exerts a 1.5- to 6-fold activation in the PdF_1 -ATPase or PdF_1F_0 -ATPase activities, with the latter coupled to enhanced transmembrane proton translocation in *P. denitrificans* (Figures 3B and 5C).

Effect of the ζ Subunit on the PdF_1F_0 -ATP Synthase and PdF_1F_0 -ATPase Activities

Although several reports show either unidirectional or bidirectional effects of IF_1 and ε on ATP synthesis and hydrolysis (Gómez-Puyou et al., 1979; Iino et al., 2009; Lippe et al., 1988; Masaike et al., 2006; Schwerzmann and Pedersen, 1986; Tsunoda et al., 2001), our results with the ζ subunit of *P. denitrificans* (Figure 3) suggest that these regulators block exclusively the CCW rotation in the F_1 -ATPase direction but not the synthetic CW direction. To determine whether ζ works as a unidirectional ζ PdF_1F_0 -ATPase inhibitor, we carried out the reconstitution of ζ into the ATP synthase of SBPs prepared from the $\text{Pd}\Delta\zeta$ mutant, taking advantage of the total lack of ζ subunit of this preparation. The reconstitution of the ζ subunit was carried out in the same conditions used for the PdF_1 -ATPase assay, in the presence of low concentrations of MgATP, which promote the productive binding and lock of the ζ subunit into the $\alpha_{\text{DP}}/\beta_{\text{DP}}/\gamma$ interface to block completely the PdF_1 or PdF_1F_0 -ATPase activity (Zarco-Zavala et al., 2014). Once the ζ subunit was reconstituted into the SBPs, approximately 100 μg of the latter were added to reaction cells pre-equilibrated at 37°C to measure the rates of ATP synthesis or ATP hydrolysis by real-time coupled assays as described in [Experimental Procedures](#). The rate of ATP hydrolysis is followed by the negative linear decay of NADH disappearance (Figure 5D, green and gray traces), whereas the rate of ATP synthesis is measured by the positive slope of NADPH production (Figure 5D, blue, black, and red traces). As can be seen, the control $\text{PdF}_1\text{F}_0^{\Delta\zeta}$ -ATPase activity (Figure 5D, green) was almost completely blocked (95% inhibition) by reconstitution with a molar excess of ζ subunit (Figure 5D, gray), consistent with the described function of ζ as total inhibitor of the PdF_1 -ATPase (Zarco-Zavala et al., 2014). In marked contrast, the control PdF_1F_0 -ATP synthase ac-

tivity (Figure 5D, black trace) was not affected at all by the same molar excess of ζ (Figure 5D, red trace) that halted almost completely the $\text{PdF}_1\text{F}_0^{\Delta\zeta}$ -ATPase activity (Figure 5D, gray trace). Indeed, the ATP synthase rates were essentially superimposed with or without previous reconstitution of the ζ subunit (Figure 5D, black and red traces). As an important blank control, the basal NADPH production in the presence of uncoupler (4 μM FCCP) and venturicidin (4 $\mu\text{g/mL}$) is indicated in blue in Figure 5D; this basal rate was subtracted from the black and red traces to obtain the net ATP synthesis rates. The experiments in Figure 5D show representative traces that were repeated at least three times, confirming clearly that the ζ subunit works as a unidirectional inhibitor of the PdF_1F_0 -ATPase activity, because it does not inhibit the PdF_1F_0 -ATP synthase activity at all.

Effect of the $\Delta\zeta$ Mutation on the Intracellular ATP Concentration of *Paracoccus denitrificans*

In order to determine whether the unidirectional PdF_1F_0 -ATPase inhibition exerted by ζ reflects on the cellular ATP concentrations, the PdWT , $\text{Pd}\Delta\zeta$, and $\text{Pd}\Delta\zeta+\zeta$ strains were grown in LB or succinate media to an absorbance of approximately 1.0 during the log phase, and the steady-state concentration of ATP was determined by the luciferin-luciferase assay (see [Experimental Procedures](#)). The results showed that, in LB, the concentration of intracellular ATP was about 4.5 mM, and it was very similar for all strains (PdWT , $\text{Pd}\Delta\zeta$, and $\text{Pd}\Delta\zeta+\zeta$), with no significant differences between them (Figure 6A). In contrast, when the concentration of [ATP] was determined in cells grown in succinate, it was nearly 3-fold higher than in LB (Figure 6B), i.e., around 13.0 mM in the WT strain (PdWT), and this dropped significantly in the $\text{Pd}\Delta\zeta$ strain to about half (6.8 mM). Furthermore, this drop in [ATP] was restored to about 12 mM in the $\text{Pd}\Delta\zeta+\zeta$ strain (Figure 6B). In summary, the key result here was that, in succinate, the $\text{Pd}\Delta\zeta$ mutant decreased its cellular [ATP] to about half that of the PdWT (Figure 6B), and this is accompanied by a slower growth rate for this mutant in succinate medium (Figure 2B). In addition, this lower [ATP] of the mutant was recovered in the $\text{Pd}\Delta\zeta+\zeta$ complemented strain (Figure 6B), together with the restored growth in succinate, as compared with the PdWT strain (Figure 2B). Furthermore, the similar intracellular [ATP] in LB media found for all strains (Figure 6A) reflects the similar growth of PdWT , $\text{Pd}\Delta\zeta$, and $\text{Pd}\Delta\zeta+\zeta$ strains in LB (Figure 2A). In summary, regardless of the differences in net [ATP] concentrations in WT strains in LB or in succinate, it is clear that the growth curves (Figure 2), ATP synthesis, and ATP hydrolysis assays (Figures 3 and 5C), as well as the intracellular [ATP] determinations (Figure 6), support each other and confirm the role of the ζ subunit as unidirectional PdF_1F_0 -ATPase inhibitor to favor ATP synthesis and cell growth in succinate respiratory media.

One may also wonder why the growth rate and the intracellular [ATP] are affected by the ζ deletion only in succinate media and not in LB (Figures 2B and 6B), if ATP comes mostly from the PdF_1F_0 -ATP synthase in either medium. As indicated in the [Supplemental Experimental Procedures](#), the $\Delta\zeta$ knockout is non-deleterious in LB, probably because the $\text{H}^+\text{PdF}_1\text{F}_0^{\Delta\zeta}$ -ATPase may be less activated than in succinate and/or because the cellular ATP pools could be restored in LB by alternative substrate-level phosphorylation pathways besides the Ox-Phos. In

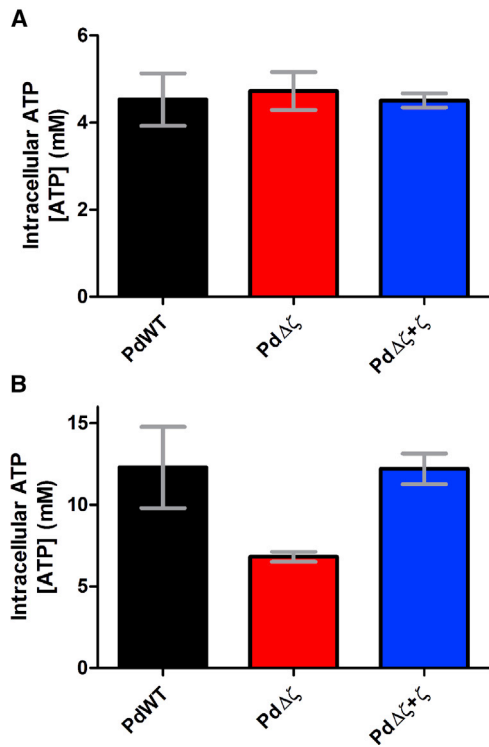


Figure 6. Determination of Intracellular ATP Concentration in PdWT, Pd $\Delta\zeta$, and Pd $\Delta\zeta+\zeta$ Strains

(A and B) The wild-type PdWT, the mutant lacking the ζ gene Pd $\Delta\zeta$, and the complemented Pd $\Delta\zeta+\zeta$ strains were separately grown to the log phase (OD of 1 at 600 nm) in LB or succinate medium at 30°C. At this point, cells were harvested by centrifugation (6,414 RCF), resuspended in 350 μ L at a concentration of approximately 3.7×10^9 cells/mL, and diluted 1:10 in lysis buffer to be processed as described in the [Experimental Procedures](#). ATP concentration was estimated by interpolation of sample data into a standard curve of ATP with a luciferin/luciferase kit. The figure shows the estimated intracellular ATP concentration in millimolar; (A) Bacterial strains grown in LB medium and (B) bacterial strains grown in succinate medium. The average of three experiments is shown with SD.

contrast, in succinate minimal medium, ATP seems to be synthesized exclusively by the PdF₁F_O-ATP synthase; therefore, here, the $\Delta\zeta$ deletion has a stronger phenotypic effect because it transforms the essentially unidirectional forward-CW-rotating H⁺PdF₁F_O $^{\zeta}$ -ATP synthase into a bidirectional H⁺PdF₁F_O $^{\Delta\zeta}$ -ATPase, thus reverting the rotation of the nanomotor from the CW-ATP synthase to the CCW-ATPase turnover, which is the only source of cellular ATP in succinate media.

Model of the PdF₁F_O- ζ Complex with the ζ Subunit Working as the Pawl of a Ratchet to Selectively Block the CCW Rotor Gyration to Favor ATP Synthesis

In its final inhibitory position, the ζ subunit inserts its N-terminal α -helix ([Figure 7](#), left panel, red) into the $\alpha_{DP}/\beta_{DP}/\gamma$ interface and contacts the γ subunit thus blocking its rotation, but apparently in both senses, i.e., in the CW-ATP synthase and in the CCW-ATPase directions; however, according to the unidirectional effects of the ζ subunit, the PdF₁F_O- ζ complex is able to gyrate its central rotor in the CW-ATP synthesis direction, but not in

the CCW direction of the PdF₁F_O-ATPase turnover ([Figure 7](#), left panel). This implies that ζ works either *mechanically* or *conformationally* as the pawl of a ratchet blocking unidirectionally γ rotation, as previously proposed ([García-Trejo et al., 2016](#)). This ζ pawl favors the “forward” ATP synthesis turnover and the overall bacterial bioenergetics to improve oxidative cell growth ([Figure 2B](#)). On the other hand, the PdF₁F_O $^{\Delta\zeta}$ mutant lacking ζ rotates in both directions (CW and CCW) to carry out both coupled ATP synthesis and hydrolysis ([Figure 7](#), right panel). In the model of [Figure 7](#), the N terminus of ζ (red) interacts directly with the γ subunit (green), thus blocking γ rotation; however, in order to allow rotation in the CW-ATP synthase direction, this ζ N terminus can either be partially or completely separated from the $\alpha_{DP}/\beta_{DP}/\gamma$ interface as induced by the $\Delta\mu_{H+}$, thus working as a conformational pawl; alternatively, it can be kept in place allowing CW rotation but not CCW rotation without its release, thus working as a mechanical pawl-ratchet. Previous studies, including ours, had shown that the $\Delta\mu_{H+}$ induces an active F₁F_O-ATPase state ([Fischer et al., 2000](#); [Gómez-Puyou et al., 1979](#); [Lippe et al., 1988](#); [Pacheco-Moises et al., 2000](#); [Zharova and Vinogradov, 2004](#)); therefore, the driving force of the $\Delta\mu_{H+}$ must be added to the ADP and P_i binding energies to drive CW rotation ([Garcia, 2000](#); [García et al., 1997](#); [Okazaki and Hummer, 2013](#); [Soidi and Penefsky, 1995](#); [Watanabe and Noji, 2014](#)); therefore, $\Delta\mu_{H+}$ and ADP/P_i binding energies can be used either to separate the N terminus of ζ from the $\alpha_{DP}/\beta_{DP}/\gamma$ interface or to overcome the torque resistance of the $\gamma/\varepsilon/c_{12}$ rotor gyration imposed by the ζ N terminus kept in the $\alpha_{DP}/\beta_{DP}/\gamma$ interface. On the contrary and reverse CCW PdF₁F_O-ATPase turnover, the smaller rotational driving force induced only by ATP binding energy and hydrolysis, working uphill against the proton gradient will probably not be enough to drive $\gamma/\varepsilon/c_{12}$ CCW rotation with the ζ N terminus bound to its inhibitory place ($\gamma/\alpha_{DP}/\beta_{DP}$ interface; [Figure 7A](#)). This would be in concordance with a relatively high rotation torque resistance of the PdF₁F_O- $\gamma/\varepsilon/c_{12}$ central rotor ([Figure 7](#)), which will require both the ADP/P_i binding energies and the $\Delta\mu_{H+}$ -driven proton flow to keep the PdF₁F_O-ATP synthase rotating in the CW direction, particularly in the presence of ζ . This could be similar, for instance, to the high torque of the unidirectional TA2.A1 ATP synthase ([McMillan et al., 2016](#)). At the moment, there is not enough experimental evidence to discern whether the ζ subunit works as a mechanical or conformational pawl. Our previous studies with *P. denitrificans* SBPs ([Pacheco-Moises et al., 2000](#)) and other studies with submitochondrial particles ([Dreyfus et al., 1981](#)) have shown a partial exposure of endogenous ζ or IF₁ upon membrane energization, respectively, thus supporting the $\Delta\mu_{H+}$ -induced conformational pawl-ratchet ζ mechanism. However, further work is necessary to resolve these details of the ζ pawl-ratchet mechanism.

Given the similarity between the ζ N terminus and the inhibitory domain of IF₁ mimicking IF₁ ([García-Trejo et al., 2016](#); [Zarco-Zavala et al., 2014](#)), it is suitable to propose that at least mitochondrial IF₁ should also work as a unidirectional F₁F_O-ATPase inhibitor, although this pawl-ratchet mechanism may also extend to the bacterial ε subunit. Indeed, the unidirectional mechanism of IF₁ has been proposed before ([Pullman and Monroy, 1963](#); [Schwerzmann and Pedersen, 1986](#)). However, this is

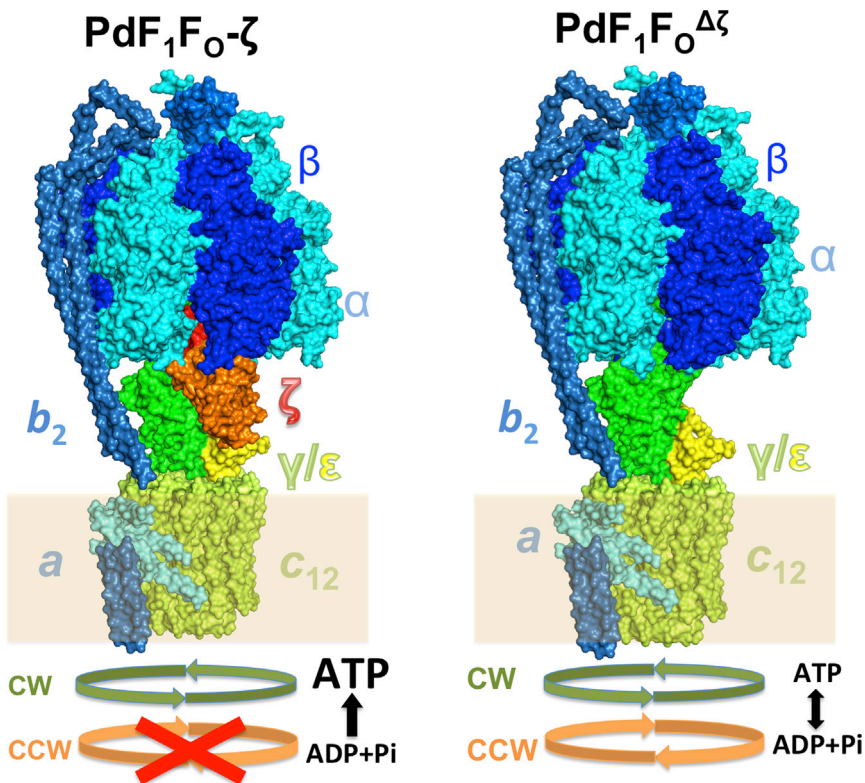


Figure 7. Structural Models of the $\text{PdF}_1\text{F}_0\text{-}\zeta$ and $\text{PdF}_1\text{F}_0^{\Delta\zeta}$ Complexes Showing the Inhibitory Binding Site and Unidirectional Pawl-Ratchet Mechanism of the ζ Subunit

The model constructed as indicated in the [Supplemental Experimental Procedures](#) shows the position of the N-terminal inhibitory domain of ζ (Zarco-Zavala et al., 2014) in red and the globular and C-terminal domain of ζ (in orange) bound into the $\alpha_{DP}/\beta_{DP}/\gamma$ interface in the left panel. The F_1 -stator complex ($\alpha_3/\beta_3/\delta/b_2/a$) is shown in shades of blue. The $\gamma/\epsilon/c_{12}$ rotor (in green and yellow) is unable to rotate in the counterclockwise (CCW) direction driving ATP hydrolysis but is able to rotate in the clockwise (CW) direction of ATP synthesis; the latter rotation is driven by the proton flow and gradient with or without partial release of the inhibitory ζ -N terminus; in either case, ζ works as a pawl-ratchet, blocking rotation of the $\gamma/\epsilon/c_{12}$ rotor only in the CCW direction. In the right panel, the $\text{PdF}_1\text{F}_0^{\Delta\zeta}$ structure is shown after removal of the ζ subunit *in silico*. In the $\text{PdF}_1\text{F}_0^{\Delta\zeta}$ complex, the $\gamma/\epsilon/c_{12}$ rotor is able to rotate in both CW and CCW directions; therefore, it can carry out both ATP synthesis and ATP hydrolysis according to the load of substrates and proton gradients. In summary, the ζ subunit favors ATP synthesis and, therefore, oxidative bacterial growth by working as a pawl-ratchet or unidirectional PdF_1F_0 -ATPase inhibitor, thus making the $\text{PdF}_1\text{F}_0\text{-}\zeta$ complex a unidirectional ATP synthase.

controversial, since several studies point to bidirectional effects of IF_1 and ϵ , whereas other studies suggest that IF_1 and ϵ work as unidirectional inhibitors (García-Bermúdez et al., 2015; Gómez-Puyou et al., 1979; Iino et al., 2009; Masaike et al., 2006; Schwerzmann and Pedersen, 1986; Tsunoda et al., 2001). Moreover, a ratchet mechanism was first proposed for the *E. coli* ϵ subunit (Tsunoda et al., 2001), and similar to our present results with $\text{Pd}\text{-}\zeta$, a recent short C-terminal deletion study of the *E. coli* ϵ inhibitory C terminus also showed detrimental effects on bacterial oxidative growth (Shah and Duncan, 2015). These studies suggest that all natural ATP synthase inhibitors (ϵ , ζ , and IF_1) may work through a similar unidirectional mechanism, since they bind to the same $\gamma/\alpha_{DP}/\beta_{DP}$ interface, named the “inhibition-general core region” (Shirakihara et al., 2015); however, further work will be required to ascertain whether ϵ , ζ , and IF_1 work with the same unidirectional mechanics. Meanwhile, the present work demonstrates that at least the ζ subunit of *P. denitrificans* and related α -proteobacteria works as a unidirectional pawl of a mechanical or conformational ratchet, blocking exclusively the PdF_1F_0 -ATPase activity and, thus, favoring the PdF_1F_0 -ATP synthase turnover, the overall cell bioenergetics, and bacterial oxidative growth.

Finally, this work establishes the biological function of a natural ATP synthase inhibitor; therefore, *P. denitrificans* and its natural PdF_1F_0 -ATPase inhibitor ζ seem suitable models to shed light on these studies. Previously, the F_1F_0 -ATPase inhibitory role of ζ has been demonstrated only *in vitro* (Morales-Ríos et al., 2010; Zarco-Zavala et al., 2014). Since the F_1F_0 -ATPase

is kinetically regulated by a number of natural intrinsic and extrinsic factors—for instance, inhibitory MgADP or activating oxyanions (Pacheco-Moisés et al., 2000, 2002; Zharova and Vinogradov, 2003, 2006a, 2006b)—it remained unclear whether these natural inhibitory proteins had a physiological F_1F_0 -ATPase regulatory role *in vivo* or whether the ATP synthase was controlled more effectively by the other factors. This work demonstrates that the ζ subunit controls the inherent rotation of the α -proteobacterial ATP synthase nanomotor to improve the overall cell bioenergetics and oxidative growth. This result is important, because the fact that bacterial growth is affected by the direct control of the ζ subunit (Figure 2) adds support for taking advantage of the bacterial ATP synthase as a target for antimicrobial drug design. Moreover, the key role of ζ as a regulatory subunit demonstrated here explains the control mechanism of this ATP synthase and why this is an essentially unidirectional ATP synthase and a poor or latent ATPase (Pacheco-Moisés et al., 2002; Pérez and Ferguson, 1990; Zharova and Vinogradov, 2003). Indeed, the ATP synthase of *P. denitrificans* has the highest ratio of ATP synthase/ATPase rates described so far (Pacheco-Moisés et al., 2002; Pérez and Ferguson, 1990; Zharova and Vinogradov, 2003). In this context, this work shows that the ζ subunit has a key role as a pawl-ratchet inhibitor to make of this enzyme from *P. denitrificans* a unidirectional ATP synthase. Further oncoming work will confirm whether mitochondrial IF_1 and inhibitory bacterial ϵ subunits have similar unidirectional pawl mechanisms and *in vivo* roles in nature as the ζ subunit does in α -proteobacteria.

EXPERIMENTAL PROCEDURES

Plasmids, Bacterial Strains, and Growth Conditions

The bacterial strains and plasmids used in this study are listed in Table S1. *Escherichia coli* strains DH5 α , (Hanahan, 1983) and S17-1 (Simon et al., 1983) were grown at 37°C in LB medium. *P. denitrificans* strains Pd1222 (PdWT) [de Vries et al., 1989], Pd $\Delta\zeta$, and Pd $\Delta\zeta+\zeta$ were grown at 30°C in LB or succinate medium (Ludwig, 1986). Antibiotics, when used, were added at the following concentrations (in micrograms per milliliter): rifampicin (Rf), 50; kanamycin (Km), 50; gentamicin (Gm), 30; and ampicillin (Ap), 100.

Knockout Mutagenesis and DNA Isolation and Manipulation

To delete the ζ gene from the Pd1222 bacterial strain, we used homologous recombination to replace the ζ gene with a kanamycin-resistance marker (Figure S1). A suicide plasmid, pJQ200SK (Gm R) (Pellici et al., 1996), was instrumental to build the construct pFMMCJG- $\Delta\zeta$. *E. coli* S17-1 (see Table S1) was transformed, and the plasmid construct was transferred to the Pd1222 strain by conjugation. Details of DNA manipulation, the construct, and complementation of the mutant *P. denitrificans* $\Delta\zeta$ (Pd $\Delta\zeta$) are indicated in the Supplemental Experimental Procedures.

Growth Curves, Cell Lysate Preparations, Protein Quantification, SDS-PAGE, and Western Blotting

Standard methods for growth curves, protein quantification, SDS-PAGE, cell extracts, and western blotting were carried out as described previously (Zarco-Zavala et al., 2014) and/or detailed in the Supplemental Experimental Procedures.

PdF₁F_O-ATP Synthase Assays

The steady-state rates of ATP synthesis activity were determined with a coupled hexokinase/glucose-6-phosphate dehydrogenase (G6PDH) assay, as described previously (Cortés-Hernández et al., 2007). Details provided in the Supplemental Experimental Procedures.

Determination of Intracellular ATP Concentration

Intracellular ATP was measured using the ATP Bioluminescent Assay Kit (Sigma-Aldrich, St. Louis, MO, USA). Details are provided in the Supplemental Experimental Procedures.

Membrane Potential Estimated by Flow Cytometry

Membrane potential was determined by flow cytometry using a BacLight Bacterial Membrane Potential Kit (Molecular Probes/Thermo Fisher Scientific, Waltham, MA, USA). Details are explained in the Supplemental Experimental Procedures.

PdF₁F_O-ATPase Assays

The steady-state rates of ATP hydrolysis activity were determined with a coupled pyruvate kinase (PK)/lactate dehydrogenase (LDH) assay as described previously (Cortés-Hernández et al., 2007). Details are described in the Supplemental Experimental Procedures.

Purification of PdF₁

Purifications of the PdF₁ fraction from Pd1222 (PdWT) and Pd $\Delta\zeta$ were obtained using chloroform extraction from inside-out vesicles of each strain as described previously (Zarco-Zavala et al., 2014), with modifications described in the Supplemental Experimental Procedures.

Inhibition Assays PdF₁ and PdF₁F_O with Reconstituted ζ Subunit

Reconstitution of the recombinant ζ subunit in PdF₁ and PdF₁F_O-ATPase complexes were carried out as described previously (Zarco-Zavala et al., 2014) and detailed in the Supplemental Experimental Procedures.

Membrane Energization of *P. denitrificans* Inverted Membranes Evidenced by ACMA Fluorescence Quenching

Succinate-driven or ATP-driven membrane energization of SBP was evidenced by the fluorescence quenching of 9-amino-6-chloro-2-methoxyacri-

dine (ACMA), as described previously (Ogilvie et al., 1997), with details explained in the Supplemental Experimental Procedures.

SUPPLEMENTAL INFORMATION

Supplemental Information includes Supplemental Experimental Procedures, four figures, and two tables and can be found with this article online at <https://doi.org/10.1016/j.celrep.2017.12.106>.

ACKNOWLEDGMENTS

This work was supported by grants from México (CONACYT) (CB-2011-01-167622) and U.N.A.M. (DGAPA) (PAPIIT- IN221216) (both to J.J.G.-T.) and partially funded by grants CONACYT 239487 and UNAM-DGAPA-PAPIIT IN204015 (both to S.U.-C.). We acknowledge Professors Alejandro Fernández-Velasco and Georgina Garza-Ramos for kindly making their fluorometer available to us. We acknowledge Héctor Adán Martínez-Torres for buffers and media preparation. This work is part of the PhD thesis of F.M.-H. at the “Programa de Maestría y Doctorado en Ciencias Bioquímicas de la Universidad Nacional Autónoma de México (U.N.A.M.), with J.J.G.-T. as PhD advisor. F.M.-H. was supported by CONACYT PhD Fellowship no. 277245, and M.Z.-Z. was supported by CONACYT Fund I0010 Fellowship no. 277592. We thank the LABNALCIT-UNAM for the technical support, acquisition, and processing of flow cytometry data, particularly Dr. Gloria Soldevila; Dr. Andrea Bedoya; Carlos Castellanos-Barba, MSc; Roxana Olguín-Alor, MSc; and Erick Espindola, MSc. Monoclonals anti- β and anti-SD70 were kind gifts of Prof. Roderick A. Capaldi. DiOC₂(3) was kindly provided by Prof. Teresita Padilla-Benavides. We acknowledge Leslie Olmedo-Nieva for her kind help on the design of figures and tables. The logistic support of Héctor Mendoza and Concepción García-Ramírez are also acknowledged. The editor and reviewers are also deeply acknowledged; their excellent work improved the final version of this paper.

This work is dedicated to the memory of Prof. Armando Gómez-Puyou for his major contributions to Bioenergetics, ATP synthase, and the structure and function of proteins and for being one of the most outstanding scientists from U.N.A.M. and México.

AUTHOR CONTRIBUTIONS

F.M.-H. designed the primers; carried out the molecular biology experiments of the $\Delta\zeta$ construction, the growth curves of all *P. denitrificans* strains, the ACMA and DiOC₂(3) membrane potential assays by fluorometry and flow cytometry, and the [ATP] determinations; purified the PdF₁^{WT} and PdF₁ ^{$\Delta\zeta$} ATPases; and wrote the first preliminary draft. A.P.-O. assisted in the construction of the Pd $\Delta\zeta$ mutant. M.A.C. designed the Pd $\Delta\zeta$ construction strategy, provided the plasmids, and advised on the molecular biology experiments. M.Z.-Z. purified the recombinant ζ subunit. R.O. and C.P.-S. assisted on the microbiology and preparation of growth media. E.E.-S. and S.U.-C. assisted with and carried out the ATP determinations by luciferin-luciferase ATP assay. J.J.G.-T. designed the research, helped with the Pd $\Delta\zeta$ design and construction, carried out the PdF₁F_O-ATP synthesis and PdF₁F_O-ATP hydrolysis assays, made the experiments of membrane energization by ACMA fluorescence quenching, helped in the determination and calculations of intracellular [ATP], constructed the PdF₁F_O- ζ structural model, advised the PhD thesis of F.M.-H., and wrote the paper.

DECLARATION OF INTERESTS

The authors declare no conflict of interests. J.J.G.-T., M.A.C., and F.M.-H. are waiting for a pending patent: MX/a/2017/016448.

Received: June 8, 2017

Revised: September 9, 2017

Accepted: December 28, 2017

Published: January 23, 2018

REFERENCES

- Berry, E.A., and Trumpower, B.L. (1985). Isolation of ubiquinol oxidase from *Paracoccus denitrificans* and resolution into cytochrome *bc*, and cytochrome *c-aa₃* complexes. *J. Biol. Chem.* 260, 2458–2467.
- Boyer, P.D. (1997). The ATP synthase—a splendid molecular machine. *Annu. Rev. Biochem.* 66, 717–749.
- Cabezón, E., Montgomery, M.G., Leslie, A.G., and Walker, J.E. (2003). The structure of bovine F1-ATPase in complex with its regulatory protein IF1. *Nat. Struct. Biol.* 10, 744–750.
- Cingolani, G., and Duncan, T.M. (2011). Structure of the ATP synthase catalytic complex (F1) from *Escherichia coli* in an autoinhibited conformation. *Nat. Struct. Mol. Biol.* 18, 701–707.
- Cortés-Hernández, P., Vázquez-Memije, M.E., and García, J.J. (2007). ATP6 homoplasmic mutations inhibit and destabilize the human F₁F₀-ATP synthase without preventing enzyme assembly and oligomerization. *J. Biol. Chem.* 282, 1051–1058.
- Cox, J.C., Ingledeiw, W.J., Haddock, B.A., and Lawford, H.G. (1978). The variable cytochrome content of *Paracoccus denitrificans* grown aerobically under different conditions. *FEBS Lett.* 93, 261–265.
- de la Rosa-Morales, F. (2005). Composición de Subunidades y Mecanismo de Regulación de la F1FoATP Sintasa de *Paracoccus denitrificans* [Composition of subunits and mechanism of regulation of the F₁F₀-ATP synthase of *Paracoccus denitrificans*]. Masters thesis. Posgrado en Ciencias Biológicas (Biología Experimental), Facultad de Ciencias [Postgraduate Program in Biological Sciences (Experimental Biology), Faculty of Sciences] (Dirección General de Bibliotecas: Universidad Nacional Autónoma de México [U.N.A.M.]). <http://132.248.9.195/ptd2005/00377/0346694/Index.html>.
- de Vries, G.E., Harms, N., Hoogendijk, J., and Stouthamer, A.H. (1989). Isolation and characterization of *Paracoccus denitrificans* mutants with increased conjugation frequencies and pleiotropic loss of a (nGATC)n DNA-modifying property. *Arch. Microbiol.* 152, 52–57.
- Dienhart, M., Pfeiffer, K., Schagger, H., and Stuart, R.A. (2002). Formation of the yeast F₁F₀-ATP synthase dimeric complex does not require the ATPase inhibitor protein, Inh1. *J. Biol. Chem.* 277, 39289–39295.
- Dreyfus, G., Gómez-Puyou, A., and Iuena de Gómez-Puyou, M. (1981). Electrochemical gradient induced displacement of the natural ATPase inhibitor protein from mitochondrial ATPase as directed by antibodies against the inhibitor protein. *Biochem. Biophys. Res. Commun.* 100, 400–406.
- Duncan, T.M., Bulygin, V.V., Zhou, Y., Hutcheon, M.L., and Cross, R.L. (1995). Rotation of subunits during catalysis by *Escherichia coli* F₁-ATPase. *Proc. Natl. Acad. Sci. USA* 92, 10964–10968.
- Fernández-Cárdenas, L.P., Villanueva-Chimal, E., Salinas, L.S., José-Núñez, C., Tuena de Gómez Puyou, M., and Navarro, R.E. (2017). *Caenorhabditis elegans* ATPase inhibitor factor 1 (IF₁) MAI-2 preserves the mitochondrial membrane potential ($\Delta\psi_m$) and is important to induce germ cell apoptosis. *PLoS ONE* 12, e0181984.
- Fischer, S., Gruber, P., and Turina, P. (2000). The activity of the ATP synthase from *Escherichia coli* is regulated by the transmembrane proton motive force. *J. Biol. Chem.* 275, 30157–30162.
- García, J.J. (2000). In *The F₀F₁-ATP Synthase: Binding Energy, Coupling and Rotational Catalysis*, First Edition (Trivandrum: Transworld Research Network).
- García, J.J., Gómez-Puyou, A., Maldonado, E., and Tuena De Gómez-Puyou, M. (1997). Acceleration of unisite catalysis of mitochondrial F1-adenosinetriphosphatase by ATP, ADP and pyrophosphate-hydrolysis and release of the previously bound [γ -32P]ATP. *Eur. J. Biochem.* 249, 622–629.
- García, J.J., Morales-Ríos, E., Cortés-Hernandez, P., and Rodríguez-Zavala, J.S. (2006). The inhibitor protein (IF1) promotes dimerization of the mitochondrial F1FO-ATP synthase. *Biochemistry* 45, 12695–12703.
- García-Bermúdez, J., Sánchez-Aragó, M., Soldevilla, B., Del Arco, A., Nuevo-Tapiolas, C., and Cuevza, J.M. (2015). PKA phosphorylates the ATPase inhibitory factor 1 and inactivates its capacity to bind and inhibit the mitochondrial H(+)-ATP synthase. *Cell Rep.* 12, 2143–2155.
- García-Trejo, J.J., Zarco-Zavala, M., Mendoza-Hoffmann, F., Hernández-Luna, E., Ortega, R., and Mendoza-Hernández, G. (2016). The inhibitory mechanism of the ζ subunit of the F1FO-ATPase nanomotor of *Paracoccus denitrificans* and related α -proteobacteria. *J. Biol. Chem.* 291, 538–546.
- Gómez-Puyou, A., de Gómez-Puyou, M.T., and Ernst, L. (1979). Inactive to active transitions of the mitochondrial ATPase complex as controlled by the ATPase inhibitor. *Biochim. Biophys. Acta* 547, 252–257.
- Hanahan, D. (1983). Studies on transformation of *Escherichia coli* with plasmids. *J. Mol. Biol.* 166, 557–580.
- Hashimoto, T., Yoshida, Y., and Tagawa, K. (1983). Binding properties of an intrinsic ATPase inhibitor and occurrence in yeast mitochondria of a protein factor which stabilizes and facilitates the binding of the inhibitor to F₁F₀-ATPase. *J. Biochem.* 94, 715–720.
- Hashimoto, T., Yoshida, Y., and Tagawa, K. (1984). Purification and properties of factors in yeast mitochondria stabilizing the F₁F₀-ATPase-inhibitor complex. *J. Biochem.* 95, 131–136.
- Hashimoto, T., Yoshida, Y., and Tagawa, K. (1987). Binding properties of 9K protein to F1-ATPase: a counterpart ligand to the ATPase inhibitor. *J. Biochem.* 102, 685–692.
- Hashimoto, T., Yoshida, Y., and Tagawa, K. (1990a). Regulatory proteins of F1FO-ATPase: role of ATPase inhibitor. *J. Bioenerg. Biomembr.* 22, 27–38.
- Hashimoto, T., Yoshida, Y., and Tagawa, K. (1990b). Simultaneous bindings of ATPase inhibitor and 9K protein to F₁F₀-ATPase in the presence of 15K protein in yeast mitochondria. *J. Biochem.* 108, 17–20.
- Hederstedt, L. (2002). Succinate:quinone oxidoreductase in the bacteria *Paracoccus denitrificans* and *Bacillus subtilis*. *Biochim. Biophys. Acta* 1553, 74–83.
- Iino, R., Hasegawa, R., Tabata, K.V., and Noji, H. (2009). Mechanism of inhibition by C-terminal alpha-helices of the epsilon subunit of *Escherichia coli* F₀F₁-ATP synthase. *J. Biol. Chem.* 284, 17457–17464.
- Iwata, S., Ostermeier, C., Ludwig, B., and Michel, H. (1995). Structure at 2.8 Å resolution of cytochrome c oxidase from *Paracoccus denitrificans*. *Nature* 376, 660–669.
- Jensen, P.R., Michelsen, O., and Westerhoff, H.V. (1993). Control analysis of the dependence of *Escherichia coli* physiology on the H⁺-ATPase. *Proc. Natl. Acad. Sci. USA* 90, 8068–8072.
- John, P., and Whatley, F.R. (1975). *Paracoccus denitrificans* and the evolutionary origin of the mitochondrion. *Nature* 254, 495–498.
- Kleinschroth, T., Castellani, M., Trinh, C.H., Morgner, N., Brutschy, B., Ludwig, B., and Hunte, C. (2011). X-ray structure of the dimeric cytochrome bc(1) complex from the soil bacterium *Paracoccus denitrificans* at 2.7-Å resolution. *Biochim. Biophys. Acta* 1807, 1606–1615.
- Kliotinsky, D.J., Brusilow, W.S., and Simoni, R.D. (1984). In vivo evidence for the role of the epsilon subunit as an inhibitor of the proton-translocating ATPase of *Escherichia coli*. *J. Bacteriol.* 160, 1055–1060.
- Kovach, M.E., Elzer, P.H., Hill, D.S., Robertson, G.T., Farris, M.A., Roop, R.M., 2nd, and Peterson, K.M. (1995). Four new derivatives of the broad-host-range cloning vector pBBR1MCS, carrying different antibiotic-resistance cassettes. *Gene* 166, 175–176.
- Ku, C., Nelson-Sathi, S., Roettger, M., Sousa, F.L., Lockhart, P.J., Bryant, D., Hazkani-Covo, E., McInerney, J.O., Landan, G., and Martin, W.F. (2015). Endosymbiotic origin and differential loss of eukaryotic genes. *Nature* 524, 427–432.
- Lippe, G., Sorgato, M.C., and Harris, D.A. (1988). Kinetics of the release of the mitochondrial inhibitor protein. Correlation with synthesis and hydrolysis of ATP. *Biochim. Biophys. Acta* 933, 1–11.
- Lu, Y.M., Miyazawa, K., Yamaguchi, K., Nowaki, K., Iwatsuki, H., Wakamatsu, Y., Ichikawa, N., and Hashimoto, T. (2001). Deletion of mitochondrial ATPase inhibitor in the yeast *Saccharomyces cerevisiae* decreased cellular and mitochondrial ATP levels under non-nutritional conditions and induced a respiration-deficient cell-type. *J. Biochem.* 130, 873–878.

- Ludwig, B. (1986). Cytochrome c oxidase from *Paracoccus denitrificans*. *Methods Enzymol.* 126, 153–159.
- Ludwig, B., and Schatz, G. (1980). A two-subunit cytochrome c oxidase (cytochrome aa₃) from *Paracoccus denitrificans*. *Proc. Natl. Acad. Sci. USA* 77, 196–200.
- Margulis, L., and Chapman, M.J. (1998). Endosymbioses: cyclical and permanent in evolution. *Trends Microbiol.* 6, 342–345, discussion 345–346.
- Masaike, T., Suzuki, T., Tsunoda, S.P., Konno, H., and Yoshida, M. (2006). Probing conformations of the beta subunit of FOF1-ATP synthase in catalysis. *Biochem. Biophys. Res. Commun.* 342, 800–807.
- McMillan, D.G., Watanabe, R., Ueno, H., Cook, G.M., and Noji, H. (2016). Biophysical characterization of a thermoalkaliphilic molecular motor with a high stepping torque gives insight into evolutionary ATP synthase adaptation. *J. Biol. Chem.* 291, 23965–23977.
- Minauro-Sanmiguel, F., Bravo, C., and García, J.J. (2002). Cross-linking of the endogenous inhibitor protein (IF1) with rotor (gamma, epsilon) and stator (alpha) subunits of the mitochondrial ATP synthase. *J. Bioenerg. Biomembr.* 34, 433–443.
- Mitchell, P. (1961). Coupling of phosphorylation to electron and hydrogen transfer by a chemi-osmotic type of mechanism. *Nature* 191, 144–148.
- Morales-Ríos, E., de la Rosa-Morales, F., Mendoza-Hernández, G., Rodríguez-Zavala, J.S., Celis, H., Zarco-Zavala, M., and García-Trejo, J.J. (2010). A novel 11-kDa inhibitory subunit in the F₁F_O ATP synthase of *Paracoccus denitrificans* and related alpha-proteobacteria. *FASEB J.* 24, 599–608.
- Morales-Ríos, E., Montgomery, M.G., Leslie, A.G., García-Trejo, J.J., and Walker, J.E. (2015a). Structure of a catalytic dimer of the alpha- and beta-subunits of the F-ATPase from *Paracoccus denitrificans* at 2.3 Å resolution. *Acta Crystallogr. F Struct. Biol. Commun.* 71, 1309–1317.
- Morales-Ríos, E., Montgomery, M.G., Leslie, A.G., and Walker, J.E. (2015b). Structure of ATP synthase from *Paracoccus denitrificans* determined by X-ray crystallography at 4.0 Å resolution. *Proc. Natl. Acad. Sci. USA* 112, 13231–13236.
- Nakamura, J., Fujikawa, M., and Yoshida, M. (2013). IF1, a natural inhibitor of mitochondrial ATP synthase, is not essential for the normal growth and breeding of mice. *Biosci. Rep.* 33, e00067.
- Noji, H., Yasuda, R., Yoshida, M., and Kinoshita, K., Jr. (1997). Direct observation of the rotation of F1-ATPase. *Nature* 386, 299–302.
- Novo, D., Perlmuter, N.G., Hunt, R.H., and Shapiro, H.M. (1999). Accurate flow cytometric membrane potential measurement in bacteria using diethyloxacarbocyanine and a ratiometric technique. *Cytometry* 35, 55–63.
- Ogilvie, I., Aggeler, R., and Capaldi, R.A. (1997). Cross-linking of the delta subunit to one of the three alpha subunits has no effect on functioning, as expected if delta is a part of the stator that links the F₁ and F_O parts of the *Escherichia coli* ATP synthase. *J. Biol. Chem.* 272, 16652–16656.
- Okazaki, K., and Hummer, G. (2013). Phosphate release coupled to rotary motion of F1-ATPase. *Proc. Natl. Acad. Sci. USA* 110, 16468–16473.
- Pacheco-Moisés, F., García, J.J., Rodríguez-Zavala, J.S., and Moreno-Sánchez, R. (2000). Sulfito and membrane energization induce two different active states of the *Paracoccus denitrificans* F_OF₁-ATPase. *Eur. J. Biochem.* 267, 993–1000.
- Pacheco-Moisés, F., Minauro-Sanmiguel, F., Bravo, C., and García, J.J. (2002). Sulfito inhibits the F1F0-ATP synthase and activates the F1F0-ATPase of *Paracoccus denitrificans*. *J. Bioenerg. Biomembr.* 34, 269–278.
- Pelicic, V., Reyrat, J.M., and Gicquel, B. (1996). Expression of the *Bacillus subtilis* sacB gene confers sucrose sensitivity on mycobacteria. *J. Bacteriol.* 178, 1197–1199.
- Pennoyer, J.D., Ohnishi, T., and Trumppower, B.L. (1988). Purification and properties of succinate-ubiquinone oxidoreductase complex from *Paracoccus denitrificans*. *Biochim. Biophys. Acta* 935, 195–207.
- Pérez, J.A., and Ferguson, S.J. (1990). Kinetics of oxidative phosphorylation in *Paracoccus denitrificans*. 1. Mechanism of ATP synthesis at the active site(s) of F0F1-ATPase. *Biochemistry* 29, 10503–10518.
- Pullman, M.E., and Monroy, G.C. (1963). A naturally occurring inhibitor of mitochondrial adenosine triphosphatase. *J. Biol. Chem.* 238, 3762–3769.
- Rondelez, Y., Tresset, G., Nakashima, T., Kato-Yamada, Y., Fujita, H., Takeuchi, S., and Noji, H. (2005). Highly coupled ATP synthesis by F1-ATPase single molecules. *Nature* 433, 773–777.
- Sabbert, D., Engelbrecht, S., and Junge, W. (1996). Intersubunit rotation in active F-ATPase. *Nature* 381, 623–625.
- Scholes, P.B., and Smith, L. (1968). Composition and properties of the membrane-bound respiratory chain system of *Micrococcus denitrificans*. *Biochim. Biophys. Acta* 153, 363–375.
- Schwerzmann, K., and Pedersen, P.L. (1986). Regulation of the mitochondrial ATP synthase/ATPase complex. *Arch. Biochem. Biophys.* 250, 1–18.
- Serrano, P., Geralt, M., Mohanty, B., and Wüthrich, K. (2014). NMR structures of alpha-proteobacterial ATPase-regulating zeta-subunits. *J. Mol. Biol.* 426, 2547–2553.
- Shah, N.B., and Duncan, T.M. (2015). Aerobic growth of *Escherichia coli* is reduced, and ATP synthesis is selectively inhibited when five C-terminal residues are deleted from the E subunit of ATP synthase. *J. Biol. Chem.* 290, 21032–21041.
- Shirakihara, Y., Shiratori, A., Tanikawa, H., Nakasako, M., Yoshida, M., and Suzuki, T. (2015). Structure of a thermophilic F1-ATPase inhibited by an epsilon-subunit: deeper insight into the epsilon-inhibition mechanism. *FEBS J.* 282, 2895–2913.
- Simon, R., Priefer, U., and Pühler, A. (1983). A broad host range mobilization system for *in vivo* genetic engineering: transposon mutagenesis in Gram negative bacteria. *Nat. Biotechnol.* 1, 784–791.
- Souid, A.K., and Penefsky, H.S. (1995). Energetics of ATP dissociation from the mitochondrial ATPase during oxidative phosphorylation. *J. Biol. Chem.* 270, 9074–9082.
- Sternweis, P.C., and Smith, J.B. (1980). Characterization of the inhibitory (epsilon) subunit of the proton-translocating adenosine triphosphatase from *Escherichia coli*. *Biochemistry* 19, 526–531.
- Tsunoda, S.P., Rodgers, A.J., Aggeler, R., Wilce, M.C., Yoshida, M., and Capaldi, R.A. (2001). Large conformational changes of the epsilon subunit in the bacterial F1F0 ATP synthase provide a ratchet action to regulate this rotary motor enzyme. *Proc. Natl. Acad. Sci. USA* 98, 6560–6564.
- Watanabe, R., and Noji, H. (2014). Timing of inorganic phosphate release modulates the catalytic activity of ATP-driven rotary motor protein. *Nat. Commun.* 5, 3486.
- Yagi, T. (1986). Purification and characterization of NADH dehydrogenase complex from *Paracoccus denitrificans*. *Arch. Biochem. Biophys.* 250, 302–311.
- Zarco-Zavala, M., Morales-Ríos, E., Serrano-Navarro, P., Wüthrich, K., Mendoza-Hernández, G., Ramírez-Silva, L., and García-Trejo, J.J. (2012). Corrigendum to “The zeta subunit of the alpha-proteobacterial F1FO-ATP synthase in *Paracoccus denitrificans*: A novel control mechanism of the central rotor.” *Biochim. Biophys. Acta* 1827, 60.
- Zarco-Zavala, M., Morales-Ríos, E., Mendoza-Hernández, G., Ramírez-Silva, L., Pérez-Hernández, G., and García-Trejo, J.J. (2014). The zeta subunit of the F1FO-ATP synthase of alpha-proteobacteria controls rotation of the nanomotor with a different structure. *FASEB J.* 28, 2146–2157.
- Zharova, T.V., and Vinogradov, A.D. (2003). Proton-translocating ATP-synthase of *Paracoccus denitrificans*: ATP-hydrolytic activity. *Biochemistry (Mosc.)* 68, 1101–1108.
- Zharova, T.V., and Vinogradov, A.D. (2004). Energy-dependent transformation of F_O•F₁-ATPase in *Paracoccus denitrificans* plasma membranes. *J. Biol. Chem.* 279, 12319–12324.
- Zharova, T.V., and Vinogradov, A.D. (2006a). Energy-linked binding of P_i is required for continuous steady-state proton-translocating ATP hydrolysis catalyzed by F_O•F₁ ATP synthase. *Biochemistry* 45, 14552–14558.
- Zharova, T.V., and Vinogradov, A.D. (2006b). Requirement of medium ADP for the steady-state hydrolysis of ATP by the proton-translocating *Paracoccus denitrificans* F_O•F₁-ATP synthase. *Biochim. Biophys. Acta* 1757, 304–310.

cell scales, based on AFM, cryo-electron tomography, mass spectrometry, crystallography, and spectroscopy data modalities. The hierarchy of time scales in the energy conversion processes was addressed via a multitude of computational models for each scale, from electronic excitation transfer to charge carrier diffusion to structure based rate kinetics, wherein the output of each model becomes an input parameter for the next scale. The EROI is formulated in relation to cell doubling time for a controlled growth environment that removes energy expenditure channels other than replication and base metabolism, such as motility, as well as energy input channels other than light absorption. Under these controlled conditions, the approach successfully reproduces light-dependence of growth behavior over nearly three orders of magnitude of illumination. Rational design principles for bioengineered energy solutions are revealed by identifying bottlenecks of energy conversion at protein level. The EROI also provides a systems-level integrative performance metric for quantifying evolutionary competitiveness between different species as well as a comparison to artificial energy harvesting systems. Current efforts extending this approach to the structural models from cyanobacterial and granal bioenergetic domains, comprising more than 4,000 proteins, will also be presented.

2068-Pos

Energetic Modelling of Mitochondrial Redox Reactions

Peter J. Gawthrop¹, Edmund J. Crampin².

¹Biomedical Engineering, University of Melbourne, Melbourne, Australia,

²Sch of Maths and Stats, Univ Melbourne, Parkville, Australia.

Mitochondria make use of redox reactions to provide the energy driving many living systems. Energetic modelling of the key components of mitochondria is thus an important challenge to systems biology. Like engineering systems, living systems are subject to the laws of physics in general and the laws of thermodynamics in particular. This fact gives the opportunity of applying engineering approaches to the modelling, analysis and understanding of living systems. The bond graph method of Paynter is one such well-established engineering approach. The mitochondrial electron transport chain transduces chemical energy to the trans-membrane protonic potential; the energy stored in this trans-membrane protonic potential is then transduced back to chemical energy by driving ATP hydrolysis in the reverse direction catalysed by ATPase. Redox reactions are a fundamental part of the electron transport chain.

Redox reactions are conveniently split into two half-reactions coupled by the transfer of electrons and thus themselves transduce chemical and electrical energy. As well as being the driver of protonic energy transduction, the electrons coupling the redox half reactions are also the source of the reactive oxygen species (ROS) superoxide and its derivatives. Thus explicit modelling of electron transfer also provides insight into ROS generation.

The bond graph approach focuses on energy transduction across physical domains and is thus an ideal modelling tool in this context.

Modular bond graphs provide a way of decomposing complex biomolecular systems into manageable parts. We show that such a modular bond graph approach, provides a flexible and powerful energy-inspired modelling method which brings engineering expertise to the analysis of biomolecular systems in general and redox reactions, ROS generation and mitochondrial chemiosmotic energy transduction in particular.

2069-Pos

Unveiling the Rate-Limiting Step of the bc_1 Complex Reaction Mechanism

Angela M. Barragan^{1,2}, Alexander V. Soudackov^{3,4},

Zaida Luthey-Schulten^{4,5}, Klaus Schulten^{1,2}, Sharon Hammes-Schiffer^{3,4},

Ilia Solov'yov⁶.

¹Department of Physics, University of Illinois at Urbana-Champaign,

Urbana, IL, USA, ²Beckman Institute for the Advancement of Science and

Technology, Urbana, IL, USA, ³Department of Chemistry, Yale University,

New Haven, CT, USA, ⁴Department of Chemistry, University of Illinois at

Urbana-Champaign, Urbana, IL, USA, ⁵Department of Physics, Center for

the Physics of Living Cells, Urbana, IL, USA, ⁶Department of Physics,

Chemistry and Pharmacy, University of Southern Denmark, Odense C,

Denmark.

The bc_1 complex is a remarkable enzyme that plays a fundamental role in the optimal conversion of energy in photosynthetic bacteria and cellular respiratory systems in higher organisms. Its contribution to this energy conversion process is to generate a proton gradient for ATP production, which occurs via a series of highly efficient charge transfer reactions between a bonded quinol and the protein itself. It is extremely challenging, however, to establish the key aspects of the bc_1 complex mechanism since it combines quantum effects at the electron level together with conformational changes at the biomolecular level. By employing computational tools such as molecular dynamics simulations together with ab-initio quantum chemistry calculations it is possible to unveil some of these key aspects. First, these techniques allowed us to confirm the coupled nature of the primary electron and proton transfer reactions. More importantly, we

were able to determine the rate constant of the respective proton-coupled electron transfer reaction that takes place at the quinol binding site of the bc_1 complex. Our results indicate good agreement between our theoretical model and experimental data. Finally, the calculation of the high kinetic isotope effect allowed us to confirm a central hypothesis regarding this reaction, namely that this is indeed the rate-limiting step of the bc_1 complex reaction mechanism.

2070-Pos

Elucidating the Role of Zinc-Bacteriochlorophyll A' in the Primary Photochemistry of *Chloracidobacterium thermophilum* Reaction Centers

Philip Charles¹, Vidmantas Kalendra¹, Zhihui He², Vasily Khurshov², Art van der Est³, John H. Golbeck⁴, Donald A. Bryant², K.V. Lakshmi¹.

¹Chemistry and Physics and The Baruch '60 Center for Biochemical Solar Energy Research, Rensselaer Polytechnic Institute, Troy, NY, USA,

²Biochemistry and Molecular Biology, Pennsylvania State University, State College, PA, USA, ³Chemistry, Brock University, St. Catharines, ON, Canada, ⁴Biochemistry and Molecular Biology and Chemistry, Pennsylvania State University, State College, PA, USA.

Chloracidobacterium (Cab.) thermophilum is a microaerophilic, chlorophototrophic species in the phylum of *Acidobacteria* that contains homodimeric Type I reaction centers (RC). Photosynthetic RCs in bacteria convert light energy into chemical energy using (bacterio)chlorophyll ((B)Chl) cofactors. In addition to participating in energy transfer in the light-harvesting complexes, the (B)Chl molecules also act as the primary electron donor and primary electron acceptor in Type I RCs. Previously, reversed-phase high-performance liquid chromatography of *Cab. thermophilum* RCs revealed the presence of (B)Chl *a*, Chl *a*, and Zn^{2+} -(B)Chl *a'* in a ratio of about 12.8:8.0:2.0. Moreover, it was shown that *Cab. thermophilum* uses chlorosomes and FMO for light harvesting, and synthesizes (B)Chl *c* in addition to (B)Chl *a*, Chl *a*, and Zn^{2+} -(B)Chl *a'*. It has been demonstrated that Chl *a* is the primary electron acceptor in *Cab. thermophilum* RC and since Zn^{2+} -(B)Chl *a'* is only present in the RC, it was suggested that it could function as the primary electron donor. In this study, we utilize high-resolution, two-dimensional (2D) ^{14}N and ^{67}Zn hyperfine sublevel correlation (HYSCORE) spectroscopy to determine the electronic and geometric structure of the primary donor cation, P_{840}^{+} , in the *Cab. thermophilum* RC. Additionally, we perform density functional theory (DFT) calculations to determine the electron spin-density distribution and electron-nuclear hyperfine coupling parameters of P_{840}^{+} for comparison with the parameters that are obtained from the experimental 2D HYSCORE measurements. Our studies indicate that the primary donor, P_{840} , of the *Cab.* RC is comprised of Zn^{2+} -sBChl *a'* molecules.

2071-Pos

The Reversible Opening of s_c Muc Demonstrates a High Potential as a Cellular Protection System

Lilia Morales-García, Salvador Uribe-Carvajal, Natalia Chiquete-Felix, Emilio Espinoza-Simon.

Instituto de Fisiología Celular, Ciudad de México, Mexico.

The mitochondrial unspecific channel in *Saccharomyces cerevisiae* (s_c MUC) is regulated by different substrates. It has been suggested that s_c MUC opening is reversible and thus physiological. Its main function would be to eliminate cations or to partially uncouple the respiratory chain to prevent radical oxygen species (ROS) overproduction. ATP and low Pi open s_c MUC, while Pi, Ca^{2+} and Mg^{2+} close it. Different groups propose other effectors such as NADH and some glycolysis intermediates, namely Fructose 1,6-biphosphate and glucose 6-phosphate). In our hands, ATP/ADP + Pi ratio seem to control opening reversibly. This would help confirm the physiological role of s_c MUC, as it opens when energy in the cell is high. Thus, s_c MUC would prevent ROS overproduction

Posters: Systems Biology and Disease

2072-Pos

Modeling of Protein Complex Architectures using Combinatorial Genetic Perturbations

Ignacia Echeverria¹, Hannes Braberg², Peter Cimermanic³, Riccardo Pellarin⁴, Dina Schneidman⁵, Anthony Shiver⁶, Carol Gross⁷, Nevan Krogan², Andrej Sali¹.

¹Dept of Bioengineering, University of California at San Francisco, San Francisco, CA, USA, ²Department of Cellular and Molecular Pharmacology, University of California at San Francisco, San Francisco, CA, USA, ³Verily, South San Francisco, CA, USA, ⁴Institut Pasteur, Paris, France, ⁵The Hebrew University of Jerusalem, Jerusalem, Israel, ⁶Stanford University, Stanford, CA, USA, ⁷Cell and Tissue Biology, University of California at San Francisco, San Francisco, CA, USA.

Mapping structure-function relationships of macromolecular assemblies plays a key role in understanding the workings of living cells. Structure



In *Saccharomyces cerevisiae*, withdrawal of the carbon source results in detachment of glycolytic enzymes from the cytoskeleton and in actin reorganization

E. Espinoza-Simón ^a, N. Chiquete-Félix ^a, L. Morales-García ^a, U. Pedroza-Dávila ^a, X. Pérez-Martínez ^a, D. Araiza-Olivera ^b, F. Torres-Quiroz ^{c, **}, S. Uribe-Carvajal ^{a, *}

^a Dept. Molecular Genetics, Inst. de Fisiología Celular, UNAM, Mexico City, Mexico

^b Dept. Biomacromol. Chemistry, Instituto de Química, UNAM, Mexico City, Mexico

^c Dept. Biochem., Inst. de Fisiología Celular, UNAM Mexico City, Mexico

ARTICLE INFO

Article history:

Received 26 June 2019

Received in revised form

20 September 2019

Accepted 9 October 2019

Available online xxx

Corresponding Editor: Steven Bates

Keywords:

Actin cytoskeleton dynamics

Fermentation

Glycolytic metabolon

Metabolic control

Starving

ABSTRACT

Metabolons are dynamic associations of enzymes catalyzing consecutive reactions within a given pathway. Association results in enzyme stabilization and increased metabolic efficiency. Metabolons may use cytoskeletal elements, membranes and membrane proteins as scaffolds. The effects of glucose withdrawal on a putative glycolytic metabolon/F-actin system were evaluated in three *Saccharomyces cerevisiae* strains: a WT and two different obligate fermentative (OxPhos-deficient) strains, which obtained most ATP from glycolysis. Carbon source withdrawal led to inhibition of fermentation, decrease in ATP concentration and dissociation of glycolytic enzymes from F-actin. Depending on the strain, inactivation/reactivation transitions of fermentation took place in seconds. In addition, when ATP was very low, green fluorescent protein-labeled F-actin reorganized from highly dynamic patches to large, non-motile actin bodies containing proteins and enzymes. Glucose addition restored fermentation and cytoskeleton dynamics, suggesting that in addition to ATP concentration, at least in one of the tested strains, metabolon assembly/disassembly is a factor in the control of the rate of fermentation.

© 2019 The Author(s). Published by Elsevier Ltd on behalf of British Mycological Society. This is an open access article under the CC BY license (<http://creativecommons.org/licenses/by/4.0/>).

1. Introduction

In the highly crowded cytoplasm, macromolecule concentrations reach 200–400 g/l (Fulton, 1982; Zimmerman and Trach, 1991). In this regard, protein and enzyme association inside living cells seems be a widespread phenomenon (Schmitt and An, 2017) and there are cases where associations improve catalytic efficiency or regulation,

work as depots for functional enzymes or constitute aggregates of dysfunctional enzymes that may even result in pathology as in Alzheimer's, Parkinson's or Huntington's diseases (O'Connell et al., 2012). Associations of enzymes catalyzing consecutive reactions would optimize metabolism: The term "metabolon" was coined to describe a complex of sequential enzymes bound to structural elements (Srere, 1985). Metabolons improve catalytic efficiency through channeling of intermediates and enhancement of enzyme stability; these have been described in the Krebs cycle (Wu and Minteer, 2015), in purine synthesis (Pedley and Benkovic, 2017) and in flavonoid synthesis (Jørgensen et al., 2005; Nakayama et al., 2019). Of interest is the ability of plants to rapidly adapt metabolons to produce different molecules as a response to challenges from the environment (Knudsen et al., 2018).

Very early, David Green proposed the existence of a "team of glycolytic enzymes" bound to membranes in both erythrocytes and yeast (Green et al., 1965). Later, glycolytic enzyme associations among themselves and with cytoskeleton elements were described in skeletal muscle (Clarke and Masters, 1975). In erythrocytes,

Abbreviations: ABP, actin binding protein; ALD, fructose 1,6 bis-phosphate aldolase; CCCP, carbonyl cyanide 3-chlorophenyl-hydrazone; FBPase, fructose 1,6 bis-phosphate phosphatase; GAPDH, glyceraldehyde 3 phosphate dehydrogenase; GFP, green fluorescent protein; HRP, horseradish peroxidase; LDH, lactate dehydrogenase; OxPhos, oxidative phosphorylation; PEPCK, phosphoenolpyruvate carboxykinase; PFK, phosphofructokinase; PGK, phosphoglycerate kinase; PKM, pyruvate kinase M; TBS, tris-buffered saline.

* Corresponding author. Circuito Exterior s/n Ciudad Universitaria, Coyoacán, 04510 D.F. Mexico. Fax: +52 55 56225630.

** Corresponding author. Circuito Exterior s/n Ciudad Universitaria, Coyoacán, 04510 D.F. Mexico. Fax: +52 55 56225630.

E-mail addresses: ftq@ifc.unam.mx (F. Torres-Quiroz), suribe@ifc.unam.mx (S. Uribe-Carvajal).

<https://doi.org/10.1016/j.funbio.2019.10.005>

1878-6146/© 2019 The Author(s). Published by Elsevier Ltd on behalf of British Mycological Society. This is an open access article under the CC BY license (<http://creativecommons.org/licenses/by/4.0/>).

Please cite this article as: Espinoza-Simón, E et al., In *Saccharomyces cerevisiae*, withdrawal of the carbon source results in detachment of glycolytic enzymes from the cytoskeleton and in actin reorganization, *Fungal Biology*, <https://doi.org/10.1016/j.funbio.2019.10.005>

proteins such as band 3, alpha-spectrin, beta-spectrin and ankyrin have been detected in association with glycolytic enzymes (Puchulu-Campanella et al., 2013). Association of the glycolytic enzymes to cytoskeletal elements include aldolase (ALD) and phosphofructokinase (PFK), which are stabilized by microtubules, optimizing their combined activity (Ra, 2000). In breast cancer cells, PFK co-localizes with pyruvate kinase (PK) or fructose 1,6 bis-phosphate phosphatase (FBPase) and phosphoenolpyruvate carboxykinase (PEPCK) (Kohnhorst et al., 2017). In hamster ovary cancer cells, glyceraldehyde-3-phosphate dehydrogenase (GAPDH) and lactate dehydrogenase (LDH) participate in a putative "glycolytic metabolon" bound to actin (Hudder et al., 2003). In this regard, it was predicted by an *in silico* assay that ALD binds actin (Menard et al., 2014).

Enzyme organization and dynamics depend on energy. In yeast, glucose starvation inhibits dynamics of chromatin and messenger ribonucleoproteins (mRNP) (Joyner et al., 2016), autophagy (Lu et al., 2004) and protein uptake (Ashe et al., 2000), while it enhances vacuolar hydrolysis (Lang et al., 2014). Also, enzymes involved in lipid biosynthesis are sequestered in foci (Suresh et al., 2015). When yeast cultures reach saturation or when incubated without glucose, enzymes, such as cytidine triphosphate synthase form filaments that disassemble upon returning to a rich medium (Noree et al., 2010).

The actin cytoskeleton plays a role in cell structure, migration, polarization, division and traffic. In yeast, actin is in equilibrium between monomeric and filamentous states (Moseley and Goode, 2006). Actin dynamics require accessory proteins such as Actin related protein (Arp2/3) and the Wiskott-Aldrich syndrome protein (Wasp) (Smith et al., 2001). Actin filaments may form actomyosin rings, cables and patches. Actin and accessory proteins as Abp1 (actin binding protein 1), Arp, Las 17 and Sla2 among others form highly motile patches that participate in endocytosis and exocytosis (Moseley and Goode, 2006). Upon cell division, patches are distributed equally into mother and daughter cells (Apodaca, 2001; Moseley and Goode, 2006). In the stationary phase, F-actin and actin-binding proteins form immobile "actin bodies". Few hours after glucose deprivation, actin cables become stabilized and myosin cables release their cargo (Xu and Bretscher, 2014). Probably actin bodies are a reservoir from which actin cables and patches assemble as soon as nutrients become available (Sagot et al., 2006).

The glycolytic *Scerevisiae* enzymes GAPDH and phosphoglycerate kinase (PGK) are inhibited by viscosity unless ALD is added. Indeed, upon association with ALD, GAPDH increases twenty times its enzymatic activity and resists viscosity-mediated inhibition (Araiza-Olivera et al., 2010). Pharmacological stabilization of F-actin increases glycolytic enzyme binding and increases the rate of fermentation. Cytochalasin-mediated monomerization of actin filaments decreases both, metabolon assembly and rate of fermentation (Araiza-Olivera et al., 2013).

It was decided to study the effect of carbon source withdrawal on the stabilization/destabilization of a glycolytic metabolon. The response to carbon source starving was tested in WT yeast or in two different oxidative-phosphorylation-deficient, fermentation obligate *S. cerevisiae* strains, namely ρ^0 (Friis and Schultz, 2016) and *pet122Δ*, which fails to produce COX-III (Costanzo and Fox, 1990). The *pet122Δ* strain lacks the ability to translate COX-III, as it lacks PET122, a translation promoter that bridges the small ribosomal subunit with the COX-III mRNA. Still, this strain is $\rho+$ and thus contains all the metabolic regulators that respond to glucose variations (Costanzo and Fox, 1990). In contrast, the ρ^0 strain has lost all its mitochondrial DNA and thus lacks many mechanisms to adapt to starvation (Friis and Schultz, 2016). Both mutants were highly sensitive to glucose starvation. ATP concentration ([ATP]) decreased and actin filaments were reorganized from patches to immotile bodies. The WT strain underwent these changes only in the

presence of an uncoupler. In all strains, glucose addition led to recovery of [ATP], actin dynamics and binding of enzymes to actin.

2. Materials and methods

2.1. Strains and culture media

The *S. cerevisiae* strains we acquired and/or generated are listed in Table 1. As indicated, culture media were: YP (1 % Yeast extract, 2 % Peptone), YPD (YP plus 2 % Dextrose), SD (Difco: YNB 1.7 g/100 mL, $(\text{NH}_4)_2\text{SO}_4$ 5 % and an amino acid mix) or SD-Gluc (SD plus 2 % glucose) at 30 °C. Cells were grown overnight at 30 °C in a rotating carrousel at 50 rpm (Cel-Gro Tissue Culture Rotator, Thermo Scientific). Where indicated, cultures were transferred to Erlenmeyer flasks and incubated under agitation at 250 rpm.

2.2. Glycolytic enzymes binding to F-actin or among themselves

Actin association of ALD, GAPDH and PGK was evaluated by co-immunoprecipitation (Araiza-Olivera et al., 2013). In addition, the association of ALD with GAPDH and PGK was evaluated using the same method. Mouse monoclonal anti-actin (ab 14128; Abcam), protein G agarose (sc-2002; Santa Cruz Biotech), mouse monoclonal anti-ALD (ab 169544; Abcam), rabbit polyclonal anti-GAPDH (FC335, Santa Cruz Biotech) and rabbit polyclonal anti-PGK (sc-28784, Santa Cruz Biotech) were used. In each case, antibodies (3 µg/mL) against actin or ALD were incubated with 20 µL protein A/G agarose during 30 min at 4 °C, mixed with cytoplasmic extract protein (1 mg/mL) and incubated at 4 °C overnight under agitation. Samples were collected and washed by centrifugation at 2000×g for 10 min twice using IP buffer (50 mM Tris-HCl, pH 7.4, 1 mM PMSF, 0.1 % Tween 20), and protease inhibitor cocktail (sc 29130; Santa Cruz). All samples were diluted in sample buffer (62.5 mM Tris, pH 6.8, 10 % glycerol, 2 % SDS, 5 % β-mercaptoethanol and 0.01 % bromophenol blue) and boiled for 5 min. SDS/PAGE were performed in 10 % polyacrylamide. Proteins were electrotransferred to polyvinylidene difluoride (PVDF) membranes and blocked with 0.5 % albumin in TBS-T (10 mM Trizma base, 150 mM NaCl, 0.1 % Tween 20, pH 7.5) for 1 h and incubated overnight at 4 °C with primary antibody, washed with TBS-T and incubated 1 h with secondary antibody. Once membranes were washed exhaustively, bands were developed with Immobilon Western Chemiluminescent HRP substrate (Millipore).

2.3. ATP concentration

The concentration of ATP was determined by bioluminescence, using the ATP dependency of the luciferase catalyzed light-emitting oxidation of luciferin, which is capable of measuring extremely low concentrations of ATP (Deluca and McElroy, 1978). Intracellular ATP was measured using the ATP Bioluminescence Assay Kit CLS II (Roche); this Kit is especially optimized for the use in luminometers, exhibits a constant light signal sustaining for several minutes. To calculate the intracellular ATP concentration, an ATP calibration curve was prepared freshly each day, as indicated by the manufacturer of the ATP Bioluminescent Kit and using lyophilized luciferase reagent. The procedure was the following, cultures were grown as mentioned above for 4 h and 1×10^7 cells/mL were taken and resuspended in 100 mM Tris-HCl, 4 mM EDTA, pH 7.8. Cells were immersed in boiling water for 2 min and cell debris were removed by centrifugation at 15 000×g. To quantify ATP concentration the supernatants were placed in the wells of a microplate and then the luciferase reagent was added. Measurements of experimental samples and standards were conducted in a POLARstar Omega luminometer (BMG Labtech, Germany) as reported by Mendoza-Hoffmann et al. (2018).

Table 1*S. cerevisiae* strains used in this study.

Strain name	Strain genotype	Source
W3031-A	MATA {leu2-3,112 trp1-1 can1-100 ura3-1 ade2-1 his3-11,15}	Dr. A. Tzagoloff
W303 1-A Abp1-GFP	MATA {leu2-3,112 trp1-1 can1-100 ura3-1 ade2-1 ABP1-GFP:HIS3}	This work
W303 ρ^0	MATA {leu2-3,112 trp1-1 can1-100 ura3-1 ade2-1 his3-11,15, rho0}	Dr. Xochitl Perez-Martinez
W303 ρ^0 Abp1-GFP	MATx {leu2-3,112 trp1-1 can1-100 ura3-1 ade2-1 ABP1-GFP:HIS3, rho0}	This work
W303 JPM66a	MATx {leu2-3,112 trp1-1 can1-100 ura3-1 ade2-1 his3-11,15 pet122delta::KANMX }	Dr. Xochitl Perez-Martinez
W303 J11 Abp1-GFP	MATx {leu2-3,112 trp1-1 can1-100 ura3-1 ade2-1 ABP1-GFP:HIS3 pet122delta::KANMX }	This work

2.4. Rate of fermentation

Yeast cells from SD-Gluc or YPD 24 h cultures were washed three times using sterile water (2900×g 5 min in an Avant J-26 XPI centrifuge, Beckman Coulter, USA) and inoculated in YP or YPD-Gluc, incubating at 30 °C for 4 h under agitation at 250 rpm in a Excella E24 incubator Shaker (New Brunswick Scientific, USA). Then, cells were washed and the pellet was resuspended again in YP or YPD. To measure the rate of fermentation, cells (1×10^7) were incubated in 20 mM glucose, for up to 6 min and 0.1 mL of 30 % trichloroacetic acid (TCA) was added. Samples were centrifuged at 2900×g for 5 min at 4 °C. The supernatant was neutralized with NaOH and ethanol was quantified using an enzymatic method coupled to NAD⁺ (1.8 mM) reduction by alcohol dehydrogenase (100 µg·µL⁻¹) (Bonnichsen, 1965). Briefly 1 mg prot./mL of each supernatant was suspended in 1 mL of 300 mM Na₄P₂O₇·10H₂O, 75 mM Semicarbazide hydrochloride, 22 mM Glycine, 66 mM NaOH pH 8.8, and 1.8 mM NAD (Bonnichsen, 1965). After 10 s, 100 µg/mL ADH was added and incubated 1 h at 24 °C. Absorbance was determined at 340 nm in an Aminco-Olis DW2000 spectrophotometer (Olis Inc., Bogart, GA, USA). Ethanol standard curve was used, and the results are reported as nmol ethanol per mg cells.

2.5. Fluorescent labeling of the actin-binding protein and of actin

In order to analyze actin distribution and dynamics, green-fluorescent protein-tagged strains were created to observe actin patches (Huckaba et al., 2004; Vasicova et al., 2015). For the actin-binding protein (Abp1p), its C-terminus of Abp1p was tagged with GFP^Y by PCR-based insertion of the gene into a chromosomal copy of ABP1 using plasmid pFA6a-link-yoEGFP-SpHis5 (gift from Wendell Lim & Kurt Thorn) (Addgene plasmid # 44836) (Lee et al., 2013) and primers Abp1fluoF, Abp1fluoR (Table S2) as described previously (Huckaba et al., 2004). Yeast were transformed using a lithium acetate protocol (Gietz et al., 1995) and the correct integration of GFP cassette at the ABP1 locus was characterized using PCR. GFP tagging had no effect on growth, glucose fermentation or actin organization (Results not shown).

To confirm the colocalization of GFP-Abp1 and actin, each GFP-Abp1-labeled strain was fixed in 3.7 % paraformaldehyde. Actin was labeled as follows: cells were washed and stained with 1.65 µM rhodamine-phalloidin (Sigma Aldrich) and incubated for 30 min at room temperature. Next, cells were washed and mounted for imaging (Higuchi-Sanabria et al., 2016). Samples were observed under a Nikon Eclipse E600 fluorescence microscope equipped with a DXM 1200 high resolution digital camera with a 460 nm–490 nm filter for GFP excitation and 530 nm–550 nm filter for rhodamine excitation. Merging was performed using ImageJ software (Hartig, 2013).

2.6. Time-lapse microscopy

To evaluate actin patch dynamics, live cells were layered onto SD agarose pads (Pemberton, 2014). Then, we evaluated actin patch dynamics in a Leica TCS-SP5 confocal microscope in a 63× objective

with an Argon laser exciting at 488 nm and generating 60 images/min. Image processing was performed with the LAS X (Leica) and ImageJ software.

2.7. Actin patch dynamics in pharmacological uncoupled yeast

To evaluate actin dynamics, the WT strain was cultured in SD-Gluc overnight and yeasts were washed and inoculated in SD. Where indicated, 20 µM carbonyl cyanide 3-chlorophenylhydrazone (CCCP) was added. Then, cells were mounted on agarose pads and analyzed with a Nikon Eclipse E600 fluorescence microscope with a DXM 1200 high resolution color digital camera.

2.8. Statistics

Where indicated, one-way ANOVA (Tukey's multiple comparisons test) was used to compare the differences between strains, using GraphPad Prism version 6 (GraphPad Software, Inc. La Jolla, CA, USA).

3. Results

3.1. Glycolytic enzyme/F-actin affinity decreased upon carbon source withdrawal

To test the modifications in actin-enzyme affinity brought by starvation, co-immunoprecipitation of three glycolytic pathway enzymes, namely ALD (Fig. 1, upper panel), PGK (Fig. 1, second panel) and GAPDH (Fig. 1, third panel) with actin was evaluated in glucose-fed (G) and in starved (S) cells. Tested strains were W303 WT, W303 ρ^0 and W303 pet122Δ. In glucose-fed strains, a strong interaction between actin and glycolytic enzymes was observed (Fig. 1, odd lanes). This was already expected from a previous report (Araiza-Olivera et al., 2013). In contrast, glycolytic enzymes from starved yeast exhibited a decrease in co-immunoprecipitation in all cases (Fig. 1, even lanes). It is interesting to observe that in starved samples GAPDH detachment seemed to be complete. Thus, the glycolytic enzyme/F-actin organization expected for a putative metabolon was disrupted by carbon source withdrawal and this should inhibit the glycolytic pathway in starved cells. To test this, it was decided to determine the association of the aforementioned enzymes in glucose-fed (G) and in starved (S) cells and whether starvation effects were magnified in the fermentative obligate strains.

3.2. Glycolytic enzyme–enzyme affinity decreased mildly upon carbon source withdrawal

The effect of glucose withdrawal on affinity among glycolytic enzymes was analyzed in extracts from G or S cells. ALD was immunoprecipitated (Fig. 2, lower panel) and co-immunoprecipitation of PGK (Fig. 2 upper panel) and GAPDH (middle panel) was evaluated. Samples from each of the strains

W303 WT (lanes 1 and 2), W303 ρ^0 (lanes 3 and 4) and W303 $pet122\Delta$ (lanes 5 and 6) were used. In all cases PGK co-immunoprecipitation decreased markedly upon starving (Fig. 2, upper panel), while GAPDH co-immunoprecipitation decreased only mildly. The effects of starving on GAPDH-ALD association were milder than those reported upon F-actin destabilization with latrunculin or cytochalasin (Araiza-Olivera et al., 2013). Thus, the glycolytic enzyme/F-actin organization expected for a putative metabolon was only mildly disrupted by carbon source withdrawal and it is not clear whether this would inhibit the glycolytic pathway in starved cells. To test this, it was decided to determine the concentration of ATP ([ATP]) in fed and starved cells from each strain and whether starvation effects were magnified in the obligate fermentative strains.

3.3. Starving decreases [ATP] in yeast. More so in obligate fermentative strains

The effect of carbon source withdrawal on [ATP] was determined, both in the WT strain (Fig. 3, black bars) and in each of the

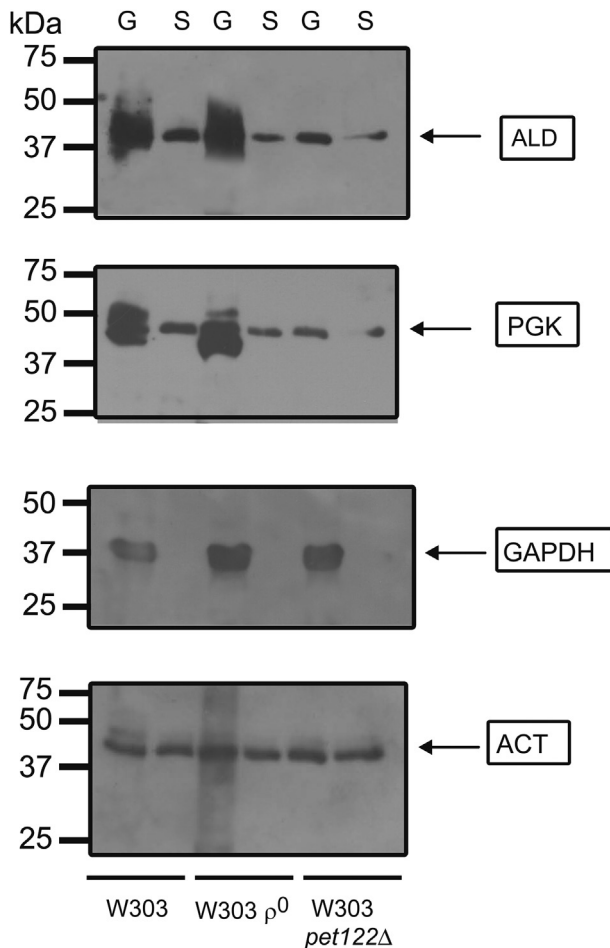


Fig. 1. Under starvation, glycolytic enzymes detach from actin. Cells were cultured overnight in SD-Gluc. Then, cells were washed and incubated in SD (S) or SD-Gluc (G) 4 h at 30 °C. Yeast extracts were obtained and actin was immunoprecipitated. Precipitates were immunoblotted against ALD (top panel), PGK (second panel) or GAPDH (third panel), with actin (ACT) as loading control (bottom panel). Lane 1: W303 WT Abp1-GFP in SD-Gluc, Lane 2: W303WT Abp1-GFP in SD, Lane 3: W303 ρ^0 Abp1-GFP in SD-Gluc, lane 4: W303 ρ^0 Abp1-GFP in SD, lane 5: W303 $pet122\Delta$ Abp1-GFP in SD-Gluc, lane 6: W303 $pet122\Delta$ Abp1-GFP in SD. Representative image of three independent experiments. Lanes with glucose-fed yeast are labeled "G" while those from starved yeast are labeled "S".

OxPhos-deficient mutants: W303 ρ^0 (Fig. 3, white bars) and W303 $pet122\Delta$ (gray bars). After incubating for 4 h in the presence of glucose, [ATP] was: in WT, [ATP] = 2.3 nmol (mg prot) $^{-1}$ and slightly higher [ATP] = 2.6–2.8 nmol (mg prot) $^{-1}$ in the fermentative mutants (Fig. 3A). Then, after a starving period of 30 min, a slight decrease was observed in WT where [ATP] = 1.8 nmol (mg prot) $^{-1}$, while in the fermentative strains [ATP] decreased to near 1.0 nmol (mg prot) $^{-1}$ in each case (Fig. 3B). After 4 h in the absence of glucose, [ATP] differences became more evident. The WT still contained high [ATP] = 2.0 nmol (mg prot) $^{-1}$ while in each of the fermentative mutants a much lower [ATP] = 0.6 nmol (mg prot) $^{-1}$ was observed (Fig. 3C). These results indicated that [ATP] was more sensitive to carbon depletion in each obligate fermentative strain than in WT. i.e., after starving for 4 h, [ATP] decreased 60–75 % in each mutant while in the WT the decrease was only 16 % (Fig. 3). The decrease in [ATP] could be due to a simple lack of substrate or might be evidencing the disorganization a glycolytic metabolon.

3.4. At low [ATP] glucose addition increased fermentation activity

Glucose withdrawal resulted in glycolytic enzyme detachment from F-actin (Fig. 1), in mild loss of enzyme–enzyme affinity (Fig. 2) and in decreased [ATP] (Fig. 3), suggesting that glycolysis was inactivated. To test this, the rate of fermentation was measured in starved (S, dots) and glucose-fed (G, circles) samples from each of the three strains (Fig. 4). In S samples the rate of fermentation was at least five times faster than in G samples (Fig. 4), suggesting that a low [ATP] activated glycolysis. In addition, while the WT (Fig. 4-A circles) and the W303 ρ^0 strain (Fig. 4-B circles) exhibited a nearly constant activity from the beginning, the fermentation rate for the W303 $pet122\Delta$ strain was slow for the first two minutes and increased at later incubation times (Fig. 4-C, circles). The WT strain, where [ATP] was higher after fasting, was the least active (Fig. 4-A, circles). The W303 $pet122\Delta$ strain exhibited an initial fermentation rate of 3 nmols EtOH (min·mg. prot $^{-1}$), which increased to 12 nmols EtOH (min·mg. prot $^{-1}$) after two minutes (Fig. 4-C, circles).

In contrast, in the G samples a very slow rate of fermentation was observed (Fig. 4, dots) in all cases. Furthermore, when these plots were magnified (Fig. 4, inserts), a slightly faster fermentation rate was detected for the first minute in each case, which decreased at later time points. In addition, for glucose-fed strains rates of fermentation were smaller than in the fasted samples. In the glucose-fed WT, the initial rate of fermentation was 3 μ mol EtOH

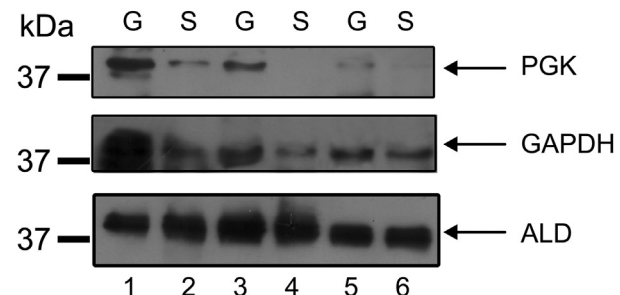


Fig. 2. Glucose withdrawal results in decreased affinity of glyceraldehyde-phosphate dehydrogenase and 2-phosphoglycerate for aldolase. Experimental conditions as in Fig. 1, except aldolase (ALD) was immunoprecipitated from yeast extracts. Precipitates were immunoblotted against PGK (upper panel) or GAPDH (middle panel), using ALD as loading control (bottom panel). Lane 1: W303 WT Abp1-GFP in SD-Gluc, Lane 2: W303WT Abp1-GFP in SD, Lane 3: W303 ρ^0 Abp1-GFP in SD-Gluc, lane 4: W303 ρ^0 Abp1-GFP in SD, lane 5: W303 $pet122\Delta$ Abp1-GFP in SD-Gluc, lane 6: W303 $pet122\Delta$ Abp1-GFP in SD. Representative image of three independent experiments. Lanes with glucose-fed yeast are labeled "G" while those from starved yeast are labeled "S".

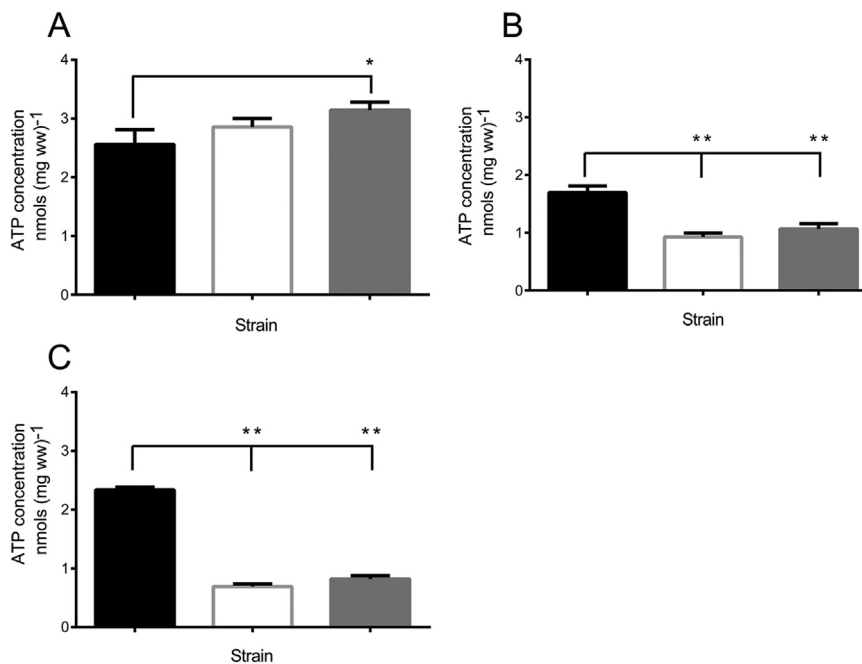


Fig. 3. ATP concentration in different yeast strains subjected to starving. Intracellular ATP in W303 Abp1-GFP (black bars), W303 ρ^0 Abp1-GFP (white bars) and W303 *pet122Δ* Abp1-GFP (gray bars) were measured. Experimental conditions as in Fig. 1. Yeasts were incubated as follows: (A) in SD-Gluc for 4 h or (B) in SD for 30 min or (C) or in SD for 4 h. Then yeasts were harvested, washed and ATP was quantified using a bioluminescence assay. Values are means \pm SD of three independent experiments, each performed in triplicate. Statistical differences were determined using One way ANOVA plus Tukey's multiple comparisons test: *P < 0.05, **P < 0.01.

(min·mg. prot⁻¹) and decreased after two minutes to 1.2 μ moles EtOH (min·mg. prot⁻¹) (Fig. 4-A insert). The W303 ρ^0 strain exhibited an initial fermentation rate of 3.6 μ moles EtOH (min·mg. prot⁻¹), which after two minutes decreased to 1.5 μ moles EtOH (min·mg. prot⁻¹) (Fig. 4-B, insert). The W303 *pet122Δ* exhibited an initial fermentation rate of 5 μ moles EtOH (min·mg. prot⁻¹), which decreased after two minutes to 2.0 μ moles EtOH (min·mg. prot⁻¹) (Fig. 4-C, insert). Thus, in the fasted samples fermentation was active, probably aiming to replenish the low ATP pool. In contrast, the glucose-fed samples were active from the start of the experiment, although these did not reach high rates probably as a result of the presence of high [ATP]. The only indication of a lag in fermentation activity after fermentation was from W303 *pet122Δ* where a one to two minute lag was observed before full activity was observed (Fig. 4-C, circles).

3.5. Actin-binding protein 1 (Abp1) reports structural cytoskeleton modifications promoted by glucose withdrawal

The glycolytic metabolon is most likely organized around the actin cytoskeleton (Araiza-Olivera et al., 2013). As actin is not amenable to labeling, it was decided to label the actin-binding protein (Abp1) instead. Then in order to confirm that the fluorescence from Abp1 was an efficient reporter of actin localization, strains were fixed and GFP-Abp1 fluorescence was followed (Fig. 5 left panels). In the same samples, F-actin was labeled using rhodamine-phalloidin (Fig. 5 middle panels) and co-localization was evaluated (Fig. 5 right panels). Green fluorescence from GFP-Abp1 co-localization with the red fluorescence from rhodamine-phalloidin was analyzed (Fig. 5). In all glucose-fed strains, and in the starved W303 WT, small fluorescent patches were detected, both in the green and in the red fluorescence channels (Fig. 5A and B, C and E), while in the starved fermentative-obligate strains large fluorescent bodies were observed both in the W303 ρ^0 (Fig. 5-D) and in the W303 *pet122Δ* (Fig. 5-F). The CCCP-uncoupled W303 WT

(to deplete ATP) also exhibited large fluorescent bodies (Result not shown). Thus, incubation without glucose led to reorganization of F-actin that correlated with the decrease in [ATP]. Upon glucose addition, [ATP] increased and modifications observed in the actin cytoskeleton were reversed (Result not shown). Images from reorganized F-actin in the S mutants (Fig. 5) suggested the presence of actin bodies, which according to the literature should be immotile (Sagot et al., 2006). To confirm the presence of immotile actin bodies, it was decided to evaluate cytoskeleton dynamics from each strain and condition.

3.6. In starving oxidative-phosphorylation-deficient strains, small, highly dynamic F-actin patches are replaced by large non-motile bodies

When yeast reach the stationary phase, actin cables and patches reorganize, forming immotile actin bodies (Sagot et al., 2006). Thus, it was decided to determine whether glucose withdrawal led to modifications of actin cytoskeleton dynamics in each strain under study, using a time-lapse microscopy assay and following the fluorescence of GFP-Abp1. In all glucose-fed strains and in the starved W303 WT strain, small, motile actin patches were observed (see supplementary videos 1, 2, 4 and 6). The W303-WT strain exhibited highly motile actin patches regardless of whether it was glucose fed (Suppl-video 1) or starved (Suppl-video 2). In contrast, the W303 ρ^0 mutant exhibited motile patches when glucose fed (Suppl-video 3), while it exhibited immotile actin bodies when starved (Suppl-video 4). The W303 *pet122Δ* strain also exhibited motile actin patches when glucose-fed (Suppl-video 5) and non-motile actin bodies when starved (Suppl-video 6).

Supplementary video related to this article can be found at <https://doi.org/10.1016/j.funbio.2019.10.005>.

The interactions of enzymes in a putative glycolytic metabolon and F-actin were explored in cells subjected to carbon source depletion. Upon starving, the cytoskeleton reorganized and lost its

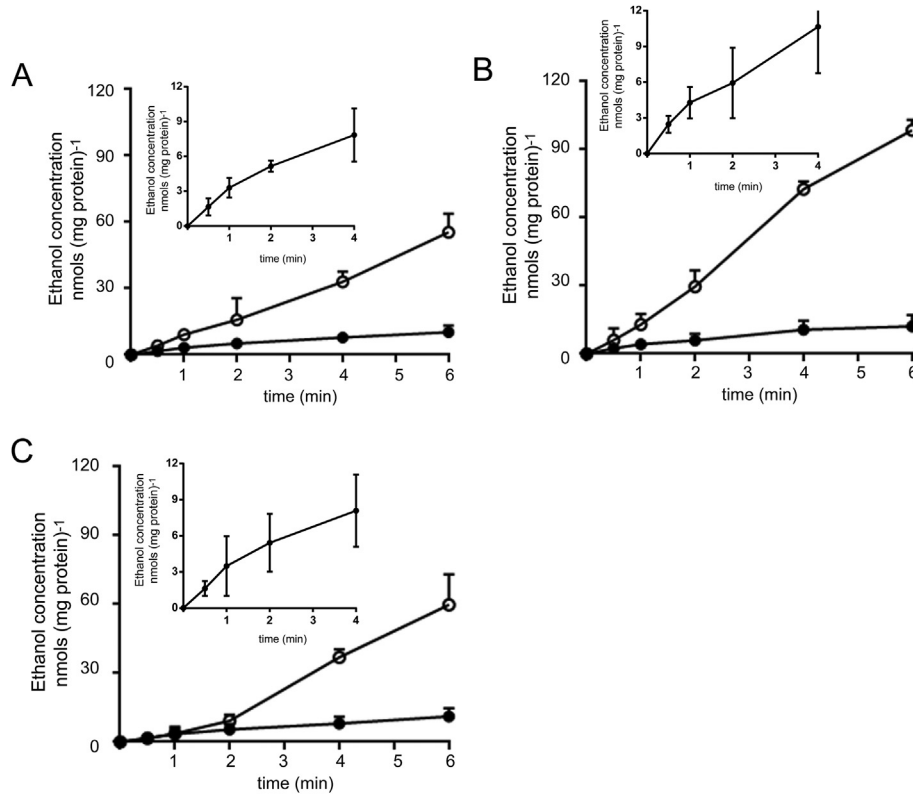


Fig. 4. In *S. cerevisiae*, the rate of fermentation reacts rapidly to glucose withdrawal and re-addition. Ethanol production kinetics were measured in (A) W303 Abp1-GFP, (B) W303 ρ^0 Abp1-GFP or (C) W303 pet122Δ Abp1-GFP. Experimental conditions, as in Fig. 1. Cells were washed and incubated 4 h in YP (empty circles) or YPD (full dots) at 30 °C. The rate of fermentation was determined at 30 s, 1, 2, 4 and 6 min. Produced ethanol was quantified using an enzyme-coupled assay (see methods). Results are reported as nmol EtOH/mg protein. Three independent experiments were performed, values are means \pm SD. *P < 0.05. Insets are a 10 time magnification of the YPD plot for each strain, aiming to show that during the first one to two minutes fermentation was slightly faster than at later points.

affinity for glycolytic enzymes. ATP concentration seemed to be an important factor regulating both cytoskeleton organization and fermentation activity. In W303 ρ^0 and W303 pet122Δ, cells that depend strongly on glycolysis for ATP production, starving also resulted in re-distribution of the cytoskeleton and in actin storage into immotile bodies. All effects disappeared upon glucose re-addition.

4. Discussion

Membrane-less enzyme complexes in the cytoplasm vary in stoichiometry and protein dwelling time (Case et al., 2019). Up to 180 intermediary metabolism enzymes may exhibit non-diffusible behavior (O'Connell et al., 2012). An interactome involving both the enzymes in a given metabolon and the membrane transporters would result in channeling of substrates from uptake by the cell all the way to the last product of the pathway (Moraes and Reithmeier, 2012). Such seems to be the case in erythrocytes, where a docking site in the vicinity of the membrane-spanning segment of band 3 binds both glycolytic enzymes and a glucose transporter (GLUT1) (Puchulu-Campanella et al., 2013). The tendency of proteins exhibiting quaternary structures to form fibers seems to be high and may optimize function as in purinosomes or become a source of disease as in sickle cell anemia or as in amyloid diseases (O'Connell et al., 2012).

Signaling pathways are another example where protein association has been reported recently (Strzyz, 2019). Actin polymerization is optimized by signaling clusters on the plasma membrane where Nephelin–Nck–N-WASP associate (Case et al., 2019). Also on the plasma membrane, the mitogen-activated protein kinase

(MAPK) pathway recruits proteins such as SOS, needed to optimize signaling (Huang et al., 2019). Protein clusters may sequester small molecules, as in adenosine A_{2A} or A_{2B} signalosomes, where each specific isoform of adenosine receptor, adenylate cyclase and A-Kinase-Anchoring Protein (AKAP) generate a sequestered cAMP pool and evoke receptor-specific responses (Guinzberg et al., 2017).

Glycolytic metabolons optimize catalysis and protect enzymes against external conditions (Araiza-Olivera et al., 2013; Menard et al., 2014). Most likely, metabolons are dynamic structures (Sweetlove and Fernie, 2018). In *C. elegans* neurons under energy stress, glycolytic enzymes move near synapses, probably with the aim of increasing local [ATP] (Jin et al., 2017). Hypoxia drives *S. cerevisiae* glycolytic enzymes into G bodies where glycolysis becomes more efficient (Jin et al., 2017).

The rate of fermentation in glucose-fed versus starved cells were explored. The energy dependence of assembly was analyzed in three different yeast strains. A WT OxPhos facultative strain (W303 WT) and two obligate fermentative strains, namely a ρ^0 (W303 ρ^0) and a strain where a promoter (PET122) needed for translation of subunit three of complex IV was deleted (W303 pet122Δ) (Costanzo and Fox, 1988). The obligate fermentative strains magnified the effects of glucose withdrawal on ATP production (Friis and Schultz, 2016). Cells were incubated four hours in the presence or in the absence of a carbon source. Under starvation, the glycolytic enzymes, ALD, GAPDH and PGK lost their affinity for F-actin (Fig. 1), and decreased enzyme–enzyme affinity (Fig. 2). Starving led to a decrease in the concentration of ATP that was more accentuated in the fermentative obligate strains (Fig. 3). When the rate of glycolysis was tested it was observed that low [ATP] led to high fermentation activity. In regard to the possible inactivation of

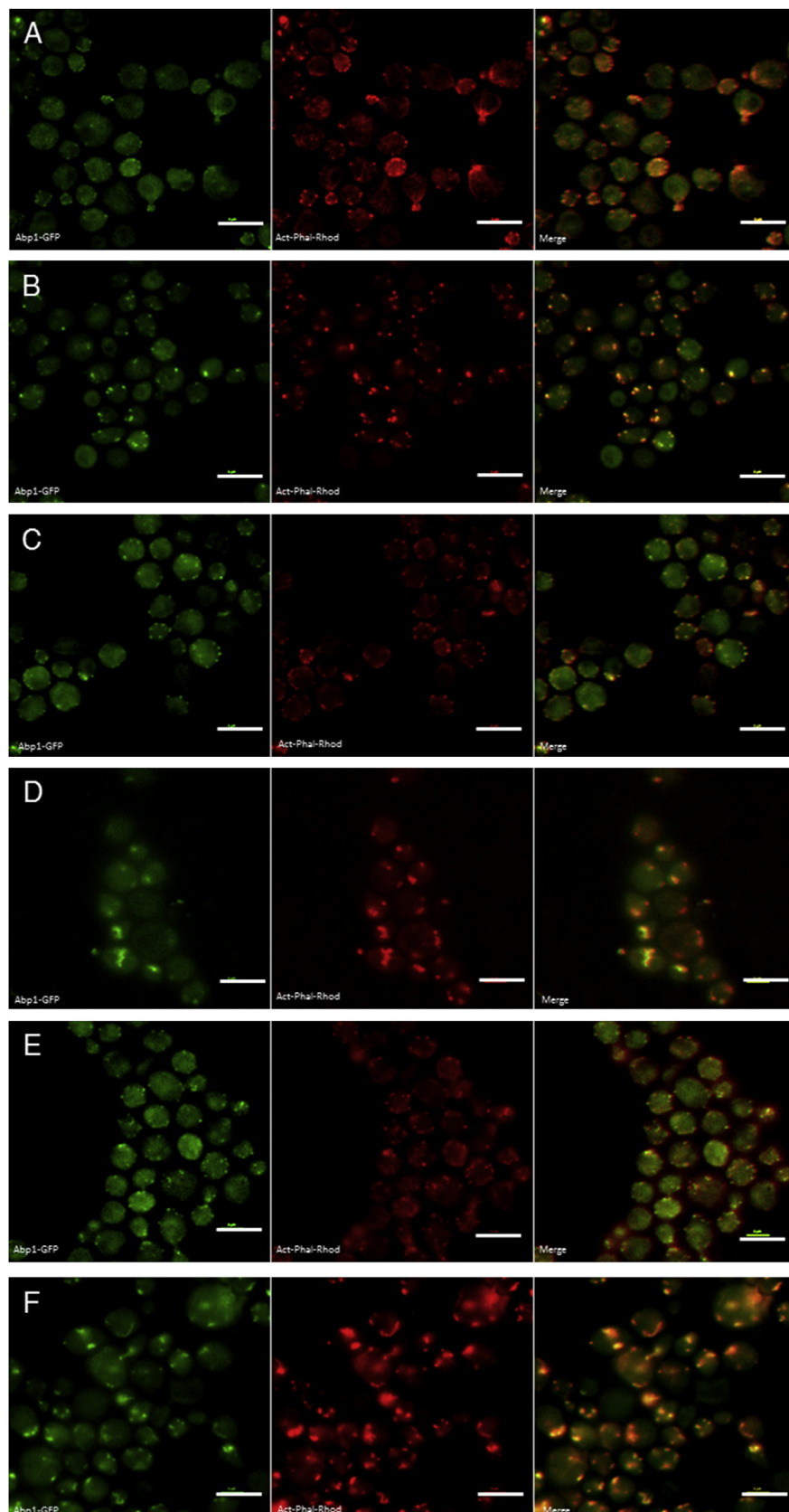


Fig. 5. Abp1-GFP and F-actin co-localize in the *S. cerevisiae* Abp1-GFP-derived W303 strains. Experimental conditions as in Fig. 4. Yeasts were incubated overnight in SD-Gluc, then cells were washed and incubated in SD-Gluc (A, C and E) or SD (B, D and F) at 30 °C and under agitation for 4 h. After incubation, cells were fixed and stained with rhodamine phalloidin for 30 min. Cell Images were obtained in an epifluorescence microscope. Strains are W303 Abp1-GFP, glucose fed (A) or starved (B) W303 p^0 Abp1-GFP, Glucose fed (C) or starved (D) and W303 *pet122Δ* A Glucose-fed (E) or starved (F). Bar = 10 μ m. Images are representative from three independent experiments.

glycolysis resulting from enzyme dissociation, only the W303 *pet122Δ* strain exhibited a degree of inactivation by starving, which rapidly reverted after two minutes (Fig. 4-C). In contrast, the rate of fermentation after glucose addition to well-fed yeast was never as high as in the starved cells and it decreased after two minutes. We suggest that [ATP] controls the rate of fermentation. The two-minute delay in activation of fermentation in the starved W303 *pet122Δ* probably reflects the need to reassemble a glycolytic metabolon. This was not observed in the W303 ρ^0 strain, perhaps due to its reported inability to respond to changes in the environment (Friis and Schultz, 2016).

The response to carbon source withdrawal was more pronounced in obligate fermentative cells, which depend heavily on glycolysis for energy production. Both OxPhos-deficient strains decreased their total ATP concentration by 80 % while in the WT the decrease was only 10 %. In addition, large reorganization of the cytoskeleton took place as F-actin was redistributed from small, dynamic patches to large immotile bodies. It has been suggested that actin bodies may be a storage form of actin designed to save energy (Sagot et al., 2006). Thus it is possible that these bodies stop functions such as cargo and endocytosis, where a motile cytoskeleton would be required (Goode et al., 2015). The cytoskeleton role as a scaffold for enzyme association in the glycolytic metabolon (Menard et al., 2014) would also be lost in large actin bodies. The critical role of the metabolon to produce energy has been documented in other systems, such as in gpdh-3 null flies which do not exhibit glycolytic complex organization in muscle, which results in the inability to fly (Wojtas et al., 1997).

Redistribution of the actin cytoskeleton into immotile bodies correlated with ATP availability. In the mutants, [ATP] decreased and the cytoskeleton was modified. However, in the WT it was necessary to uncouple oxidative phosphorylation in order to obtain immotile bodies. Actin cytoskeleton redistribution experiments were conducted using the GFP-Abp1, which as expected from the literature (Sagot et al., 2006), remained bound to actin following its distribution, regardless of the metabolic conditions in the cell.

In *S. cerevisiae*, a carbon source starve-feed cycle controlled the rate of fermentation. It is likely that the mechanism of control involved the assembly/disassembly of a putative glycolytic metabolon that used the F-actin cytoskeleton as a scaffold. In addition, the concentration of ATP was a major factor controlling the maximal rate of fermentation. Obligate fermentative strains were more sensitive to the effects of starving on their metabolism and on cytoskeleton dynamics.

Declaration of Competing Interest

The authors have no conflicts of interest to declare.

Acknowledgements

Partially funded by DGAPA-PAPIIT, UNAM, Mexico, Grant numbers: SUC: IN204015; FTQ: IA202217 and IN209219 and by Conacyt Mexico SUC: Grant: 239487. EES was a CONACYT Mexico PhD fellow, LMG and UPD are CONACYT fellows, EES and UPD are enrolled in the Biochemistry Graduate Program at UNAM. LMG is in the Biomedical Research Graduate program at UNAM. We received technical help from the Microscopy (R. Rincón Heredia), Molecular Biology and Computation units at the IFC.

Appendix A. Supplementary data

Supplementary data to this article can be found online at <https://doi.org/10.1016/j.funbio.2019.10.005>.

References

- Apodaca, G., 2001. Endocytic traffic in polarized epithelial cells: role of the actin and microtubule cytoskeleton. *Traffic* 2, 149–159. <https://doi.org/10.1034/j.1600-0854.2001.020301.x>.
- Araiza-Olivera, D., Chiquete-Felix, N., Rosas-Lemus, M., Sampedro, J.G., Peña, A., Mujica, A., Uribe-Carvajal, S., 2013. A glycolytic metabolon in *Saccharomyces cerevisiae* is stabilized by F-actin. *FEBS J.* 280, 3887–3905. <https://doi.org/10.1111/febs.12387>.
- Araiza-Olivera, D., Sampedro, J.G., Mujica, A., Peña, A., Uribe-Carvajal, S., 2010. The association of glycolytic enzymes from yeast confers resistance against inhibition by trehalose. *FEMS Yeast Res.* 10, 282–289. <https://doi.org/10.1111/j.1567-1364.2010.00605.x>.
- Ashe, M.P., Long, S.K., De Sachs, A.B., 2000. Glucose depletion rapidly inhibits translation initiation in yeast. *Mol. Biol. Cell* 11, 833–848.
- Bonnichsen, R., 1965. Ethanol: determination with alcohol dehydrogenase and DPN. In: *Methods of Enzymatic Analysis*, pp. 285–289. <https://doi.org/10.1016/B978-0-12-395630-9.50061-X>.
- Case, L.B., Zhang, X., Ditlev, J.A., Rosen, M.K., 2019. Stoichiometry controls activity of phase-separated clusters of actin signaling proteins. *Science* 363, 1093–1097. <https://doi.org/10.1126/science.aau6313> (80).
- Clarke, F.M., Masters, C.J., 1975. On the association of glycolytic enzymes with structural proteins of skeletal muscle. *Biochim. Biophys. Acta* 381, 37–46. [https://doi.org/10.1016/0304-4165\(75\)90187-7](https://doi.org/10.1016/0304-4165(75)90187-7).
- Costanzo, M.C., Fox, T.D., 1990. Control of mitochondrial gene expression in *Saccharomyces cerevisiae*. *Annu. Rev. Genet.* 24, 91–113. <https://doi.org/10.1007/BF00219314>.
- Costanzo, M.C., Fox, T.D., 1988. Specific translational activation by nuclear gene products occurs in the 5' untranslated leader of a yeast mitochondrial mRNA. *Proc. Natl. Acad. Sci. U.S.A.* 85, 2677–2681. <https://doi.org/10.1073/pnas.85.8.2677>.
- Deluca, M., McElroy, W.D., 1978. Purification and properties of firefly luciferase. In: *Methods in Enzymology. Bioluminescence and Chemiluminescence*, 57. Acad. Press, San Diego, New York, pp. 3–15.
- Friis, R.M.N., Schultz, M.C., 2016. Attenuation of transcriptional and signaling responses limits viability of ρ^0 *Saccharomyces cerevisiae* during periods of glucose deprivation. *Biochim. Biophys. Acta - Gen. Subj.* 1860, 2563–2575. <https://doi.org/10.1016/j.bbagen.2016.07.029>.
- Fulton, A.B., 1982. How crowded is the Cytoplasm? *Minireviews. Water* 30, 345–347. [https://doi.org/10.1016/0092-8674\(82\)90231-8](https://doi.org/10.1016/0092-8674(82)90231-8).
- Gietz, R.D., Schiestl, R.H., Willem, A.R., Woods, R.A., 1995. Studies on the transformation of intact yeast cells by the LiAc/SS??DNA/PEG procedure. *Yeast* 11, 355–360. <https://doi.org/10.1002/yea.320110408>.
- Goode, B.L., Eskin, J.A., Wendland, B., 2015. Actin and endocytosis in budding yeast. *Genetics* 199, 315–358. <https://doi.org/10.1534/genetics.112.145540>.
- Green, D.E., Murer, E., Richardson, S.H., Salmon, B., Brierley, G.P., Baum, H., 1965. Association of integrated metabolic pathways with membranes. *Arch. Biochem. Biophys.* 112, 635–647.
- Guinzberg, R., Díaz-Cruz, A., Acosta-Trujillo, C., Vilchis-Landeros, M.M., Vázquez-Meza, H., Lozano-Flores, C., Chiquete-Felix, N., Varela-Echavarría, A., Uribe-Carvajal, S., Riveros-Rosas, H., Piña, E., 2017. Newly synthesized cAMP is integrated at a membrane protein complex signalosome to ensure receptor response specificity. *FEBS J.* 284, 258–276. <https://doi.org/10.1111/febs.13969>.
- Hartig, S.M., 2013. Basic image analysis and manipulation in imgel. *Curr. Protoc. Mol. Biol.* 1–12 <https://doi.org/10.1002/047142727.mb1415s102>.
- Higuchi-Sanabria, R., Swayne, T.C., Boldogh, I.R., Pon, L.A., 2016. Imaging of the actin cytoskeleton and mitochondria in fixed budding yeast cells. In: Gavin, R.H. (Ed.), *Cytoskeleton Methods and Protocols: Methods and Protocols*. Springer New York, New York, NY, pp. 63–81. https://doi.org/10.1007/978-1-4939-3124-8_3.
- Huang, W.Y.C., Alvarez, S., Kondo, Y., Kwang Lee, Y., Chung, J.K., Monatrice Lam, H.Y., Biswas, K.H., Kuriyan, J., Groves, J.T., 2019. A molecular assembly phase transition and kinetic proofreading modulate Ras activation by SOS. *Science* 363, 1098–1103. <https://doi.org/10.1126/science.aau5721> (80).
- Huckaba, T.M., Gay, A.C., Pantaleo, L.F., Yang, H.C., Pon, L.A., 2004. Live cell imaging of the assembly, disassembly, and actin cable-dependent movement of endosomes and actin patches in the budding yeast, *Saccharomyces cerevisiae*. *J. Cell Biol.* 167, 519–530. <https://doi.org/10.1083/jcb.200404173>.
- Hudder, A., Nathanson, L., Deutscher, M.P., 2003. Organization of mammalian cytoplasm. *Mol. Cell. Biol.* 23, 9318–9326. <https://doi.org/10.1128/MCB.23.24.9318-9326.2003>.
- Jin, M., Han, T., Yao, Y., Alessi, A.F., Freeberg, M.A., Inoki, K., Klionsky, D.J., Kim, J.K., Jin, M., Klionsky, D.J., Han, T., Freeberg, M.A., Karnovsky, A., Moresco, J.J., Yates, J.R., Baba, M., Gitler, A.D., Inoki, K., Fuller, G.G., Alessi, A.F., Freeberg, M.A., Roach, N.P., Kim, J.K., Han, T., 2017. Glycolytic enzymes coalesce in G bodies under hypoxic stress. *Cell Rep.* 20, 895–908. <https://doi.org/10.1016/j.celrep.2017.06.082>.
- Jørgensen, K., Rasmussen, A.V., Morant, M., Nielsen, A.H., Bjarnholt, N., Zagrobelny, M., Bak, S., Møller, B.L., 2005. Metabolon formation and metabolic channeling in the biosynthesis of plant natural products. *Curr. Opin. Plant Biol.* 8, 280–291. <https://doi.org/10.1016/j.pbi.2005.03.014>.
- Joyner, R.P., Tang, J.H., Helenius, J., Dultz, E., Brune, C., Holt, L.J., Huet, S., Müller, D.J., Weis, K., 2016. A glucose-starvation response regulates the diffusion of macromolecules. *Elife* 5, 1–26. <https://doi.org/10.7554/elife.09376>.

- Knudsen, C., Gallage, N.J., Hansen, C.C., Møller, B.L., Laursen, T., 2018. Dynamic metabolic solutions to the sessile life style of plants. *Nat. Prod. Rep.* 11, 1140–1155. <https://doi.org/10.1039/c8np00037a>.
- Kohnhorst, C.L., Kyoung, M., Jeon, M., Schmitt, D.L., Kennedy, E.L., Ramirez, J., Bracey, S.M., Luu, B.T., Russell, S.J., An, S., 2017. Identification of a multienzyme complex for glucose metabolism in living cells. *J. Biol. Chem.* 292, 9191–9203. <https://doi.org/10.1074/jbc.M117.783050>.
- Lang, M.J., Martinez-Marquez, J.Y., Prosser, D.C., Ganser, L.R., Buelto, D., Wendland, B., Duncan, M.C., 2014. Glucose starvation inhibits autophagy via vacuolar hydrolysis and induces plasma membrane internalization by down-regulating recycling. *J. Biol. Chem.* 289, 16736–16747. <https://doi.org/10.1074/jbc.M113.525782>.
- Lee, S., Lim, W.A., Thorn, K.S., 2013. Improved blue, green, and red fluorescent protein tagging Vectors for *S. cerevisiae*. *PLoS One* 8, 4–11. <https://doi.org/10.1371/journal.pone.0067902>.
- Lu, M., Sautin, Y.Y., Holliday, L.S., Gluck, S.L., 2004. The glycolytic enzyme aldolase mediates assembly, expression, and activity of vacuolar H⁺-ATPase. *J. Biol. Chem.* 279, 8732–8739. <https://doi.org/10.1074/jbc.M303871200>.
- Menard, L., Maughan, D., Vigoreux, J., 2014. The structural and functional coordination of glycolytic enzymes in muscle: evidence of a metabolon? *Biology (Basel)* 3, 623–644. <https://doi.org/10.3390/biology3030623>.
- Mendoza-Hoffmann, F., Pérez-Osegueda, Á., Cevallos, M.Á., Zarco-Zavala, M., Ortega, R., Peña-Segura, C., Espinoza-Simón, E., Uribe-Carvajal, S., García-Trejo, J.J., 2018. The biological role of the ζ subunit as unidirectional inhibitor of the F1FO-ATPase of paracoccus denitrificans. *Cell Rep.* 22, 1067–1078. <https://doi.org/10.1016/j.celrep.2017.12.106>.
- Moraes, T.F., Reithmeier, R.A.F., 2012. Membrane transport metabolons. *Biochim. Biophys. Acta* 1818, 2687–2706. <https://doi.org/10.1016/j.bbamem.2012.06.007>.
- Moseley, J.B., Goode, B.L., 2006. The yeast actin cytoskeleton: from cellular function to biochemical mechanism. *Microbiol. Mol. Biol. Rev.* 70, 605–645. <https://doi.org/10.1128/MMBR.00013-06>.
- Nakayama, T., Takahashi, S., Waki, T., 2019. Formation of flavonoid metabolons: functional significance of protein-protein interactions and impact on flavonoid chemodiversity. *Front. Plant Sci.* 10 <https://doi.org/10.3389/fpls.2019.00821>.
- Noree, C., Sato, B.K., Broyer, R.M., Wilhelm, J.E., 2010. Identification of novel filament-forming proteins in *Saccharomyces cerevisiae* and *Drosophila melanogaster*. *J. Cell Biol.* 190, 541–551. <https://doi.org/10.1083/jcb.201003001>.
- O'Connell, J.D., Zhao, A., Ellington, A.D., Marcotte, E.M., 2012. Dynamic reorganization of metabolic enzymes into intracellular bodies. *Annu. Rev. Cell Dev. Biol.* 28, 89–111. <https://doi.org/10.1146/annurev-cellbio-101011-155841>.
- Pedley, A.M., Benkovic, S.J., 2017. A new View into the regulation of purine metabolism: the purinosome. *Trends Biochem. Sci.* 42, 141–154. <https://doi.org/10.1016/j.tibs.2016.09.009>.
- Pemberton, L.F., 2014. Preparation of yeast cells for live-cell imaging and indirect immunofluorescence. In: Smith, J.S., Burke, D.J. (Eds.), *Yeast Genetics: Methods and Protocols*. Springer New York, New York, NY, pp. 79–90. https://doi.org/10.1007/978-1-4939-1363-3_6.
- Puchulu-Campanella, E., Chu, H., Anstee, D.J., Galan, J.A., Tao, W.A., Low, P.S., 2013. Identification of the components of a glycolytic enzyme metabolon on the human red blood cell membrane. *J. Biol. Chem.* 288, 848–858. <https://doi.org/10.1074/jbc.M112.428573>.
- Ra, B., 2000. Quantitative characterization of homo- and heteroassociations of muscle phosphofructokinase with aldolase. *Biochim. Biophys. Acta Gen. Subj.* 1479, 303–314.
- Sagot, I., Pinson, B., Salin, B., Daignan-Fornier, B., 2006. Actin bodies in yeast quiescent cells: an immediately available actin reserve? *Mol. Biol. Cell* 17, 4645–4655. <https://doi.org/10.1091/mbc.E06>.
- Schmitt, D.L., An, S., 2017. Spatial organization of metabolic enzyme complexes in cells. *Biochemistry* 56, 3184–3196. <https://doi.org/10.1021/acs.biochem.7b00249>.
- Smith, M.G., Swamy, S.R., Pon, L. a., 2001. The life cycle of actin patches in mating yeast. *J. Cell Sci.* 114, 1505–1513.
- Srere, P.A., 1985. The metabolon. *Trends Biochem. Sci.* 10, 109–110. [https://doi.org/10.1016/0968-0004\(85\)90266-X](https://doi.org/10.1016/0968-0004(85)90266-X).
- Strzyz, P., 2019. Phase separation tunes signal transduction. *Nat. Rev. Mol. Cell Biol.* 20, 263. <https://doi.org/10.1038/s41580-019-0121-7>.
- Suresh, H.G., da Silveira dos Santos, A.X., Kukulski, W., Tyedmers, J., Riezman, H., Bukau, B., Mogk, A., 2015. Prolonged starvation drives reversible sequestration of lipid biosynthetic enzymes and organelle reorganization in *Saccharomyces cerevisiae*. *Mol. Biol. Cell* 26, 1601–1615. <https://doi.org/10.1091/mcb.E14-11-1559>.
- Sweetlove, L.J., Fernie, A.R., 2018. The role of dynamic enzyme assemblies and substrate channelling in metabolic regulation. *Nat. Commun.* 9, 2136. <https://doi.org/10.1038/s41467-018-04543-8>.
- Vasicova, P., Lejskova, R., Malcova, I., Hasek, J., 2015. The stationary-phase cells of *Saccharomyces cerevisiae* display dynamic actin filaments required for processes extending chronological life span. *Mol. Cell. Biol.* 35, 3892–3908. <https://doi.org/10.1128/MCB.00811-15>.
- Wojtas, K., Laurence, S., Sullivan, D., 1997. Flight muscle function in *Drosophila* requires colocalization of glycolytic enzymes. *Mol. Biol. Cell* 8, 1665–1675.
- Wu, F., Minteer, S., 2015. Krebs cycle metabolon: structural evidence of substrate channeling revealed by cross-linking and mass spectrometry. *Angew. Chemie - Int. Ed.* 54, 1851–1854. <https://doi.org/10.1002/anie.201409336>.
- Xu, L., Bretscher, A., 2014. Rapid glucose depletion immobilizes active myosin v on stabilized actin cables. *Curr. Biol.* 24, 2471–2479. <https://doi.org/10.1016/j.cub.2014.09.017>.
- Zimmerman, S.B., Trach, S.O., 1991. Estimation of macromolecule concentrations and excluded volume effects for the cytoplasm of *Escherichia coli*. *J. Mol. Biol.* 222, 599–620. [https://doi.org/10.1016/0022-2836\(91\)90499-V](https://doi.org/10.1016/0022-2836(91)90499-V).

ORIGINAL ARTICLE

Open Access



Metabolism, ATP production and biofilm generation by *Staphylococcus epidermidis* in either respiratory or fermentative conditions

Ulrik Pedroza-Dávila¹, Cristina Uribe-Alvarez¹, Lilia Morales-García¹, Emilio Espinoza-Simón¹, Ofelia Méndez-Romero², Adriana Muhlia-Almazán², Natalia Chiquete-Félix¹ and Salvador Uribe-Carvajal^{1*}

Abstract

Staphylococcus epidermidis is a Gram-positive saprophytic bacterium found in the microaerobic/anaerobic layers of the skin that becomes a health hazard when it is carried across the skin through punctures or wounds. Pathogenicity is enhanced by the ability of *S. epidermidis* to associate into biofilms, where it avoids attacks by the host and antibiotics. To test the effect of oxygen on metabolism and biofilm generation, cells were cultured at different oxygen concentrations ($[O_2]$). As $[O_2]$ decreased, *S. epidermidis* metabolism went from respiratory to fermentative. Remarkably, the rate of growth decreased at low $[O_2]$ while a high concentration of ATP ([ATP]) was kept. Under hypoxic conditions bacteria associated into biofilms. Aerobic activity sensitized the cell to hydrogen peroxide-mediated damage. In the presence of metabolic inhibitors, biofilm formation decreased. It is suggested that at low $[O_2]$ *S. epidermidis* limits its growth and develops the ability to form biofilms.

Keywords: *Staphylococcus epidermidis*, Oxygen concentration, Metabolism, Biofilms, Rate of oxygen consumption, Fermentation

Introduction

Saprophytic microorganisms control pathogenic bacteria, digest nutrients and synthesize coenzymes, prosthetic groups and amino acids (Foster et al. 2005; Berg 1996; Sender et al. 2016). In the skin, *Staphylococcus epidermidis* inhibits colonization by *Staphylococcus aureus* or *Streptococcus pyogenes* secreting antimicrobial compounds and proteases (Cogen et al. 2010; Iwase et al. 2010). In the skin, *S. epidermidis* inhabits the epidermis, dermis and the nearly anoxic sebaceous glands (Grice and Segre 2011).

Staphylococcus epidermidis is frequently introduced through wounds and surgical procedures. A recent study reported the presence of antibiotic-resistant

S. epidermidis strains in 46% of hospital secondary infections (Chabi and Momtaz 2019). Many of these strains were resistant to at least three antibiotics (Chabi and Momtaz 2019). Indeed, many antibiotics have to be tested in order to treat *S. epidermidis* nosocomial infections (Roujansky et al. 2020). *S. epidermidis* is also found frequently in implanted devices such as valves and catheters. There is an active search for materials to coat implant surfaces which may prevent biofilm formation (Rabin et al. 2015). Among these, zirconium nitride has shown promise in orthopaedic implants (Pilz et al. 2019), while sphingosine coating is being used with success on implant titanium-surfaces (Beck et al. 2019). Inside the body, this bacterium has to face attack from the immune system, high $[O_2]$ (Fang et al. 2016) and antibiotics (Leid 2009), most likely triggering a stress response. Within the organism, *S. epidermidis* may find areas with low $[O_2]$, similar to its natural habitat; it is likely that the bacterium will make an effort to remain in the hypoxic

*Correspondence: suribe@ifc.unam.mx

¹ Department of Genetics and Molecular Biology, Instituto de Fisiología Celular, Universidad Nacional Autónoma de México (UNAM), Mexico City, Mexico

Full list of author information is available at the end of the article

area, adhering to the surface and organizing into biofilms (Lewis 2007; Uribe-Alvarez et al. 2016). In regard to hypoxic environments within the host, these are often found at or near artificial devices such as catheters or prosthetic valves, where biofilms may force removal of implanted devices (Fey and Olson 2010; Büttner et al. 2015).

Understanding the *S. epidermidis* response to different $[O_2]$ would help optimize treatments (Cotter et al. 2009). We have reported that growing *S. epidermidis* at different $[O_2]$ modifies expression of respiratory chain enzymes and the ability to form biofilms (Uribe-Alvarez et al. 2016). At high $[O_2]$, cytochrome oxidases and NADH dehydrogenases are abundant and biofilms are minimal. In contrast, $[O_2]$ depletion increases nitrate reductase expression and association into biofilms (Uribe-Alvarez et al. 2016).

Here, the effect of $[O_2]$ on both, the aerobic and anaerobic metabolism of *S. epidermidis* was evaluated, together with [ATP]. In addition, the sensitivity of *S. epidermidis* to the toxic effects of hydrogen peroxide was tested. In each case, the biofilm-forming activity of cells was measured (Lewis 2007). When ATP synthesis was inhibited to different degrees by inhibitors of respiration (cyanide) (Uribe-Alvarez et al. 2016) or glycolysis (1,4-bisphosphobutane) (Hartman and Barker 1965; Rosas-Lemus et al. 2016a), biofilm formation also decreased. It is suggested that *S. epidermidis* associates into biofilms as a strategy to avoid high $[O_2]$.

Materials and methods

Bacterial strain and growth media

Staphylococcus epidermidis strain ATCC 12228 was a kind donation from Dr. Juan Carlos Cancino Díaz (Instituto Politécnico Nacional, México). A loophole from the bacterium was suspended in 5 mL of 3% tryptic soy broth (Fluka, Sigma) and incubated at 37 °C for 24 h. Pre-cultures were added to 1 L LB medium (1% tryptone, 0.5% yeast extract, 1% NaCl) plus 2% glucose and incubated 24 h at 30 °C under aerobic (shaking 150 rpm), microaerobic (5% CO₂, no agitation) or anaerobic (static in oxygen-depleted sealed acrylic chamber) conditions. Then the cells were washed three times at 5000×g for 10 min with distilled water and resuspended in 10 mM HEPES pH 7.4 (Uribe-Alvarez et al. 2016).

Cytoplasmic extracts

All procedures were conducted at 4 °C. Cells (grown under aerobic, microaerobic or anaerobic conditions) were centrifuged at 5000×g for 10 min, washed three times with distilled water and resuspended in 50 mL 10 mM HEPES, pH 7.4, supplemented with one tablet of protease-inhibitor cocktail (Complete) and 1 mM

PMSF. Cells were disrupted by sonication using a Sonics VibraCell sonicator (Sonics & materials, Inc., Newtown, CT) 7 × 20 s with 20 s intervals. To remove unbroken cells the suspension was centrifuged at 10,000×g for 10 min and the supernatant was recovered.

Protein concentration

Protein concentrations from intact *S. epidermidis* cells were determined by the biuret method (Gornall et al. 1949). Absorbance (540 nm) was measured in a Beckman-Coulter DU50 spectrophotometer. For cytoplasmic extracts, protein concentration was measured by Bradford at 595 nm, using 1 or 2 μL aliquots of the sample in a PolarStar Omega (BMG labtech, Ortenberg, Germany) (Bradford 1976).

Rate of oxygen consumption

The rate of oxygen consumption was measured in 10 mM HEPES pH 7.4 plus the indicated respiratory substrate. Bacteria, 0.5 mg prot mL⁻¹ were added to a water-jacketed 1 mL chamber at 37 °C equipped with a Clark type electrode connected to a Strathkelvin model 782 oxymeter. Data were analyzed using the 782 Oxygen System Software (Warner/Strathkelvin Instruments) (Uribe-Alvarez et al. 2016).

Ethanol production

Fermentation by cell cytoplasmic extracts (0.5 mg prot. mL⁻¹) was measured in 0.1 M MES-TEA, pH 7.0, 1.8 mM NAD plus either glucose or glycerol and incubated at 30 °C for 0, 2.5, 5 or 10 min. The reaction was stopped with 30% TCA, 0.1 mL and neutralized with NaOH. Ethanol was measured adding a 10 μL aliquot (0.005 mg) of the supernatant to 0.2 mL 114 mM K₂HPO₄, pH 7.6. After 1 min, 30 μg ADH mL⁻¹ was added, the sample was incubated for 30 min and O.D. was determined at 340 nm in a POLARstar Omega. Ethanol is reported as μmol ethanol (mg prot)⁻¹ (Araiza-Olivera et al. 2013).

ATP concentration

ATP was measured in cytoplasm extracts resuspended to 0.025 mg protein in 0.15 mL reaction buffer (20 mM KH₂PO₄, 40 mM Na₂HPO₄, 80 mM NaCl, 1 mM MgSO₄). An ATP calibration curve was prepared freshly each day using lyophilized luciferase (Sigma-Aldrich). Luciferase was prepared following instructions by the provider and 0.02 mL was added to each sample in a 96-well microplate. Bioluminescence was detected in a POLARstar Omega luminometer (BGM LABTECH, Offenburg, Germany). [ATP] was reported as μmol (mg prot)⁻¹ (Palikaras and Tavernarakis 2016; Mendoza-Hoffmann et al. 2018).

Susceptibility to hydrogen peroxide-mediated damage

The effect of $[H_2O_2]$ on the viability of *S. epidermidis* was determined as previously reported (Macvanin and Hughes 2010). Briefly, cells were adjusted to an O.D.=0.1 (600 nm) and then H_2O_2 (0 to 25 mM as indicated) was added to the reaction mixture. After 30 min, serial dilution of the cultures was performed in 0.9% NaCl and 10 μ L of the 1:1000 diluted sample was plated in LB, 2% glucose agar plates and incubated 24 h at 37 °C. Colony forming units (CFU) mL^{-1} were counted. The sample taken before H_2O_2 addition was assigned as 100%. The average of three experiments is shown with SD. ANOVA test and Tukey's multiple comparison-test were used. Significance was $*P < 0.0001$.

Biofilm formation and detection

Biofilm generation was measured in sterile Costar 96-well polystyrene plates as previously reported (Calà et al. 2015; Uribe-Alvarez et al. 2016). Briefly, in each well, 0.4% crystal violet in 33% glacial acetic acid was mixed with the indicated, inhibitors sodium cyanide (NaCN) (100 μ M), butane-1,4-bisphosphate (B1,4BP) (1 mM) or, carbonyl cyanide *m*-chlorophenyl hydrazone (CCCP) (0.1, 0.5, or 1 μ M, as indicated). Then bacteria were added to O.D. 0.02. Final volume 200 μ L. The plate was incubated 24 h at 37 °C with 5% CO₂. After incubation, wells were washed twice with 200 μ L phosphate-buffered saline (PBS) to remove non-adherent bacteria. Plates were dried for 1 h at 60 °C, stained with 0.4% crystal violet for 10 min and washed under running tap water to remove excess stain. Absorbance (492 nm) was measured using a microplate reader (Polar Star Omega, BMG Labtech). Each sample was tested in three independent triplicate experiments and compared against the non-treated control using one-way variance analysis (ANOVA) plus Dunnett's post hoc test.

Results

Oxygen is among the most important factors driving evolution (Lane 2002). Its partial reduction products, the reactive oxygen species (ROS) destroy nucleic acids, proteins and membranes (Ezraty et al. 2017). Thus, to profit from its remarkable electron acceptor properties, organisms have to deal carefully with the dangerous oxygen molecule (Lane 2002; Rosas-Lemus et al. 2016b). *S. epidermidis* lives in hypoxic/anoxic environments, although it can adapt to high [O₂]. In order to follow the metabolic adaptation of *S. epidermidis* it was cultivated at different [O₂]. After 24 h under aerobic conditions biomass yield was 8.58 g/L, three times higher than

under microaerobiosis, 2.11 g/L or anaerobiosis, 1.75 g/L.

In order to further explore the basis for biomass yield variations at different [O₂], the activity of the respiratory chain from *S. epidermidis* grown at different [O₂] was measured (Fig. 1). As expected from previous respiratory chain protein expression results (Uribe-Alvarez et al. 2016), the ability of cells to consume oxygen was proportional to [O₂] in the growth medium. In aerobic conditions and in the presence of lactate the rate of oxygen consumption was 70 natgO (mg prot. min)⁻¹, at least five times higher than in microaerobic media, where the rate was 5 natgO (mg prot. min)⁻¹ or in those grown under anaerobic conditions, where it was negligible (Fig. 1). Under normoxia the best respiratory fuel was lactate, which was oxidized around three times as fast as glucose or ethanol (Fig. 1).

In *S. epidermidis* respiratory chain activities correlated with growth rates. However, it was reasoned that in hypoxia glycolysis may constitute an important source of energy (Somerville and Proctor 2009). Furthermore, as *S. epidermidis*, normally lives at low [O₂], fermentation may be the preferred energy-yielding pathway in this bacterium. To test this, *S. epidermidis* was grown at different [O₂] and ethanol production from either glucose (Fig. 2a) or glycerol (Fig. 2b) was measured at 2.5, 5 and 10 min of incubation. Both substrates were equally efficient. However, at different [O₂] large variations in the rate of fermentation were observed: bacteria from anaerobic media were the most active, (Fig. 2), suggesting that fermentation increases as [O₂] decreases.

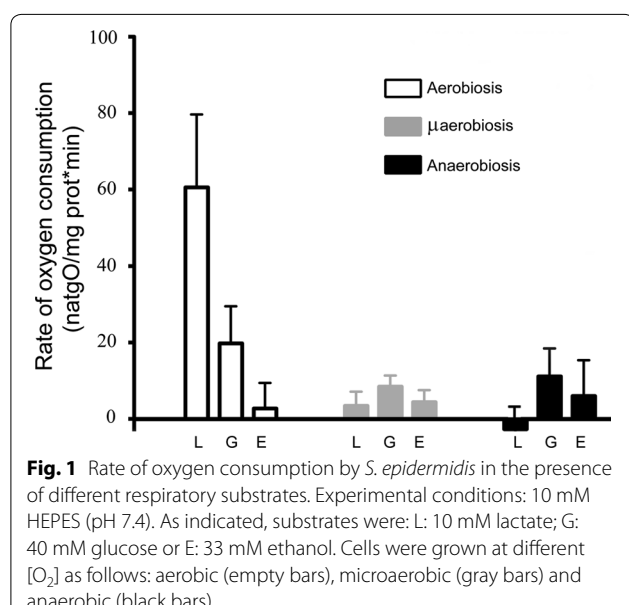
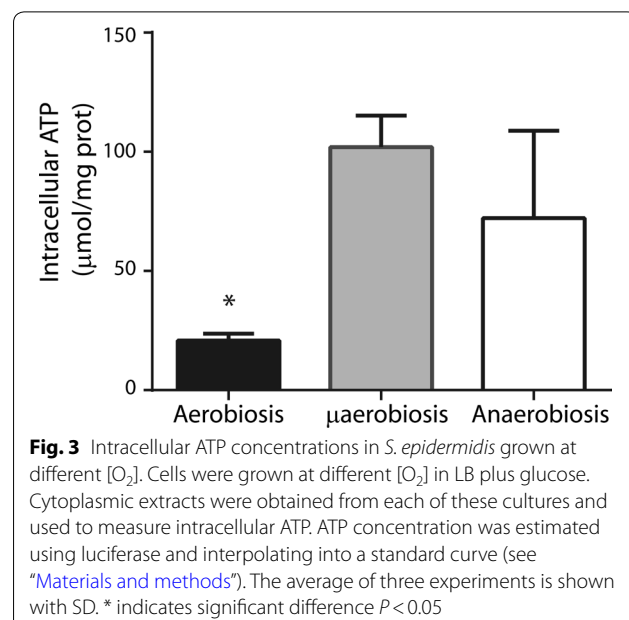
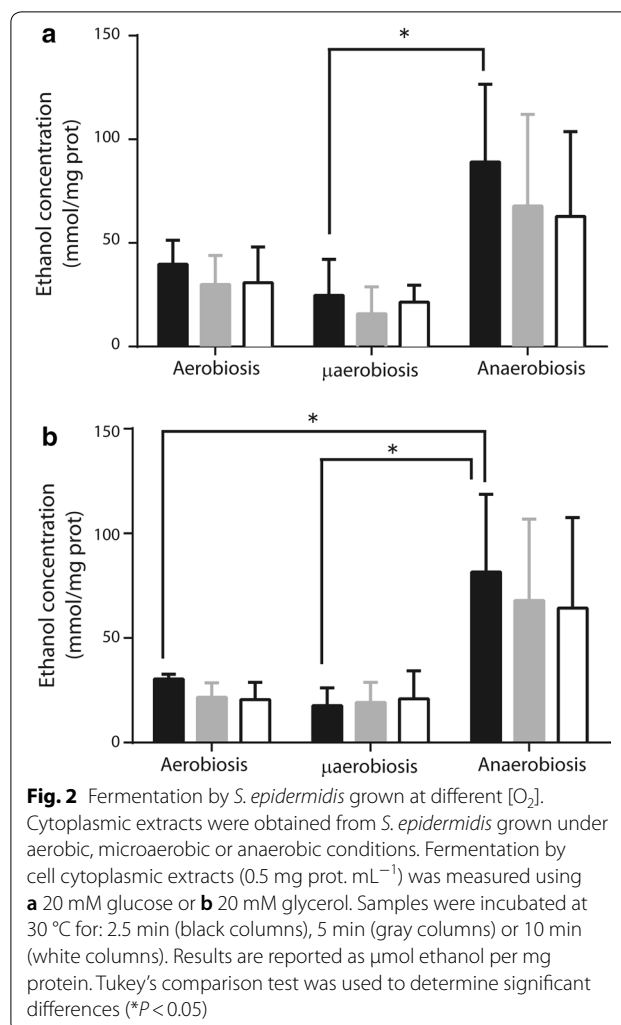


Fig. 1 Rate of oxygen consumption by *S. epidermidis* in the presence of different respiratory substrates. Experimental conditions: 10 mM HEPES (pH 7.4). As indicated, substrates were: L: 10 mM lactate; G: 40 mM glucose or E: 33 mM ethanol. Cells were grown at different [O₂] as follows: aerobic (empty bars), microaerobic (gray bars) and anaerobic (black bars)



In *S. epidermidis*, increasing $[O_2]$ increased the rate of oxygen consumption while fermentation was inhibited. To determine which of these pathways produced more energy, the concentration of ATP ([ATP]) was measured in *S. epidermidis* grown under normoxia, hypoxia or anoxia (Fig. 3). Contrary to what we expected from the low growth rate and the slow respiratory activity observed, in hypoxia- and anoxia-grown cells, [ATP] was higher than in normoxia as aerobiosis, [ATP] increased roughly five times in hypoxia and three times in anoxia as compared to normoxia (Fig. 3).

In *S. aureus* a deficient respiratory chain confers resistance to H_2O_2 toxicity (Painter et al. 2017), suggesting that anaerobiosis-adapted cells resist oxidative stress better. Thus, we decided to test *S. epidermidis* grown at different $[O_2]$ for its sensitivity to H_2O_2 (Fig. 4) (Lobritz et al. 2015). Even at the lowest concentrations of H_2O_2 we used (0.5 mM), viability decreased in all cells. Aerobic-grown cells exhibited the poorest survival rates, while

cells grown under anaerobiosis survived best, such that even at the highest H_2O_2 concentration tested (25 mM H_2O_2) a small amount of viable cells was detected (Fig. 4). The increase in sensitivity to ROS observed in aerobically grown *S. epidermidis* was probably due to increased expression of the redox enzymes in the respiratory chain (Uribe-Alvarez et al. 2016). These redox enzymes contain different coenzymes and prosthetic groups, which normally become free radicals during their catalytic cycle (Quinlan et al. 2013; Rosas-Lemus et al. 2016b). Thus, as reported for *S. aureus* (Painter et al. 2017) at high $[O_2]$ *S. epidermidis* expressed an active respiratory chain and its sensitivity to H_2O_2 increased.

The highest [ATP] was detected in cells grown at low $[O_2]$, which exhibited a slow growth rate. This seemingly contradictory situation may be explained by proposing that when *S. epidermidis* finds a low $[O_2]$, which resembles that found in its normal niche, it makes an effort to attach itself to a surface, redirecting its energy use from growth to produce polysaccharides and proteins for biofilm generation (Beenken et al. 2004; Lewis 2007). To analyze whether biofilm was dependent on [ATP], *S. epidermidis* was grown under hypoxia and in the presence and absence of different metabolic inhibitors. In hypoxic grown-cells both oxidative phosphorylation and fermentation are active. It was observed that cells incubated in the presence of the respiratory chain inhibitor cyanide or the glycolytic inhibitor 1,4-bisphosphobutane, formed smaller biofilms than the control and that addition of both inhibitors led to even less biofilms (Fig. 5a). This would suggest that biofilm

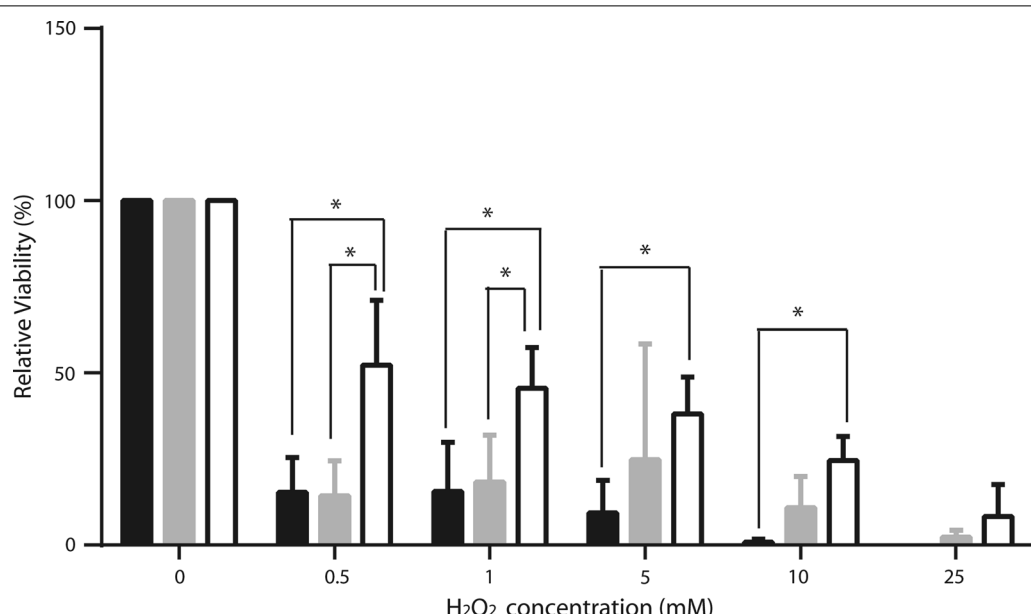


Fig. 4 H₂O₂ effect on cellular viability. *S. epidermidis* susceptibility to hydrogen peroxide was determined using 0, 0.5, 1, 5, 10 or 25 mM H₂O₂ in each group: aerobiosis (black bar), microaerobiosis (gray bar) or anaerobiosis (white bar). After 30 min of incubation with H₂O₂, the samples were diluted 1:1000, 10 µL were taken and plated in LB plus 2% glucose-agar. CFU/mL were counted. Samples without treatment were assigned as 100% viable cells. The average of three experiments is shown with SD. Significance *P<0.0001

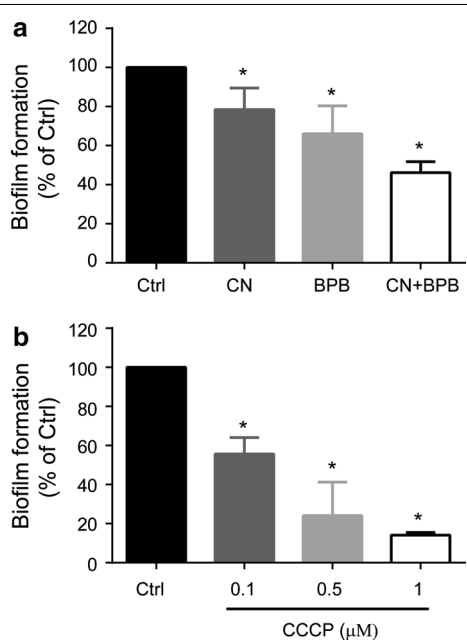


Fig. 5 *In vitro* biofilm inhibition assay. *S. epidermidis* was grown under microaerobic conditions. **a** Different metabolic inhibitors were added as indicated: 100 µM NaCN, 1 mM B1,4BP or both inhibitors. **b** Different concentrations of the uncoupler CCCP (0.5, 1.0 and 1.5 µM) were added to deplete ATP. After 24 h of incubation biofilm generation was evaluated by measuring the absorbance at 492 nm with a microplate reader. Each sample was compared with the control (without additions). Statistics were applied using ANOVA and Dunnett's post hoc test. Significance *P<0.0001

formation activity is proportional to [ATP]. In addition, the uncoupler CCCP was used at concentrations below those where it killed cells (Result not-shown), observing that biofilm generation decreased further as uncoupler concentration increased (Fig. 5b). These results suggest that, regardless of its source, in *S. epidermidis* high [ATP] is needed to form biofilms.

Discussion

Antibiotic-resistant strains of *S. epidermidis* are increasingly found in nosocomial infections (Chabi and Momtaz 2019). Implant removal due to *S. epidermidis* biofilm colonization is also quite frequent (Gristina 1987; Raad et al. 1998). *S. epidermidis* is frequently found in coagulase-negative staphylococci-caused prosthetic valve infective endocarditis cases (Mack et al. 2013), in 30–43% implant infections (Zimmerli et al. 2004) and in 50–70% catheter-related infections (von Eiff et al. 2002). Understanding the physiology of the bacterium is a must in order to design new treatment and prevention methods (Uribe-Alvarez et al. 2016). In biofilms, *S. epidermidis* cells are protected from the host. Thus, it is most important to analyse the association and specialization processes of the cells involved in the genesis of biofilms.

Diverse facultative bacteria adapt to wide [O₂], differentially expressing redox enzymes in its respiratory chain. *S. epidermidis* does express different enzymes

at varying $[O_2]$ (Uribe-Alvarez et al. 2016). Aerobic metabolism enabled cells to grow more (Baez and Shiloach 2014). Still, enhanced growth resulted in higher sensitivity to H_2O_2 , suggesting that high contents of redox enzymes make cells vulnerable to ROS. Indeed, when grown at high $[O_2]$, sensitivity to ROS is enhanced in *S. aureus* and *Enterococcus faecalis*, while their mutant counterparts, lacking an efficient respiratory chain resist ROS better (Painter et al. 2017).

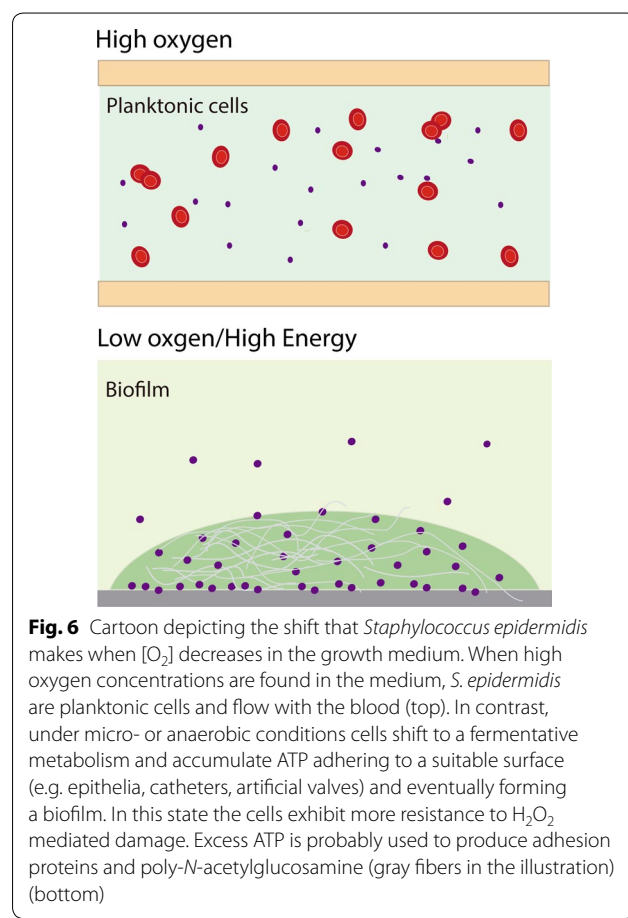
When exposing *S. epidermidis* grown in different $[O_2]$ to oxygen peroxide, we observed a similar phenomenon: cells grown in hypoxic or anoxic environments, which exhibited low respiratory rates were more resistant to oxygen peroxide (Fig. 4). Thus, as in *S. aureus*, the lack of an efficient respiratory chain in *S. epidermidis* enabled cells to survive ROS. This is probably useful when bacteria detached from a biofilm reach other tissues where they may be confronted with the oxidative burst generated by the immune system (Jensen et al. 1992).

The rate of oxygen consumption in aerobic grown cells was highest when lactate was the substrate. This is probably due to the direct donation of electrons to the menaquinone pool by lactate dehydrogenase (Götz and Mayer 2013; Kane et al. 2016). The slower rates observed for alcohol, may be due to an additional step as alcohol dehydrogenase electrons are first donated to Ndi2 (Artzatbanov and Petrov 1990). The rate of respiration was also slow for glucose, probably for the same reason, as intermediaries have to undergo many reactions before releasing electrons to the respiratory chain (Ferreira et al. 2013). In contrast, under anaerobiosis, lactate-dependent oxygen consumption disappeared completely while a small rate of glucose-dependent oxygen consumption was still present. In contrast, in *S. aureus* increased lactate dehydrogenase expression anaerobiosis has been reported (Fuchs et al. 2007).

The normal habitat for *S. epidermidis* is the microaerobic environment found in different epidermic and dermic layers (Peyssonnaux et al. 2008). One strategy *S. epidermidis* uses when confronted with high $[O_2]$ is the differential expression of a diverse number of redox enzymes in the respiratory chain. Reports indicate that when microaerophilic or anaerophilic bacteria find a suitable environment, they react manufacturing proteins and polysaccharides that enable them to form biofilms and attach to surfaces at low $[O_2]$. Avoiding high $[O_2]$ involves both, anchoring in low oxygen environments and building biofilms as barriers against penetration of ROS or toxic substances (Palikaras and Tavernarakis 2016). Metabolic adaptation has also been reported for *Neisseria gonorrhoeae*, when it is stimulated to form biofilms. A proteomic analysis of *N. gonorrhoeae* biofilms evidenced up-regulation of proteins involved in

anaerobic metabolism such as glycolysis and TCA cycle plus increased expression of those proteins involved in biofilm generation like pilus-associated proteins (Phillips et al. 2012). In addition, some oxidative stress genes are required for normal biofilm formation in *N. gonorrhoeae* (Falsetta et al. 2011).

The increase in ATP prior to biofilm formation has been reported in others bacterium. *Bacillus brevis* and *Escherichia coli* react to substrate depletion by adhering to glass surfaces and at the same time increase [ATP] two to fivefold as compared to planktonic cells (Hong and Brown 2009). So, the conditions where bacteria need to make biofilms promote saving ATP even at the expense of the growth rate. ATP is most likely needed to synthesize the extracellular proteins and the polysaccharide fibers that anchor cells to surfaces and to each other. Inhibiting ATP production in micro- or anaerobic conditions by adding cyanide or 1,4-bisphosphobutane resulted in a reduced biofilm formation (Fig. 5). This phenomenon is also observed when treating *S. epidermidis* with the nitrate reductase inhibitor methylamine in anaerobic conditions (Uribe-Alvarez et al. 2016). In contrast, in aerobiosis cyanide promotes biofilm formation (Uribe-Alvarez et al. 2016).



Even when facultative bacteria such as *S. epidermidis* survive at high [O₂], their habitat in the skin is hypoxic to anoxic. While they survive in aerobic environments their susceptibility to ROS-mediated damage and possibly to attack by macrophages increases. They thus present an oxygen avoidance behavior, anchoring and associating in hypoxic environments (Fig. 6). Learning how avoidance works in *S. epidermidis* and other bacteria would impact both the physiologic and therapeutic field.

Aiming to understand such rise in ATP, we found that other bacteria, e.g. *Bacillus brevis* and *Escherichia coli*, react to substrate depletion by adhering to glass surfaces and at the same time increase [ATP] two- to fivefold in comparison to planktonic cells (Hong and Brown 2009). In this regard, it has been reported that hypoxic stimuli induce biofilm formation in *S. epidermidis* (Uribe-Alvarez et al. 2016).

Acknowledgements

Partially funded by UNAM/DGAPA/PAPIIT grant IN203018 to SUC and CONACYT 241670 grant to AMA. UPD (MsSc) and EES (PhD) are graduate students in the Biochemistry Program at UNAM. LMG is in the Biomedical PhD program at UNAM. OMR is a graduate student at CIAD. UPD, LMG and OMR are CONACYT fellows. CUA present address: Fox-Chase Cancer Center, Philadelphia, PA. Technical help from Ramón Méndez-Franco is acknowledged.

Authors' contributions

UPD, participated in all experiments and in discussions helping to write and edit the manuscript. CUA contributed to the original idea, she was the first author of the previous paper, participated in oxymetry experiments and in discussions helping to write and edit the manuscript. LMG participated in oxygen-consumption experiments and discussions on the manuscript. EES, participated in fermentation experiments and in discussions. OMR participated in the experiments performed both at CIAD and at UNAM and in discussions. AMA contributed with early ideas and designed some protocols, she provided reagents and facilities at CIAD and edited the manuscript. NCF taught graduate students the techniques involved in each experiment, supervising experimental work and protocols. SUC helped develop the original idea, designed the project, helped in technique application and wrote the manuscript. He provided facilities and found funding. Participated in lab discussions. All authors read and approved the final manuscript.

Ethics approval and consent to participate

This article does not contain any studies with human participants or animals performed by any of the authors.

Competing interests

The authors declare that they have no competing interests.

Author details

¹ Department of Genetics and Molecular Biology, Instituto de Fisiología Celular, Universidad Nacional Autónoma de México (UNAM), Mexico City, Mexico. ² Centro de Investigación y Desarrollo en Alimentos (CIAD), Hermosillo, Sonora, Mexico.

Received: 28 January 2020 Accepted: 31 January 2020

Published online: 11 February 2020

References

- Araiza-Olivera D, Chiquete-Felix N, Rosas-Lemus M, Sampedro JG, Peña A, Mujica A, Uribe-Carvajal S (2013) A glycolytic metabolon in *Saccharomyces cerevisiae* is stabilized by F-actin. FEBS J 280:3887–3905. <https://doi.org/10.1111/febs.12387>
- Artzatbanov VYU, Petrov VV (1990) Branched respiratory chain in aerobically grown *Staphylococcus aureus*—oxidation of ethanol by cells and protoplasts. Arch Microbiol 153:580–584
- Baez A, Shiach J (2014) Effect of elevated oxygen concentration on bacteria, yeasts, and cells propagated for production of biological compounds. Microb Cell Fact 13:181. <https://doi.org/10.1186/s12934-014-0181-5>
- Beck S, Sehl C, Voortmann S, Verhasselt HL, Edwards MJ, Buer J, Hasenberg M, Gulbins E, Becker KA (2019) Sphingosine is able to prevent and eliminate *Staphylococcus epidermidis* biofilm formation on different orthopedic implant materials in vitro. J Mol Med. <https://doi.org/10.1007/s00190-018-0188-x>
- Beenken KE, Dunman PM, McAleese F, Macapagal D, Murphy E, Projan SJ, Blevins JS, Smeltzer MS (2004) Global gene expression in *Staphylococcus aureus* biofilms. J Bacteriol 186:4665–4684. <https://doi.org/10.1128/JB.186.14.4665-4684.2004>
- Berg RD (1996) The indigenous gastrointestinal microflora. Trends Microbiol 4:430–435. [https://doi.org/10.1016/0966-842X\(96\)10057-3](https://doi.org/10.1016/0966-842X(96)10057-3)
- Bradford MM (1976) A rapid and sensitive method for the quantitation of microgram quantities of protein utilizing the principle of protein-dye binding. Anal Biochem 72:248–254
- Büttner H, Mack D, Rohde H (2015) Structural basis of *Staphylococcus epidermidis* biofilm formation: mechanisms and molecular interactions. Front Cell Infect Microbiol 5:14. <https://doi.org/10.3389/fcimb.2015.00014>
- Calà C, Amadio E, Di Carlo E, Virruso R, Fasciana T, Giannanca A (2015) Biofilm production in *Staphylococcus epidermidis* strains, isolated from the skin of hospitalized patients: genetic and phenotypic characteristics. N Microbiol 38:521–529
- Chabi R, Momtaz H (2019) Virulence factors and antibiotic resistance properties of the *Staphylococcus epidermidis* strains isolated from hospital infections in Ahvaz, Iran. Trop Med Health 47:56. <https://doi.org/10.1186/s41182-019-0180-7>
- Cogen AL, Yamasaki K, Sanchez KM, Dorschner RA, Lai Y, MacLeod DT, Torpey JW, Otto M, Nizet V, Kim JE, Gallo RL (2010) Selective antimicrobial action is provided by phenol-soluble modulins derived from *Staphylococcus epidermidis*, a normal resident of the skin. J Invest Dermatol 130(1):192–200
- Cotter JJ, O'Gara JP, Mack D, Casey E (2009) Oxygen-mediated regulation of biofilm development is controlled by the alternative sigma factor sigma(B) in *Staphylococcus epidermidis*. Appl Environ Microbiol 75:261–264. <https://doi.org/10.1128/AEM.00261-08>
- Ezraty B, Gennaris A, Barras F, Collet J-F (2017) The gain of single electrons by oxygen (O²) generates partially reduced reactive oxygen species (ROS), including superoxide anions (O²⁻). Nat Publ Gr. <https://doi.org/10.1038/nrmicro.2017.26>
- Falsetta ML, Steichen CT, McEwan AG, Cho C, Ketterer M, Shao J, Hunt J, Jennings MP, Apicella MA (2011) The composition and metabolic phenotype of *Neisseria gonorrhoeae* biofilms. Front Microbiol 2:75. <https://doi.org/10.3389/fmicb.2011.00075>
- Fang FC, Frawley ER, Tapscott T, Vázquez-Torres A (2016) Bacterial stress responses during host infection. Cell Host Microbe 20:133–143. <https://doi.org/10.1016/j.chom.2016.07.009>
- Ferreira MT, Manso AS, Gaspar P, Pinho MG, Neves AR (2013) Effect of oxygen on glucose metabolism: utilization of lactate in *Staphylococcus aureus* as revealed by in vivo NMR studies. PLoS ONE 8:e58277. <https://doi.org/10.1371/journal.pone.0058277>
- Fey PD, Olson ME (2010) Current concepts in biofilm formation of *Staphylococcus epidermidis*. Future Microbiol 5:917–933. <https://doi.org/10.2217/fmb.10.56>
- Foster J, Ganatra M, Kamal I, Ware J, Makarova K, Ivanova N, Bhattacharyya A, Kapral V, Kumar S, Posfai J, Vincze T, Ingram J, Moran L, Lapidus A, Omelchenko M, Kyripides N, Ghedin E, Wang S, Goltsman E, Joukov V, Ostrovskaya O, Tsukerman K, Mazur M, Comb D, Koonin E, Slatko B (2005) The Wolbachia genome of *Brugia malayi*: endosymbiont evolution within a human pathogenic nematode. PLoS Biol 3:e121. <https://doi.org/10.1371/journal.pbio.0030121>
- Fuchs S, Pané-Farré J, Kohler C, Hecker M, Engelmann S (2007) Anaerobic gene expression in *Staphylococcus aureus*. J Bacteriol 189:4275–4289. <https://doi.org/10.1128/JB.00081-07>
- Gornall AG, Bardawill CJ, David MM (1949) Determination of serum proteins by means of the biuret reaction. J Biol Chem 177:751–766

- Götz F, Mayer S (2013) Both terminal oxidases contribute to fitness and virulence during organ-specific *Staphylococcus aureus* colonization. MBio 4:e00976-13. <https://doi.org/10.1128/mBio.00976-13>
- Grice EA, Segre JA (2011) The skin microbiome. Nat Rev Microbiol 9:244–253. <https://doi.org/10.1038/nrmicro2537>
- Gristina AG (1987) Biomaterial-centered infection: microbial adhesion versus tissue integration. Science 237:1588–1595. <https://doi.org/10.1126/science.3629258>
- Hartman FC, Barker R (1965) An exploration of the active site of aldolase using structural analogs of fructose diphosphate*. Biochemistry 4:1068–1075. <https://doi.org/10.1021/bi00882a014>
- Hong Y, Brown DG (2009) Variation in bacterial ATP level and proton motive force due to adhesion to a solid surface. Appl Environ Microbiol 75:2346–2353. <https://doi.org/10.1128/AEM.02671-08>
- Iwase T, Uehara Y, Shinji H, Tajima A, Seo H, Takada K, Agata T, Mizunoe Y (2010) *Staphylococcus epidermidis* Esp inhibits *Staphylococcus aureus* biofilm formation and nasal colonization. Nature 465:346–349. <https://doi.org/10.1038/nature09074>
- Jensen ET, Kharazmi A, Höiby N, Costerton JW (1992) Some bacterial parameters influencing the neutrophil oxidative burst response to *Pseudomonas aeruginosa* biofilms. APMIS 100:727–733. <https://doi.org/10.1111/j.1699-0463.1992.tb03991.x>
- Kane AL, Brutinel ED, Joo H, Maysonet R, VanDrisse CM, Kotloski NJ, Gralnick JA (2016) Formate metabolism in *Shewanella oneidensis* generates proton motive force and prevents growth without an electron acceptor. J Bacteriol 198:1337–1346. <https://doi.org/10.1128/JB.00927-15>
- Lane N (2002) Oxygen: the molecule that made the world. Oxford University Press, Oxford
- Leid JG (2009) Bacterial biofilms resist key host defenses. Microbe 4:66–70
- Lewis K (2007) Persister cells, dormancy and infectious disease. Nat Rev Microbiol 5:48–56. <https://doi.org/10.1038/nrmicro1557>
- Lobritz MA, Belenky P, Porter CBM, Gutierrez A, Yang JH, Schwarz EG, Dwyer DJ, Khalil AS, Collins JJ (2015) Antibiotic efficacy is linked to bacterial cellular respiration. Proc Natl Acad Sci USA 112:8173–8180. <https://doi.org/10.1073/pnas.1509743112>
- Mack D, Davies AP, Harris LG, Jeeves R, Pascoe B, Knobloch JK-M, Rohde H, Wilkinson TS (2013) *Staphylococcus epidermidis* in biomaterial-associated infections. Biomaterials associated infection. Springer, New York, pp 25–56
- Macvanin M, Hughes D (2010) Assays of sensitivity of antibiotic-resistant bacteria to hydrogen peroxide and measurement of catalase activity. Methods in molecular biology. Humana Press, Clifton, pp 95–103
- Mendoza-Hoffmann F, Pérez-Osegueda Á, Cevallos MÁ, Zarco-Zavala M, Ortega R, Peña-Segura C, Espinoza-Simón E, Uribe-Carvajal S, García-Trejo JJ (2018) The biological role of the ζ subunit as unidirectional inhibitor of the F1FO-ATPase of *Paracoccus denitrificans*. Cell Rep 22:1067–1078. <https://doi.org/10.1016/j.celrep.2017.12.106>
- Painter KL, Hall A, Ha KP, Edwards AM (2017) The electron transport chain sensitizes *Staphylococcus aureus* and *Enterococcus faecalis* to the oxidative burst. Infect Immun. <https://doi.org/10.1128/IAI.00659-17>
- Palikaras K, Tavernarakis N (2016) Intracellular assessment of ATP levels in *Caenorhabditis elegans*. Bio-Protocol. <https://doi.org/10.21769/BioProtoc.2048>
- Peyssonnaux C, Boutin AT, Zinkernagel AS, Datta V, Nizet V, Johnson RS (2008) Critical role of HIF-1 α in keratinocyte defense against bacterial infection. Invest Dermatol 128:1964–1968. <https://doi.org/10.1038/JID.2008.27>
- Phillips NJ, Steichen CT, Schilling B, Post DMB, Niles RK, Bair TB, Falsetta ML, Apicella MA, Gibson BW (2012) Proteomic analysis of *Neisseria gonorrhoeae* biofilms shows shift to anaerobic respiration and changes in nutrient transport and outermembrane proteins. PLoS ONE 7:e38303. <https://doi.org/10.1371/journal.pone.0038303>
- Pilz M, Staats K, Tobudic S, Assadian O, Presterl E, Windhager R, Holinka J (2019) Zirconium nitride coating reduced *Staphylococcus epidermidis* biofilm formation on orthopaedic implant surfaces: an in vitro study. Clin Orthop Relat Res 477:461–466. <https://doi.org/10.1097/CORR.0000000000000568>
- Quinlan CL, Perevoshchikova IV, Hey-Mogensen M, Orr AL, Brand MD (2013) Sites of reactive oxygen species generation by mitochondria oxidizing different substrates. Redox Biol 1:304–312. <https://doi.org/10.1016/j.redox.2013.04.005>
- Raad I, Alrhawan A, Rolston K (1998) *Staphylococcus epidermidis*: emerging resistance and need for alternative agents. Clin Infect Dis 26:1182–1187. <https://doi.org/10.1086/520285>
- Rabin N, Zheng Y, Opoku-Temeng C, Du Y, Bonsu E, Sintim HO (2015) Biofilm formation mechanisms and targets for developing antibiofilm agents. Future Med Chem 7:493–512
- Rosas-Lemus M, Chiquete-Félix N, Ruiz-Pérez K, Rigoulet M, Devin A, Hernández-Rodríguez M, Uribe-Carvajal S (2016a) Sensitivity of the mitochondrial unspecific channel of *Saccharomyces cerevisiae* to butane-1,4-bisphosphate, a competitive inhibitor of fructose-1,6-bisphosphate-aldolase. ChemistrySelect 1:2930–2934. <https://doi.org/10.1002/slct.201600303>
- Rosas-Lemus M, Uribe-Alvarez C, Contreras-Zentella M, Luévano-Martínez LA, Chiquete-Félix N, Morales-García NL, Simón EE, Muñoz-Almazán A, Escamilla-Marván E, Uribe-Carvajal S (2016b) Oxygen: from toxic waste to optimal (toxic) fuel of life. Free radicals and diseases. Rijeka, Intech
- Roujansky A, Martin M, Gomart C, Hulin A, Mounier R (2020) Multidrug-resistant *Staphylococcus epidermidis* ventriculostomy-related infection successfully treated by intravenous ceftaroline after failure of daptomycin treatment. World Neurosurg. <https://doi.org/10.1016/j.wneu.2020.01.013>
- Sender R, Fuchs S, Milo R (2016) Revised estimates for the number of human and bacteria cells in the body. PLoS Biol. <https://doi.org/10.1371/journal.pbio.1002533>
- Somerville GA, Proctor RA (2009) At the crossroads of bacterial metabolism and virulence factor synthesis in *Staphylococci*. Microbiol Mol Biol Rev 73:233–248. <https://doi.org/10.1128/MMBR.00005-09>
- Uribe-Alvarez C, Chiquete-Félix N, Contreras-Zentella M, Guerrero-Castillo S, Peña A, Uribe-Carvajal S (2016) *Staphylococcus epidermidis*: metabolic adaptation and biofilm formation in response to different oxygen concentrations. Pathog Dis 74:ftv111. <https://doi.org/10.1093/fmp/ftv111>
- von Eiff C, Peters G, Heilmann C (2002) Pathogenesis of infections due to coagulase-negative staphylococci. Lancet Infect Dis 2:677–685. [https://doi.org/10.1016/S1473-3099\(02\)00438-3](https://doi.org/10.1016/S1473-3099(02)00438-3)
- Zimmerli W, Trampuz A, Ochsner PE (2004) Prosthetic-joint infections. N Engl J Med 351:1645–1654. <https://doi.org/10.1056/NEJMra040181>

Publisher's Note

Springer Nature remains neutral with regard to jurisdictional claims in published maps and institutional affiliations.